Molecular Pathophysiology and Stem Cell Treatment for Mitochondrial Diseases: Insights from the French-Canadian Variant of Leigh Syndrome

Alexanne Cuillerier

Thesis submitted to the University of Ottawa
in partial fulfillment of the requirements for the Ph.D. program in Cellular and Molecular Medicine

July 19th, 2021

Cellular and Molecular Medicine
Faculty of Medicine
University of Ottawa

Authorizations

All research conducted as part of this thesis had been approved by the following ethics committees:

- Animal work was approved by the University of Ottawa Institutional Animal Care Committee and conducted according to the directives of the Canadian Council on Animal Care.
- Work performed on LSFC patient cells was approved by Research Ethics Committees of the Centre de santé et de services sociaux de Chicoutimi, and the University of Ottawa. Skin biopsies were obtained from subjects after receiving written informed consent from either the subject or their legal guardian(s).
- Work performed using healthy Human bone marrow derived stem cells was approved by the Ottawa Hospital Research Institute Ethics Board (REB) under Study Number 20120929-01H.

All previously published work obtained permissions from the publishers for publication within this document. Licenses are provided below, as well as the student's contributions:

1- **Loss of hepatic LRPPRC alters mitochondrial bioenergetics, regulation of permeability transition and trans-membrane ROS diffusion**
   Alexanne Cuillerier, Shamisa Honarmand, Virgilio J. J. Cadete, Matthieu Ruiz, Anik Forest, Sonia Deschênes, Claudine Beauchamp, LSFC Consortium, Guy Charron, John D. Rioux, Christine Des Rosiers, Eric A. Shoubridge, Yan Burelle
   Human Molecular Genetics, 2017
   Contribution: 80% designed study, performed experiments, analyzed data, wrote manuscript
   License: 5102601454757; Open Access
2- **Hybrid clear/blue native electrophoresis for the separation and analysis of mitochondrial respiratory chain supercomplexes**
   Alexanne Cuillerier, Yan Burelle
   JoVE, 2019
   Contribution: 85% designed study, performed experiments, analyzed data, wrote manuscript
   License: Permission to reuse material in thesis, pursuant to the Author License Agreement for Open Access.

3- **Adaptive optimization of the OXPHOS assembly line partially compensates LRPPRC-dependent mitochondrial translation defect in mice**

Alexanne Cuillerier, Matthieu Ruiz, Caroline Daneault, Anik Forest, Jenna Rossi, Goutham Vasam, George Cairns, Virgilio Cadete, LSFC Consortium, Christine Des Rosiers, Yan Burelle

Communications Biology, 2021

Contribution: 80% designed study, performed experiments, analyzed data, wrote manuscript

License: Communications Biology is a fully open access journal and articles are freely accessible on publication under a CC BY License (Creative Commons Attribution 4. 0 International License).

4- **Testing the potential of stem cell therapy for mitochondrial diseases using the French-Canadian variant of Leigh syndrome – a pilot study**

Alexanne Cuillerier, Virgilio Cadete, Nicholas Cober, Conor O'Dwyer, Fengxia Xiao, George Cairns, Chantal Pileggi, Jenna Rossi, Mary-Ellen Harper, Morgan Fullerton, Dylan Burger, Duncan Stewart, Yan Burelle

Unpublished

Contribution: 80% designed study, performed experiments, analyzed data, wrote manuscript

License: Manuscript not submitted at the moment of submission of this thesis

Abstract

The French-Canadian variant of Leigh syndrome (LSFC) is a distinct and particularly severe presentation of Leigh syndrome characterized by the onset of unpredictable acidotic crises leading to death of 80% of them before the age of five. This autosomal recessive disorder is caused by mutations in *LRPPRC*, encoding an mRNA binding protein of the same name with a high affinity for mitochondrial transcripts. As a result of the mutations, levels of LRPPRC are decreased in all tissues and cause a severe deficiency of complex IV of the respiratory chain, with a deeper involvement of brain and liver. To gain better knowledge on the pathophysiology of this disease, and of the impact of the OXPHOS defect on the liver, our research consortium developed a mouse model of the disease harboring a liver specific inactivation of *Lrpprc* (H-*Lrpprc*). The goal of this thesis is to investigate the *in vivo* consequences of hepatic *Lrpprc* inactivation and to test potential therapy for mitochondrial diseases. The characterization of this model and the analysis of the mitochondrial phenotype are presented in Chapter 2 (*Cuillerier et al, Human Molecular Genetics, 2017*). Despite this severe phenotype, H-*Lrpprc* mice show no signs of overt liver failure and maintain energy levels, suggesting mechanisms are in place to sustain residual complex IV function. The underlying compensatory mechanisms granting these mice a remarkable resilience were explored and are presented in Chapter 4 (*Cuillerier et al, Communications Biology, 2021*). Along this project, we developed a protocol, and the optimized conditions of this method are described in Chapter 3 (*Cuillerier and Burelle, JoVE, 2019*). Although great progress has been made, there are currently no effective or curative treatments for LSFC and mitochondrial diseases. Recently, extensive pre-clinical and clinical studies supported the emergence and safety of mesenchymal stem cells therapy in the treatment of various diseases. Following transplantation, MSCs promote repair through various mechanisms including secretion of cytokines/exosomes, and transfer of mitochondria directly to target cells with impaired mitochondria offering a possibility to replace mutant dysfunctional organelles, which is relevant in the context of genetic mitochondrial diseases. Based on this, the objective of the last chapter of this thesis is to test the therapeutic potential of MSCs for genetic mitochondrial disorders using MSC-based approaches and LSFC as a disease model. Unfortunately, we encountered several obstacles along the way, including the departure of our main collaborator and stem cell expert, and delays in experimental procedures due to the COVID-19 pandemic. Consequently, this study was not completed at the moment of submission of this thesis, and is therefore presented as a pilot study in the form of a manuscript in Chapter 5. Overall, these projects unveiled alterations of mitochondrial functions that go beyond OXPHOS, a

complex network of compensatory mechanisms in place to palliate these defects, and finally, encouraging preliminary results suggest MSC therapy could be beneficial for the treatment of mitochondrial diseases.

Acknowledgments

First, I would like to thank the patients and their family for trusting us. I sincerely hope our work brings them comfort and optimism.

I would like to acknowledge my supervisor, Dr. Yan Burelle. I walked into your office for an interview for my honor's project with no experience, and you gave me a chance. Then, despite the financial and technical challenges, you let me work on the LSFC project throughout my graduate studies and always supported me. I cannot express how grateful I am to you for giving me this opportunity. Thank you for your contagious passion for science, and especially mitochondria. It made me realize how much I like science and rare diseases and now want to pursue a career in this field. Thank you for your teaching, mentoring, encouragements, understanding and for questioning my crazy hypotheses because it shaped me into the scientist I have become. I really enjoyed when you took the time to come to the lab to troubleshoot protocols with me, or simply to be my extra pair of hands when I needed help with experiments. I truly hope we can keep working together in the future through collaborations and shared projects.

I would like to thank the members of our research consortium on LSFC for developing the tools I had the privilege to use for my projects, for their scientific input, help, guidance and support for the LSFC project. I would like to extend a special thank you to Dr. Christine Des Rosiers and Dr. Matthieu Ruiz for their contribution to my projects, especially all their work on lipidomics. Moreover, their advice and insights were extremely valuable, and I greatly appreciated their help and support throughout my graduate studies.

I would like to thank my advisory committee members, for their mentorship, insights, encouragements, and guidance: Dr. Mary-Ellen Harper, Dr. Ruth Slack, Dr. Matthew Lines and Dr. Hanns Lochmuller. I would like to add a special thanks to Dr. Mary-Ellen Harper for making me feel as part of her lab, although I was not one of her students.

I would like to thank my colleague and close friend, Dr. Chantal Pileggi. You are always there for me, cheering me up when I need it and helping me with experiments and other things when I am overwhelmed. Thank you for sharing your office with me during the time I was writing my thesis. You are a true mitochondriac, an outstanding scientist and a great inspiration. I am glad we work together on various projects in the lab, and I am delighted to know we will keep collaborating in the future.

When I first started in Dr. Burelle's lab, I had the privilege to work with a wonderful team who trained me and ignited my passion for what I do. I do not think I would be where I am today without them. I keep a fond memory of our time at the University of Montreal.

Thank you, Sonia Deschênes, for all you taught me, for your advice, your encouragements, for your funny jokes, our more serious conversations, and everything else. I really enjoyed working with you and I miss it every day.

Thank you, François Brisebois, for trusting me with your experiments during my first week at the lab, for the philosophic and scientific discussions, for your famous quotes that Nicolas and I still refer to, and for your friendship during our masters.

Thank you, Dr. Virgilio Cadete, for teaching me so many skills, for being a great mentor, for collaborating with me on the stem cell project and initiating this project. Thank you for being there for me as a colleague and as a friend in the good and the bad times. I am very grateful for your support and encouragements when I moved to Ottawa and started my Ph. D.

Thank you, Nicolas Sgarioto, for training me with so many things, for your patience, your passion for science and dedication to doing things the right way. We started as lab mates, and you have now become one of my closest friends. Thank you for your support throughout my graduate studies, for your understanding and your advice. I enjoy every each of our adventures, and I am thrilled to know there are many more to come. I miss working with you on a daily basis, and I hope we get the chance to share the same lab again one day.

I would like to thank the other past and present members of the Burelle Lab: Ali Al-Rewashdy, Jenna Rossi, Asma Bouali, Gaurav Kumar Jain, Nikita Larionov, George Cairns, Jess Thumiah-Mootoo, Jeremy Racine and Mah Rukh Abbasi. Thank you for all the good moments, the great scientific discussions and for sharing my daily life at the lab.

I would like to thank my parents, Monique and Michel, for their love and continuous support throughout this chapter of my life. Thank you for always encouraging us to study what we like and to pursue a career that fulfills us, and thank you for feeding my curiosity and interest in sciences as I was growing up. Dad, you taught us a good work ethic, to be thorough, to help people whenever we can, and above all to be resilient. I am extremely grateful because these skills shaped me into the scientist I am and contribute to my success. I would like to thank my sister, Laurence, of whom I am very proud. Thank you, Laurence, for always listening to me, for your advice, for making me laugh and for your interest in my research. You are a brilliant executive nurse advisor and scientist, and it is always a pleasure to discuss scientific topics with you.

A special thank you to my dearest friend Dr. Cécilia Tremblay. We embarked on this journey together while we were still undergrads and have made our way through graduate studies. You always support me, encourage me, and understand every step and challenge that comes along the way. You are an amazing scientist and I admire you so much. I truly cherish our friendship and I hope that one day, our scientific paths cross again.

I would also like to thank all the other collaborators, students and people, whose name I did not mention, that I encountered and had the chance to work with during my doctorate. For some, although our paths may have parted, I appreciated our time together and it contributed to making me the scientist and person I am today, so thank you.

Finally, I would like to acknowledge all the funding agencies who supported my research through grants awarded to Dr. Burelle (La Fondation du Grand Défi Pierre Lavoie, the University of Ottawa, the Ottawa Institute for Regenerative Medicine, the National Sciences and Engineering Council of Canada and the Canadian Institutes of Health Research) and who supported me through doctoral scholarships (La Fondation du Grand Défi Pierre Lavoie, the University of Ottawa, and the Canadian Institutes of Health Research).

Table of Contents

List of tables

List of figures

Supplemental Material:

List of abbreviations

2D	2 Dimensions
AA	Antimycin A
ADP	Adenosine Di-Phosphate
AFG3L2	ATPase Family Gene 3 Like Matrix AAA Peptidase Subunit 2
AGC	Automatic Gain Control
ANT	Adenine Nucleotide Translocator
APOO	Apolipoprotein O
APOOL	Apolipoprotein O Like
AQP8	Aquaporin 8
ATAD3	ATPase Family AAA Domain Containing 3A
ATP	Adenosine Tri-Phosphate
ATP5A1	ATPsynthase F1 Subunit alpha
BAT	Brown Adipose Tissue
BG	Background
BN-PAGE	Blue-Native Polyacrylamide Gel Electrophoresis
BSA	Bovine Serum Albumin
Ca^{2+}	Calcium
$CaCl_2$	Calcium Chloride
CB	Coomassie Blue
CCCP	Carbonyl Cyanide m-Chlorophenyl hydrazone
CI	Complex I
CID	Collision Induced Dissociation
CIHR	Canadian Institutes of Health Research
CII	Complex I
CIII	Complex III
CIV	Complex IV
CIV1	Monomer of Complex IV
CIV2	Dimer of Complex IV
CL or CLs	Cardiolipin(s)
CN-PAGE	Clear Native-Polyacrylamide Gel Electrophoresis

CN/BN-PAGE	Clear/Blue Native-Polyacrylamide Gel Electrophoresis
CoA	Coenzyme A
CoQ	Coenzyme Q
CoreII	Subunit of the Respiratory Chain Protein Ubiquinol Cytochrome c Reductase
COX	Cytochrome c Oxidase
COX1-3	Cytochrome c Oxidase subunits 1-3
COX10	Cytochrome c Oxidase subunits 10
COXIV	Cytochrome c Oxidase subunits 4
CRC	Calcium Retention Capacity
CS	Citrate Synthase
CsA	Cyclosporin A
CV	Complex V or ATPsynthase
CypD	Cyclophilin D
DAB	3,3'-Diaminobenzidine
DDA	Data Dependent Acquisition
DDM	n-dodecyl-β-D-maltoside
DHA	Docosahexaenoic acid
DNA	Deoxyribonucleic Acid
DOI	Digital Object Identifier
$\Delta\psi$	Membrane Potential
EDTA	Ethylenediaminetetraacetic acid
EGTA	Ethylene glycol-bis(2-aminoethylether)-N,N,N′,N′-tetraacetic acid
EMC	Endoplasmic Reticulum Membrane Complex
ER	Endoplasmic Reticulum
ETC	Electron Transport Chain
ex-em	Excitation-Emission
FA	Fatty Acid
FC	Fold Change
FDR	False Discovery Rate
GM or G/M	Glutamate/Malate
GPL	Glycerophospholipids
GRP75	Glucose-Related Protein 75

H&E	Haematoxylin & Eosine
H2O2	Hydrogen Peroxide
HCL	Hydrochloric Acid
HEPES	N-(2-Hydroxyethyl)piperazine-N′-(2-ethanesulfonic acid)
HPLC	High Performance Liquid Chromatography
HSP /HSPA	Heat Shock Protein
IMM	Inner Mitochondrial Membrane
IP3R	Inositol Triphosphate Receptor 3
IQR	Interquartile Range
JoVE	Journal of Visual Experiments
K	Potassium
K-MES	2-(N-Morpholino) ethanesulfonic acid potassium salt
K2HPO4	Dipotassium Hydrogen Phosphate
KCN	Potassium Cyanide
KH2PO4	Potassium Dihydrogen Phosphate
KO	Knock-out
KOH	Potassium Hydroxide
LC-MS	Liquid Chromatography-Mass Spectrometry
LC-QTOF	Liquid Chromatography Quadrupole Time-of-flight
LONP1	Lon Peptidase 1
LPE	Lysophosphatidylethanolamine
LRPPRC	Leucine Rich pentatricopeptide repeat containing
LSFC	Leigh Syndrome French-Canadian
MAM/ MAMs	Mitochondria Associated Membranes
MFN2	Mitofusin 2
Mg^{2+}	Magnesium ion
MgCl2	Magnesium Chloride
MICOS	Mitochondria Contact Site and Cristae Organizing System
MOPS	3-(N-Morpholino) Propane Sulfonic Acid
MPAT	Mitochondrial Polyadenylation Tail Length
MPP	Mass Profiler Professional
mRNA	Messenger Ribonucleic Acid
MRPl	Mitochondrial Ribosomal Protein L

MRPs	Mitochondrial Ribosomal Protein S
MS	Mass Spectrometry
MS/MS	Tandem Mass Spectrometry
MTBE	Methanol/acetonitrile/methyl tert-butyl ether
mtDNA	Mitochondrial Deoxyribonucleic Acid
mtRNA	Mitochondrial Ribonucleic Acid
mtUPR	Mitochondrial Unfolded Protein Response
NaCl	Sodium Chloride
NAD^+	Nicotinamide Adenine Dinucleotide
NADH	Nicotinamide Adenine Dinucleotide + Hydrogen
NaPi	Sodium Phosphate
ND3	NADH Dehydrogenase 3
NDUFA9	NADH:Ubiquinone Oxidoreductase Subunit A9
NH_3	Ammonia
NSERC	Natural Sciences and Engineering Research Council
OIRM	Ontario Institute for Regenerative Medicine
ON	Ontario
OSCP	Oligomycin Sensitivity Conferral Protein
OXPHOS	Oxidative Phosphorylation
PA	Phosphatidic Acid
PBS	Phosphate-buffered Saline
PC	Phosphatidylcholine
PCR	Polymerase Chain Reaction
PDH	Pyruvate Dehydrogenase
PE	Phosphatidylethanolamine
PG	Phosphatidylglycerol
PGC1α	Peroxisome proliferator-activated receptor gamma coactivator-1 alpha
PHB1	Prohibitin 1
PHB2	Prohibitin 2
Pi	Inorganic Phosphate
PMID	Pub Med Identifier
Ppif	Peptidylprolyl Isomerase F
prot.	Protein

PTP	Permeability Transition Pore
PVDF	Polyvinylidene Difluoride
Q-PCR	Quantitative Polymerase Chain Reaction
QTOF	Quadrupole Time of Flight
RNA	Ribonucleic Acid
ROS	Reactive Oxygen Species
RT	Real Time
SC or SCs	Supercomplexes
SCAF1	Supercomplexes Assembly Factor 1
SDH	Succinate Dehydrogenase
SDHA	Succinate Dehydrogenase Complex Flavoprotein Subunit A
SDS-PAGE	Sodium Dodecyl-sulfate Polyacrylamide gel electrophoresis
SEM	Standard Error of the Mean
SLIRP	Stem-loop-interacting RNA-binding Protein
SMP	Submitochondrial Particles
SOD2	Superoxide Dismutase 2
SPG7	Spastic Paraplegia Type 7
Succ	Succinate
Surf1	Surfeit locus protein 1
TBE	Tris-borate-EDTA
TBST	Tris-buffered Saline + Tween
TCA	Tricarboxylic Acid Cycle
TE Buffer	Tris-EDTA Buffer
TEM	Transmission Electron Microscopy
TFAM	Transcription Factor A
TG	Triglyceride
TIM/TOM	Translocase of inner membrane/Translocase of outer membrane
TMPD	N′-Tetramethyl-p-phenylenediamine
UQCR2	Ubiquinol Cytochrome c Reductase
USA	United States of America
VDAC	Voltage Dependent Anion Channel
WT	Wild-type
YME1L1	YME1 Like 1

Chapter 1: Introduction

Mitochondria play a crucial role in the cell which goes beyond energy production in the form of ATP through oxidative phosphorylation, and is involved in reactive oxygen species production, calcium homeostasis and apoptosis. Abnormalities of mitochondrial functions have been identified in a myriad of diseases including cancers, diabetes, Alzheimer's disease, Huntington's disease, Parkinson's disease, and amyotrophic lateral sclerosis to only name a few. [1, 2] Whether mitochondrial dysfunctions contribute to the pathogenesis of these disorders or if they are secondary, remains elusive. On the other hand, primary mitochondrial diseases are defined as genetic disorders leading to dysfunction of oxidative phosphorylation or mitochondrial structure and function, and form a group of diseases which is complex from the clinical, genetic and biochemical standpoint. [3] The estimated prevalence of primary mitochondrial disorders is 1 in 5000 live births. [4]

1.1 Genetic Mitochondrial Diseases

A major contributing factor to the complexity of these disorders is the dual governance of the mitochondria by both the nuclear and mitochondrial genomes. [5] The mitochondrial DNA (mtDNA) is transmitted exclusively by the mother and is found in hundreds to thousands of copies, tightly associated to the inner mitochondrial membrane, in each cell. [6, 7] Although it has greatly evolved, the mtDNA still displays features of its bacterial ancestor, including a circular genome, and encodes for the two mitochondrial ribosomes, 22 tRNA and 13 polypeptides forming the catalytic cores of complexes I, III, IV and ATPsynthase. [8] The rest of the nearly 1,500 mitochondrial proteins are encoded by the nuclear DNA, translated on cytosolic ribosomes, and imported to the mitochondria through the TIM/TOM (translocase of inner membrane/translocase of outer membrane) complex. [9, 10] Proteins synthesized in the cytosol harboring a mitochondrial targeting sequence are unfolded before translocation to the mitochondria, where they are processed and re-folded by proteases and chaperones. [11] The expression of mitochondrial proteins by both genomes is tightly regulated to avoid any imbalance between nuclear and mitochondrial proteins. Genetic mitochondrial diseases can be caused by mutations in either the nuclear or mitochondrial DNA and can be transmitted through the five modes of inheritance: autosomal recessive/dominant,

X-linked recessive/dominant, and mitochondrial (maternal). [12] Up to now, nearly 600 different causative mutations in both the mitochondrial and nuclear genomes have been identified. [4, 13]

1.1.1 Mitochondrial DNA

Over 300 mutations of mtDNA have been identified [14] and are found in most adult patients with mitochondrial diseases. [15] Alteration of the mitochondrial genome ranges from single nucleotide variants to depletion syndromes defined by quantitative reduction of absolute number of mtDNA copy number. [13] Mutations can cause complex-specific disorders, if the mutation is in one of the genes encoding any subunit of the respiratory complexes I, III, IV or ATPsynthase, or multicomplex disorders if the mutations affect rRNA or tRNA genes, thus impacting the translation and synthesis of all mitochondria encoded respiratory complexes subunits. [16]

1.1.1.1 Heteroplasmy and threshold effect

The rate of mutation of mtDNA is extremely high because of the absence of histones, the lack of effective repair mechanisms, and the proximity to sites of production of reactive oxygen species. [17] When a copy of mtDNA is mutated, the cell then contains a mixture of wild-type and mutant DNA and this state is termed heteroplasmy. Levels of heteroplasmy can be different from cell to cell, and from tissue to tissue within a same individual. [18-20] As the mtDNA will replicate and the cell will divide, the ratio of mutated/wild type mtDNA will vary and a daughter cell can eventually reach the state of homoplasmy, where all copies of mtDNA are mutated. Due to this heteroplasmy/homoplasmy phenomenon, the same mtDNA mutation can generate drastically different phenotypes among patients, even within the same family, depending on the amount of mutated mtDNA. [18, 21] For a given mutation, some patients can be asymptomatic, and symptoms arise when the mutation load reaches a certain percentage; this is termed the threshold effect. Interestingly, levels of heteroplasmy can also decrease, especially in rapidly dividing tissues, leading to a progressive recovery in this organ. [22, 23]

1.1.2 Nuclear DNA

Over 1,500 mitochondrial proteins are encoded in the nucleus [24], and these include 1) subunits of respiratory chain complexes and assembly factors, 2) proteins involved in the integrity and replication of mtDNA, 3) proteins forming channels for protein importation in the

mitochondria, 4) complexes responsible for phospholipids synthesis in the mitochondria and 5) proteins responsible for mitochondrial dynamics (fusion and fission). Since proper functioning of mitochondria requires these numerous proteins, causative mutations of mitochondrial diseases are more abundantly found in the nuclear genome. [25]

1.1.2.1 Subunits of respiratory chain complexes and assembly factors

Mutations falling into this category can affect the respiratory chain either directly or indirectly. Direct hits affect the components of the respiratory chain and include mutations in the nuclear genes encoding 38 subunits of complex I, the totality of complex II with 4 subunits, 10 subunits of complex III, 10 subunits of complex IV, 14 subunits of ATPsynthase, and the mobile electron carriers CoQ10 and cytochrome *c*. [26] Indirect hits affect proteins that do not form the respiratory chain, but which are essential for the proper assembly, function, and stability of the OXPHOS complexes. These include chaperones and assembly factors, also called ancillary proteins, that participate in the intricate process of respiratory complex assembly.

1.1.2.2 Integrity and replication of mtDNA

Given its reduced size, the mtDNA relies heavily on the nuclear genome for the synthesis of factors essential for its proper functioning and replication, such as TFAM, POLG, Twinkle, and indirectly by OPA1 and MFN2. [13, 27, 28] Mutations in these factors can cause qualitative or quantitative alteration of the mtDNA. Qualitative alterations are characterized by multiple deletions of mtDNA (loss of genomic segments) and directly affect the nucleotide pool available in the mitochondria. [29] On the other hand, quantitative alterations are characterized by mtDNA depletion (reduced mtDNA content in cells) and create an imbalance in mtDNA/nuDNA ratios.

1.1.2.3 Mitochondrial protein importation

Nuclear encoded mitochondrial proteins are synthesized in the cytoplasm and are imported to the proper compartment of the organelle. Several proteins are involved in their transport across the outer and inner mitochondrial membranes and include factors, docking proteins, chaperonins, and proteases. [30] Mutations in this category can be found in the targeting sequence of mitochondrial proteins, or less frequently in the transport machinery. Mutation of the translocase of

inner mitochondrial membrane (TIMM) AFK and DNAJC19 [31, 32] are included in this category. More details on the reported mutations withing this category are found in Table 1.

1.1.2.4 Mitochondrial lipid synthesis

The highly specialized and complex mitochondrial membranes each harbor a distinct set of proteins and lipids which are evolutionary conserved. [33-35] Mitochondrial membranes consist of a balance between bilayer and non-bilayer forming lipids, with an asymmetric distribution of phospholipids. [36, 37] The outer mitochondrial membrane is mainly composed of bilayer forming lipid phosphatidylcholine (PC) and non-bilayer forming lipid phosphatidylethanolamine (PE), representing approximately 80% of total lipids. [34] The inner mitochondrial membrane is also mainly composed of PE and PC, and contain 10-15% of the essential anionic lipid cardiolipin. Cardiolipin is exclusively found in the inner mitochondrial membrane where it interacts with respiratory complexes and is synthesized in the organelle. Mitochondrial membranes contain very low amounts of cholesterol and sphingolipids compared to other organelles. [34] In addition, mitochondrial membranes contain PC and PE plasmalogens, which contain a vinyl-ether bond, supporting membrane fusion. As for its proteins, the mitochondria is capable of synthesizing some of its lipids and the rest is imported, mainly from the endoplasmic reticulum. [38] Mutations in this category affect either lipid synthesis or importation to the organelle and are listed in Table 1. Among them, mutations in Tafazin (*TAZ)* cause Barth syndrome, a CIV disease characterized by altered cardiolipin maturation. [39, 40]

1.1.2.5 Mitochondrial dynamics

Mitochondria travel within the cell through dynamin and undergo cycles of fission and fusion, adapting to the energy needs. Mutations in this category affect proteins involved in the transportation of mitochondria or the fission/fusion machinery and alter the distribution of the organelle or its structure. These include, but are not limited to, mutations in proteins MFF, MFN and OPA1. [27, 28, 41] More details are found in Table 1.

1.1.3 Advancement of sequencing

As for most rare diseases, the determination of a molecular diagnosis in patients with mitochondrial diseases is a complex process. Sadly, a large proportion of patients enter a “diagnosis

odyssey", that can last for years, where they consult with an average of 8 physicians before obtaining a diagnosis. [42] Traditionally, the diagnosis of mitochondrial diseases was achieved by excluding other metabolic disorders, performing brain imaging and invasive muscle biopsy, and biochemical analysis through enzymology. [13, 43, 44] However, these biochemical assays are challenging and performed only in some laboratories. [28] In addition, protocols vary among institutions and subtle defects are poorly captured by these tests. [45, 46] Over the last decade, new sequencing technologies, and their constantly decreasing costs, have uncovered hundreds of causative mutations and have significantly increased the diagnostic yield of mitochondrial diseases. [47-49] Because of its greater sensitivity, next generation sequencing is particularly useful in detecting low levels of mtDNA heteroplasmy without targeting specific sites. [50, 51] Whole-Exome Sequencing is the most commonly used method for suspected mitochondrial disease and is useful in patients with less specific presentations. [44] Otherwise, specific panels for mitochondrial diseases with candidate genes are available to physicians if a mitochondrial disease is suspected. [49]

As these tools become more accessible and are used more frequently, the databases grow, and targeted panels are refined enabling a more rapid diagnosis for patients.

1.1.4 Classification of genetic mitochondrial diseases

Mitochondrial disorders were first termed mitochondrial myopathies, and a few years later the term mitochondrial encephalomyopathies was introduced after the observation of brain involvement in addition to muscle in some patients. [52, 53] As knowledge on this group of diseases expanded, it became clear that mitochondrial diseases are not limited to myopathies and are very complex. Heterogeneous clinical presentation and overlapping of spectrum of phenotypes makes it challenging to classify this group of disorders. [4] There is no universal classification of mitochondrial diseases, however most reviews present classifications based on clinical feature, organ involvement, affected OXPHOS complex or genetic cause. [3, 4, 54-56]

Table 1.1: Classification of Mitochondrial Diseases

Adapted from: [3, 4, 12, 56, 57]

Disease Mechanisms		***DNA***	***Gene Defects***	***Example Syndromes***
OXPHOS complexes	Complex I Subunits	Nuclear	*NDUFA1, NDUFA2, NDUFA6, NDUFA9, NDUFA10, NDUFA11, NDUFA12, NDUFA13 NDUFB3, NDUFB8, NDUFB9, NDUFB10, NDUFB11, NDUFS1, NDUFS2, NDUFS3, NDUFS4, NDUFS6, NDUFS7, NDUFS8, NDUFV1, NDUFV2, NDUFAF1, NDUFAF2, NDUFAF3, NDUFAF4, NDUFAF5, NDUFAF6, NDUFAF7, NDUFAF8, ACAD9, ECSIT, FOXRED1, NUBPL, TIMMDC1, TMEM126B*	Leigh syndrome, ACAD9 deficiency
		Mitochondrial	*MT-ND1, MT-ND2, MT-ND3, MT-ND4, MT-ND4L, MT-ND5, MT-ND6*	LHON
	Complex II	Nuclear	*SDHA, SDHAF1, SDHB, SDHC, SDHD, SDHAF2*	Leigh syndrome
	Complex III	Nuclear	*UQCRB, UQCRC2, UQCRFS1, UQCRQ, UQCC2, UQCC3, CYC1, BCS1L, HCCS, TTC19, LYRM7*	Bjornstad syndrome, GRACILE
		Mitochondrial	*MT-CYB*	N/D
	Complex IV	Nuclear	*COX7B, COX4I1, COX4I2, COX5A, COX6A1, COX6A2, COX6B1, COX8A, NDUFA4, SURF1, SCO1, SCO2, COX10, COX14, COX15, COX20, COA3, COA5, COA6, COA7, FASTKD2, PET100, PET117, CEP89*	Leigh syndrome

		Mitochondrial	*MT-CO1, MT-CO2, MT-CO3*	Leigh syndrome
	ATPsynthase	Nuclear	*ATP5F1A, ATP5F1D, ATP5F1E, ATP5MD, ATPAF2, TMEM70*	TMEM70 deficiency
		Mitochondrial	*MT-ATP6, MT-ATP8*	NARP
	Multi-complexes assembly factor	Nuclear	*OXA1L*	Encephalopathy
mtDNA maintenance	Nucleotide pool maintenance	Nuclear	*RRM2B, DGUOK, TK2, MPV17, TYMP, ABAT, SAMHD1*	Myopatic MDDS, Encephalomyopathic MDDS, MNGIE, Hepatocerebral MDDS, PEO
	Replication	Mitochondrial	*POLG, POLG2, TWNK, DNA2, SSBP1, MGME1, RNNASEH1, TOP3A, FBXL4*	Alpers syndrome, IOSCA, Perrault syndrome, hepatocerebral MDS, PEO, Infantile-onset spinocerebellar ataxia
Mitochondrial gene expression	Mitochondrial transfer RNAs	Mitochondrial	*MT-TA, MT-TC, MT-TD, MT-TD, MT-TE, MT-TF, MT-TG, MT-TH, MT-TI, MT-TK, MT-TL1, MT-TL2, MT-TM, MT-TN, MT-TP, MT-TQ, MT-TR, MTTS, MT-TT, MT-TV, MT-TW, MT-TY, MT-DEL*	MELAS, MERRF

	Mitochondrial aminoacyl-tRNA synthetase	Nuclear	*AARS2, CARS2, DARS2, EARS2, FARS2, GARS, HARS2, IARS2, KARS, LARS2, MARS2, NARS2, PARS2, RARS2, SARS2, TARS2, VARS2, WARS2, YARS2, QRSL1, GATB, GATC, HSD17B10*	MLASA, DARS2 deficiency, HUPRA, Perrault syndrome, RARS2 deficiency, VARS2 deficiency, YARS2 deficiency
	Mitochondrial transcript processing and modification	Nuclear	*TFAM, POLRMT, MTFMT, TRIT1, TRMT5, TRMT10C, TRNT1, PNPT1, MTO1, TRMU, GTPBP3, PUS1, THG1L, ELAC2, MTPAP, NSUN3, PDE12*	MLASA, SIFD, TRMU deficiency, Hypertrophic cardiomyopathy, Leigh syndrome
	Mitoribosome (ribosomal RNA and protein subunits, assembly and recycling factors, translation initiation, elonfation and termination factors)	Nuclear	*MRPL3, MRPL12, MRPL44, MRPS2, MRPS7, MRPS14, MRPS16, MRPS22, MRPS23, MRPS25, MRPS28, MRPS34, PTCD3 (MRPS39), MRM2, ERAL1, RMND1, C12orf65, GFM1, GFM2, GUF1, LRPPRC, TACO1, TSFM, TUFM*	Leigh syndrome, RMND 1 deficiency, Perrault syndrome
		Mitochondrial	*MT-RNR1, MT-RNR2*	Late onset nonsyndromic hearing loss and deafness
Mitochondrial membrane lipids, import, dynamics and quality control	Mitochondrial membrane phospholipid metabolism and protein import machinery	Nuclear	*TAZ, TIMM8A, AGK, CHKB, DNAJC19, GFER, PAM16, SERAC1, PLA2G6, TIMM22, TIMM50, TIMMDC1*	Barth syndrome, Sengers, MEGDEL, X-linked deafness-dystonia syndrome

	Mitochondrial solute carriers	Nuclear	*SLC25A11, SLC25A24, SLC25A4, SLC25A1, SLC25A3, SLC25A10, SLC25A12, SLC25A13, SLC25A15, SLC25A19, SLC25A20, SLC25A21, SLC25A22, SLC25A26, SLC25A32, SLC25A38, SLC25A42, SLC25A46, GOT2, MICU1, MICU2*	combined D-2- and L-2-hydroxyglutaric aciduria, carnitine-acylcarnitine carrier deficiency, hyperornithinemia-hyperammonemia-homocitrillinuria (HHH) syndrome, early infantile epileptic encephalopathy type 3, Amish microcephaly, aspartate/glutamate isoform 1 deficiency, congenital sideroblastic anemia, Fontaine progeroid syndrome, and citrullinemia type II
	Mitochondrial dynamics	Nuclear	*DNM1L, MFN2, OPA1, GDAP1, MSTO1, MFF, STAT2, TRAK1, MIEF2*	OPA1 disease
	Intermembrane space and MICOS complex	Nuclear	*CHCHD10, CHCHD2, QIL1*	QIL1 deficiency
	ER-mitochondrial tethering	Nuclear	*EMC1*	N/D
	Mitochondrial protein quality control	Nuclear	*CLPX, HSPE1, AFG3L2, ATAD3A, SPG7, HSPA9, HSPD1, HTRA2, PMPCA, PMPCB, MIPEP, XPNPEP3, CLPB, CLPP, LONP1, PITRM1, SACS, TRAP1, PRKN, PINK1, YME1L*	Perrault syndrome, Ataxia, Spastic paraplegia

	Toxicity	Nuclear	*ETHE1, HIBCH, ECHS1, SQOR*	Ethylmalonic encephalopathy
	Antioxidant defense	Nuclear	*TXN2, TXNIP*	Familial glucocorticoid deficiency
Vitamins and cofactors metabolism	Coenzyme Q10 biosynthesis	Nuclear	*PDSS1, PDSS2, COQ2, COQ4, COQ5, COQ6, COQ7, COQ8A, COQ8B, COQ9*	CoQ10 disorders
	Iron-sulfure cluster protein biosynthesis	Nuclear	*ABCB7, ISCA1, ISCA2, ISCU, FDXR, FDX2, FXN, LYRM4, NFS1, NFU1*	Freidreich ataxia
	Lipoc acid biosynthesis	Nuclear	*BOLA3, GLRX5, IBA57, LIAS, LIPT1, LIPT2, MECR*	N/D
	Cytochrome c synthesis	Nuclear	*CYCS*	N/D
	Biotin metabolism	Nuclear	*BTD, HLCS*	N/D
	Thiamine metabolism and transport	Nuclear	*TPK1, SLC19A2, ALC19A3*	N/D
	Riboflavin metabolism and transport	Nuclear	*SLC52A1, FLAD1, SLC52A2, SLC52A3*	N/D
	Nicotinamide metabolism	Nuclear	*NMNAT1, NADK2, NAXD, NAXE, NNT*	N/D

	Coenzyme A metabolism	Nuclear	*COASY, PANK2, PPCS*	N/D
	Copper and manganese metabolism	Nuclear	*SLC33A1, CCS, SLC39A8*	N/D
	Selenocystein metabolism	Nuclear	*SECISBP2, SEPSECS*	N/D
Other cellular defects associated with mitochondrial dysfunction	Calcium homeostasis	Nuclear	*WFS1, ANO10, C19ORF70, CISD2, CYP24A1*	Wolfram syndrome
	Haem biosynthesis	Nuclear	*ALAS2, ABCB6, SFXN4*	N/D
	Apoptosis defects	Nuclear	*AIFM1, DIABLO, APOPT1, PTRH2*	Cowchock syndrome
	DNA repair	Nuclear	*APTX, XRCC4*	N/D
	Miscellaneous	Nuclear	*PNPLA4, CTBP1, FGF12, KIF5A, STXBP1, ALDH18A1, C19ORF12, DCC, DIAPH1, OPA3, CA5A, C1QBP, PNPLA8, POP1, PPA2, ROBO3, RTN4IP1, SPART, SPATA5, TANGO2, TMEM65, TMEM126A*	N/D

1.1.5 Clinical presentation, disease progression and diagnosis approach

Although mitochondrial disorders can affect a single organ, most affected patients have non-classical multisystemic disease presentations affecting any organ in the body. [4, 15, 26] Classically, mitochondrial diseases present with prominent neurologic or myopathic features. Each patient presents with a different constellation of clinical features and disease progression, making diagnosis and disease management extremely challenging. [15] To add to the complexity of these diseases and make diagnosis even more challenging, a defined syndrome can be caused by different mutations in different genes and can involve both the nuclear and mitochondrial genomes. [58] The opposite is also true where a given mutation can cause a range of different phenotypes. [59] In some cases, specific clusters of clinical features are associated with distinct syndromes such as Kearns-Sayre Syndrome (pigmentary retinopathy, heart block, progressive external ophthalmoplegia)[60], CPEO (external ophthalmoplegia, bilateral ptosis, mild proximal myopathy) [60], MELAS (mitochondrial encephalomyopathy with lactic acidosis and stroke-like episodes) [61], MERRF (myoclonus epilepsy with ragged-red fibres) [62], NARP (neurogenic muscle weakness, ataxia and retinitis pigmentosa) [63] and LS (elevated blood and CSF lactate levels, neurodevelopmental regression, symptoms related to basal ganglia and brain stem dysfunction)[64]. [26]

Mitochondrial diseases can present in both childhood and adulthood and can follow a non-linear progression. Typically, more severe syndromes present during infancy and are caused by mutations in the nuclear genomes, whereas milder syndromes usually present in older individuals and are caused by mutations in the mtDNA. [65-67] In some cases, symptoms occur or are aggravated by metabolic stresses such as infections and nutrition. [13] Developmental milestones are either not met in patients or acquired skills are lost with time.

A few key clinical features, including stroke-like episode, acquired ptosis accompanied or not by ophthalmoplegia, sideroblastic anaemia and epilepsia partialis continua, usually arise suspicion for a mitochondrial disease. [26, 68] Moreover, biomarkers such as high blood or CSF lactate, plasma alanine and urinary 3-methylglutaconic acid are usually associated with these disorders. [15] Otherwise, diagnosis approach includes family history, metabolic investigation, muscle biopsy, neuroimaging, and genetic testing. [4, 69]

Important hallmarks in family history include consanguinity, previous early neonatal deaths or stillbirths. If parents have a family history of mitochondrial disease, they can benefit from prenatal molecular genetic testing for the pathogenic variant(s). [26] Physical examination usually includes electrocardiography and echocardiography, neurological assessment (ptosis, optic atrophy, pigmentary retinopathy, hypotonia, muscle weakness, dystonia, spasticity), muscle strength and exercise tolerance. [70] Metabolic investigation is achieved by testing blood, urine, and CSF metabolites such as lactate and pyruvate. [71] Muscle biopsies are performed to provide evidence of respiratory chain enzyme deficiency and used to be first line of investigation. However, with the increased availability and use of genetic testing for mitochondrial diseases, invasive muscle biopsies are now reserved for critical cases where there is no time for genetic testing and immediate care is required. [44] Neuroimaging can reveal indicative white matter disturbances or leukoencephalopathy, but also very specific phenotypes characteristic of defined syndromes that can be used for diagnosis. One example is the distinct symmetrical lesions in the basal ganglia and brain stem seen by MRI in the case of Leigh Syndrome. [72]

1.2 Leigh Syndrome

Leigh syndrome (LS) was first described by Denis Leigh in 1951 [73], and was first termed subacute necrotizing encephalomyelopathy based on the cerebral lesions observed. It is the most common paediatric presentation of a mitochondrial disease affecting 1/40,000 live births worldwide, with the broadest genetic heterogeneity. [15] Clinical evolution is rapid, and patients develop a wide range of symptoms, including failure to thrive, developmental regression, hypotonia and dystonia, typically at 2 years of age following a normal development. [74, 75] Disease onset is possibly triggered by a metabolic stress, such as infection, nutrition or surgery, and morbidity is considerably high with the majority of affected children not surviving past three years of age. [74] Despite heterogeneity in the clinical presentation, patients must meet the following criteria for diagnosis: 1) syndrome is neurodegenerative and progressive, 2) symptoms are associated with mitochondrial dysfunctions caused by a genetic defect, and 3) the presence of symmetric bilateral necrotic lesions in basal ganglia and brainstem by MRI. [15] These characteristic lesions are remarkably consistent and consist of necrotic tissue, demyelination, gliosis, and vascular proliferation. [76] These lesions also show elevated lactate by magnetic resonance spectroscopy. Lactate and pyruvate are two key biomarkers of LS and are unusually high in blood and cerebrospinal fluid of patients. [15, 75, 77]

Additional abnormalities include low bicarbonate levels in blood and abnormally low fasting blood sugar.

On the molecular level, high blood lactate is indicative of a reorientation of metabolism towards glycolysis. Chronic hyperlacticacidemia with abrupt and sudden increase in lactate levels can trigger metabolic crisis. Furthermore, high blood lactate and pyruvate, and low blood sugar are indicative of impaired gluconeogenesis occurring in the liver. [72, 74, 78] In this regard, the activity of pyruvate carboxylase, a key gluconeogenesis enzyme converting pyruvate to oxaloacetate in the mitochondria, is severely impaired in some variants of LS. [78] Hepatic anomalies including steatosis, fibrosis, cirrhosis, and abnormal mitochondrial proliferation are indicative of bioenergetics impairment and have also been reported in LS patients. [79, 80] It is suggested that the impairment of energy generation greatly contributes to the cerebral lesions' pathogenesis. In fact, the observed gliosis in patients is likely a consequence of ATP depletion, although other factors cannot be excluded. [76] In turn, the affected microglia and astrocytes become activated and defective, causing neuronal death and the formation of fibrous scar tissue. Interestingly, the vulnerable cerebral regions in LS have a high ATP consumption and glucose metabolism early in life under basal conditions and seem particularly susceptible to energy deprivation. [76]

Over 75 mutations causing LS have been identified in both nuclear and mitochondrial genomes [15, 81], and the most redundant ones are found in the nuclear gene *Surf1* [52] (encoding a complex IV assembly factor), and the mitochondrial gene *Atpase6* [82] (encoding a subunit of ATPsynthase). Biochemically, deficiency of complex I is the most frequent presentation of LS. Overall, all five respiratory complexes can be affected individually or jointly in LS, and more rare deficiencies in PDH and coenzyme Q have also been reported. [74] Recently, mutations in *LRPPRC* were identified to cause a phenotypically distinct and expanding form of LS: the French-Canadian variant of Leigh Syndrome (LSFC). [83, 84]

1.3 LSFC

LSFC was first identified in a population from the geographically isolated region of Saguenay-Lac-Saint-Jean, in Quebec, where the carrier rate is estimated at 1/23 and 1/2000 live births is affected. [85, 86] A few years later, additional cases involving novel mutations of *LRPPRC* have also been reported in populations outside of Québec, notably in Italy, China, and in the UK in patients of Caucasian, Pakistani, Indian, Turkish, and Iraqi origin. [87-89]

1.3.1 Phenotype

The LSFC phenotype is characterised by developmental delay, failure to thrive, regression, hypotonia, striking paucity of facial and limb movement, mild facial dysmorphism, unexpressive facies, anteverted nares, arched eyebrows, prominent forehead, hirsutism, and chronic well-compensated metabolic acidosis. [86] Bicarbonate levels in the blood are moderately decreased with normal blood pH. [86] Levels of lactate are mildly elevated in blood and CSF, and usually higher in the latter. [86] Unlike what is reported in classic LS, LSFC patients show no clinical or echocardiographic evidence of cardiomyopathy and lack severe myopathy. [86] Despite the absence of a cardiac phenotype, metabolomics analysis of patient plasma recently revealed alterations in cholesterol and insulin levels suggestive of a higher cardiometabolic risk compared to healthy controls. [90] All autopsy samples reveal microvesicular steatosis of the liver, and all patients display typical LS cerebral lesions. [86] The clinical course is variable between patients, but only a few survive past 2 years of age, with moderate mental handicap. [86]

1.3.2 Acidotic crises and stroke like episodes

Although the phenotype is similar to classic LS, LSFC is characterised by the onset of unpredictable subacute lactic acidosis crises that cause severe neurologic damage, and lead to death of most affected children before 5 years of age. [91, 92] The trigger of these fatal crises still remains to be identified, but metabolic challenges such as nutritional stress are strongly suspected, and most LSFC patients experienced a crisis during a major febrile infection. [91] Drowsiness and ataxia have been reported in the days preceding the lactic acidosis crises and signs of acidosis develop within 1-2 hours. During the crises, patients present with Kussmal respiration, stupor or coma, parenchymal lung infiltrates, hypoxia and shock. In addition, lactate levels are exacerbated during

lactic acidosis crises. The evolution is usually fulminant leading to a coma and shock, and cerebral lesions typical of LS are aggravated during the episode. The lactic acidosis crises mostly occur under two years of age and is fatal in 91% of patients. [86]

Another type of crisis can occur in LSFC patients, independently of lactic acidosis crises. Stroke like episodes have been reported in some patients and are characterised by frontal cortical lesions, ischemia-like lesions in the brain parenchyma, cerebral vasomotor abnormalities, and systemic acid-base imbalance. [92] Arteriography during acute phase shows capillary shunting delimited by neuroanatomy rather than vascular boundaries. [92] The affected structures eventually develop in LS characteristic brain lesions and therefore, brain vasomotor changes are probably linked to the pathogenesis of the disease. In all cases, stroke-like episodes followed an infection and two patients presented with paralysis. [92]

Both types of crises are unpredictable, have severe physiological consequences, and are lethal in most patients. *In vitro* experiments testing factors relevant to the acidotic crises patients undergo, have shown that patient cells are more vulnerable to pathophysiological stressors. When exposed to BSA-conjugated palmitate to mimic nutritional overload, LSFC fibroblasts release a significantly greater amount of the cell death marker LDH, and display increased caspase 3/7 activities. [93] Moreover, the palmitate-induced cytotoxicity is enhanced when lactate concentrations are concomitantly high, and this decreases cellular ATP levels by 50%. Under these stress conditions CIV activity was not further decreased. Interestingly, high lactate alone had no effect on LDH release and caspase 3/7 activity, supporting the notion that high lactate is a consequence of disease state and not a pathological contributor. [93]

1.3.3 Biomarkers

Among the many challenges patients and clinicians face in the context of mitochondrial diseases are diagnosis and monitoring of disease progression. [4, 77] There are no universal markers of mitochondrial diseases, and the clinical heterogeneity is a major hurdle. The identification of specific biomarkers would be extremely valuable, especially if they could predict the onset of the fulminant lactic acidosis crises and allow for more rapid and tailored interventions that could

potentially save patients. Ideally, signature biomarkers can be identified in samples that require minimally invasive sampling like urine or blood and can be used to assess the presence or absence of a disease and its progression. [77]

Recent studies performed on LSFC patients' and disease model plasma and urine revealed the presence of a metabolomic signature that includes both classic and unexpected metabolites. [90, 93] The analysis provided insight into the metabolic alterations in LSFC, and the most discriminant metabolites identified are higher in LSFC patients and include lactate, β-hydroxybutyrate, acylcarnitines (particularly myristoylcarnitine and palmitoylcarnitine) and α-hydroxybutyrate. These markers are indicative of perturbations in NADH/NAD^+ ratios, citric acid cycle reactions, fatty acid oxidation and amino acid catabolism. [90] Additionally, conjugated bile acids and plasmalogens levels are lower in patients. These markers suggest the perturbations go beyond mitochondria metabolism and also affect peroxisomal lipid metabolism. [94]

1.3.4 Molecular Genetics of LSFC

The LSFC gene locus was one of the first disease-causing genes to be identified through linkage disequilibrium, which mapped it to chromosome 2p16-21. [95] Shortly after this discovery, integrative genomics revealed two mutations, a missense alanine to valine base change (A354V) and a deletion (C1277STOP), in the *LRPPRC* gene (encoding a protein of the same name) as causative of LSFC. [84] Patients from the Saguenay-Lac-Saint-Jean region are all homozygous for the A354V mutation, except for one compound heterozygote patient who harbours both A354V and C1277STOP mutations. [84, 91] LRPPRC (or LRP130) is an mRNA-binding protein of 130kDa that belongs to the pentatricopeptide repeat (PPR) protein family. [84]

1.3.5 PPR Proteins

PPR proteins bind RNA to regulate gene expression at the post-translation level and are involved in RNA processing, splicing, stability, editing and translation. [96-98] All PPR proteins have the same basic structure, the PPR cassette, composed of tandemly repeated helical sequence motifs made of 35 amino acids forming two antiparallel helices. [99, 100] The series of cassettes

vary in numbers, ranging from 2 to 26, which forms a superhelix with a central groove that allows the binding to RNA molecules. [99, 100] To bind RNA, PPR proteins undergo conformation changes and form homodimers. [101, 102] The binding between PPR proteins and RNA is sequence specific and occurs through van der Waals interactions. [102, 103] Interestingly, recent advances have shown that PPR proteins can be engineered to recognize target RNA sequences, which could have therapeutic potential. [104, 105] These proteins are highly conserved across species and are found in all eukaryotic lineages. [106] Up to now, seven Human PPR proteins have been identified. [97] They all mainly localize in the mitochondria, and some of them to a lesser extend in the nucleus. [107, 108] They are categorized in two classes, each divided in subclasses. Mitochondrial RNA polymerase POLRMT, one subunit of mitochondrial ribosomes MRPS27, PRCD1-2-3, MRPP3 and LRPPRC all belong to the human PPR family. [109]

1.3.6 LRPPRC

LRPPRC was the first Human PPR protein to be identified. [84] It has been associated with anti-apoptotic effects in tumors, but it is primarily known to cause LSFC upon mutation. LRPPRC contains a leucine-rich PPR cassette and is necessary for polyadenylation of mitochondrial transcripts. [110-112] It forms a stable complex with a 12kDa protein named SLIRP (stem-loop RNA-binding protein) with a 1:1 stoichiometry, that sequesters and stabilizes pools of polyadenylated mitochondrial mRNAs protecting them from degradation prior to translation. [113, 114] Studies on LSFC patient myoblasts, myotubes and fibroblasts have revealed that LRPPRC and SLIRP are interdependent and essential for mitochondrial translation. [113] When LRPPRC levels are decreased by siRNA, SLIRP follows a similar trend, and vice-versa. Interestingly, depletion of SLIRP causes a destabilization of mt-RNAs similar to the defect induced by reduced levels of LRPPRC, and phenocopies LSFC in fibroblasts. [113] This suggests the cardiac tissue uses alternative pathways for the post-transcriptional handling of mitochondrial-encoded proteins, and highlights the fact that mitochondrial mRNAs are handled in a tissue specific way. [113] Additional studies in primary hepatocytes revealed that LRPPRC also localises in the nucleus where it physically interacts with the transcriptional coactivator PGC1-α (peroxisome proliferator-activated receptor coactivator 1-α). PGC1-α, a coactivator of numerous nuclear receptors and transcription factors, drives mitochondrial biogenesis in several tissues and regulates hepatic glucose homeostasis by activating gluconeogenesis genes. [100, 115-117] Although the interaction with PGC1-α is preserved upon mutation of LRPPRC, when LRPPRC is reduced by 85% it impacts

PGC1-α levels and decreases them by 40%. [108] Conversely, forced expression of LRPPRC increases levels of PGC1-α mRNAs, but also PEPCK and G6P, two key gluconeogenic enzymes. This upregulation is abolished when LRPPRC is depleted, and consequently the coactivator ability of PGC1-α to increase the transcription of PEPCK and G6P, indicating that LRPPRC and PGC1-α act together to regulate the expression of mitochondrial and gluconeogenesis genes. [118-120] However, levels of LRPPRC do not affect all targets of PGC1-α, such that CPT1 and HNF4α, for example, are unaffected by modulation of LRPPRC levels, indicating only specific pathways are modulated by the two proteins. [108] Moreover, forced expression of LRPPRC enhances OXPHOS through mitochondria remodelling, including higher cristae density, independently of mitochondrial biogenesis. [118] These findings were obtained through modulation of the levels of normal LRPPRC, it is therefore not known if the nuclear function of mutated LRPPRC is affected in LSFC.

1.3.7 Distinct tissue pattern involvement

Despite the mutation, LRPPRC's putative mitochondrial targeting sequence is unaltered, and the protein is correctly imported to the mitochondria and not mis-targeted, as shown by immunofluorescence assays in patient fibroblasts. [93, 121] LRPPRC carrying the A354V mutation is unstable, and steady-states levels are reduced by 70% in all tissues in patients. [113, 121] This decrease has a variable impact on the different organs since normal expression of LRPRPC is high in skeletal muscle and heart, and significantly lower in liver and brain. [109, 121] Therefore, tissues with naturally lower levels of normal LRPPRC are greatly affected by the mutation. This contributes to the distinct LSFC phenotype, and liver and brain involvement distinguishes it from classic LS. [113, 121] Mutation of LRPPRC results in a decrease of COXI and COXIII mRNA levels, and thus a decrease of these core subunits and of assembled complex IV in LSFC tissues. [113, 121] Interestingly, differentiated patient myotubes display a combined OXPHOS defect with reduced levels of assembled CIV and CI. *In vitro* studies revealed that depletion of normal LRPPRC in fibroblasts and myotubes to the same level as the mutated form (i. e. 30%) results in a similar phenotype. [122] These results highlight the fact that mutated LRPPRC could still be functional, and it is rather its lowered level that causes the OXPHOS deficiency observed in patients. Furthermore, when normal LRPPRC levels are reduced by 100% with siRNA, all mitochondria encoded respiratory chain complexes display an assembly defect. [122] This strongly suggests the steady states level of LRPPRC determines the extend of the OXPHOS defect. In patient liver samples, assembled CIV is barely detectable, whereas levels are reduced to 50% in heart samples,

but both tissues have increased levels of assembled CI and CIII. [113] Similarly to what was observed *in vitro*, muscle samples display a decrease of assembled CIV and CI. [113] Other proteins involved in mitochondrial translation show a tissue specific response. In fact, the levels of the small mitochondrial ribosome subunit MRPS27 and the fully assembled small ribosome are both decreased in LSFC liver samples, and the large ribosome is not affected, whereas levels of both the small and large ribosomes are increased in LSFC heart mitochondria. [113] This suggests the onset of adaptive mechanisms in response to mutated LRPPRC in this tissue.

Another interesting factor related to tissue involvement patterns is the existence of tissue specific isoforms of some complex IV subunits that are developmentally regulated. [123] This modulation is sensitive to energy demand and responds to external regulators such as hormones and second messengers in highly specialized organs like heart, liver, brain, kidney, and skeletal muscle. [123] The isoforms are encoded on different chromosomes, indicating they are not the product of alternative splicing of the same gene. Subunits VIa and VIIa exist as two isoforms: heart and liver. The liver isoform is ubiquitously expressed and is replaced by the heart isoform in heart and skeletal muscle after birth. [123] The specific function of the different isoforms is not well understood. However, it is noteworthy to mention that heart and muscle have a high mitochondrial density and can rely on both aerobic and anaerobic energy production, whereas liver and brain depend on aerobic energy production and have a lower mitochondrial load. [124]

1.3.8 Biochemistry and pathophysiology

Models of whole-body knockout of *Lrpprc* are embryonic lethal, highlighting the importance of LRPPRC in mouse embryonic development. [112, 125] Only tissue specific disruption of the protein leads to viable mouse models. Heart specific knockout of *Lrpprc* causes cardiomyopathy and a severely shorten lifespan. [112] Almost all mitochondrial mRNAs are decreased in absence of heart LRPPRC, except for the ribosomal mRNAs (12S rRNA and 16S rRNA) which are increased. To compensate, some mRNAs are translated at a higher level, but the product is unstable and prematurely degraded. Despite this, only the amount of CIV subunits is decreased and CI, CII and ATPsynthase subunits are at normal levels. [112] The amount of fully assembled CIV is decreased and further characterization highlighted decreased amount of assembled CI and ATPsynthase, and the presence of sub-assembled ATPsynthase of lower

molecular weight. [112, 126] This ATPsynthase assembly defect leads to abnormal cristae structure. [126] Complex IV enzyme activity is reduced in absence of heart LRPPRC, whereas the other respiratory complexes are only slightly affected. [112] Functionally, mitochondrial respiration is decreased in the phosphorylating state whereas the uncoupled respiration is spared, and reactive oxygen species production is increased in absence of heart LRPPRC. [126]

Biochemically, the homozygous A345V mutation of *LRPPRC* translates into a severe complex IV (cytochrome c oxidase, COX) deficiency of the mitochondrial respiratory chain. [85, 93, 113] The enzyme deficiency is spread across tissues following the same pattern as the enzyme assembly defect, significantly affecting liver and brain. [113, 121] Hence, LSFC differs from classic LS, and most COX diseases, by a lesser involvement of heart, skeletal muscle and kidney. Recent studies performed on patients' fibroblasts revealed additional dysfunctions, indicating that *LRPPRC* mutation's impact goes beyond OXPHOS and affects other important facets of mitochondria. [93] LSFC fibroblasts present morphological and functional abnormalities such as a fragmented mitochondrial network, reduced membrane potential, lower maximal ADP-driven respiration in presence of substrates feeding CI and CII, and an increased susceptibility to PTP opening when challenged with increasing amounts of calcium. [93] Despite these multiple dysfunctions at baseline, cellular ATP levels are not compromised, and ROS production is unaltered. An enhanced glycolysis could compensate and help maintain normal levels of ATP in LSFC fibroblasts. When fibroblasts are given exogenous carbon 13 labelled glucose, its incorporation in pyruvate, lactate and alanine is increased by 41%, 61% and 52% respectively in patient cells, which could be explained by an enhanced glycolysis. [127] As a natural compensatory mechanism, aerobic glycolysis is triggered in LSFC fibroblasts as illustrated by increased levels of HIF1-a and phosphorylated PDH1. The phosphorylated form of PDH1 is inactive, and therefore there is a metabolic switch from oxidative metabolism in mitochondria to glycolysis. [127] These transcription factors are normally under the control of mTORC1, but intriguingly the increase of HIF1-a levels and phosphorylated PDH1 is independent of the complex in patient cells as there is no change in the ratio of phosphorylated to non-phosphorylated mTOR. [127] Inhibition of mTOR with rapamycin further decreases the levels of LRPPRC, and consequently COX-IV, without affecting the levels of ATP in LSFC fibroblasts. [127] This indicates that patient cells rely on extra-mitochondrial metabolism to maintain normal levels of cellular ATP, and more importantly, that compensatory mechanisms are in place to support cell viability.

Given these dysfunctions at baseline in fibroblasts, where LRPPRC levels are reduced by 50%, it is fair to stipulate those mitochondrial functions are altered to a similar, if not greater extend, in liver and brain where LRPPRC is nearly absent. In this context, mouse models become useful to investigate the pathophysiology of the disease, and the severity of COX deficiency in organs that are predominantly affected in LSFC patient. Our research consortium has dedicated a lot of work towards the development of mouse models to study LSFC in the past decade. Unfortunately, our group has found that germline knock-in of the A354V mutation is embryonic lethal, and we and others have found the ubiquitous knockout of LRPPRC to also be lethal. [112, 125] However, mice with tissue specific disruption of Lrpprc are viable, and amenable to study the in vivo function of hepatic LRPPRC. In order to gain better knowledge on the pathophysiology and the underlying mechanisms of LSFC, our research consortium developed a mouse model harbouring a liver specific inactivation of LRPPRC. Results from the characterization of this model are detailed in the first paper of this thesis (Chapter 2).

1.4 Compensatory Mechanisms

Despite a severe CIV deficiency, LSFC patient fibroblasts are able to maintain normal ATP levels and some patients make it to adulthood, indicating compensatory mechanisms are in place to support mitochondria functions and allow survival. [91, 93] Beyond LSFC, it is fair to suspect most cells will try to mount compensatory responses to survive in the presence of a primary mitochondrial defect. This concept has not been examined a lot, and it might provide insights to inform therapeutic strategies.

In a healthy state, mitochondrial signals, including ROS and reactive metabolic intermediates, modulate the expression of several thousands of genes linked to various cellular functions. [128-130] Moreover, mitochondria are responsible for numerous essential functions in the cell. Therefore, impairment of mitochondrial functions can result in a broad transcriptional reprogramming involving epigenetics and have a dramatic effect. [131, 132]

Interestingly, unusual cases of COX deficiency show spontaneous recovery. [66, 133] Patients present exclusively with myopathy in early infancy, resulting in severe muscle weakness and

hypotonia, and they often require assisted ventilation. [66] Muscle biopsy is identical to fatal COX deficiency, with red ragged fibers, swollen mitochondria and faint or no reaction for COX. [66] After this life-threatening period, children surprisingly recover around the age of three, where muscle biopsy is normal, and they show no more clinical symptoms. Sequencing identified a homoplasmic variant in the mtDNA, but this mutation alone is not sufficient to cause the disease since only 1/100 carriers develop COX deficiency. [66, 134] The additional heterozygous mutation in *EARS2* or *TRMU* is required for disease onset. Other cases of mitochondrial diseases involving mutations in these two genes also show a reversible disease course. [134] A recent study suggests the spontaneous recovery in patients with digenic mutations is mediated by compensatory mechanisms, including the integrated stress response and mTOR activation. [134] These rare cases of reversible COX deficiency truly highlight the power of these compensatory mechanisms. [66, 133, 134]

1.4.1 Broad mechanisms

1.4.1.1 The Integrated Stress Response

Several studies have linked mitochondrial dysfunctions to a specific gene expression program associated with the integrated stress response (ISR; represented schematically in Figure 1.1). [135, 136] In mammalian cells, the ISR can be triggered by nutrient deficiency, unfolded protein stress or pathogen infection. [136, 137] The activation of the ISR occurs through a family of four distinct kinases (PERK, GCN2, PKR, HRI) that phosphorylate the transcription factor eIF2α, which in turn inhibits global protein synthesis and promotes the translation of specific mRNAs harbouring up-stream open reading frames (uORFs). [135] The induced transcriptional program varies across tissues and the four kinases, sharing a conserved catalytic core, are activated by different triggers. [138]

Figure 1.1: Integrated Stress Response Pathway. Adapted from [138]

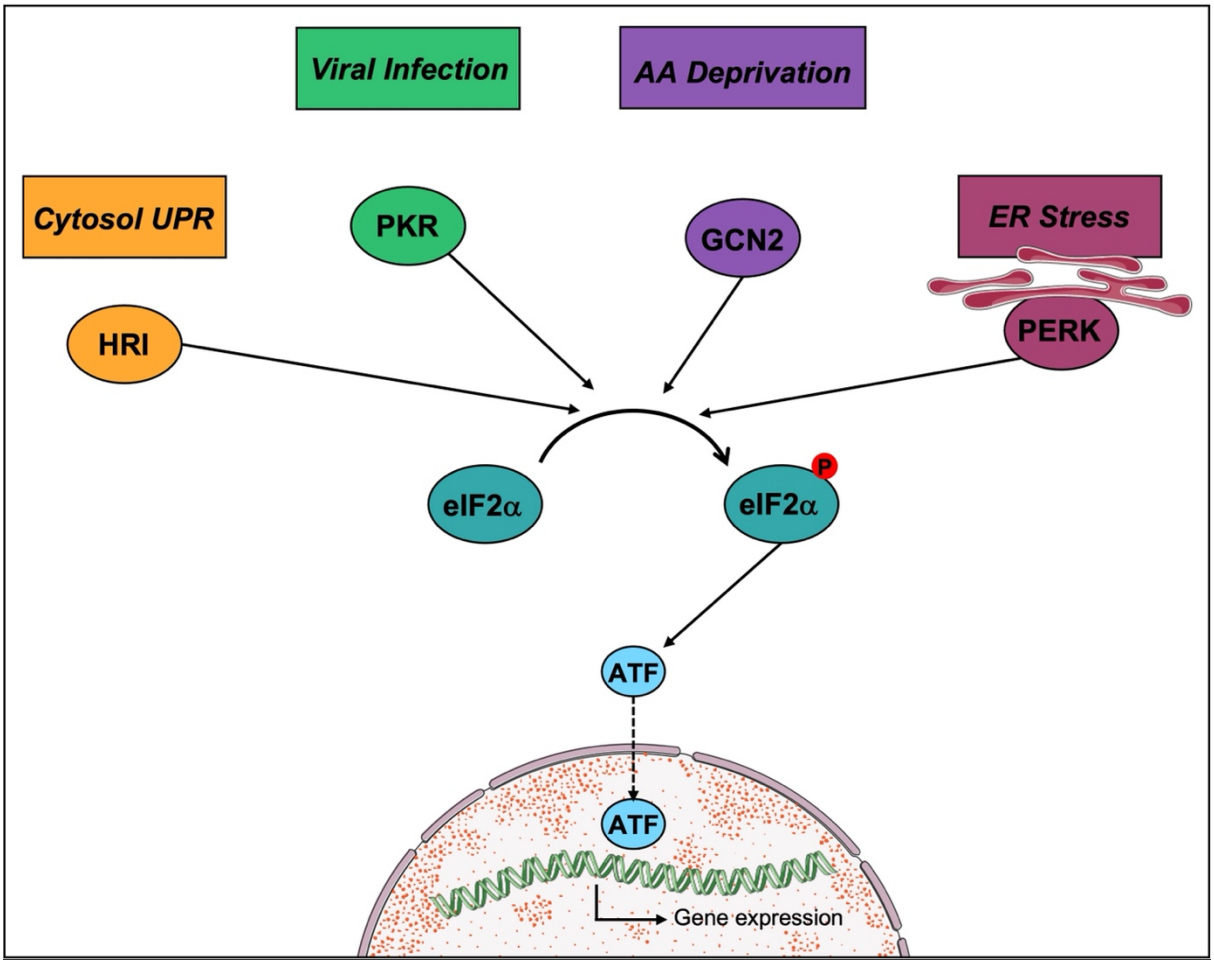

1.4.1.1.1 PERK

Protein Kinase R-like endoplasmic reticulum kinase (PERK) localizes to the ER and is activated by the unfolded protein response (UPR) in this organelle. [139, 140] Under stress induced by ROS, PERK has been shown to modulate mitochondrial functions and it has also been suggested to mediate signaling between the ER and mitochondria. [141] Overall, PERK can modulate the capacity of mitochondria to adapt to the metabolic needs of the ER. A metabolic adaptation study where cells were grown in galactose media revealed the activation of PERK, and subsequent phosphorylation of eIF2α, activates the translation of ATF4, which triggers the translation of supercomplex assembly factor 1 (SCAF1). [142] This assembly factor is believed to promote the formation of supra-arrangements of respiratory chain complexes into supercomplexes (SCs) (see section 1.4.2 3 for details on SCs), optimizing mitochondrial respiration. [143] PERK also activates LONP1, a mitochondrial chaperone and protease that binds mtDNA. [144]

1.4.1.1.2 GCN2

General Control Nonderepressible 2 (GCN2) responds to nutrient deprivation and phosphorylates eIF2α under amino acid limitation. [138, 145-147] To adapt to this condition, GCN2 upregulates non-essential amino acid synthesis and downregulates lipogenesis through SERBP to allow metabolic adaptation. GCN2 is generally found associated to ribosomes and its activation is potentially modulated by ribosome stalling. [146] GNC2 is also activated when mitochondrial translation is inhibited in mammals. [148]

1.4.1.1.3 PKR

Protein Kinase R (PKR) responds to viral infection, through the binding of double stranded RNA. [149, 150] The subsequent phosphorylation of eIF2α and interruption of protein synthesis serves to prevent viral protein production in the infected cell. In absence of pathogens, PKR is activated by endogenous RNA, proteins, and inflammation caused by UPR in the ER. [151-153] Additionally, PKR mediates the mitochondrial UPR in states of inflammation. [154] Once activated, PKR phosphorylates eIF2α, which in turn activates mitochondrial chaperone HSP60. [135]

1.4.1.1.4 HRI

Heme-regulated inhibitor (HRI) responds to UPR in the cytosol and stimulates the expression of chaperones and proteases. [155, 156] It is essential for the pro-inflammatory response to bacterial infection. [157] Activated HRI phosphorylates eIF2α, activating ATF4 which upregulates heat shock protein HSPB8, essential for sustained activation of NF-κB signaling. [155] HRI is also activated by OMA1, mitochondrial stress activated protease, and DELE1, a mitochondrial protein. [157] Under normal conditions during erythroblast differentiation, HRI regulates mitochondrial biogenesis, translation, and activity. [156]

Among the mRNAs harboring uORFs, transcription factors ATF4, ATF5 and CHOP respond to mitochondrial dysfunction and require phosphorylated eIF2α to initiate their translation. These transcription factors activate chaperones and pathways that rewire cellular metabolism and increase

mitochondrial proteostasis. [158-161] Although ATF4, ATF5 and CHOP all play a role during mitochondrial stress, it remains unclear if they act individually or together. [162-164] Loss of LONP1 during mitochondrial stress, causing insoluble protein aggregates accumulation in the mitochondrial matrix and ribosome biogenesis alteration, also triggers the ISR. [165] In mitochondrial diseases, the ISR activates the one carbon pathway and is thought to be involved in the secretion of FGF21 and GDF15 in the circulation, two known biomarkers of mitochondrial translation defects. [56]

It is still debated whether the ISR plays a protective role or if it contributes to pathogenesis. However, it has been shown that prolonged activation of the ISR in muscle is not protective in mitochondrial myopathy. [166]

In the compensatory mechanisms' hierarchy, the ISR is known to be an essential precursor of the mitochondrial UPR (UPR^{mt}) activation. [162]

1.4.1.2 UPR^{mt}

Mitochondrial dysfunctions trigger the mitochondrial unfolded protein response (UPR^{mt}), a transcriptional response regulated by nuclear-mitochondrial crosstalk that promotes repair and recovery of the mitochondria to maintain cellular function and survival. [167-170] Although the UPR^{mt} is an essential compensatory mechanism, it becomes detrimental if its activation is prolonged or altered and can promote the propagation of mutant mtDNA. [171] Therefore, its regulation is tightly executed at multiple levels and can be coordinated between cells and tissues.

Upon mitochondrial dysfunction (OXPHOS impairment, ROS, impaired respiratory chain complexes assembly/mito-nuclear protein imbalance, unfolded protein) in *C. elegans*, the import of protein to the organelle is impaired. [169] Therefore, the import of transcription factor ATFS-1 to the mitochondria is suspended and it is instead redirected to the nucleus where it upregulates genes encoding proteases and chaperones to promote recovery and maintain homeostasis. [169] Upon mitochondrial stress, the UPR^{mt} suspends OXPHOS genes transcription and shifts metabolism to glycolysis to promote organelle recovery. [170, 172] Although the UPR^{mt} was initially described in rat cells, the underlying mechanisms have been studied and described in detail in *C. elegans*, but

unfortunately they remain incomplete in mammals. Activation of the UPR^{mt} in mammals is more complex and follows activation of the ISR and is triggered by mtDNA depletion or accumulation of misfolded proteins in the mitochondria. [173] The response involves bZIP transcription factors ATF4 and ATF5 (mammalian homolog of ATFS-1), and CHOP, pre-activated during the ISR. [138, 174-176] Ultimately, these factors upregulate mitochondrial proteases and chaperones (most notably: HSP60, ClpP, LONP1, AFG3L2), to re-establish mitochondrial proteostasis by degrading misfolded or damaged proteins and promoting *de novo* protein folding (schematically represented in Figure 1.2). In addition, UPR^{mt} modulates the one carbon metabolism, promoting cellular redox balance and nucleotide synthesis. [177-179]

Figure 1.2 : Mammalian mtUPR. Adapted from [173, 180].

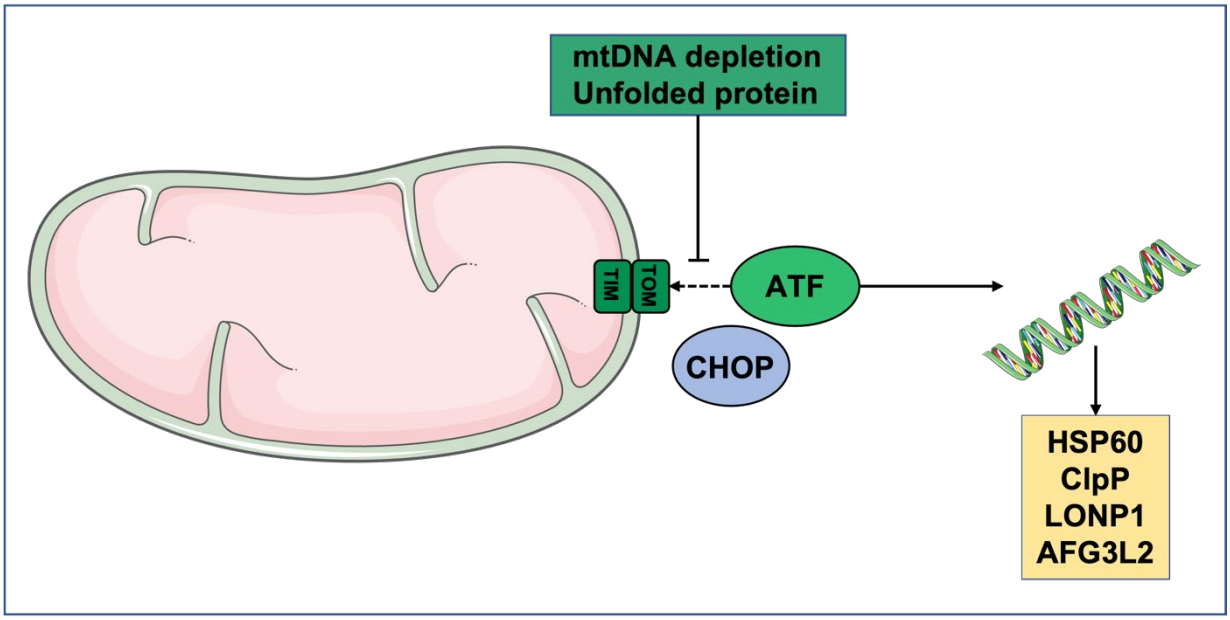

Increased levels of transcripts associated with the UPR^{mt} have been reported in patients with mitochondrial myopathies, in mouse model of mitochondrial cardiomyopathy [181, 182], and model of ALS with CI deficiency. [183]

1.4.2 Specific mechanisms

A recent study generated cybrids with increasing percentage of heteroplasmy for the mtDNA mutation 3234A>G in the tRNA$^{Leu(UUR)}$, to elucidate the basis of abrupt phenotype changes among

patients. [19] A total of seven groups were created (0%, 20%, 30%, 50%, 60%, 90%, and 100%) since the clinical phenotype for this mutation will vary depending on these specific heteroplasmy levels, causing diabetes and autism (10-30%), encephalomyopathies (50-90%) or perinatal lethality (90-100%). [19] The authors elegantly demonstrated how different epigenetic programs are triggered depending on the extend of the bioenergetic defect, and which adaptive mechanisms is privileged depending on the heteroplasmy level (Table 1.2). [19]

Table 1.2: Adaptative Mechanisms in Response to Heteroplasmy. Adapted from [19].

	Heteroplasmy level					
Compensatory Mechanism	*20%*	*30%*	*50%*	*60%*	*90%*	*100%*
Mitochondrial Chaperones (HSP60 and HSP10)	Up-regulated	Up-regulated	Down-regulated	Down-regulated	Up-regulated	Down-regulated
Genes related to mitochondrial functions (OXPHOS, TCA cycle)			Up-regulated	Up-regulated	Up-regulated	
Mitochondrial Biogenesis (PGC1-α, ribosomal genes)			Up-regulated	Up-regulated	Up-regulated	
Glycolytic genes			Increased	Increased	Increased	Low

Variations in mitochondrial dysfunctions results in nuclear DNA remodelling, triggering adaptive responses. These strategies correlate with changes in energy availability and depend on the length and extend of the defect. In condition of low energy availability, the cell adapts by conserving

energy (decreased utilization, increased repair). In more severe and prolonged conditions of energy deficiency, the cell adapts by up regulating the energy generating systems, such as mitochondrial biogenesis and/or glycolysis. [19]

1.4.2.1 Mitochondria biogenesis

Mitochondrial biogenesis is the process by which pre-existing mitochondria grow and divide, resulting in variation of number, size, and mass of the organelle. [184] It is regulated by the co-transcriptional regulation factor PGC1-α that promotes the expression of Tfam through activation of transcription factors NRF-1 and NRF-2. [115, 185, 186] Tfam ultimately drives mtDNA transcription and replication. [186] In parallel, other targets of NRF stimulate the TCA (tricarboxylic acid) cycle and β-oxidation to provide sufficient energy for the process. To a lesser and more restricted extend, PGC1-β, which shares similar structure and function with PGC1-α, can also stimulate mitochondria biogenesis through NRF. [187] Several stimuli activate the PGC1-α cascade, including AMPK, PPARγ, CaMKIV, nitric oxide, SIRT1, TORC, calcineurin, p38 MAPK and RIP140, in response to exercise, caloric restriction, cold and ATP depletion. [184]

In several cases of mitochondrial diseases, especially in mitochondrial myopathies, increased biogenesis is reported. [188, 189] The classic Red-Ragged Fibers (RRF), an abnormal accumulation of dysfunctional mitochondria in the muscle fibers, is a great example. Mitochondrial biogenesis occurs as an attempt to meet the cellular energetic needs upon mitochondrial dysfunction. [190] It has also been suggested that the upregulation of mitochondria biogenesis could be protecting against caloric overload. [188] In fact, high-calorie diet aggravates mitochondrial dysfunctions, and physicians recommend their patients eat smaller meals more often during the day instead of three large meals to decrease the number of calories taken in at a time. [191] In addition to mitochondrial biogenesis, other genes related to energy metabolism are upregulated in response to respiratory deficiency. [189] In cases of mitochondrial diseases caused by mutations in mtDNA, the upregulation of this gene program correlates with the level of heteroplasmy once a certain threshold is reached. [19] This suggest the response is triggered only past a given degree of bioenergetic inhibition, and it probably varies across tissues.

1.4.2.2 Activation of glycolysis and mTOR pathway

Glycolysis consists of ten reactions by which one molecule of glucose is converted into two molecules of pyruvate in the cytosol, with a net production of two molecules of ATP and two molecules of NADH. [192] During glycolysis, two molecules of ATP and NAD^+ are consumed, making it a costly energy generating process and the reactions are limited by NAD^+ availability in the cell. [192] In anaerobic conditions, pyruvate is no longer oxidized by the Krebs cycle and quantities of NAD^+ become limiting and glycolysis decreases. To overcome this, pyruvate is converted to lactate by lactate dehydrogenase through fermentation, using two molecules of NADH to generate two molecules of NAD^+ to resume glycolysis. The accumulated lactate is eventually released in the bloodstream. In aerobic conditions, pyruvate is imported to the mitochondria and converted into two molecules of acetyl-CoA by pyruvate dehydrogenase to feed the Krebs cycle, and ultimately the respiratory chain. [192]

Aerobic glycolysis, also known as the Warburg effect, can be upregulated when mitochondrial respiration is altered, and was suggested by Otto Warburg himself in his original hypothesis. [193, 194] This process occurs mainly in cancer cells to meet the biosynthetic requirements of the cells but has also been reported in Parkinson's and Alzheimer's, concomitant with mitochondrial dysfunction. [194] In human cybrid models of mitochondrial diseases, glycolysis is induced at high levels of heteroplasmy (50-90%) and is associated with cell growth. [19] Moreover, circulating lactate levels are often high in patients with mitochondrial diseases, suggesting an up-regulation of glycolysis to compensate for the energy production defect. [4]

Among the pathways regulating metabolism, mammalian target of rapamycin (mTOR) coordinates cell growth with environment conditions, such as nutrient and oxygen availability. [195] Feeding activates mTOR to promote growth and energy storage and inhibits catabolism. On the other hand, mTOR is inhibited in conditions of fasting, low ATP levels, hypoxia, or DNA damage to promote catabolism. [195, 196] In hematopoietic and cancer cells, mTOR promotes aerobic glycolysis through AKT and HIF-1α to support cell differentiation and meet the energy demand of rapid cell growth, respectively. [197] The AKT/mTOR cascade mediates mitochondrial function through glucose metabolism and the activation of AKT has been shown to drive a shift in metabolism and a resistance to autophagy under mitochondrial stress. [196, 197] Interestingly, a study revealed mTOR complex I (mTORC1) controls the integrated mitochondrial stress response (ISRmt) in

models of mitochondrial myopathy. [166] In these models, caused by mtDNA defects, the OXPHOS deficiency in muscle correlates with the increased phosphorylation of downstream targets of mTORC1. [166] Treatment with rapamycin, a mTOR inhibitor, significantly improves the phenotype of mitochondrial myopathy models, and of other mitochondrial diseases models [198], suggesting it might be a promising therapeutic option. However, rapamycin is not effective for all mitochondrial diseases, and its potential is hardly predictable as evidenced by contrasting effects of the drug in different patients. [198]

The role of mTOR in the pathogenesis of LSFC has been investigated in patient fibroblasts. [127] The preserved levels of ATP and increased lactate point towards the up-regulation of glycolysis in LSFC, potentially mediated by mTOR. [93] Despite an increase in the expression of HIF-1α and PDHK1 (another target of mTOR), mTOR levels and phosphorylation were not different from the healthy controls and were not altered by rapamycin treatment, indicating this cascade is activated by another upstream kinase. [127] Treatment of LSFC fibroblasts with rapamycin further decreased the levels of LRPPRC and COX IV, suggesting a role of mTOR in the regulation of expression of these proteins. [127]

1.4.2.3 Supercomplexes

Our view of the organization of respiratory chain complexes within the inner mitochondrial membrane has been challenged in the past two decades. Models of dynamic supra-arrangements of individual OXPHOS complexes into SCs have been proposed, and these arrangements respond to various stimuli in both non-pathological and pathological conditions. [199-202] An increasing number of studies are suggesting SCs are rearranged to promote and maintain oxidative phosphorylation. [202-205]

Figure 1.3 : Supercomplexes Formation and Roles. Adapted from [201, 206].

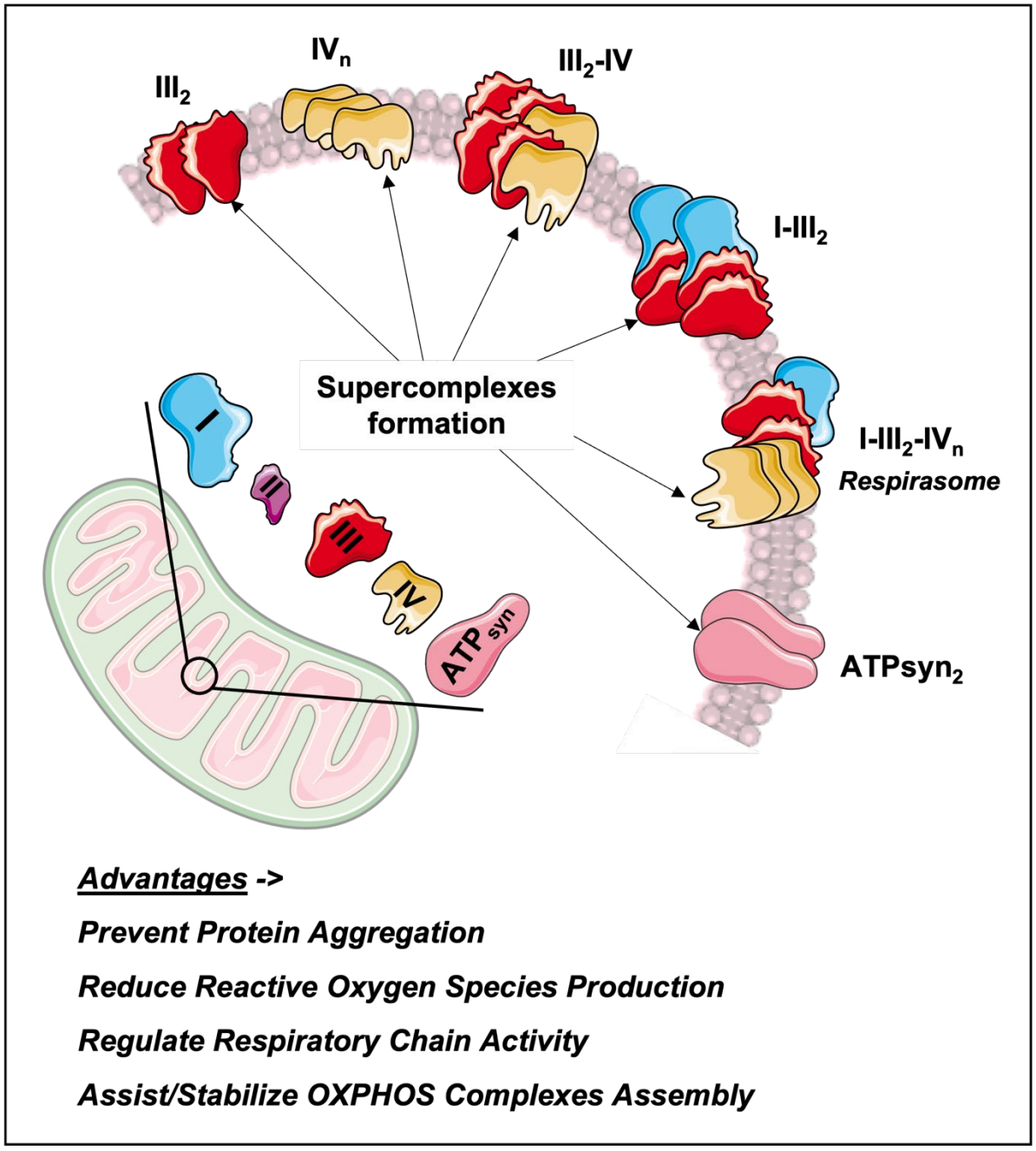

1.4.2.3.1 The respiratory chain

The electron transport chain, composed of respiratory complexes I to IV, oxidizes reducing equivalents coming from the Krebs cycle, glycolysis, or fatty acid oxidation, and uses the energy generated to pump protons across the inner mitochondrial membrane. [192] The proton motive force created is used by ATPsynthase to phosphorylate ADP to ATP. The oxidative reactions begin at CI with the oxidation of NADH and the transfer of two electrons to coenzyme Q. This creates enough

energy for CI to pump 2 protons in the intermembrane space. [192] Electrons can also enter the chain at CII through the oxidation of succinate to fumarate. This reaction reduces FAD to $FADH_2$, which rapidly donate its electrons to coenzyme Q, but the energy produced is insufficient to pump protons across the IMM. [192, 207] Reduced coenzyme Q shuttles the electrons from CI and CII to CIII, providing enough energy for CIII to pump 4 protons in the intermembrane space. [192] The electrons are then transferred from CIII to cytochrome c, which carries them to CIV. The last complex accepts the electrons, pumps 2 protons and catalyzes the reduction of molecular oxygen to water. [192] The electrochemical gradient generated by these reactions is used by ATPsynthase. The protons from the intermembrane space pass through ATPsynthase, causing its rotation and the coupled phosphorylation of ADP to ATP. [192]

1.4.2.3.2 Description

The advancement of native electrophoresis techniques and optimization of mitochondria solubilization with digitonin allowed the resolution of high molecular weight supramolecular arrangements of OXPHOS complexes. [199, 208, 209] The simplified view of the respiratory chain as individual complexes aligned in the inner mitochondrial membrane is now replaced by a dynamic organization which consists in various arrangements of the respiratory chain complexes with each other termed supercomplexes (SCs) (See Figure 1.3 for a schematic representation of SCs). Further characterization revealed not all OXPHOS complexes are incorporated in SCs and there is a balance between free complexes and complexes incorporated in SCs, defining the "plasticity" model. [201] It is estimated that 85-90% of CI, 55-65% of CIII and only 15-25% of CIV is incorporated in SCs, the remaining is arranged in either monomers, dimers, or oligomers. [204, 210] The different SCs stoichiometry include CI-$CIII_2$, $CIII_2$-CIV_{1-2} and CI-$CIII_2$-CIV_{1-4}. [204, 210] Arrangements containing CI, CIII, CIV, together with mobile electrons carriers coenzyme Q and cytochrome c, are capable of oxidation of NADH by molecular oxygen *in vitro* and are called respirasomes. [200] Structural analysis revealed the interaction between CI and CIII is dominated by the supernumerary subunits of CI. [211] The two specific interactions are between subunits NDUFA11 and NDUFB4 of CI with subunit UQCRQ of CIII, and subunits NDUFB9 and NDUFB4 of CI with subunits UQCRC1 and UQCRFS1 of CIII. [212, 213] The interactions formed by CIV with CI and CIII are less tight and vary among species. [213] In ovine mitochondria, the contacts are between subunit COX7A of CIV and subunits UQCR1 and UQCR11 of CIII. [212]

1.4.2.3.3 Raison d'être

SCs arrangements have been characterized in various tissues from numerous species, but their true *raison d'être* remains elusive. Several studies have proposed possible advantages of SCs formation. Among them:

1) Prevent protein aggregation in the protein rich IMM. Proteins make up to 70% of the IMM. The weak interactions between complexes forming SCs potentially maintain the fluidity of the membrane. [214]

2) Decrease ROS production. Studies on bovine mitochondria and liposomes containing CI and CIII have shown SCs decrease ROS produced by CI. [215] Moreover, the amount of CI incorporated in SCs inversely correlates with ROS production in neurons and astrocytes. [216]

3) Regulate the respiratory chain activity. Physiological stresses such as exercise lead to an increased SCs formation in Humans, possibly linking enhanced SCs assemblies to increased energy demand. [204]

4) Assist and stabilize the assembly of individual OXPHOS complexes. This is exemplified in models where a combined OXPHOS defect is caused by a mutation or knockdown of one subunit of a specific complex. Typically, CI defects will also affect CIII, likely because unstable CI cannot properly form the CI-CIII SC. [217, 218] Likewise, defects of CIII often affect CI and CIV, with a decrease in respirasome formation. [217, 219] Besides, an increasing number of studies are showing SCs rearrangement is promoted under stress conditions to palliate an isolated or combined OXPHOS defect. [203, 220, 221]

Mild acidosis caused by hypoxia in neurons has been shown to preserve mitochondrial function through adaptive mechanisms including SCs remodeling. Monomeric CI was decreased in favor of SCs, while arrangements containing CI, CIII and CIV were preserved, functionally increasing maximal respiratory capacity and reserve capacity. [222] Patients suffering from Leigh syndrome caused by mutations in *NDUFS4* have a decreased CI stability and activity. Despite this, active and fully assembled CI are found in SCs in a mouse model of the disease, indicating the supramolecular assembly of CI is favored to promote its function. [220] Additionally, studies performed on patient fibroblasts with a complex IV deficiency caused by different mutations have shown the residual CIV is preferentially incorporated in SCs, specifically the respirasome, and barely in the monomeric form. [203]

Once more, this highlights how SCs formation, as a compensating mechanism, favors the stability and function of deficient OXPHOS complexes.

1.4.2.3.4 Assembly factors

Although the existence of SCs is now well accepted, the molecular mechanisms underlying their formation are poorly understood. Several proteins have been suggested to be required for SCs formation and stability. In yeast, knockdown studies suggest respiratory complex factors 1 and 2 (RCF1 and RCF2) are required for the late assembly steps of CIV are for the formation and stabilization of CIII-CIV SCs. [223-225] Conversely, *Rcf* knockout strains have decreased CIV activity but are still capable of forming SCs. [226] The mammalian orthologs of RCF1, Higd1a and Higd2a, participate in the biogenesis of CIII and CIV and stably interact with both complexes to maintain their structure and functional integrity. [223, 227, 228] It is suggested Higd1a and Higd2a might affect SCs assembly in a manner like Rfc1 in yeast.

Knockout studies in mice suggest the CIV subunit COX7A2 promotes the interaction between CIV and CIII in SCs formation. [143, 229] Comparisons between mouse strains revealed the existence of two different isoforms of this protein: a long isoform (COX7A2L) is present in CD1 and an unstable short one in C57BL/6J and C57BL/6N. [230] Several studies performed in various mouse tissues have shown contradictory results regarding the necessity of COX7A2L in the formation of the respirasome, containing CI, CIII and CIV. However, the conclusion that can be drawn is that COX7A2L is dispensable for the respirasome formation but required for the formation of $CIII_2$-CIV SC. [231] Therefore, it is now proposed the long isoform COX7A2L interacts with the subunit UQCR11 of CIII and replaces subunit COX7A of CIV upon formation of SC containing CIII and CIV, which precedes the respirasome assembly. [232] In the absence of the long isoform, CIII and CIV do not interact with each other but still individually associate with CI and form a weaker respirasome. [143, 230]

Nevertheless, the necessity of these factors is controversial, and it is still debated as to whether these proteins act directly on SCs formation and assembly or indirectly by promoting the assembly of individual complexes. [206]

1.4.2.3.5 Lipid environment

Beyond assembly factors, growing evidence indicates membrane lipid composition plays a role in the assembly and stability of multi-protein complexes, including OXPHOS complexes. [37, 233] Cardiolipin (CL), a signature phospholipid of the mitochondria present in high concentration in the inner membrane, has been shown to be important for SCs formation and stability in yeast and bovine mitochondria. [234-237] Self-assembly experiments realized through molecular dynamics simulation approach revealed how CL determines SC interfaces. Accordingly, the interacting regions between CIII and CIV are specifically enriched in CL, which act as a glue. The strength of CL binding relies on a delicate balance of electrostatic and Van der Waals forces. [214, 235] In Humans suffering from Barth syndrome, mutation in *Tafazzin* prevents the indispensable CL remodeling and disrupts SCs. [40] Proteins involved in CL synthesis inevitably play an indirect role in SCs assembly, to an extend like OXPHOS complexes assembly factors and chaperones.

On the other hand, the role of phosphatidylethanolamine (PE) in SCs formation and stability is controversial. Despite being the most abundant membrane lipid in mitochondria and binding respiratory complexes, PE depletion in yeast correlates with stabilization of high molecular weight SCs, suggesting increased amounts of PE disrupt SCs. [238] However, other groups reported that depletion of PE, and of PC, in yeast neither perturbed or promoted SCs assemblies [36, 239].

Altogether, this suggests a correct balance of mitochondrial membrane phospholipids is crucial for SCs stability and disruption of the equilibrium could contribute to the onset of mitochondrial dysfunctions.

LSFC patient fibroblasts maintain near normal ATP levels despite a severe CIV defect, indicating compensatory mechanisms are also in place in the presence of mutated LRPPRC. Based on the evidence in the literature and the variety of mechanisms described in models of mitochondrial dysfunctions, it is fair to stipulate that some of the aforementioned mechanisms are present in LSFC patient fibroblasts and in the H-Lrpprc$^{-/-}$ mouse model. The identification and characterization of these compensatory mechanisms is of great importance as it could lead to the development of therapeutic options targeting those to promote mitochondria repair. In order to investigate this, we

first developed a native electrophoresis technique that aims to preserve the most labile interactions between the OXPHOS complexes forming SCs. The development, details and advantages of this method are described in the second paper of the thesis (Chapter 3). Results from the investigation of compensatory mechanisms in LSFC models are described in the third paper of this thesis (Chapter 4).

1.5 Therapies for mitochondrial diseases

Despite all the advances made in the last couple of decades in the field of mitochondrial diseases, the biggest challenge remains the lack of effective and curative treatments. The current options include vitamins and supplements, and are used as antioxidants, mitochondrial substrates, cofactors, or enhancers of respiratory chain flux. [240] Unfortunately, their efficacy remains controversial, and a Cochrane review found little evidence supporting their use. [241] Moreover, although recent guidelines recommend the use of one supplement at a time, most mitochondrial disease patients take a cocktail of at least four supplements. [241, 242]

1.5.1 Options for Leigh Syndrome

In Leigh syndrome, molecules with antioxidant properties have shown promising results in cell models and in patients enrolled in an open label study. [243-245] However, these options are not as relevant for the treatment of LSFC since ROS production is not significantly increased in patient fibroblasts and treating the cells with various antioxidants (idebenone, N-acetyl cysteine, and resveratrol) exacerbated their phenotype. [93] Other preclinical studies used Rapamycin to treat a mouse model of Leigh syndrome and patient neurons to enhance the elimination of damaged mitochondria through mitophagy by inhibiting mTOR. Rapamycin moderately improved the symptoms and increased lifespan. [246, 247] Once more, the use of this compound was not effective in LSFC fibroblasts as it did not affect mTOR, and it further decreased the levels of COX IV and LRPPRC. [127] Gene therapy is being explored to treat Leigh syndrome, and other mitochondrial diseases, caused by mutations in the mtDNA and seems promising. Studies using AAV-PHP. B to deliver *Ndufs4* have shown it alleviates the symptoms in Ndufs4$^{-/-}$ mice but also displays strain and species dependent efficacy. [248, 249] Unfortunately, these genetic treatments are tailored to a specific mutation and cannot be transposed to other Leigh syndromes caused by mutations in a different gene such as LSFC.

Ideally, an effective therapy for Leigh syndrome should have multiple targets to match the heterogeneous phenotype, and hopefully be used for other mitochondrial diseases. Interestingly, a recent CRISPR-Cas 9 screen identified the inhibition of the Von Hippel-Lindau (VHL) factor as the most effective at suppressing mitochondrial disease. [250] In normoxic conditions, VHL targets the hydroxylated hypoxia-inducible transcription factors (HIFs) for degradation. During hypoxia, or when VHL is inhibited, HIF is stabilized and activates the hypoxia transcriptional program. Mimicking hypoxia (through VHL knockout or the use of a hypoxia triggering molecule) in cells and zebra fish increases the resistance of OXPHOS complexes to their specific inhibitors. [250] Since the pharmacologic inhibitors poorly cross the blood-brain barrier, a mouse model of Leigh syndrome was instead exposed to mild hypoxia at 11% O_2, a level known to be tolerated by Humans living at high altitude. [250] Surprisingly, chronic hypoxia prevented the onset of several symptoms and prolonged lifespan. [250] A follow-up study later demonstrated chronic hypoxia can even reverse the neurodegenerative lesions in the brain of the mouse model when the exposure begins after the onset of symptoms. [251] Unfortunately, the effects of hypoxia do not persist in time and hypoxia must be maintained continuously, making it challenging to translate this as a therapy for patients. [251] Other options, such as HIF targets or treating the mice with CO_2, are not as effective and have severe side effects. [252] More studies are required to explore alternative ways to reproduce the beneficial effects of hypoxia safely and effectively.

1.5.2 Stem cell therapy

In the past years, extensive pre-clinical and clinical data supported the emergence and safety of mesenchymal stem cells (MSCs) in the treatment of various human diseases. [253] MSCs consist of a heterogeneous subset of pluripotent stromal stem cells and can be isolated from bone marrow, adipose tissue, umbilical cord, and umbilical cord blood. [254] Bone marrow and adipose tissue derived MSCs are the most commonly used in clinical studies and regenerative medicine. [255]

1.5.2.1 Beneficial effects in various diseases

In 2020, over 1,000 registered clinical trials using MSCs as a therapeutic agent were listed on clinicaltrials.gov. MSCs therapy has shown beneficial effects in various conditions, including acute organ failure, graft-versus-host disease, ischemic heart disease, cardiovascular disease, liver disease, inflammatory diseases, diabetes, spinal cord injuries, bone and cartilage injuries

(summarized in [256]). In the more current context of the COVID-19 pandemic, several clinical trials investigating the potential of MSCs therapy for pneumonia and respiratory distress syndrome have been registered. [256, 257] The latter clearly highlights the potential of MSCs for the treatment of inflammatory and immune diseases.

1.5.2.2 MSCs characteristics

The minimal criteria defining MSCs are self-renewal, three mesenchymal lineages differentiation (osteoblasts, chondrocytes and adipocytes), adherence to plastic *in vitro*, and specific antigen expression (express CD105, CD73, CD90 and lack CD45, CD34, CD11, CD79a and CD19.) [258] MSCs have low immunogenicity and can be xenotransplanted without immunosuppression in the host. Upon transplantation, they secrete a large number of functional molecules and home to the damaged tissue or site of inflammation through their ability to detect and react to inflammation markers. [259]

1.5.2.3 MSCs-based mechanism of action

In the original hypothesis, injected MSCs migrated to the target tissue, engrafted, and differentiated into functional cells to regenerate the damaged tissue. [260] However, several studies have shown the high cell mortality rate of MSCs upon injection and therefore the low probability of tissue regeneration by cell differentiation and replacement. [261, 262] Nevertheless, MSCs therapy still has a beneficial effect in recipients, and this must occur through other mechanisms (summarized in Figure 1.4). This is now supported by evidence in various models, both *in vitro* and *in vivo*, notably in heart disease. [261, 263, 264] Therefore, in addition to cell replacement and differentiation, the revised hypothesis of MSC therapy includes the alternative modes of rescue and repair:

- Paracrine activity of secreted growth factors, cytokines, and hormones. Through this mechanism, MSCs can modulate inflammation by up-regulating anti-inflammatory cytokines while reducing pro-inflammatory factors, and support cell survival by secreting growth factors, cytokines, and extracellular matrix. [257, 260, 265] The paracrine activity of MSCs has an impact on fibrosis by reducing the infiltration of inflammatory cells, oxidative stress, and the activity of extra-cellular matrix secreting cells. [266] In murine models of liver disease, MSC therapy significantly reduces liver fibrosis *in vivo*. [267, 268]

- Material transfer from cell to cell through tunneling nanotubes (TNTs). [269] This network made of F-actin formed between MSCs and target cells allows communication and intercellular transport. Proteins, peptides, and complete organelles, such as lysosomes and mitochondria, can be transferred by TNT. [270-275]
- Release of extra-cellular vesicles. [276, 277] These membrane bound vesicles can be divided by size in exosomes (30-100nm, of endocytic origin), microvesicles (50-1000nm, non-endocytic origin) and apoptotic bodies (1-5µm, released during apoptosis). [278] Exosomes are of particular interest and are released when multivesicular bodies traffic to and fuse with the plasma membrane. [279] Their cargo is broad and includes mRNA, microRNA, proteins, and lipids. [280] The interest in their therapeutic potential is growing and their utilization may eventually surpass MSCs therapy.

Figure 1.4: MSCs-based Mechanisms of Action. Adapted from [260].

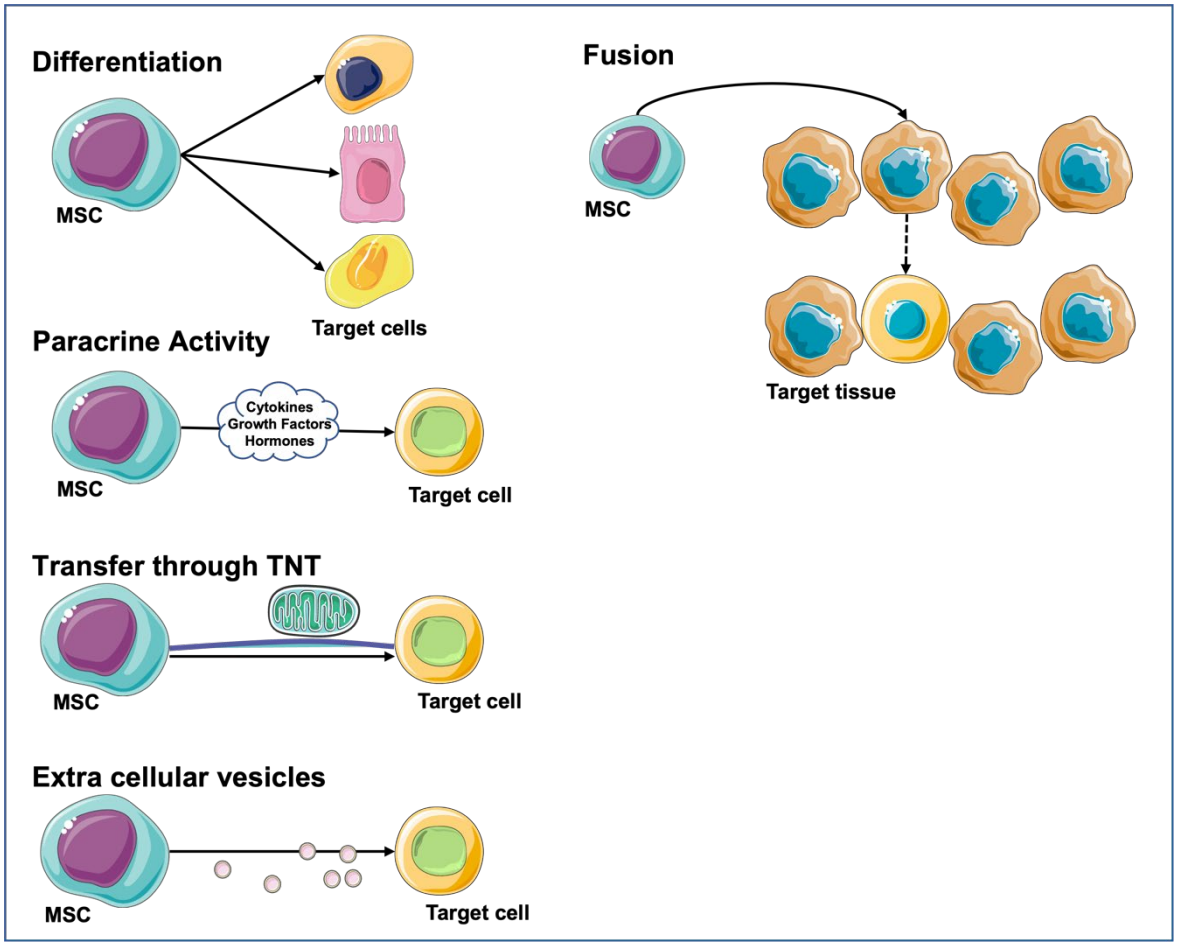

In the context of developing a therapy for mitochondrial diseases, two mechanisms are particularly appealing: mitochondrial transfer and extra-cellular vesicles (EVs).

1.5.2.4 Mitochondrial Transfer

The first evidence of mitochondria transfer through TNT was gathered from co-cultures experiments of Human MSCs with rho-0 lung epithelial cells. [274] Labelling techniques were used to monitor organelle and mtDNA transfer from the MSCs to the rho-0 cells, resulting in cell growth, restoration of mitochondrial respiration and increased ATP production. [274] Additional studies reported mitochondria transfer in various cell types and *in vivo* models. [270-272, 275, 281] The regulation of this process and the number of transferred mitochondria was shown to be regulated by Miro-1, an outer mitochondrial membrane GTPase, by gain of function approaches. [282, 283] Over-expression of this protein in MSCs increases mitochondrial transfer to target cells. [282] Undoubtedly, other proteins involved in the intracellular trafficking of mitochondria may also play a role in intercellular mitochondria transfer. The damage or injury signals triggering mitochondria transfer are still unknown. However, the transfer always originates from a healthy MSC as it was shown that MSCs containing dysfunctional mitochondria do not transfer them to the target cells. [284] Interestingly, MSCs derived from pluripotent stem cells display enhanced TNT formation and mitochondria transfer compared to adult derived MSCs. [285]

1.5.2.5 Extra-cellular Vesicles

Recent studies emphasize the contribution of EVs in the paracrine activity of MSCs. Conditioned MSCs media, and subsequent EVs isolation, were found to have therapeutic effects comparable to MSCs in rodent models. [286-288] Similar to MSCs, EVs have immunomodulatory capabilities, promote tissue repair and reduce fibrosis. [289] EVs have also been shown to activate the mTOR signaling pathway through AKT. [290] Among the advantages of EV therapy, their smaller size allows them to go through the pulmonary circulation (as opposed to MSCs who tend to get stuck in the lungs) and cross the blood-brain barrier. [291, 292] The efficacy of their cargo greatly depends on the donor, cell passage number and culture microenvironment. On the other hand, it is possible to modulate those conditions and pre-treat the cells to obtain a specific EV cargo, and a more tailored treatment. EVs isolated from cancer cells and astrocytes were shown to contain substrates of the TCA cycle, the *ND1* gene (encoding a subunit of CI), and the complete mtDNA. [293] Moreover, EVs increase mitochondrial respiration in an *in vitro* model of pulmonary

hypertension. [294] These features are extremely relevant in the optic of developing a therapy for mitochondrial diseases.

The potential of stem cell therapy for mitochondrial diseases has not been explored yet. Considering the emergence and safety of MSC therapy, and the impact of their therapeutic mechanisms on mitochondria, the third project of this thesis aims to explore the potential of stem cell therapy for mitochondrial diseases using LSFC as a model. Unfortunately, this project was not completed at the time of submission of this thesis, and it remains an exploratory study. Therefore, the results are only observatory and are summarized in chapter 5.

Chapter 2

Loss of Hepatic LRPPRC Alters Mitochondrial Bioenergetics, Regulation of Permeability Transition and Trans-membrane ROS diffusion

Alexanne Cuillerier[1,#], Shamisa Honarmand[2], Virgilio J. J. Cadete[1,$], Matthieu Ruiz[3], Anik Forest[3], Sonia Deschênes[1,4], Claudine Beauchamp[3], LSFC Consortium, Guy Charron[3], John D. Rioux[3], Christine Des Rosiers[3,4], Eric A. Shoubridge[2], Yan Burelle[*,1,#]

[1]Faculty of Pharmacy, University of Montreal, Montreal, QC, Canada

[2]Department of Human Genetics, Montreal Neurological Institute McGill University, Montreal, QC, Canada

[3]Research Center, Montreal Heart Institute, Montreal, QC, Canada

[4]Faculty of Medicine and Department of Nutrition, Université de Montréal, Montreal, QC, Canada

[#]Current Address: Interdisciplinary School of Health Sciences, Faculty of Health Sciences and Department of Cellular and Molecular Medicine, Faculty of Medicine, University of Ottawa, Ottawa, ON, Canada

[$]Current Address: Ottawa Hospital, Sinclair Centre for Regenerative Medicine, Ottawa, ON, Canada

Human Molecular Genetics, 2017; PMID: 28575497; DOI 10. 1093/hmg/ddx202

2.1 ABSTRACT

Background and aims: The French-Canadian variant of Leigh Syndrome (LSFC) is an autosomal recessive oxidative phosphorylation (OXPHOS) disorder caused by a mutation in *Lrpprc*, coding for a protein involved in the stability of mitochondrially-encoded mRNAs. Low levels of LRPPRC are present in all patient tissues, but result in a disproportionately severe OXPHOS defect in the brain and liver, leading to unpredictable subacute metabolic crises.

Methods: To investigate the impact of the OXPHOS defect in the liver, we analyzed the mitochondrial phenotype in mice harboring an hepatocyte-specific inactivation of *Lrpprc*.

Results: Loss of LRPPRC in the liver caused a generalized growth delay, and typical histological features of mitochondrial hepatopathy. At the molecular level, LRPPRC deficiency caused destabilization of polyadenylated mitochondrial mRNAs, altered mitochondrial ultrastructure, and a severe complex IV (CIV) and ATP synthase (CV) assembly defect. The impact of LRPPRC deficiency was not limited to OXPHOS, but also included impairment of long-chain fatty acid oxidation, a striking dysregulation of the mitochondrial permeability transition pore, and an unsuspected alteration of trans-membrane H_2O_2 diffusion, which was traced to the ATP synthase assembly defect, and to changes in the lipid composition of mitochondrial membranes.

Conclusion: This study underscores the value of mitochondria phenotyping to uncover complex and unexpected mechanisms contributing to the pathophysiology of mitochondrial disorders.

2.2 INTRODUCTION

Leigh Syndrome is the most common paediatric presentation of autosomal recessive oxidative phosphorylation (OXPHOS) diseases. This syndrome is an early onset, subacute neurodegenerative disorder accompanied by characteristic brain stem lesions, psychomotor regression, hypotonia, ataxia, and lactic acidosis. [73, 295, 296] The so-called classical form of the syndrome can be caused by mutations in subunits of the pyruvate dehydrogenase (PDH) complex, or more frequently, by mutations in the structural subunits of OXPHOS complexes, or of factors required for their assembly, resulting in isolated or multi-complex deficiencies affecting Complex I, II, IV (CI, CII, CIV) and the ATP synthase (CV). [72, 297]

In addition to classic LS, a variant known as Leigh Syndrome French Canadian (LSFC; OMIM #220111) has a characteristic pattern of tissue involvement, and a different clinical evolution, with acute metabolic crises usually leading to very early fatality. [85, 86, 91] LSFC is caused by a mutation in *Lrpprc*, which codes for an RNA-binding protein involved in the stabilization of most mtDNA-encoded mRNAs. [84, 112, 122] Most patients examined to date are homozygous for a single missense mutation, which results in low (*i. e.* less than 20% of normal levels) steady state amounts of LRPPRC protein in all tissues. [87, 113, 122] This causes a pronounced complex IV (C-IV) deficiency in the liver and brain (20% of normal activity), a moderate C-IV deficiency in fibroblasts and heart (50% of normal activity) and a combined C-IV and complex I (C-I) defect in skeletal muscle (40 % of normal activity). [85, 87, 113, 122] LSFC fibroblasts recapitulated several alterations in mitochondrial function including mitochondrial fragmentation, a decrease mitochondrial membrane potential, and reduced ADP-stimulated respiration. [87, 93] Consistent with these findings, a case-control prospective metabolic profiling study in LSFC patients revealed a metabolic signature of disrupted oxidative phosphorylation, which include markers reflecting changes in $NAD^{+,}$ lipid and amine metabolism. [90] Additional mutations in the *Lrpprc* gene have recently been identified outside the French-Canadian population, resulting in similar multi-systemic and neurological phenotypes. [87] The reasons underlying this spectrum of biochemical defects remains unclear, but is likely related to differences in the way mitochondrial mRNAs are handled in different tissues, and the ability of some cell types, but not others, to compensate for the absence of LRPPRC through adaptive changes in their mitochondrial translation machinery. [113]

The aim of the present study was to examine the impact of LRPPRC deficiency on key aspects of the liver mitochondrial phenotype. We generated an hepatic knockout mouse model to investigate in detail the impact of LRPPRC deficiency on the phenotype of liver mitochondria. Our results reveal that loss of hepatic LRPPRC triggers a multi-faceted phenotypic remodelling that extends beyond OXPHOS impairment, and includes mitochondrial ultrastructure abnormalities, impaired lipid metabolism, dysregulation of the permeability transition pore, and changes in ROS dynamics, thus highlighting the complex pathogenesis of OXPHOS disorders.

2.3 RESULTS

2.3.1 Loss of hepatic LRPPRC results in growth delay, and pronounced liver histopathological abnormalities.

Homozygous knockout mice were viable, had a normal appearance and locomotor activity under normal cage bound conditions, but had reduced body weight at 5 weeks-old compared to littermate controls (Fig 2.1A). After an overnight fast, only 2 % (2 out of 98) of *H-Lrpprc*$^{-/-}$ mice were found lethargic in their cage due to hypoglycaemia (≤ 3. 1 mmol/L), indicating a relatively preserved capacity to sustain hepatic glucose production. Of note, immunoblot analysis indicated the presence of residual amounts of LRPPRC (Fig 2.2A), which is likely attributable to liver regeneration as previously observed in liver-specific COX10 knockout mice. [298]

Livers of *H-Lrpprc*$^{-/-}$ mice displayed several macroscopic abnormalities. Liver mass was 25% greater than in control animals (Fig. 2.1B), liver lobes displayed scattered pale coalescing areas, characteristic of multifocal hepatic necrosis, and the gall bladder was severely swollen. Microscopically, the geometry of liver lobules was disrupted and numerous blood vessels were dilated (Fig. 2.1C). Cholestasis, focal necrosis, infiltration of inflammatory cells and microvesicular steatosis was also evident following H&E and Oil Red O staining (Fig. 2.1C-D). Consistent with a C-IV deficiency, a severe reduction of COX staining was present in liver sections from *H-Lrpprc*$^{-/-}$ mice. Furthermore, the normal peri-portal zonation of nuclear encoded CII (*e. g.* SDH) activity was lost in favour of a more homogeneous distribution across liver lobules (Fig. 2.1E).

Transmission electron microscopy showed the presence of notable abnormalities in mitochondria from H-*Lrpprc*$^{-/-}$ livers. In general, mitochondria appeared larger than in control mice, and many displayed altered cristae morphology characterized by loss of cristae ridges, and the presence of large vacuolar structures or patches of stacked cristae (Fig. 2.1F).

Figure 2.1: General Phenotype and Liver Histology in Normal and Liver-Specific LRPPRC Deficient Mice.

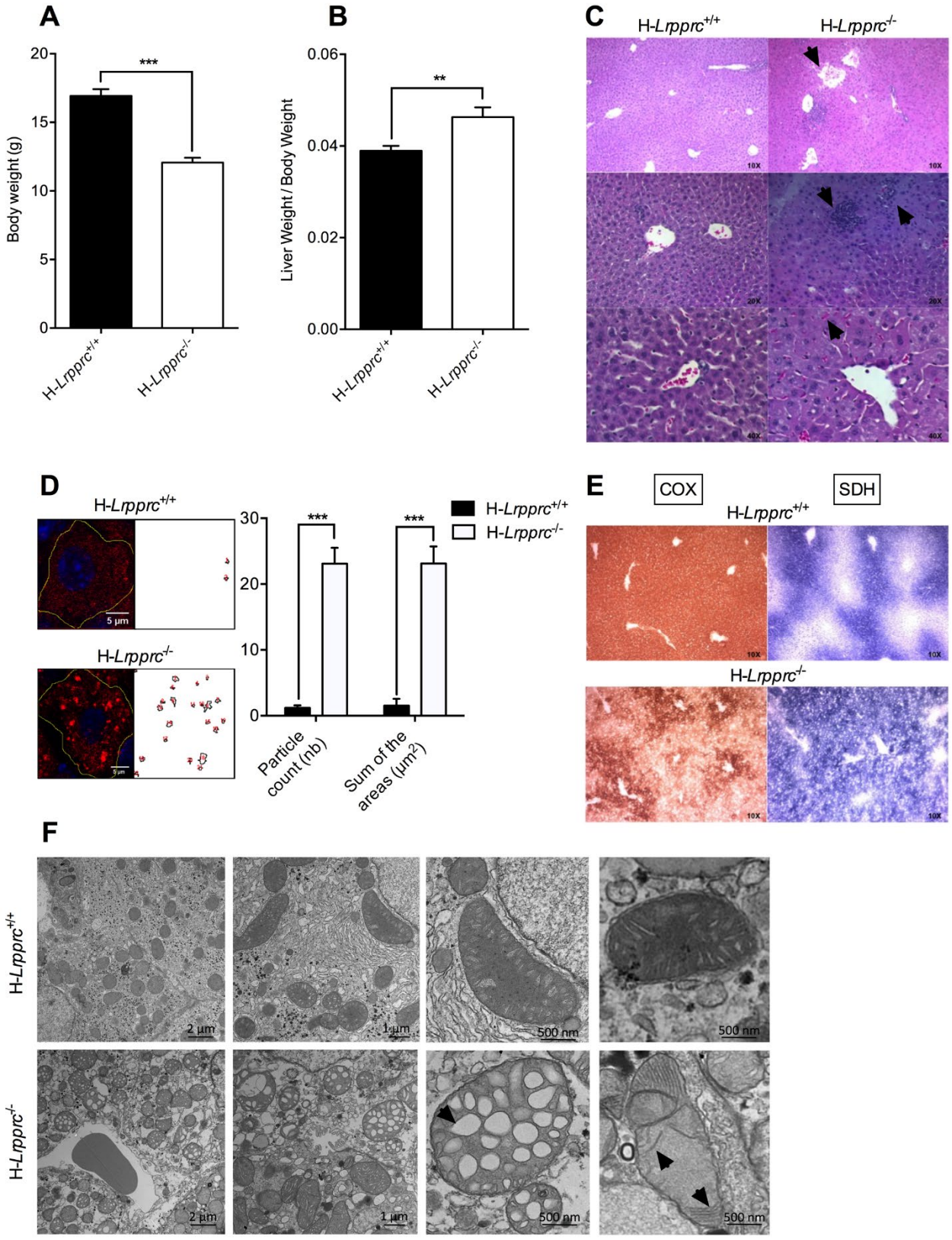

Panels A and B show mean body weight (n = 30), and ratio of liver to body weight (n = 16-17) in H-Lrpprc$^{+/+}$ and H-Lrpprc$^{-/-}$ mice. Panel C shows representative images of H&E staining. Loss of

*lobular structure and dilated vessels (top), focal necrosis and infiltration of inflammatory cells (middle), and cholestasis (bottom) are visible in the H-Lrpprc$^{-/-}$ samples (arrows). Panel D shows the quantification of Oil Red'O staining intensity in individual hepatocytes from H-Lrpprc$^{+/+}$ and H-Lrpprc$^{-/-}$ livers (n = 10). Panel E shows representative images of serial liver sections stained for COX (brown staining) and SDH (blue staining) activity. Panel F shows transmission electron micrographs from both mouse strains. Arrows point to large vacuolar structures and stacked cristae, which were commonly observed in H-Lrpprc$^{-/-}$mitochondria. Difference between H-Lrpprc$^{+/+}$ and H-Lrpprc$^{-/-}$ was assessed with a Student t-test: **: $p < 0.01$; ***: $p < 0.001$.*

2.3.2 Loss of hepatic LRPPRC induces a multi-faceted bioenergetic phenotype

LRPPRC deficiency resulted in the reduction of the steady state levels of most mtDNA-encoded transcripts in mice at ten weeks of age, particularly COX1-3 and ATP6, while rRNA levels were normal (Fig. 2.2E). Furthermore, in H-*Lrpprc*$^{-/-}$ mice, a high proportion (70-91%) of transcripts for COX1, COX2 and ND3 were oligo adenylated with less than 10A's, or lacked stop codons, and had short and variable chain lengths (Fig. 2.2F). However, there was no relationship between the severity of mRNA downregulation and the polyA tail length based on ND3 analysis.

In five weeks old mice, SDS-PAGE experiments indicated a near complete absence of LRPPRC in whole liver extracts (Fig. 2.2A), which was accompanied by a drastic reduction of the LRPPRC binding partner SLIRP (Fig. 2.2B). The abundance of the mitochondria-encoded CIV subunit COX1 was also significantly reduced as compared to control mice, while the abundance of CI (NDUFA9) and CII (SDHA) subunits were normal (Fig. 2.2A-B). Measurement of enzyme activities and BN-PAGE analysis confirmed a severe (>80%) decrease in the activity (Fig. 2.2C), and assembly of CIV (Fig. 2.2D). At this age, the activity of the TCA-cycle enzyme CS, and the amounts of assembled CI, CII, and CIII were similar to controls (Fig. 2.2C-D). However, at ten weeks of age, the amount of all three complexes was higher in *H-Lrpprc*$^{-/-}$ mice, suggesting a compensatory upregulation of other electron transport chain complexes over time (Fig. S2.1).

Figure 2.2 Impact of LRPPRC Deficiency on the OXPHOS System

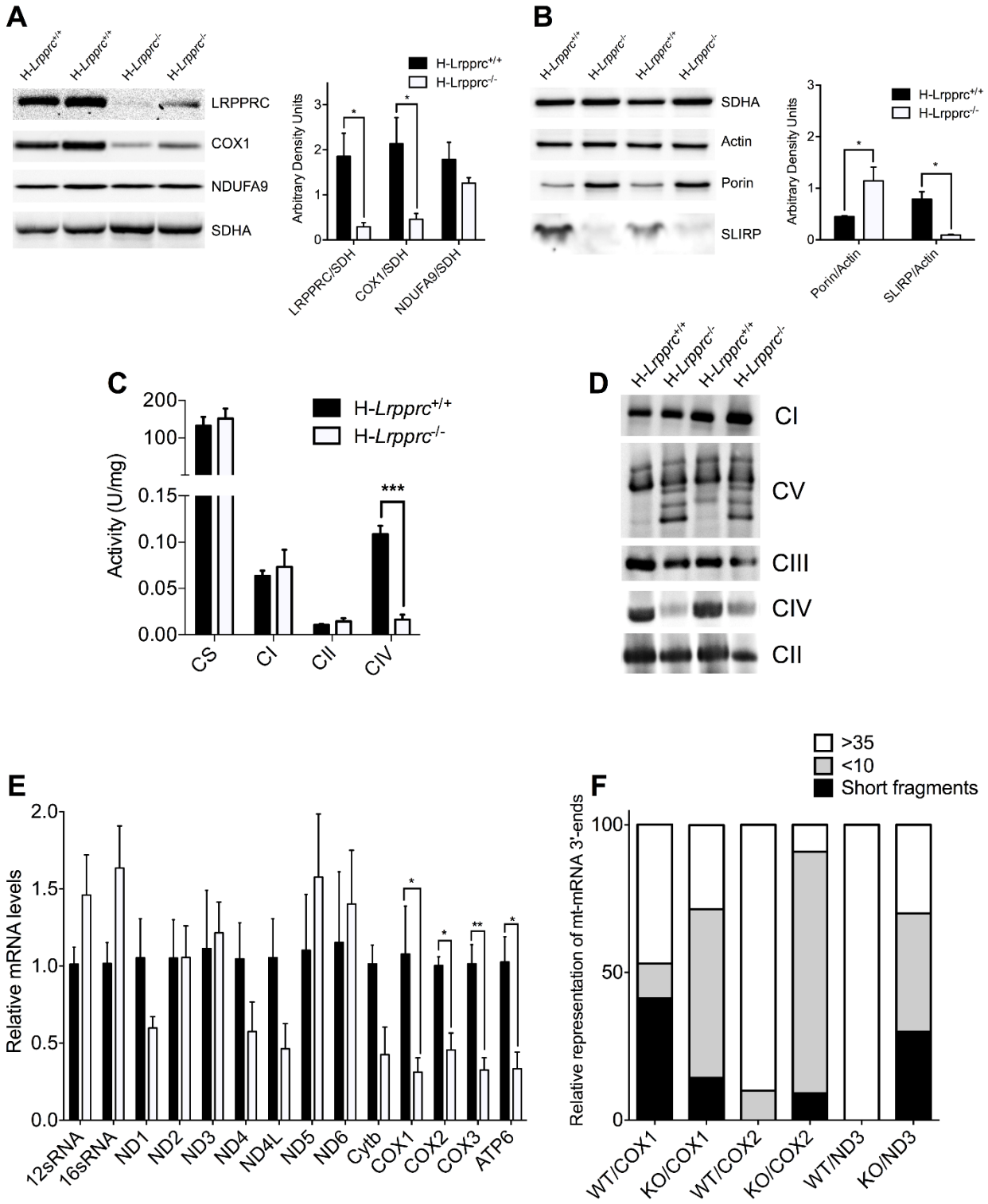

Panel A and B: SDS-PAGE blots and densitometry analysis (n=4-6 mice per group) showing the impact of LRPPRC deficiency on SLIRP and selected components of CI (NDUFA9), CII (SDHA), CIV (COX1), and outer membrane (Porin). SDH and Actin were used as loading controls. Panel C: Activity of OXPHOS (CI, CII, CIV) and TCA cycle (CS) enzymes in isolated liver mitochondria. Enzyme activity measured spectrophotometrically (n= 4-8 mice per experimental group). Panel D:

*BN-PAGE blot of OXPHOS complexes in normal and H-Lrpprc$^{-/-}$ mice. Antibodies to detect OXPHOS complexes were NDUFA9 (CI), SDHA (CII), UQCRC2 (CIII), COXIV (CIV) and ATP5A1 (CV). Data are representative of 4 independent experiments. Panel E: Expression of mitochondrial ribosomal subunits, and of selected mitochondrial and nuclear encoded transcripts in wild type and H-Lrpprc$^{-/-}$ mice. Data were obtained at 10 weeks of age (n=3-5). Panel F: Polyadenylated tail length analysis for COX1, COX2 and ND3 mRNA. Data shows the proportion of mRNA 3' end displaying PolyA short, >10 and >35 chain length in wild type and Lrpprc-knockout mice. Data were obtained at 10 weeks of age (3 experimental replicates per group, using pooled RNA from 3 WT and 3 KO mice). Difference between H-Lrpprc$^{+/+}$ and H-Lrpprc$^{-/-}$ was assessed using one-way ANOVA: *: $p < 0.05$; **: $p < 0.01$, ***: $p < 0.001$.*

We also investigated whether or not in addition to a CIV deficiency, mitochondria from *H-Lrpprc$^{-/-}$* mice also displayed abnormalities at the level of the phosphorylation machinery, particularly the ATPsynthase (CV). As shown in Fig. 2.3A, CV activity was similar in the two experimental groups. However, an important loss of sensitivity to inhibition by oligomycin was noted in *H-Lrpprc$^{-/-}$* samples, suggesting a CV defect. BN-PAGE analysis in DDM-solubilized mitochondrial extracts indicated a reduction in the amount of assembled CV monomers in *H-Lrpprc$^{-/-}$* samples (Fig. 2.3B). Moreover, lower molecular weight ATPα immuno-reactive bands were visible, suggesting an accumulation of sub-assembled CV (Fig. 2.3B). CN-PAGE and in-gel activity measurements were also performed in digitonin-solubilized mitochondria to resolve CV dimers (Fig. 2.3C). These experiments confirmed the assembly defect, and further indicated an important reduction in amount of assembled CV dimers in *H-Lrpprc$^{-/-}$* mice.

Figure 2.3: Impact of LRPPRC Deficiency on ATP synthase (CV) Activity and Assembly.

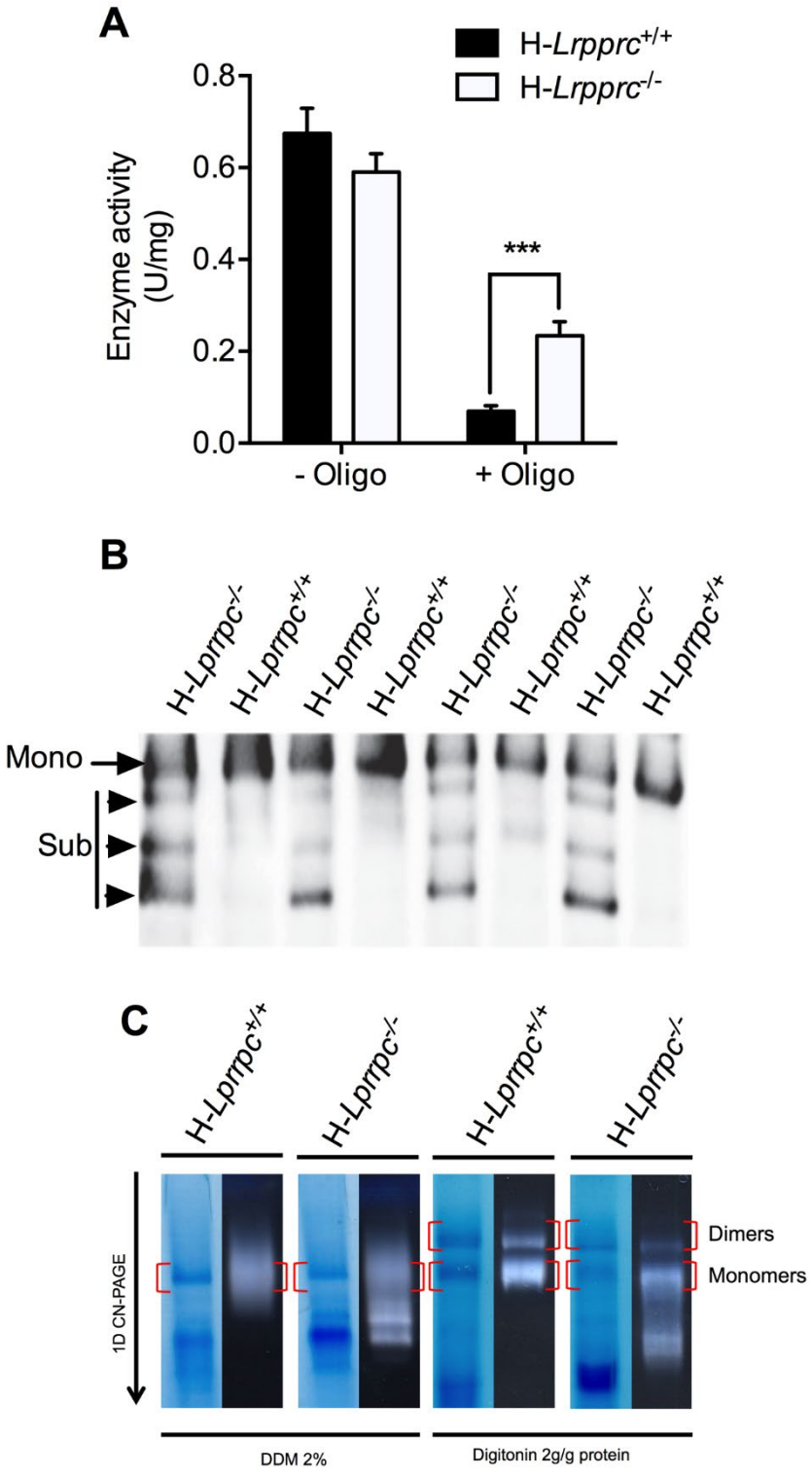

Panel A: Enzyme activity measured spectrophotometrically in mitochondrial extracts in absence and presence of the CV inhibitor Oligomycin (1. 2 µM). Data are expressed as fold changes vs wild type values (n=6-8). Panel B: BN-PAGE blot of DDM-solubilized mitochondria from wild type and H-Lrpprc$^{-/-}$ mice. Membranes were probed with anti-ATPα, Mono: CV monomers, Sub: Sub-assembled CV complexes. Panel C: Supramolecular assembly of CV revealed by in gel activity

*measurement. CN-PAGE was performed in duplicates for each sample. The first gel was used for in gel activity measurements (right lanes for each sample), while the other gel was stained with coomassie blue. Experiments were performed following extraction with DDM, which fully dissociates CV into monomers or with digitonin to preserve dimeric, and oligomeric CV complexes. Blots are representative of at least 3 independent experiments. Significantly different from the H-Lrpprc$^{+/+}$ group: ** $p < 0.01$.*

Respirometry studies were performed to examine the bioenergetic consequences of these OXPHOS defects. While subtle differences in baseline state 2 respiration were apparent, the most striking abnormality was a 40-60% reduction of maximal ADP-stimulated respiration in presence of CI or CII substrates (Fig. 2.4A). This reduction was attributable to the ATP synthase defect, rather than to loss of CIV activity, since mitochondria from control and *H-Lrpprc*$^{-/-}$ mice had similar maximal respiration rates following uncoupling with CCCP (Fig. 2.4A). Since the activity of CIV measured in solubilized extracts was reduced by 80% in *H-Lrpprc*$^{-/-}$ mitochondria (Fig. 2.3A), the surprizing capacity of residual CIV to support normal rates of respiration was investigated by monitoring CIV activity in its native membrane environment using TMPD/Ascorbate as a respiratory substrate (Fig 2.4B). Under those conditions, CIV activity of *H-Lprrpc*$^{-/-}$ mitochondria was only 30% lower than in controls ($p = 0.07$), indicating that the detergent extraction step used for the spectrophotometric assessment of CIV activity amplifies the defect in *H-Lrpprc*$^{-/-}$ mitochondria. Interestingly, CIV was significantly more sensitive to cyanide (Fig 2.4C) in *H-Lrpprc*$^{-/-}$ mitochondria compared to controls, indicating a greater vulnerability to inhibition.

Mitochondria from *H-Lrpprc*$^{-/-}$ mice also showed a 50 % reduction in ADP-stimulated respiration in presence of palmitoyl-CoA (Fig. 2.4A). Because the respiration rates observed with palmitoyl-CoA, are less than half those achieved with CII substrates, this result suggest that in addition to causing OXPHOS defects, *Lrpprc* deficiency has a direct impact on mitochondrial fatty acid oxidation capacity.

Figure 2.4: Impact of LRPPRC Deficiency on the Mitochondrial Bioenergetics Phenotype.

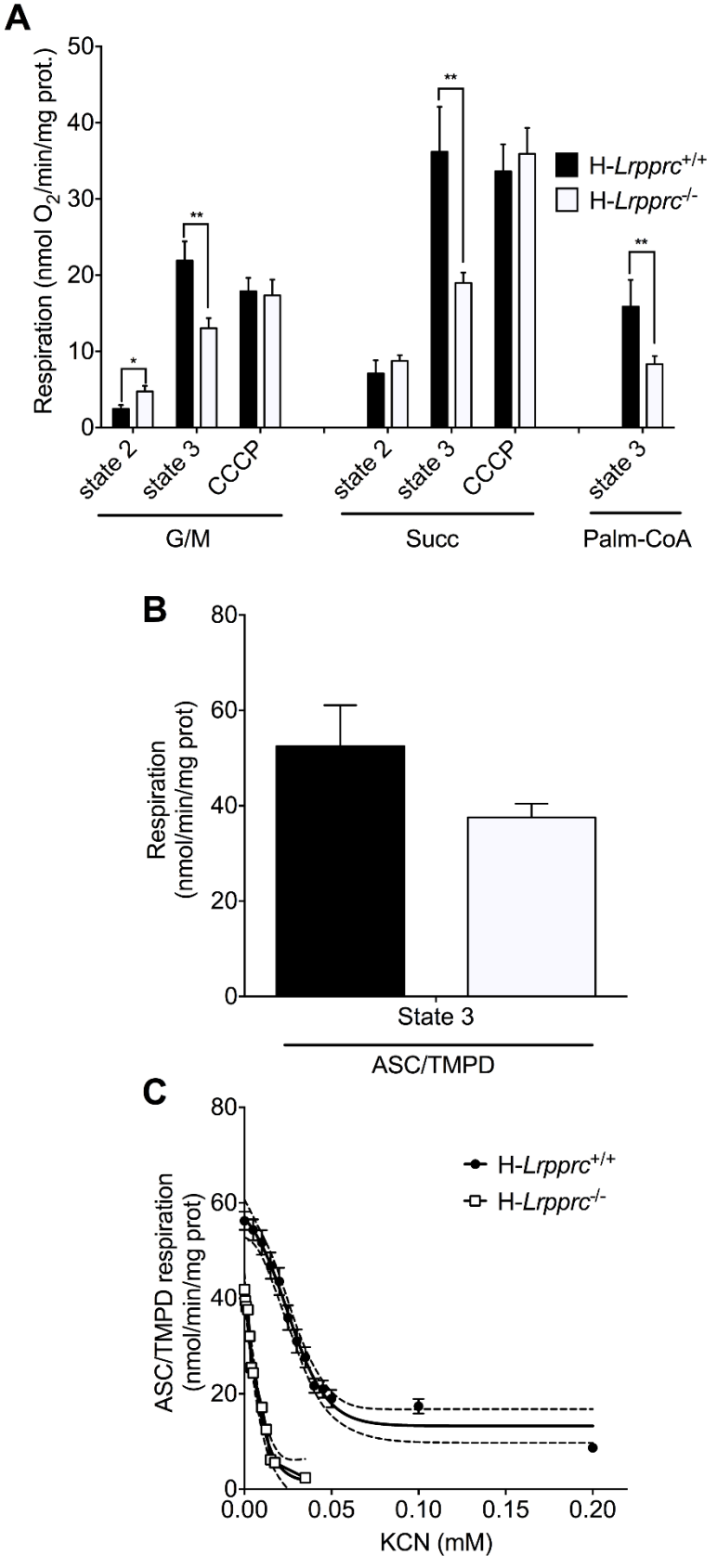

Panel A: Baseline state 2, state 3 (1 mM ADP), and CCCP (0. 03 µM)-uncoupled respiration in liver mitochondria energized with CI (glutamate/malate [GM: 5/2. 5 mM]), CII (Succinate 5 mM) substrates, or following stimulation of long-chain fatty acid oxidation (palmitoyl-CoA [20µM]) (n=5-9). Panel B: Maximal state 3 respiration in isolated liver mitochondria energized with CIV substrates (ascorbate/TMPD: 9mM/0. 9mM) (n= 5). Panel C: Titration of CIV-driven (Ascorbate/TMPD 9/0.9 mM) state 3 respiration with potassium cyanide (KCN) in wild type and H-Lrpprc$^{-/-}$ mitochondria. Best fit and 95% confidence intervals are shown for each dataset (n=5).

2.3.3 The ATP synthase assembly defect associated with LRPPRC deficiency alters the mitochondrial permeability transition pore.

Recent studies suggest that ATP synthase dimers may constitute the structural core of the PTP. [299, 300] In the presence of increased Ca^{2+} concentrations and Pi, which are key triggers of pore opening, Ca^{2+} is suggested to displace Mg^{2+} from catalytic sites on the F1 sector. Under this condition, CV would adopt a conformation that induces pore formation at the interface between the two CV monomers. In this model, the OSCP subunit, located on the lateral stalk of CV is suggested to act as a negative modulator of PTP opening, presumably by limiting access of the Ca^{2+} binding sites on the F1 ATPase. [299, 300] Importantly, this negative modulation is suggested to be relieved when Cyclophilin-D (CypD), a key pore-sensitizing protein present in the mitochondrial matrix, is recruited to OSCP. [299, 300]

Given the CV assembly defect observed in *H-Lrpprc*$^{-/-}$ mice, Ca^{2+} retention capacity (CRC) experiments were performed in presence of Pi to determine whether pore regulation was altered. As shown in Fig. 2.5A and 2.5D, CRC was nearly two-fold greater in mitochondria from *H-Lprrpc*$^{-/-}$ mice, indicating a striking resistance to PTP opening. CRC was also performed in presence of Mg^{2+}, ADP, and oligomycin, to delineate the nature of this resistance. Under this condition, CRC was increased by 2.3 - 2.5 fold in both experimental groups, indicating normal sensitivity in *H-Lrpprc*$^{-/-}$ mitochondria to ligands of the catalytic F1 sector, and the OSCP subunit (Fig. 2.5C and 2.5D). Furthermore, OSCP levels in whole mitochondrial lysate and extracts used for CN-PAGE were similar between the two experimental groups (Fig. 2.5F). CRC experiments were also performed in presence of Cyclosporin-A (CsA), which delays PTP opening by preventing recruitment of CypD to OSCP. [299, 300] As expected, CsA increased resistance to Ca^{2+}-induced PTP opening by more than 2.5 fold in control mice. In contrast, mitochondria from *H-Lrpprc*$^{-/-}$ mice were largely

insensitive to CsA (Fig. 2.5B and 2.5D). Lack of sensitivity to CsA is normally observed in cells that express low levels of CypD[301, 302], and in tissues from CypD-KO mice [303]. However, this was not the case in *H-Lrpprc*$^{-/-}$ mice since total mitochondrial CypD content was twofold higher than in controls (Fig. 2.5E). Together, these data indicate that in *H-Lrpprc*$^{-/-}$ mitochondria the CV assembly defect leads to intrinsic resistance to pore opening, through a loss of regulation by CypD.

Figure 2.5: Impact of LRPPRC Deficiency on the Permeability Transition Pore.

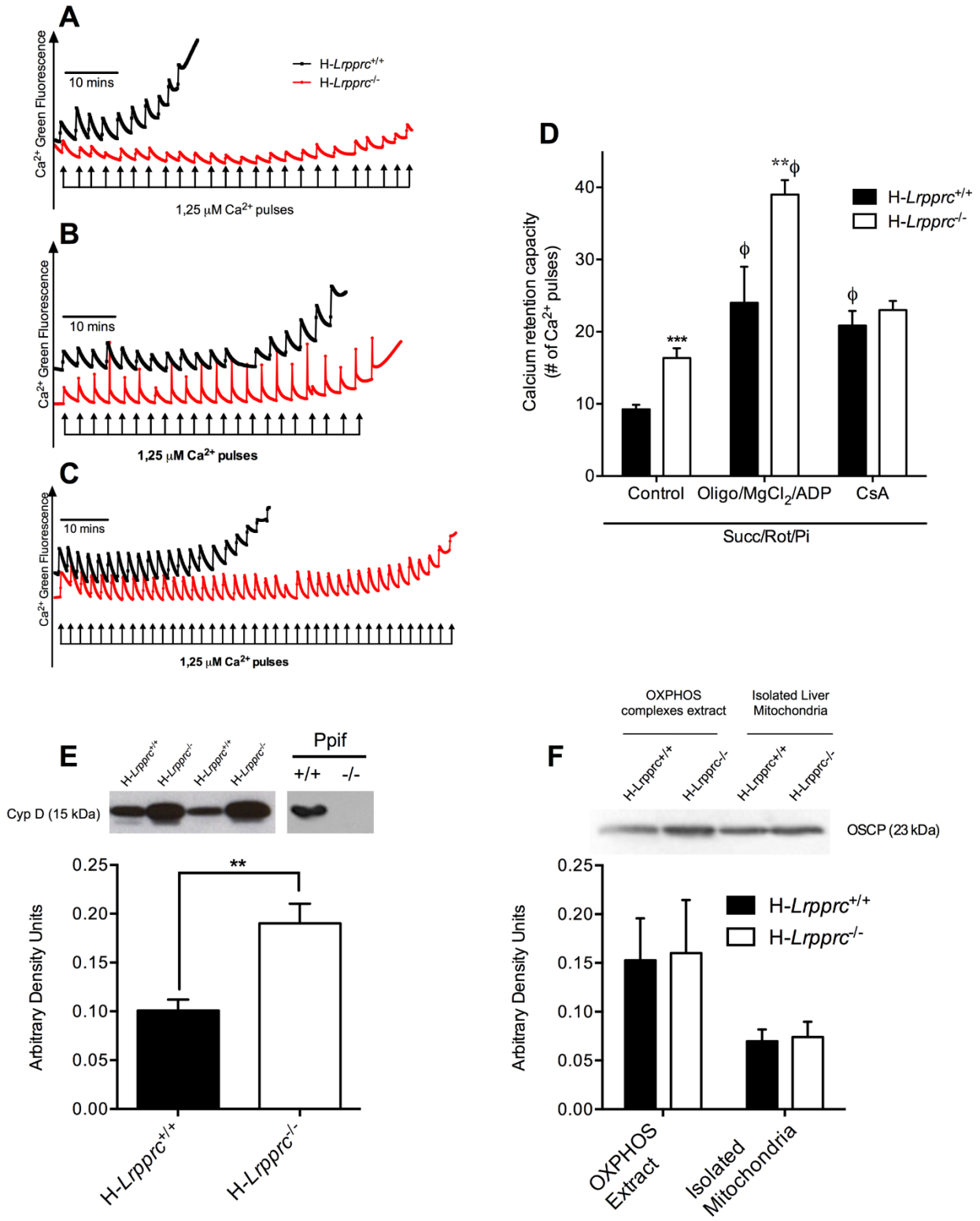

Panel A-C: Representative tracings of mitochondrial calcium retention capacity (CRC) in isolated liver mitochondria exposed to consecutive pulses of calcium (2.5 μmole/mg protein per pulse). All experiments were performed in presence of Succinate (5 mM), Rotenone (1 μM) and Pi (10 mM).

*In panel B and C, the incubation buffer was respectively supplemented with Cyclosporin-A (1μM), or a combination of ADP (12 μM), MgCl2 (0.6 mM) and Oligomycin (27 μM). Panel D: Average Calcium Retention Capacity observed in the three experimental conditions described in A-C (n= 8-11). Panel E: Immunoblot and densitometric analysis of Cyclophilin-D (CypD) content in isolated liver mitochondria from wild type and H-Lrpprc$^{-/-}$ mitochondria. Mitochondrial lysates from wild-type and CypD deficient Ppif$^{-/-}$ mice were run as controls control (n= 6). Panel F: Immunoblot and densitometric analysis of OSCP content in whole mitochondrial lysates and OXPHOS extracts obtained following digitonin treatment. Significantly different from wild type mice: ** p < 0.01, ***: p < 0.001; Significantly different from control condition: ***: p<0.001.*

2.3.4 Hepatic LRPPRC deficiency induces pronounced changes in mitochondrial H_2O_2 dynamics

An important factor believed to underlie cellular dysfunction in genetic mitochondrial diseases is enhanced production of mitochondrial ROS, which can disrupt normal ROS-dependent cellular signal transduction, and trigger oxidative damage to cellular components. [304, 305] To address whether LRPPRC deficiency had an impact on mitochondrial ROS dynamics, net mitochondrial H_2O_2 release was measured in respiring mitochondria. Strikingly, mitochondria from *H-Lrpprc*$^{-/-}$ mice released tenfold less H_2O_2 compared to controls in conditions where superoxide production is promoted through reverse electron flow (*i.e.* during state 2 respiration with succinate ± glutamate/malate) (Fig. 2.6A). To investigate factors underlying this striking difference, mitochondrial membrane potential, which is an important determinant of superoxide production, was measured. As shown in Fig. 2.6B, membrane potential was reduced by 2-3 mV in *H-Lrpprc*$^{-/-}$, which can account for no more than ~7% of the difference in H_2O_2 release observed vs wild type. [306, 307]

To determine whether enhanced ROS scavenging was responsible for the dramatic reduction of mitochondrial H_2O_2 release in *H-Lrpprc*$^{-/-}$ mice, the capacity to scavenge a pulse of exogenous H_2O_2 was also measured directly in respiring mitochondria. This scavenging rate represents the sum of the rate of all mitochondrial H_2O_2 consuming systems. Surprisingly, mitochondria from *H-Lrpprc*$^{-/-}$ mice were completely unable to scavenge exogenous H_2O_2 (Fig. 2.6C). The level of key antioxidant enzymes was therefore measured. The expression of SOD2 was similar in the two groups, while the levels of catalase were modestly reduced, suggesting no major collapse of the

antioxidant machinery (Fig. 2.6D). This observation was overall compatible with results of the H_2O_2 release experiment, since a collapse of antioxidant systems would have caused an increase in H_2O_2 release, not a drastic reduction as observed. Together, the lack of endogenous H_2O_2 emission and exogenous H_2O_2 scavenging pointed to a major barrier hindering H_2O_2 diffusion in and out of mitochondria in *Lrpprc*-deficient mice.

To address this possibility, respiring mitochondria were titrated with increasing concentration of digitonin (0.01 to 0.03%) to achieve progressive membrane permeabilization. As shown in Fig 2.6E, addition of digitonin to *H-Lrpprc*$^{-/-}$ mitochondria progressively raised the amount of H_2O_2 released in the media to the level observed in non-permeabilized mitochondria from control mice, suggesting trapping of H_2O_2 in mitochondria from *H-Lrpprc*$^{-/-}$ mice. To test this hypothesis, H_2O_2 production was measured in inside-out sub-mitochondrial, where respiratory chain complexes generate H_2O_2 directly in the incubation medium, bypassing the normal diffusion step across the lipid bilayer. In this condition, H_2O_2 release was actually higher in *H-Lrpprc*$^{-/-}$ compared to control (Fig. 2.6F), confirming that LRPPRC deficiency induced a strong reduction of mitochondrial permeability to H_2O_2.

Figure 2.6: Impact of LRPPRC Deficiency on Mitochondrial H_2O_2 Dynamics.

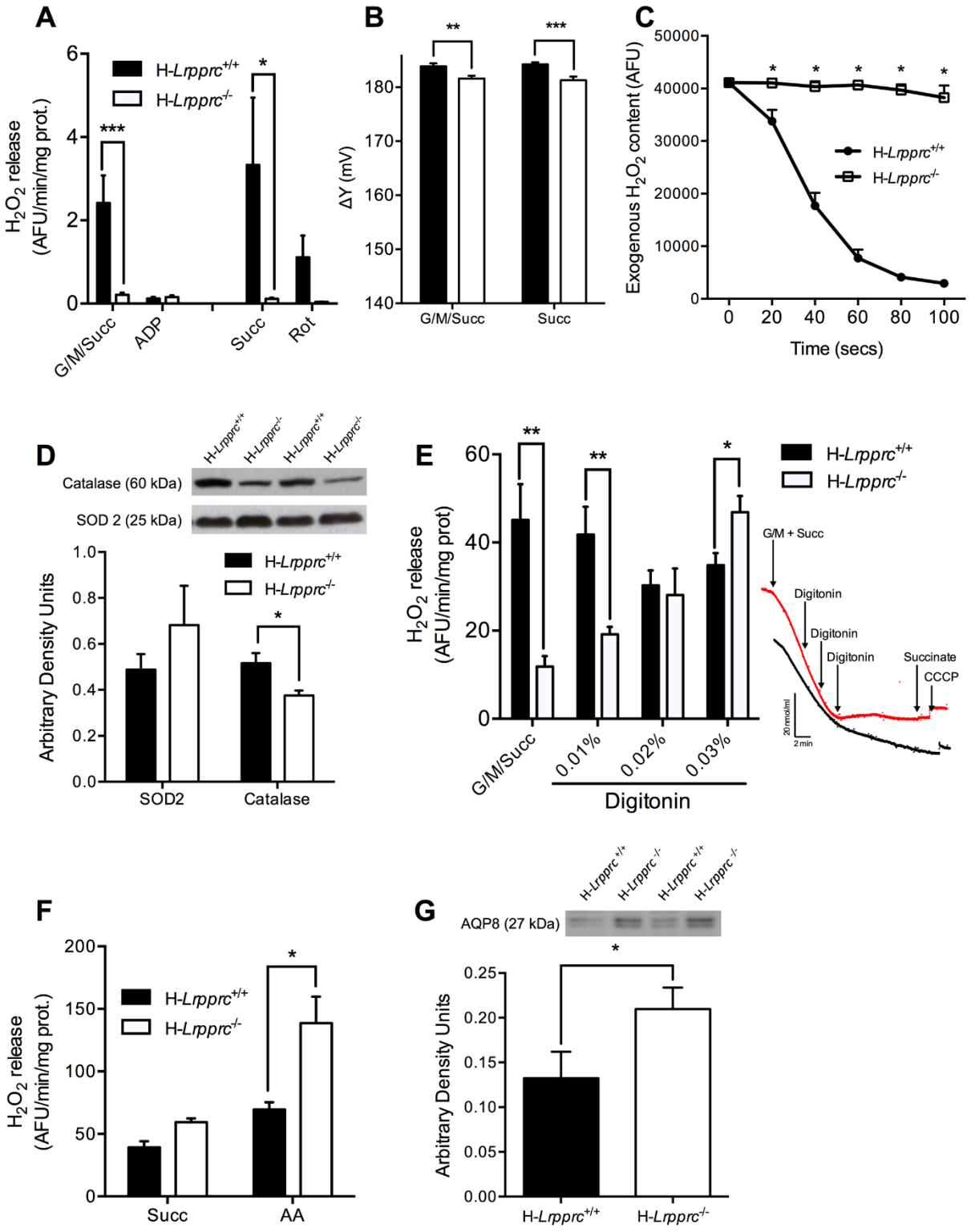

Panel A: Net H_2O_2 release from mitochondria under state 2 and state 3 (1 mM ADP) conditions in presence of substrates for CI + CII (G/M/Succ: 5/2. 5/5 mM) (n=8-16). In some experiments (n=3), net H2O2 release was measured in presence of succinate alone (Succ: 5 mM) and rotenone (1 µM) was added to confirm that H_2O_2 release occurred mainly through reverse electron backflow to CI.

*Panel B: Mitochondrial membrane potential measured on respiring isolated liver mitochondria energized with complex I + II (G/M/Succ: 5/2. 5/5 mM) or complex II (succinate 5mM) substrates. (n= 6). Panel C: Kinetics of scavenging of an exogenous H_2O_2 load (3 nmoles) by mitochondria energized with CI substrates (Gutamate/Malate: 50/20 µM) (n=6). Panel D: Immunoblot and densitometric analysis of SOD2 and catalase content in mitochondria from wild type and H-Lrpprc$^{-/-}$ mice (n=6). Panel E: Net H_2O_2 release from mitochondria under state 2 conditions in presence of substrates for CI+CII (G/M/Succ: 5/2.5/5 mM). Following baseline measurements, digitonin was progressively added and changes in H_2O_2 release were monitored (n= 6). Insets in panel E shows progressive inhibition of respiration in H-Lrpprc$^{+/+}$(black tracing) H-Lrpprc$^{-/-}$ (grey tracing) in response to progressive permeabilization with digitonin. Panel F: H_2O_2 production measured in sub-mitochondrial particles (SMP) in presence of succinate (5 mM) alone, or with Antimycin-A (AA: 2 µM) (n= 4). Panel G: Immunoblot and densitometric analysis of AQP8 content in mitochondria from wild type and H-Lrpprc$^{-/-}$ mitochondria (n=6). Significantly different from wild type mice: * $p < 0.05$, ** $p < 0.01$, ***: $p < 0.001$.*

To investigate the underlying mechanism, the expression of aquaporin-8 channels, which are known to facilitate the diffusional transport of H_2O_2 across the inner mitochondrial membrane [308, 309] was measured. AQP-8 content was 35% higher in *H-Lrpprc$^{-/-}$* mice, indicating that changes in AQP8 expression were not responsible for the altered H_2O_2 diffusion (Fig. 2.6G). Non-targeted lipidomic analysis was also performed to examine potential changes in the membrane lipid composition. In *H-Lrpprc$^{-/-}$* mitochondria, 65 features reached the established significance threshold (FC>2 and FDR<5%, corresponding to a *p* value of 0.01) (Fig 2.7A). From these features, thirty-three distinct lipids were identified in *H-Lrpprc$^{-/-}$* mitochondria of which 14 were upregulated and 18 downregulated. Interestingly, increased lipids were essentially glycerophospholipids mostly represented by phosphatidylcholines (PC) and few phosphatidylethanolamine (PE), while decreased lipids species were more diversified. The latter included in particular 7 triglycerides, 2 diglycerides, 6 sphingomyelins, as well as cholesterol and cholesterol sulfate (Fig 2.7B). Together, these results indicated that loss of LRPPRC triggers broad changes in the lipid composition of mitochondrial membranes, which likely underlie the impairment of H_2O_2 diffusion in and out of mitochondria.

Figure 2.7: Impact of LRPPRC Deficiency on Mitochondrial Membrane Lipid Composition.

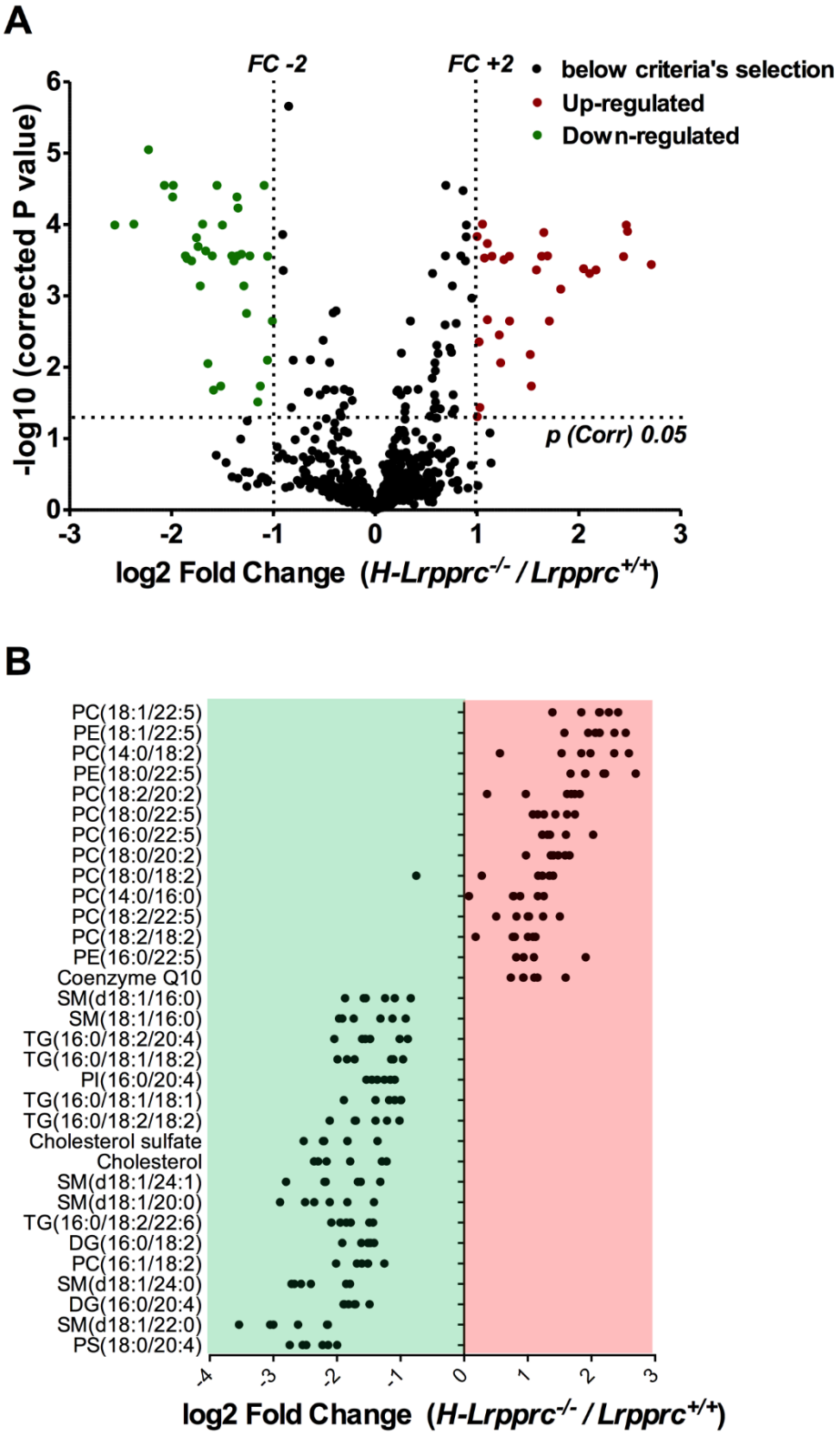

Panel A: Volcano plot showing entities that were identified as differentially expressed, either up or downregulated, in H-Lrpprc$^{-/-}$ mitochondria according to the following selection criteria: fold change > 2 and corrected p value < 0.05. Panel B: Individual lipid species found to be significantly up or down-regulated on H-Lrpprc$^{-/-}$ mitochondria. Each dot represents a Log2-transformed ratio

of an individual H-Lprrpc$^{-/-}$ mitochondria relative to the mean value obtained in the wild type group (n=6 per group).

2.4 DISCUSSION

Our results reveal that specific loss of LRPPRC in the liver induces a generalized growth delay, and typical histological features of severe mitochondrial hepatopathy. At the molecular level, LRPPRC deficiency causes destabilization of polyadenylated mitochondrial mRNAs, resulting in a severe CIV and CV assembly defect that compromises OXPHOS capacity. Importantly, our data show that the impact of LRPPRC deficiency is not limited to OXPHOS, but also includes impairment of long-chain fatty acid oxidation, a striking dysregulation of the mitochondrial permeability transition pore, and an unsuspected alteration of trans-membrane H_2O_2 diffusion. Dysregulation of the PTP and changes in mito-cellular H_2O_2 exchanges can be traced to the ATP synthase assembly defect, and to changes in the lipid composition of mitochondrial membranes, revealing novel intricacies of mitochondrial OXPHOS deficiencies that have potential clinical impact.

2.4.1 Bioenergetics phenotype of hepatic LRPPRC deficiency.

Previous studies have shown that CIV activity is reduced by 80% in liver samples from LSFC patients [85, 113], which is expected to have severe bioenergetic consequences. Yet, some patients survive several years, with no signs of chronic liver dysfunction despite the presence of steatosi. [91] Our data suggest that this may be explained in part by the fact that biochemical measurement of CIV activity following detergent extraction exaggerates the actual severity of the enzyme defect. Indeed, when measured in intact mitochondria, our data shows that CIV activity was only reduced by 30% in LRPPRC-deficient livers, as opposed to 80% when measured following detergent extraction. This significant residual activity was sufficient to sustain normal respiration with substrates feeding the ETC at the level of CI or CII, albeit at a higher percentage of maximal CIV capacity, which likely put cells at greater risk of bioenergetic crisis in presence of factors that negatively modulate CIV activity *in vivo*. [93]

Sensitivity of CIV to inhibition in presence of detergents has been reported previously in cells from *Surf1* patients [310], although the underlying mechanisms were not established. One factor that likely plays a role is membrane lipids which are known to be crucial for proper assembly, and function of ETC complexes. [238, 239] For CIV in particular, mass spectrometry coupled to X-ray structure analysis has identified thirteen lipids including CL, PCs, PEs, PGs and TGs that are integral to the complex, and likely play a structural and functional role. [311] Interestingly, one

intrinsic PC [PC(16:1/18:2)], and three TGs [TG(16:0/18:1/18:1); TG(16:0/18:1/18:2) believed to stabilize the dimeric state of CIV, and the assembly between the three core subunits (COX1-3), and the nuclear encoded subunits were significantly reduced in *H-Lrpprc*$^{-/-}$ mitochondria. These results suggest that the reduced abundance in key structural lipids could increase the lability of CIV in LRPPRC-deficient mitochondria, making the enzyme more vulnerable to inhibition in presence of detergents. An interesting question that remains to be investigated is whether the reduced abundance of these lipids is simply a consequence of the lower level of assembled CIV. However, the fact that several other lipids are also modified in *H-Lrpprc*$^{-/-}$ mitochondria suggests that it is part of a more global remodelling of membrane lipid composition.

Results from our study also show that the impact of LRPPRC-deficiency in the mouse liver is not limited to CIV but also includes a CV assembly defect that was largely responsible for the impairment of OXPHOS capacity we observed. While a similar CV defect was reported following Cre-mediated inactivation of *Lrpprc* in the mouse heart [126], recent results from our group indicate that this abnormality is likely absent in the liver and heart from LSFC patients. Indeed, the only defect observed is a severe (80%) reduction in CIV assembly in the liver, and a more moderate (50%) reduction in the heart [113] with no signs of other OXPHOS complexes being affected. Absence of CV defect was also recently reported in patients with a mutation of LRPPRC that is distinct from the one causing LSFC. [87] This difference could be explained by the presence of greater residual amounts of LRPPRC in patient tissues compared to knockout mice tissues, which would be sufficient to allow proper assembly of CV. However, we consider this possibly unlikely since in LSFC patients the levels of LRPPRC in both organs is either undetectable, or extremely low (<10%) [113]. Moreover, when the level of LRPPRC is further decreased in patient fibroblasts using siRNAs, it is the assembly of all OXPHOS complexes, not just CV, that is compromised. [122] Therefore, the CV assembly defect reported in the liver and heart likely represents a species-specific response to LRPPRC deficiency.

In addition to affecting OXPHOS directly, our data shows that LRPPRC deficiency impairs mitochondrial long-chain acyl-CoA oxidation which is consistent with our recent metabolic profiling of plasma from LSFC patients. [90] Indeed, we identified elevated circulating acylcarnitines irrespective of chain length suggesting the existence of multiple defects in mitochondrial fatty acid β-oxidation. Because oxidation of long-chain fatty acid is controlled by steps located upstream of the ETC [312, 313], this impairment is unlikely to be explained by the

reduction of OXPHOS capacity *per se*. Although we did not pursue this further, previous studies indicate that knockdown of *Lrpprc* in primary hepatocytes does not lower the expression of key genes involved in mitochondrial fatty acid uptake and β-oxidation, despite reducing overall cellular fatty acid uptake, and oxidation. [118, 314] It is therefore likely that post-translational changes secondary to the OXPHOS defect, or broader changes in lipid metabolism revealed by our lipidomic analysis, underlie the reduced fatty acid uptake/oxidation capacity and drive steatosis in the *Lrpprc*-deficient liver.

2.4.2 PTP dysregulation in LRPPRC-deficient mitochondria

The PTP, located in the mitochondrial inner membrane, plays an important role in the physiological regulation of ROS production, mitochondrial Ca^{2+} release, and cellular differentiation, as well as pathological activation of cell death (see [315] for recent review). Despite being well characterized functionally, the molecular identity of the PTP continues to be a subject of debate. Several molecular candidates have been proposed including ANT [316], VDAC [317] and the Pi carrier [318]. However, none of these putative pore components has survived experimental scrutiny. Recently, studies in yeast, and mammalian cell models have provided strong evidence that CV acts as the core constituent of the PTP. [300, 319, 320] Our study, by showing a striking dysregulation of the PTP in a mouse model of primary CV defect, provides support for this model. Interestingly, in fibroblasts from LSFC patients, we previously reported an enhanced sensitivity to PTP opening in presence of Ca^{2+} [93], which may be due to the absence of CV assembly defects in patient cells.

The molecular mechanism by which CV shifts from an ATP synthetizing unit to a high conductance non-specific pore remains largely unknown. [299, 321] One model proposes that the PTP forms at the interface of CV dimers. [299, 322] At this level, several subunits of the Fo sector (a, e, f, g and A6L) bind together, and stabilize the central c-ring of the Fo sector, and the lateral stalk of the F-ATPase [323-326], which contributes to the formation of 86°-angled CV dimers that define areas of high membrane curvature at the level of cristae ridges. [327-329] In the presence of increased Ca^{2+} concentrations, Ca^{2+} is suggested to displace Mg^{2+} from catalytic sites on the F1 sector. Under this condition, CV would adopt a conformation that induces pore formation at the interface between the two CV monomers. [299, 322] The exact mechanism of pore formation currently remains unclear. The c-ring was initially proposed as the pore-forming channel [320], but recent studies

strongly argue against this possibility [330]. Subunits of the Fo sector that are required for the stabilization of CV dimers [331] however remain serious candidates [299]. Results showing that knockout of subunits e and g induces a strong resistance to PTP opening argue in favor of this model. [319] Irrespective of the exact mechanism of pore formation, studies show that CV is regulated by binding of CypD to the OSCP subunit of the lateral stalk, which induces a conformational change that facilitates pore formation. [300, 332]

Our data shows that the CV assembly defect associated with the loss of LRPPRC induces a marked resistance to PTP opening that can be explained by a loss of control of PTP sensitization by CypD. This effect is not related to reduced CypD expression, as the protein level is upregulated twofold in absence of LRPPRC. Since OSCP levels were comparable across the two experimental groups, and that OSCP is present in CV monomers and dimers following cardiac inactivation of *Lrpprc* [126], it is also unlikely that lack of CypD binding sites on CV is responsible for pore desensitization in LRPPRC deficient mitochondria. One possibility is that post-translational modifications of OSCP, such as a reduction of K40 acetylation, could impair CypD recruitment, as recently shown [333]. Alternately, loss of mitochondrially-encoded subunits a (ATP6) and A6L (ATP8) (Fig 2.2A and [126]) and potentially other associated Fo subunits may lead to alterations in the assembly between the Fo sector, and the peripheral stalk which prevent CypD binding from exerting its pore-promoting conformational changes. More detailed structure-function studies are required to elucidate the precise mechanisms involved.

2.4.3 Altered ROS dynamics in LRPPRC-deficient mitochondria

Oxidative stress is considered a significant contributor to the pathogenesis of OXPHOS defects. [304, 305] Mitochondrial ROS production, and its consequences on signaling pathways, and mitochondrial/cellular injury is generally viewed as the result of a disequilibrium between the production of ROS by dysfunctional ETC complexes, and their elimination by various mitochondrial antioxidant systems. However, our results show the importance of considering mitochondrial membranes as potential diffusion barriers that can affect mito-cellular ROS dynamics in pathological states. Indeed, we show that lack of LRPPRC drastically reduced the capacity of mitochondria to release and take-up H_2O_2. This effect occurred in absence of major remodelling of key antioxidant enzymes (Catalase and SOD2) and was abolished by progressive permeabilization with small amounts of digitonin. Furthermore, mitochondrial $O_2^{-\bullet}$ and H_2O_2 production was higher

in LRPPRC-deficient mice when measured in inside-out submitochondrial particles, suggesting that reduced membrane permeability to H_2O_2 in LRPPRC-deficient livers confined ROS to the mitochondrial compartment.

Although H_2O_2 is generally considered to diffuse freely across membranes, increasing evidence suggest that this process may be regulated. One of the mechanisms involves diffusion-facilitating channels of the aquaporin family, particularly AQP8 isoforms, which are expressed in mitochondrial membranes, where they are thought to assist diffusion of water, NH_3, and H_2O_2. [308, 309] Knockdown of AQP8 was shown to inhibit mitochondrial H_2O_2 release [309], and cause mitochondrial dysfunctions including oxidative stress, respiratory impairments, and loss of membrane potential. [308, 309] Based on these results, lower expression of AQP8 might have been expected in *H-Lrpprc*$^{-/-}$ mitochondria; however, our results indicate that AQP8 expression was in fact higher in absence of LRPPRC, indicating that this is not the primary mechanism responsible for the impaired diffusion of H_2O_2. In fact, our results would suggest that in absence of LRPPRC AQP8 expression may be upregulated in an attempt to compensate the H_2O_2 diffusion deficit.

In view of our results, changes in the lipid composition of membranes in LRPPRC-deficient mitochondria appear as the main factor responsible for the impaired diffusion of H_2O_2. Although the precise mechanism remains unclear, one possibility is that loss of membrane cholesterol, which is already present at low levels in mitochondrial membranes [34], contributes to the H_2O_2 diffusion impairment. Lipid composition and their arrangement in the bilayer, as well as physicochemical parameters of lipids surrounding cholesterol molecules, might have an impact on lipid packing density and thickness which could eventually lead to a packing defect. In *H-Lrpprc*$^{-/-}$ mitochondria, the significant decrease in cholesterol as well as the increase amount in PC-containing polyunsaturated FA highlighted perturbations on mitochondrial membranes physical properties thereby promoting increased membrane fluidity, decreased thickness and major packing defects [33, 334], which could interfere with H_2O_2 diffusion. Support for a role of cholesterol and its lipid interactome in affecting trans-membrane H_2O_2 diffusion comes from studies in yeast showing that downregulation of ergosterol (the main sterol in in fungi and protozoa) during the stationary phase reduces H_2O_2 diffusion into cells, while upregulation of ergosterol content during exponential growth facilitates H_2O_2 diffusion out of cells. [335, 336] Studies in yeast also showed that gain of function mutation of the ergosterol synthesis pathway enhanced H_2O_2 permeability. [337] Together, these data have led to the suggestion that in yeast, modulation of ergosterol content is part of a

cellular strategy to manage oxidative stress in the face of pronounced metabolic transitions. [335-337] Interestingly, in mammalian erythrocytes, upregulation of membrane cholesterol content was found to decrease the trans-membrane diffusion of oxygen [338], which is compatible with a role of cholesterol in facilitating the diffusion of small molecules. As for cholesterol sulfate, it is suggested to play a role in the stabilization of erythrocyte membrane [339], but whether its downregulation could alter diffusion is unknown. It should however be noted that under normal healthy conditions, mitochondrial membranes may not constitute a major diffusion barrier, since in our experiments progressive permeabilization of mitochondrial membranes with digitonin did not reveal evidence of H_2O_2 trapping in wild-type mitochondria. Pathological loss of cholesterol and specific changes in the lipid composition of mitochondrial membranes may be required to observe a diffusion limitation.

In summary, our mouse model of hepatic LRPPRC deficiency reveals that genetic OXPHOS defects can be accompanied by broad and surprising phenotypic alterations that cannot easily be predicted based on knowledge of the causal genetic defect. From a clinical perspective, our results also indicate that investigation of PTP dysregulation is warranted in patients harboring CV assembly defects. Furthermore, the substantial remodeling of the lipid composition of mitochondrial membranes in our mouse model suggests that membrane lipidomics should be performed in patients with genetic OXPHOS defects as this might assist diagnosis and have significant impact on mitochondrial functions and the disease phenotype.

2.5 MATERIALS AND METHODS

2.5.1 Animal care and generation of conditional Lrpprc knockout mice

All experiments on animals were approved by the Université de Montréal Institutional Animal Care Committee and conducted according to the directives of the Canadian Council on Animal Care. Mice were maintained in ventilated cage racks by groups of 4-6 mice. All mice were kept on a regular 12h-12h light-dark cycle, and had access to food and water *ad libitum*. To disrupt LRPPRC expression in the liver, the *Lrpprc* knock-out mice line *Lrpprc*$^{tm1a(KOMP)Wtsi}$ produced in C57BL/6N embryonic stem (ES) cells was acquired from KOMP repository (University of California, California). The mutated locus was transmitted through the germline to obtain heterozygous *Lrpprc*$^{+/lox\text{-}neo}$ animals. These animals were then bred with *flp* producing animal B6(C3)-Tg(Pgk1-FLPo)10Sykr/J (The Jackson Laboratory) in order to excise the neomycin resistance cassette, recreating a LRPPRC protein producing locus having *lox* sites in intron 3 and 5. The resulting *Lrpprc*$^{+/loxP}$ mice were then mated to get homozygous *Lrpprc* $^{loxP/loxP}$ mice and only animals that were exempt of the *flp* allele were kept. To achieve liver specific inactivation of *Lrpprc*, *Lrpprc* $^{loxP/loxP}$ mice were crossed with B6. Cg-Tg(Alb-cre)21Mgn/J (The Jackson Laboratory) mice producing the *Cre* recombinase under the control of the albumin promoter and bred to homozygous state, Hep-Cre$^{cre/cre}$. These mice were then bred with the *Lrpprc* $^{loxP/loxP}$ to generate double homozygous mice Hep-*Lrpprc*$^{loxP/loxP;cre/cre}$. However, in order to simultaneously generate homozygous knockout and wild type littermate controls, Hep-*Lrpprc*$^{loxP/loxP;cre/0}$ individuals were inter-crossed.

All animals were genotyped at weaning via tail biopsies (20 mg/ml), which were incubated at 55°C for 4 h in buffer (50 mM Tris, 30 mM EDTA, and 0.25% SDS) containing (1,000 µg/ml) proteinase K (Sigma, St. Louis, MO). After digestion, the samples were diluted 1:250 in DNAse/RNAse free water along with 15 mg chelex-resin (Bio-Rad Laboratories, Hercules, CA) and heated at 95°C for 5 min. They were then analyzed in duplicate by quantitative qPCR with 2X Platinum SYBR Green qPCR Supermix-UDG, according to the manufacturer's specifications (Invitrogen Life Technologies, Carlsbad, CA). Cycling was achieved in a MX3005p cycler (Stratagene, Mississauga, Ontario, Canada) with the following conditions: 95°C for 10 min and 40 cycles of 95°C for 30 s, 47°C for 45 s, and 72°C for 45 s. The primers for qPCR were designed to target the Cre gene cassette (reverse: CCAGCTTGCATGATCTCC; forward:

CGCTAAGGATGACTCTGG), and the corresponding PCR signal was expressed relative to cyclophilin A (*Ppia*) genomic DNA (reverse: GCCGCCAGTGCCATTATG; forward: CCGATGACGAGCCCTTGG). Lox allele containing LRPPRC was detected by end-point PCR. The primers for PCR were designed to target the lox containing neighbouring sequences located in the third LRPPRC intron (reverse: ATGAGTTCGATTCCCAGCAAC; forward: CGTAGGCAGTATCCACAC). The lox-containing PCR amplicon is 474 bp while the endogenous amplicon is 386 bp. Animals used (males and females) for experiments were euthanized by cervical dislocation at 5 or 10 weeks of age following an overnight fast. Unless indicated otherwise, results presented were obtained using 5 weeks-old mice.

2.5.2 Histology

Haematoxylin/Eosin: For a general assessment of histopathology, livers were rapidly excised and fixed overnight in 10% formalin. Samples were embedded in paraffin and 5µm thick sections were stained with Haematoxylin and Eosin.

Oil Red'O: To quantify steatosis, livers were snap frozen in liquid nitrogen for Oil red'O staining. 10µm thick sections were fixed in 10% neutral buffered formalin for 5 minutes, washed 4 times in distilled water and stained for 30 minutes at room temperature with either Oil Red'O (working solution: 0.5% Oil Red'O in propylene glycol) or propylene glycol. Following thorough rinsing with distilled water, slides were mounted using Pro-long Gold anti-fade reagent with DAPI (Invitrogen) and examined by confocal microscopy. Lipid droplet number and morphology in individual hepatocytes was quantified using ImageJ (NIH).

COX/SDH activity: Cytochrome *c* oxidase (COX) and succinate dehydrogenase (SDH) activity staining was adapted from[340]. Serial cryostat sections were cut 10µm thick, brought to room temperature and were left to air dry for 1 hour. The first section of each sample was incubated for COX activity staining (in mM: 3.75 DAB, 0.1 Cytochrome C, pinch of catalase in 0.1 NaPi buffer, pH 7.0) for 30 minutes at 37°C. The second section was incubated for SDH activity staining (in mM: 130 Na- Succinate, 0.2 PMS, 0. 1 Sodium Azide, 1.5 NBT in 0.1 NaPi buffer, pH 7.0) for 30 minutes at 37°C. The third section was incubated for COX activity staining buffer first, washed with distilled water and incubated for SDH activity staining buffer to achieve double staining.

Sections were washed with distilled water and mounted with glycerol gelatine. Slides were examined by light microscopy.

2.5.3 Transmission electron microscopy

Following anaesthesia (8% chloral hydrate; 600mg/kg), mice were perfused with 10ml PBS and 5ml 2.5% glutaraldehyde via the vena cava. Livers were excised, sliced and fixed over night at 4°C in 2.5% glutaraldehyde in phosphate buffer. After sample preparation, 90-100 nm thick sections were mounted onto a 200 mesh copper grid (Electron Microscopy Sciences) and imaged with a FEI Tecnai 12 120 kV transmission electron microscope equipped with an AMT XR80C 8 megapixel CCD camera as previously described. [341]

2.5.4 Preparation of Isolated Liver Mitochondria

Liver mitochondria were isolated as described [342] with slight modifications. Following cervical dislocation, livers were rapidly excised and transferred to cold isolation buffer (in mM: 300 sucrose, 10 Tris-HCl, 1 EGTA-Tris Base; pH 7.2). The tissue was minced using scissors and 4mm^2 pieces were allowed to sediment. The decanted suspension was transferred in 15ml Potter-Elvehjem homogeniser and homogenised with 5 strokes, the pestle rotating at 500rpm. The homogenate was centrifuged 10 minutes at 1000Xg, 4°C and the supernatant was transferred in a clean tube and re-centrifuged at the same speed. The resulting supernatant was transferred using a syringe attached to a metal filling cannula and centrifuged 10 minutes at 8000Xg, 4°C. The supernatant was aspirated and the pellet was re-suspended in suspension buffer (in mM: 300 sucrose, 10 Tris-HCl, 0.05 EGTA-Tris Base; pH 7.2). The suspension was centrifuged 10 minutes at 8000Xg, 4°C; and the last two steps repeated twice. The final pellet was re-suspended in 300µl suspension buffer and kept on ice until use.

2.5.5 Preparation of Sub-mitochondrial Particles

Submitochondrial particles were prepared as in [343-345]. Frozen isolated liver mitochondria were thawed on ice and centrifuged for 10 minutes at 8000Xg, 4°C. The pellet was re-suspended in sonication buffer (in mM: 250 sucrose, 10 K-phosphate, 10 Tris-HCl, 2 EGTA, 2 $MgCl_2$; pH 7.4) and sonicated 5x15 seconds using a Branson sonicator at 50% amplitude. The suspension was centrifuged 10 minutes at 10 000Xg, 4°C; the supernatant was transferred and centrifuged 60

minutes at 100 000Xg, 4°C in a swinging-bucket rotor. The final pellet was re-suspended in a small volume (25µl or less) of suspension buffer (in mM: 1 EDTA, 1 $MgCl_2$, 75 sodium phosphate; pH 7.4) and kept on ice until use.

2.5.6 Mitochondrial Functions

Respirometry: Respiration was measured using Clark-type electrodes at 23 ºC under continuous stirring based on previous protocols [342]. Mitochondria (0.3 mg prot. /ml) were suspended in respiration buffer (in mM: 10 KCl, 5 K_2HPO_4, 10 MOPS, 9 Pi, 2,5 $MgCl_2$, 1mg/ml BSA; pH 7.4). Following baseline recording, respiration was measured following sequential additions: *i)* glutamate + malate (5:2. 5 mM) for Complex-I (CI) or succinate (5 mM) for complex-II (CII), *ii)* ADP (1 mM), and *iii)* and carbonyl cyanide m-chlorophenylhydrazone (CCCP: 0.03 µM). To measure to oxidation of long-chain fatty acids, respiration was measured following supplementation with palmitoyl-carnitine (20 µM) in presence of malate (2.5 mM) and ADP (1 mM). To measure the activity of complex-IV (CIV) under native conditions, maximal ADP stimulated respiration was measured in presence of TMPD/Ascorbate (5/0.3 mM), and titrated with increasing concentrations of potassium cyanide, which allowed to correct respiration values for the auto-oxidation of TMPD/Ascorbate.

Ca^2- induced opening of the permeability transition pore (PTP): Mitochondria (0.5 mg prot. /ml) were incubated in a sucrose buffer (in mM: 250 sucrose, 0.005 EGTA-Tris base, 10 Tris-MOPS; pH 7.55) containing succinate (5 mM), rotenone (1 µM) and Pi (10 mM). Changes in extra-mitochondrial calcium concentration were monitored fluorimetrically (Hitachi, F4500 spectrofluorometer) using Calcium-green 5N (1 µM, ex–em: 505–535 nm) as described previously[343]. Residual calcium concentration was adjusted to the same level at the beginning of every experiment by adding a small amount of EGTA. Calcium pulses (2.5 µmol/mg protein) were added at 2 min intervals until a Ca^{2+}-induced Ca^{2+} release was observed. In some experiments, the following PTP inhibitors were added prior to Ca^{2+} pulses: Cyclosporin-A (1 µM), $MgCl_2$ + ADP + Oligomycin (1.2, 0.6, and 0.00127 mM respectively). In all experiments, Calcium Retention Capacity (CRC) was taken as the total amount of Ca^{2+} accumulated by mitochondria prior to the Ca^{2+} pulse triggering Ca^{2+} release.

Mitochondrial membrane potential: Mitochondria (0.25mg prot. /ml) were incubated at room temperature in a K-MES buffer (in mM: 110 K-MES, 35 KCl, 1 EGTA, 5 K_2HPO_4, 3 $MgCl_2$, 0.5mg/ml BSA) supplemented with the potentiometric probe Rhodamine 123 (0.2 µM, ex-em: 503–525 nm) and either glutamate:malate (5: 2.5 mM) or succinate (5 mM). Membrane potential ($\Delta\Psi$) was calculated from changes in the concentration of extra-mitochondrial Rhodamine 123 as per [344] using the equation $\Delta\Psi$=59 x log [Rhodamine]in / [Rhodamine]out. To calculate the intra-mitochondrial concentration of Rhodamine, the amount of Rhodamine taken-up by mitochondria was determined by measuring changes in fluorescence following addition of respiratory substrates. A matrix distribution volume of 1 µl / mg protein, and a non-specific binding of rhodamine to mitochondria of 30% was assumed in all groups. [344]

Mitochondrial H_2O_2 release and membrane permeabilization: Mitochondria (0.2 mg prot. /ml) were incubated at room temperature in a K-MES buffer (in mM: 110 K-MES, 35 KCl, 1 EGTA, 3 $MgCl_2$,10 K_2HPO_4, 0. 5mg/ml BSA; pH 7.55) supplemented with the H_2O_2-sensitive probe Amplex red (1.5µM; ex-em: 563-587nm) and horseradish peroxidase (1.2U/ml), as previously described [345]. Net mitochondrial H_2O_2 release was measured: i) under state 2 conditions in presence of succinate (5 mM) alone or with glutamate-malate (5:2.5 mM) to elicit reverse electron flow, ii) under state 3 conditions following addition of ADP (1 mM) and iii) under state 2 following inhibition of reverse electron flow with rotenone (1 µM). To assess mitochondrial H_2O_2 trapping, net H_2O_2 release was first measured under state 2 conditions and membranes were subsequently permeabilized by adding increasing pulses of digitonin (0.01% per pulse) at regular interval. An increase in H_2O_2 emission above basal levels was used as an indicator of H_2O_2 entrapment.

H_2O_2 Scavenging: H_2O_2 scavenging was measured fluorimetrically in a 96 well plate reader using a protocol modified from[345]. Briefly, mitochondrial aliquots (0.1 mg prot/ml) were distributed in 7 wells in K-MES buffer supplemented with glutamate (50 µM) and malate (20 µM). A pulse of 3 nmoles of H_2O_2 was added to the first well at *t*=0 sec, and to each subsequent well at 20 sec intervals. At t=100 sec, 100 µL of K-MES buffer supplemented with 10µM Amplex Red, and 0.5U/ml horseradish peroxidase was added to all wells, and fluorescence corresponding to the amount un unscavenged H_2O_2 remaining in each well was immediately measured in end-point measurement mode. In all experiments a control well containing no mitochondria was used as the baseline control.

2.5.7 Immunoblotting

SDS-PAGE: Whole liver extracts or isolated mitochondria were extracted in 1% lauryl maltoside/PBS, and 10, 20 or 50 µg of protein per sample were loaded and run on 12 or 15% polyacrylamide gels, then transferred to PVDF membrane and used for the detection of LRPPRC (1/1000; in house), SLIRP (1/50; in house), COX I (1/2000; Abcam #ab14705), NDUFA9 (1/1000; Abcam #ab14713), SDHA (1/1000; Abcam #ab14715), SOD2 (1/2000; Abcam #ab16956), CoreII (1/100; in house), Catalase (1/1000; Abcam #ab52477), Cyclophilin-D (1/1000; Pierce Thermos-Fisher #PA1-028), AQP8 (1/1000; Abcam #203682), OSCP (1/1000; Santa Cruz #365162), Porin (1/2000; Abcam #14734), and Actin (1/1000; Genescript #A00702). LRPPRC polyclonal antibodies were prepared by immunizing rabbits with peptides of 22 amino acids corresponding the sequence CEPPESFEFYAQQLRKLRENSS (antibody 295–313; Zymed Laboratories, San Francisco, CA). The density of immunoreactive bands was determined using ImageJ. Unless indicated in the figure legend, all results were normalised by ponceau staining of the membranes.

Clear-Native-PAGE and in gel ATPase activity: OXPHOS complexes were extracted from isolated mitochondria using either Dodecylmaltoside (DDM: 2%) or digitonin (2g digitonin/1g mitochondrial protein) in extraction buffer (in mM: 30 HEPES, 150 K-acetate, 2 6-aminocaproic acid, 1 EDTA, 12% glycerol; 10µl buffer/100µg protein). The suspension was incubated on ice for 30 minutes and centrifuged for 45 minutes at 20 400Xg at 4°C. The supernatant was supplemented with 750µM 6-aminocaproic acid, and separated by Clear Native (CN)-PAGE on 3-12% Bis-Tris Novex gels (Life Technologies). Half of gel was stained with coomasie blue. The other half of the gel was incubated in an ATP synthase activity buffer (in mM: 50 glycine, 5 $MgCl_2$, 50 HEPES, 30 $CaCl_2$, 10 ATP; pH 7.8) overnight at 4°C under agitation to resolve native ATP synthase complexes.

Blue-Native-PAGE: Mitochondria extracts were solubilised in 1% lauryl maltoside, 10 µg of protein was loaded on 6-15% polyacrylamide gradient gel and then transferred to nitrocellulose membrane. Individual structural subunits of complexes I (NDUFA9; 1/1000; Abcam #ab14713), II (SDHA; 1/1000; Abcam #ab14715), III (CoreII; 1/100; in house), IV (COX I; 1/2000; Abcam #ab14705) and V (ATP5a; 1/5000; Abcam #ab14748) were detected.

2.5.8 Enzyme activities

Activities of CI (NADH-CoQ reductase), CII (succinate dehydrogenase), CIV (cytochrome oxidase), CV (ATP synthase) and citrate synthase (CS) were measured spectrophotometrically in a plate reader using standard coupled enzyme assays adapted from [342] and from [346] for CV. Activities were expressed in mU. min^{-1}. mg mitochondrial $prot^{-1}$. To facilitate comparisons, all enzymes activities were subsequently expressed as fold difference *vs* H-*Lrpprc*$^{+/+}$.

2.5.9 Mitochondrial Polyadenylation Tail Length Assay (MPAT)

The MPAT assay was performed as per[347]. A universal linker DNA oligonucleotide 5'-phospho-ATG TGA GAT CAT GCA CAG TCA TA-3'-NH2 was ligated to the 3' termini of total RNA (2.5 µg) by T4 RNA ligase (New England Biolabs) at 37°C for 3h. The ligated RNA was subjected to phenol/chloroform extraction and ammonium acetate/ethanol precipitation and then amplified using one-step RT-PCR kit (QIAGEN) with anti-linker primer (5' TAT GAC TGT GCA TGA TCT CAC AT 3'). A first round of PCR (35 cycles) was applied using a gene-specific upper primer and the anti-linker primer, followed by a second round of 10-cycle PCR using a gene-specific lower primer and the anti-linker primer. Half of the reaction product was resolved by 10% polyacrylamide gel electrophoresis in TBE buffer, dyed with SYBR green (Invitrogen) and visualized by PhosphorImage, and the remaining half was cloned in TOPO TA cloning vector (Invitrogen) and a large number of clones were subjected to Sanger sequencing.

2.5.10 Mitochondrial membrane lipid composition using LC-MS analysis

Procedures for lipid extraction and analysis were adapted as previously described (Matyash V, JLR, 2008; Sandra K, j Chromatogr A, 2010). Briefly, lipids were extracted from isolated mitochondria (200 µg protein), which had been spiked with six internal standards. Samples (equivalent to 2.6 µg of protein extract) were injected onto a 1290 Infinity HPLC coupled with a 6530 accurate mass QTOF (Agilent, Santa Clara, USA) via a dual electrospray ion source. Lipids were eluted on a Zorbax Eclipse plus C18, 2. 1 x 100 mm, 1. 8µm (Agilent, Santa Clara, USA) kept at 40°C with a gradient of 83 min and were analysed in both negative and positive scan mode. Each feature or entity characterized by a specific mass and retention time, were identified using Mass Hunter B. 07. 00 software (Agilent, Santa Clara, USA). A frequency filter of 100 % was applied and signal intensities were normalized using Quantile algorithm with Mass Profiler Pro. software (MPP, Agilent, Santa Clara, USA). MS entities that discriminated the two conditions based on a false

discovery rate of 5% and a fold change >2, were subjected to tandem mass spectrometry for lipid identification. Note that for cholesterol, identification was also confirmed by LC-MS analysis of the corresponding standard.

2.5.11 Statistical Analyses

Unless indicated, data are presented as mean ± SEM. Unpaired student's *t*-test or a one-way analysis of variance (ANOVA) followed by Bonferroni multiple comparison *post hoc* analysis was used to determine significant difference between two or among multiple groups, respectively. Statistically significant differences were considered for $p<0.05$. All analyses were performed on Prism 6.0 for Mac OS-X. For lipidomics analysis, data were analyzed with Mass Profiler Professional (MPP) using unpaired student's t-test followed by Benjamini Hochberg correction and statistical significance was set at a false discovery rate of 5%; data are depicted as a volcano plot.

2.6 Funding

This work was supported by the Canadian Institutes of Health Research (CIHR; Grant #102168 to JDR, YB, EAS, CDR for the CIHR Emerging Team in Leigh Syndrome French Canadian (LSFC): Translating gene discovery into treatments for patients.

2.7 Acknowledgements

We would like to thank Mélanie Burnette, François Brisebois, Nicolas Morin and Nicolas Sgarioto for technical assistance. This work was supported by the Canadian Institutes of Health Research (CIHR ; Grant #102168 to the CIHR Emerging Team in Leigh Syndrome French Canadian (LSFC) : Translating gene discovery into treatments for patients (awarded to CDR, YB, JDR, and EAS), the Lactic Acidosis Association (AAL) and Fondation du Grand Défi Pierre Lavoie. YB is a Ottawa University Chair in Integrative Mitochondrial Biology. JDR holds the Canada Research Chair in Genetics and Genomic Medicine. AC is recipient of a graduate scholarship from Fondation du Grand Défi Pierre Lavoie.

2.8 CONSORTIA

Members of the LSFC consortium at the time this study was initiated were in alphabetical order: Bruc G. Allen, Claudine Beauchamp, Chantal Bemeur, Yan Burelle, Guy Charron, Lise Coderre, Alexanne Cuillerier, Christine Des Rosiers, Sonia Deschênes, François Labarthe, Jeanine Landry, Catherine Laprise, Geneviève Lavallée, Pierre Lavoie, Sylvie Lesage, Bruno Maranda, Charles Morin, Yvette Mukazena, John D. Rioux, Marie-Eve Rivard, Eric A. Shoubridge, Jessica Tardif, Julie Thopson-Legault, Nancy Tremblay, Vanessa Tremblay-Vaillancourt, Luc Vachon, and Josée Villeneuve.

2.9 Conflict of interest statement

The authors declare no conflicts of interest.

2.10 Authors contribution

Concept and design (YB, AC, EAS, CDR, JDR); Experiments, procedures and data analysis (AC, AF, CB, CDR, EAS, GC, JDR, MR, SD, SH, VJJC, YB); Manuscript writing (YB, AC); Manuscript review (EAS, JDR, CDR, MR)

Chapter 3

Hybrid clear/blue Native Electrophoresis for the Separation and Analysis of Mitochondrial Respiratory Chain Supercomplexes

Alexanne Cuillerier, Yan Burelle

Interdisciplinary School of Health Sciences, Faculty of Health Sciences

and Department of Cellular and Molecular Medicine, Faculty of Medicine, University of Ottawa, Ottawa, ON, Canada

JoVE, 2019; PMID: 31157764; DOI: 10.3791/59294

3.1 KEYWORDS

Mitochondria, respiratory chain, respiratory chain supercomplexes, Native electrophoresis

3.2 SUMMARY

Here we present a protocol to extract, resolve and identify mitochondrial supercomplexes which minimizes exposure to detergents and Coomassie Blue. This protocol offers an optimal balance between resolution, and preservation of enzyme activities, while minimizing the risk of losing labile protein-protein interactions.

3.3 ABSTRACT

Complexes of the oxidative phosphorylation machinery form supramolecular protein arrangements named supercomplexes (SCs), which are believed to confer structural and functional advantages to mitochondria. SCs have been identified throughout species, from yeast to mammal, and an increasing number of studies report disruption of their organization in genetic and acquired human diseases. As a result, an increasing number of laboratories are interested in analyzing SCs, which can be methodologically challenging. This article presents an optimized protocol that combines the advantages of Blue- and Clear-Native PAGE methods to resolve, and analyze SCs in a time-effective manner. With this hybrid CN/BN-PAGE method, mitochondrial SCs extracted with optimal amounts of the mild detergent digitonin are exposed briefly to the anionic dye Coomassie Blue (CB) at the beginning of the electrophoresis, without exposure to other detergents. This short exposure to CB allows to separate and resolve SCs as effectively as with traditional BN-PAGE methods, while avoiding the negative impact of high CB levels on in gel activity assays, and labile protein-protein interactions within SCs. With this protocol it is thus possible to combine precise and rapid in gel activity measurements with analytical techniques involving 2D electrophoresis, immuno-detection and/or proteomics for advanced analysis of SCs.

3.4 INTRODUCTION

Mitochondria produce energy through oxidative phosphorylation, where respiratory complexes I-II-III-IV oxidize substrates and transfer electrons to oxygen, generating a gradient that allows phosphorylation of ADP by the ATP synthase (CV). In the past years, extensive studies have shown that respiratory chain complexes are not solely incorporated in a linear way in the inner mitochondrial membrane, but are also organised into supercomplexes (SCs) arrangements. [200, 348] In mammalian mitochondria, SCs exist in varying stoichiometry: CI/CIII2/CIV1-4 (named respirasome, is capable of NADH:O2 oxidoreduction in vitro)2, CI/CIII2 and CIII2/CIV1-2. [204, 210] Furthermore, respiratory complexes are distributed under different ratios between their free form and SCs arrangements. Therefore, it is estimated that 85-100% of CI, 55-65% of CIII, and 15-25% of CIV are found in SCs. [210] These supramolecular structures are thought to decrease ROS production, stabilize or assist in the assembly of individual complexes, regulate respiratory chain activity, and prevent protein aggregation in the protein rich IMM. [201, 202, 206, 349] Their remodelling ability upon variation in energy demand, and their importance in the pathogenesis of diseases is being investigated in several labs. [203-205, 349-353] Studies have demonstrated that pathological changes in SCs assembly are present in a variety of disorders, including, but not limited to, genetic defect in cardiolipin synthesis [40], heart failure [354], ischemia-reperfusion [355], diabetes [351], and aging [356].

Native electrophoresis and immunodetection are widely used in SCs studies to resolve OXPHOS complexes quaternary arrangements. [200, 357, 358] Native electrophoresis can further be combined with specific in gel activity assays or 2D-SDS PAGE to enable precise molecular determination of the various SCs assemblies. [348, 357] The ability to study SCs is critically dependent on the extraction conditions, including type and concentration of detergent used, ionic strength and pH, as well as on electrophoretic migration conditions, which comprise buffer composition, presence of CB, gel size and acrylamide percentage. [200]

Protocols and SCs band resolution vary greatly among papers, making comparison between studies difficult, and adaptation of methods challenging. [359] Therefore, this paper proposes a robust and optimal protocol to extract SCs from isolated mitochondria of different sources with the non-ionic detergent digitonin, and to resolve high molecular weight SCs bands. The optimized detergent

concentration, composition of the extraction buffer, and the absence of Coomassie Blue in sample preparation minimize disruption of protein complexes. This protocol combines CN-PAGE and BN-PAGE for optimal SCs assemblies resolution on large gel, and is compatible with in-gel activity assays allowing better visualization of reactive bands, along with the use of immunodetection for a detailed analysis SCs arrangements and composition.

3.5 PROTOCOL

Figure 3.1: Assay workflow. Schematic components of the figure are from Servier Medical Art.

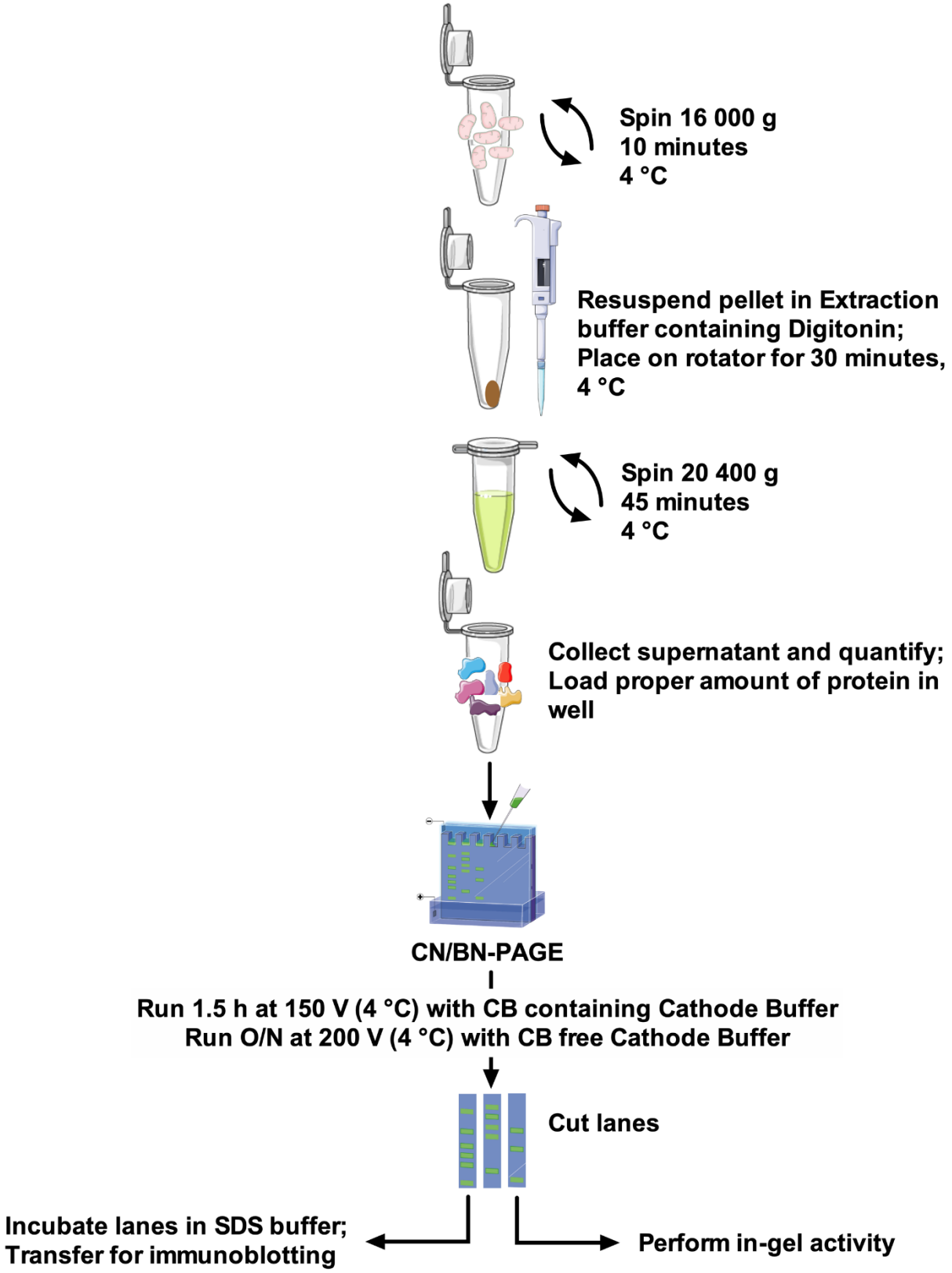

1. SC Extraction

1.1. Prepare 100 mL of Extraction buffer (see table 3.2) by dissolving EDTA in water. Increase pH with KOH until completely dissolved, then adjust pH to 7.5 with HCl. Add remaining components to the solution, complete to final volume with water, and keep on ice. In a tube, dissolve digitonin in extraction buffer to make a 10% stock solution, vortex thoroughly until completely dissolved, and keep on ice.

Note: Extraction buffer can be prepared in advance and kept at 4 °C for 2 months maximum. If wavy bands start to appear at the bottom of the gel, it means extraction buffer is too old. When preparing the 10% digitonin solution, prepare a stock volume counting 500 µl per sample if using mouse liver mitochondria.

1.2. Mitochondria isolated from animal tissue (mouse heart, muscle, liver; rat heart) or cells human fibroblast) using standard protocols [360-362] can be used for the extraction of SCs. Once mitochondria are obtained, quantify protein content using the bicinchoninic acid assay kit according to the manufacturer's recommendations. Isolated mitochondria can be supplemented with proteases and phosphatases inhibitors at this step.

Note: SCs can be extracted on either fresh or thawed mitochondria. It is recommended to extract SCs from all samples at the same time, to insure they are treated with the same batches of solutions and under the same conditions.

1.3. Based on the mitochondrial protein concentration obtained, and the final digitonin/protein ratio desired, calculate the volume of stock digitonin solution and extraction buffer required as per Table 1. For SC extraction, 1 µL of extraction buffer (Table 3.2) containing digitonin is added for each 10 µg of mitochondrial protein. The digitonin/protein ratio can vary from 2-8 g/g. A digitonin titration should always be performed for each new type of sample used (See figure 3.2 for an example).

1.4. Pellet mitochondria, in a 1.5 mL tube by centrifugation at 16 000 x g for 10 minutes at 4 °C.

1.5. Discard supernatant and re-suspend the mitochondrial pellet in the calculated volume of ice-cold extraction buffer containing digitonin. Place tubes on a mini tube rotator and incubate for 30 minutes at 4 °C at a medium rotation speed. Make sure that samples are getting properly mixed.

1.6. Centrifuge samples at 20 400 x g for 45 minutes at 4 °C to remove insolubilized fragments.

1.7. Transfer supernatant in a new tube on ice and quantify proteins. This fraction represents the respiratory supercomplexes extract. If electrophoresis is not performed on the same day store samples at -80 °C.

Note 1: Avoid freeze/thaw cycles of the extract, as this disrupts higher molecular arrangements of SCs. Aliquot sample before the first freeze/thaw cycle if needed.

Note 2: To perform a standard BN-PAGE experiment, CB should be added to the SCs extract at this step. CB should be added in a 1g/8g ratio relative to the amount of detergent used.

2. Gradient gel Casting and Electrophoresis

2.1. Prepare 3x gradient buffer and acrylamide stocks for making the gradient gel, aliquot and store at – 20 °C (see table 3.3).

2.2. Prepare anode and cathode buffers, and keep at 4 °C (see table 3.5).

2.3. Open the casting chamber and place an outer glass plate (20 cm x 22 cm) in the chamber. Position one set of spacers (1.5 mm) using the alignment card to ensure they are seated firmly against the side and corners of the chamber. Place an inner glass plate (20 cm x 20 cm) on top of the spacers (this forms the gel sandwich), and put a plastic separation sheet on top of the glass plate.

2.4. Repeat step 2.3 until the desired number of gels to cast is reached. For this protocol, 4 gels are casted. The Biorad Casting Chamber system allows the casting of a maximum of 10 gels at a time. Take-up the remaining space in the chamber by first adding as many acrylic blocks as needed, and then glass plates if needed.

Note: The montage has to be tightly sealed; there should be no space between the gel sandwiches in the chamber.

2.5. Place a strip of parafilm in the groove before seating the gasket firmly in the gasket notch. Place the sealing plate on the chamber and tighten all 6 screws. Stand the casting chamber.

2.6. Place gradient former on a stir plate with a magnetic stirrer in the “light” mixing chamber. Connect the tubing of casting chamber to the gradient former, secure the tubing in the cassette of the peristaltic pump, and make sure the stopcock of the gradient former is closed.

2.7. To cast 4 gels, prepare 60 mL of 4% and 60 mL of 12% gel solutions (see table 3.4) in Erlenmeyer and swirl thoroughly to mix. Pour 60 mL of 4% gel solution in the “light” mixing

chamber, and 60 mL of 12% in the “heavy” reservoir chamber of the gradient former. Set stir speed of the stir plate at 350 rpm. Open the stopcock and turn on the pump at 35 rpm.

2.8. Once the light fraction is lower than the heavy fraction, pause the pump and open the valve stem between “light” and “heavy” reservoirs, let fractions volume equilibrate, and restart the pump.

Note: it is important that no bubbles enter the system and get trapped between glass plates. If this happens, undo montage, wash and redo.

2.9. Once the gradient gel is completely poured, stop the pump, and overlay water (about 1 mL) on each gel sandwich to prevent drying of the gel. Let polymerize for 2 hours.

2.10. Prepare 25 mL stacking gel in Erlenmeyer and swirl to mix thoroughly. Remove water and insert 15 well combs in each gel sandwich. Pour stacking gel and let polymerize for 2 hours.

Note: Gels can be casted and kept at 4 °C for 1 week.

2.11. Insert gel in sandwich clamps and remove comb. With the short glass plate facing down, insert the gel sandwich in the cooling core. Repeat on the other side, and place core in the electrophoresis tank.

2.12. Pour 300 mL of Blue Cathode Buffer in inner chamber of the electrophoresis tank.

Note: The electrode has to be submerged in cathode buffer, which requires approximately 300 mL.

2.13. Load between 75 µg and 175 µg of protein per well. Run gel at 150 V for 1h30 (or until samples have all entered the gradient gel) in cold room (4 °C).

Note 1: A minimum of 75 µg per well is required for good resolution of in-gel activity bands. Loading over 175 µg of protein will lead to a loss of clear bands due to excessive enzyme activity.

Note 2: Replicates of the sample should be loaded in separate wells to enable parallel determination of in-gel activities and immunoblot analysis of OXPHOS complexes. Parallel determination of IGA for CI, CII, CIV and CV requires a minimum of 300 µg. Parallel immunoblot analysis of CI, CII, CII, CIV and CV requires a minimum of 375 µg.

2.14. Remove Blue Cathode Buffer with pipet or vacuum, replace by 300 mL Coomassie Blue-free Cathode Buffer, and run gel at 200 V overnight (16-20h) in cold room (4 °C). Proceed to step 3 or 4 for In gel activity measurement or immunoblotting.

3. In-gel Activity for Complexes I, II, IV and CV

3.1. Before the end of electrophoresis, prepare in-gel activity buffers according to Table 6, and keep in the dark at RT. 20 mL of in-gel activity buffer is sufficient for 3 sample lanes.

Note: This CV in-gel activity assay is based on the reverse activity of ATPsynthase (i.e. ATP hydrolysis), and uses calcium as a co-factor, which precipitates in the gel. Calcium is less harmful than the lead used in other protocols. Furthermore the use of this protocol does not require a pre-activation/conditioning of the gel. [360]

3.2. Stop electrophoresis and retrieve gel. Cut lanes, if necessary, and transfer gel lanes in plastic bags (3 sides cut, and plastic bag opened like a book). Seal 2 of the 3 sides with a heat sealer.

Note: To compare the composition of SC bands between experimental groups, it is recommended to run the same samples in replicates on the same gel. Cut lanes to incubate each replicate in different in-gel activity buffers (CI, II, IV, V). To confirm the specificity of the assays, additional replicates can be prepared to run in gel activities in presence of specific respiratory chain inhibitors.

3.3. For 3 experimental samples (i.e. 3 wells), add 20 mL of in-gel activity buffer, remove bubbles and seal 4th side of plastic bag.

Note: Add inhibitors in negative control experiments if performed: CI: Rotenone 1 µM; CII: Sodium Malonate 10 mM; CIII: Antimycin-A 8 µM; CIV: KCN 0.6 mM; CV: Oligomycin 0.5 µ

3.4. Incubate gel lanes at 37 °C in the dark, and check every 15 minutes. Incubation time varies depending on the amount of protein and complexes. CI will react faster than CIV or CV. Optimal staining usually occurs after 2h for CI, 4h for CIV and 6h for CII and CV.

3.5. Rinse gel lanes in water to stop reaction, and image on a white background for CI, CII, CIV, or black background for CV.

Note: Gels can be kept in plastic bags at RT or 4°C for several months.

4. Immunoblotting

4.1. Prepare transfer buffer according to table 7, and keep at RT. Prepare TBST and keep at RT.

4.2. Place the entire gel, or selected lanes, in a container and add transfer buffer supplemented with SDS (0. 25% final in transfer buffer). Place container on rocker and incubate for 1h.

4.3. Cut PVDF membrane (size corresponding to the size of the gel) and activate in 20 mL of methanol under agitation for 2 minutes. Replace by 20 mL transfer buffer and place under agitation for 2 minutes.

4.4. Prepare transfer sandwich, from bottom to top, making sure there is no bubble between gel and activated PVDF membrane: clear side of cassette / black sponge / blotting paper /membrane / gel / blotting paper / black sponge / black side of cassette. Close and lock the cassette.

4.5. Place transfer sandwich in transfer tank, with clear side of the sandwich facing the red side of the electrode, and pour transfer buffer to immerge the gel. Connect cooling system to the transfer tank and set at 4°C. Connect to power-pac and set at 40 mAmps, run for 24 hours.

4.6. Retrieve membranes, block for 1h in 5% BSA in TBST and incubate in primary antibody solution prepared in 5% BSA in TBST over night at 4°C.

4.7. Rinse membranes in TBST, 3 times for 10 minutes.

4.8. Incubate membranes in secondary antibody solutions prepared in 5% BSA in TBST for 2 hours at room temperature.

4.9. Rinse membranes in TBST, 3 times for 10 minutes.

4.10. Add chemiluminescent solution to membranes and image.

5. Analysis

5.1. In-gel activity assay images or immunoblots can be used to analyze SCs. To analyze composition of bands, align replicates and validate which complex reacted positively for each given band.

5.2. To analyze the distribution of complexes, in various supramolecular assemblies, open images in ImageJ and use the Gel analysis tool (see Figure 3. 5 for an example).

5.2.1. Select lanes with the rectangle tool, and plot lanes.

5.2.2. Draw lines to close the area under the curve of each bands of interest and click on each area with the wand tool to generate a table containing the area under the curve values.

5.2.3. To calculate the distribution of the complex, report the values for each band relative to that of the monomer.

3.5.1 Buffers and solutions

See Table 3. 2-8 for detailed buffers composition, and antibodies.

Digitonin 10 %, dissolved in SC extraction buffer (prepare fresh). Digitonin solubility varies upon provenance and product lot. For this protocol, digitonin #D141 from Sigma-Aldrich was used, which is soluble in the extraction buffer at RT.

3.5.2 Equipment

All equipment used for large gel casting, electrophoresis and transfer was purchased from Biorad (Protean® II xi system), and is listed in the Table of Materials.

All images were batch processed using Affinity Photo to build figures.

3.6 REPRESENTATIVE RESULTS

Figure 3.2 shows results from a digitonin titration experiment aimed to identify the proper amount of digitonin required for the extraction of SCs. This amount will vary depending on the tissue/cell type and whether the sample was frozen or not. For this experiment, a CIV in-gel activity was performed to visualize SCs isolated from fresh mouse liver mitochondria. Ratios from 2/1 to 10/1 g digitonin/g of protein were tested. The optimal amount of digitonin for this sample is 4 g/g, as it provides a good resolution of monomeric CIV, and high molecular weight SCs. At a lower ratio, bands are not clear and resolve into a smear during electrophoresis, whereas the use of higher ratio of digitonin leads to disruption of high molecular weight SC.

Figure 3.2: Digitonin Titration to Extract Supercomplexes from Fresh Mouse Liver Mitochondria.

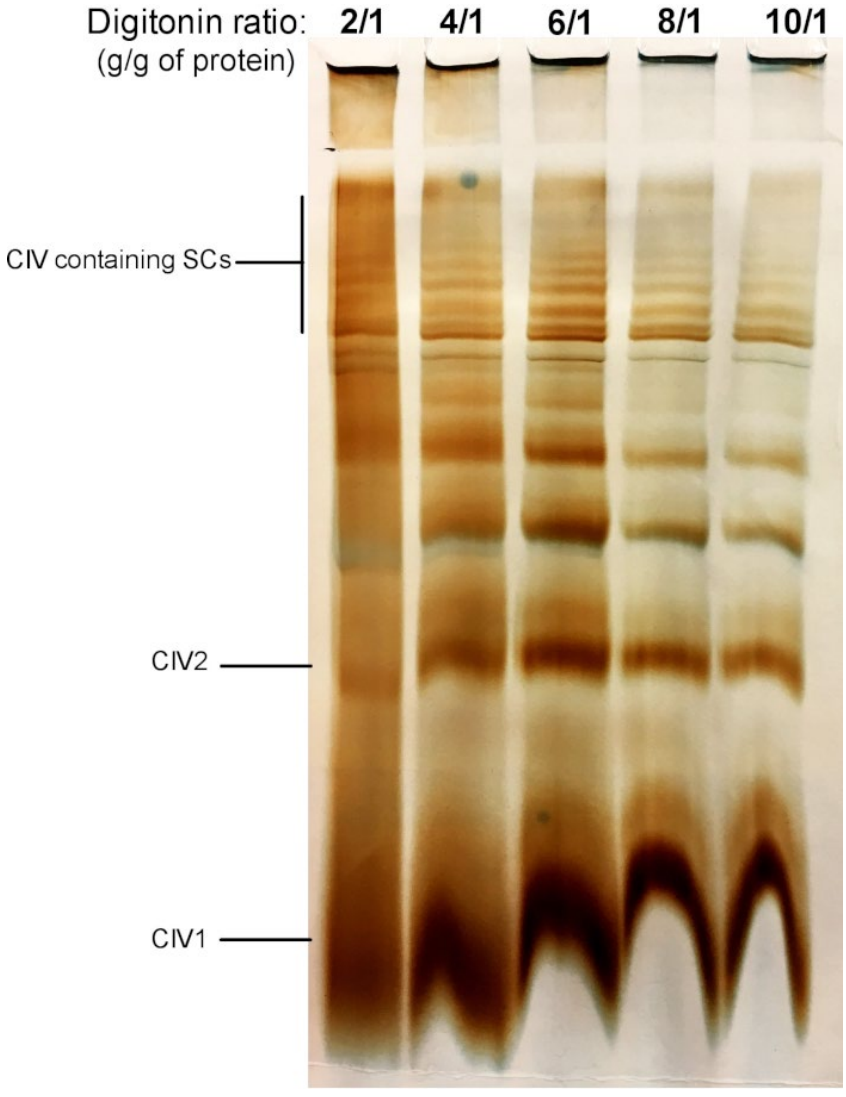

Digitonin titration to extract supercomplexes from fresh mouse liver mitochondria. This example shows aliquots of mouse liver mitochondria, isolated from one animal that were treated with increasing amounts of digitonin to extract respiratory supercomplexes. Samples were then resolved by Hybrid CN/BN PAGE, and in-gel activity of CIV was determined. CIV1: complex IV monomers; CIV2: Complex IV dimers; SC: supercomplexes.

Figure 3.3 and 3.4 show the results of a complete experiment performed on a preparation of mouse liver mitochondria extracted with 4 g digitonin /g protein. Proteins were separated using hybrid BN/CN-PAGE, standard BN-PAGE, or CN-PAGE. All three gels were casted at the same time and lanes were loaded with replicates of the same sample. Following electrophoresis, individual lanes were cut and processed for in gel activity measurement (CI, CII, CIV and CV on Figure 3) and immunoblotting (CI, CII, CIII, CIV, CV on Figure 4).

Addition of CB either momentarily in cathode buffer (i.e. hybrid CN/BN-PAGE) or in sample and cathode buffer throughout electrophoresis (i.e. BN-PAGE), considerably improves the mobility and resolution of SC bands, and individual respiratory complexes compared to CN-PAGE (Figure 3.3). Bands are easily distinguishable with the hybrid technique or BN-PAGE after in-gel activity for CIV, whereas in the same sample resolved by CN-PAGE, SCs and monomeric CIV reactive bands cannot be identified.

Figure 3.3: In-gel activity of OXPHOS Complexes Following Hybrid CN/BN-PAGE, BN-PAGE or CN-PAGE.

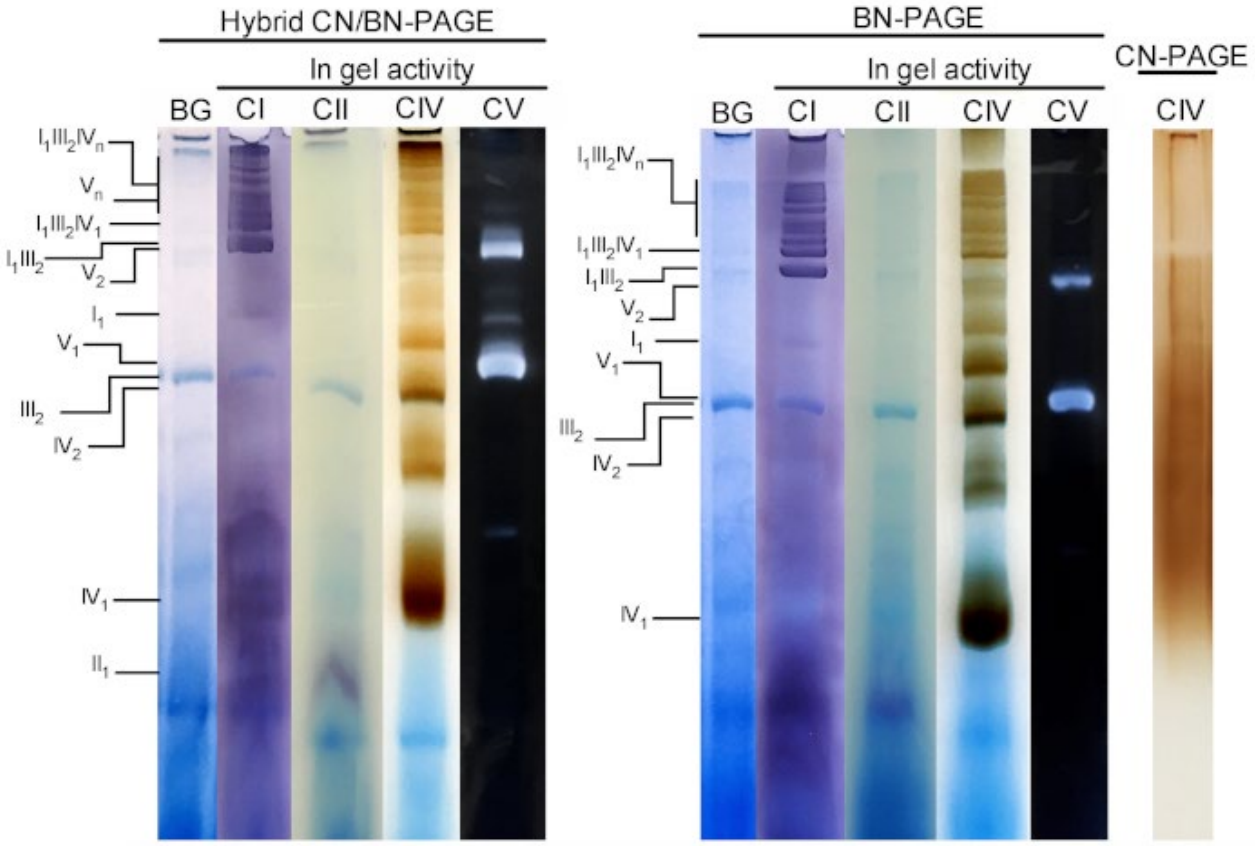

In-gel activity of OXPHOS complexes following hybrid CN/BN-PAGE, BN-PAGE or CN-PAGE. Liver mitochondria isolated from one mouse were treated with digitonin (4 g/g ratio digotonin/protein) to extract respiratory supercomplexes. Aliquots of this sample were then loaded on multiple wells in three distinct gels and submitted to CN/BN-PAGE, BN-PAGE or CN-PAGE. Each replicate lane within each gel was then cut and immediately used for in-gel activity assays (labeled CI, CII, CIV and CV). One lane was used as control to show background (labeled BG) staining with Coomassie Blue. OXPHOS complexes and supramolecular assemblies are identified using the standard nomenclature, with numbers in indices indicating the molecular stoichiometry of each OXPHOS complex. It should be noted that the position of CIII-containing supramolecular assemblies is based on immunodetection since in-gel activity for CIII was not performed in this particular experiment.

Figure 3.4: Immunoblot Analysis of OXPHOS Complexes Following Hybrid CN/BN-PAGE or BN-PAGE.

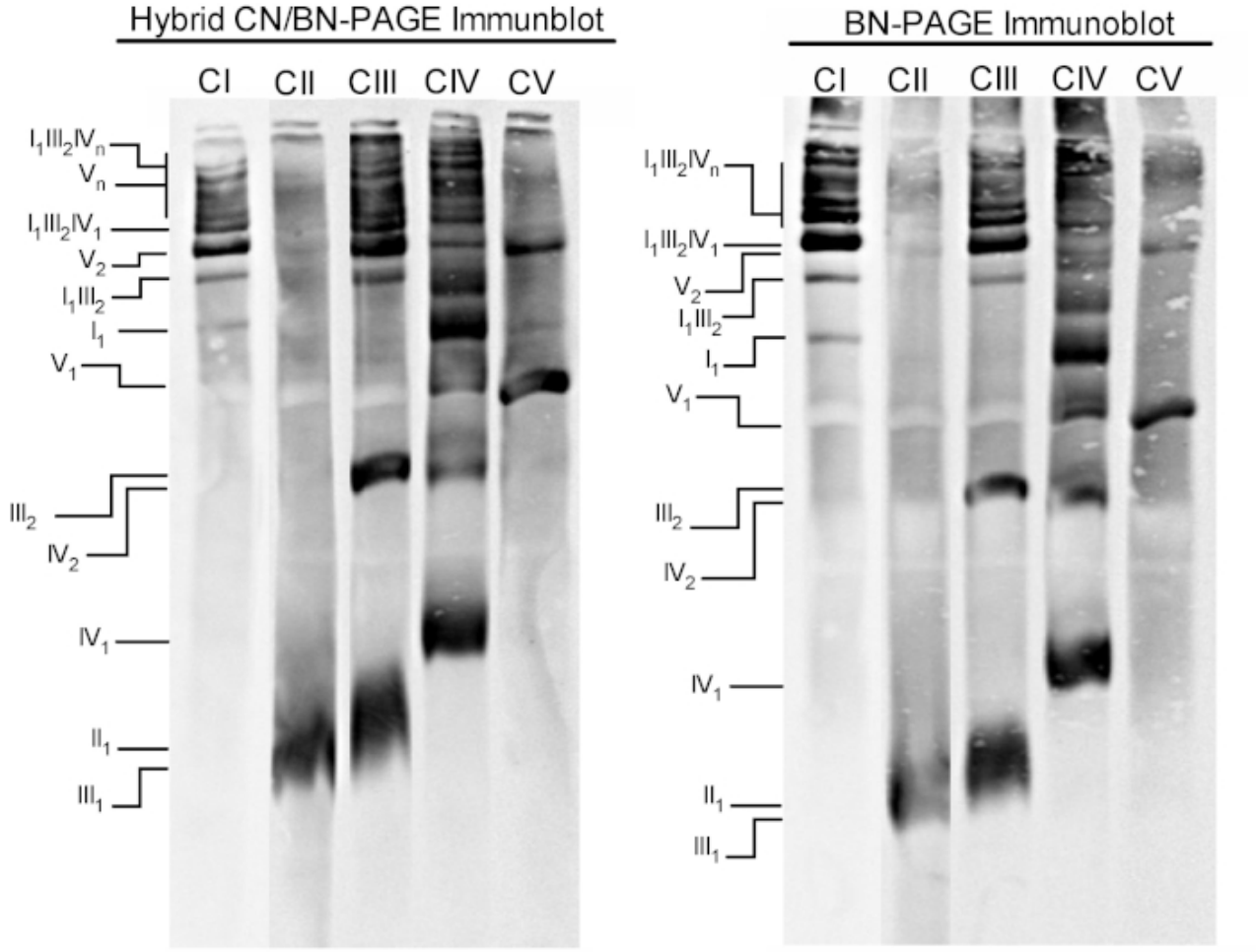

Immunoblot analysis of OXPHOS complexes following hybrid CN/BN-PAGE or BN-PAGE. Replicates from the experiments described in the figure 3 legend were electro-transferred on a single membrane. After transfer individual lanes were cut and incubated with specific antibodies recognizing CI, CII, CIII, CIV and CV. OXPHOS complexes and supramolecular assemblies are identified using the standard nomenclature, with numbers in indices indicating the molecular stoichiometry of each OXPHOS complex.

Figure 3.3 and 3.4 show that the resolution and banding pattern of OXPHOS monomers and supramolecular assemblies is qualitatively comparable between hybrid CN/BN-PAGE and BN-PAGE. However, notable differences exist. First, the electrophoretic mobility of OXPHOS complexes is slightly reduced when proteins are separated using hybrid CN/BN-PAGE conditions vs standard BN-PAGE, due to reduced amount of CB. This mobility shift is greater for CIV monomers, followed by CV monomers, and CI (Figure 3.3-3.4). Second, the blue background is lower in the hybrid CN/BN-PAGE compared to BN-PAGE (Figure 3.3 left lanes). As a result, high

background levels following BN-PAGE completely masks the in-gel activity staining for CII, and enhances the background noise associated with the activity of CIV dimers (Figure 3). Third, the activity of CV is higher when samples are run under hybrid CN/BN-PAGE conditions compared to BN-PAGE (Figure 3.3), due to the reduced amount of CB, which is known to interfere with CV catalytic activity [208]. CN/BN-PAGE also allows better preservation of CV supramolecular assemblies, as shown by a greater proportion of total CV activity being associated with CV dimers (Figure 3.3). Moreover, CV oligomers are visible under CN/BN-PAGE, while they are completely dissociated under BN-PAGE conditions. Interestingly, distinct bands displaying CV activity are also observed between CV monomers and dimers, when samples are run under CN/BN-PAGE (Figure 3.2).

Figure 3.5 shows a representative analysis of OXPHOS complex distribution in supramolecular assemblies. The image shows CI in gel activity of samples obtained from 4 distinct healthy mouse liver mitochondria preparations. Densitometry analysis allows to measure the area under the curve of CI-reactive bands, and to present the relative distribution of C1 activity in the monomeric (I1) and supramolecular forms (I1III2, I1III2IV1, I1III2IVn). Similar analysis can be performed following immunoblot.

Figure 3.5: Quantification of CI Distribution in Monomeric and Supramolecular Assemblies.

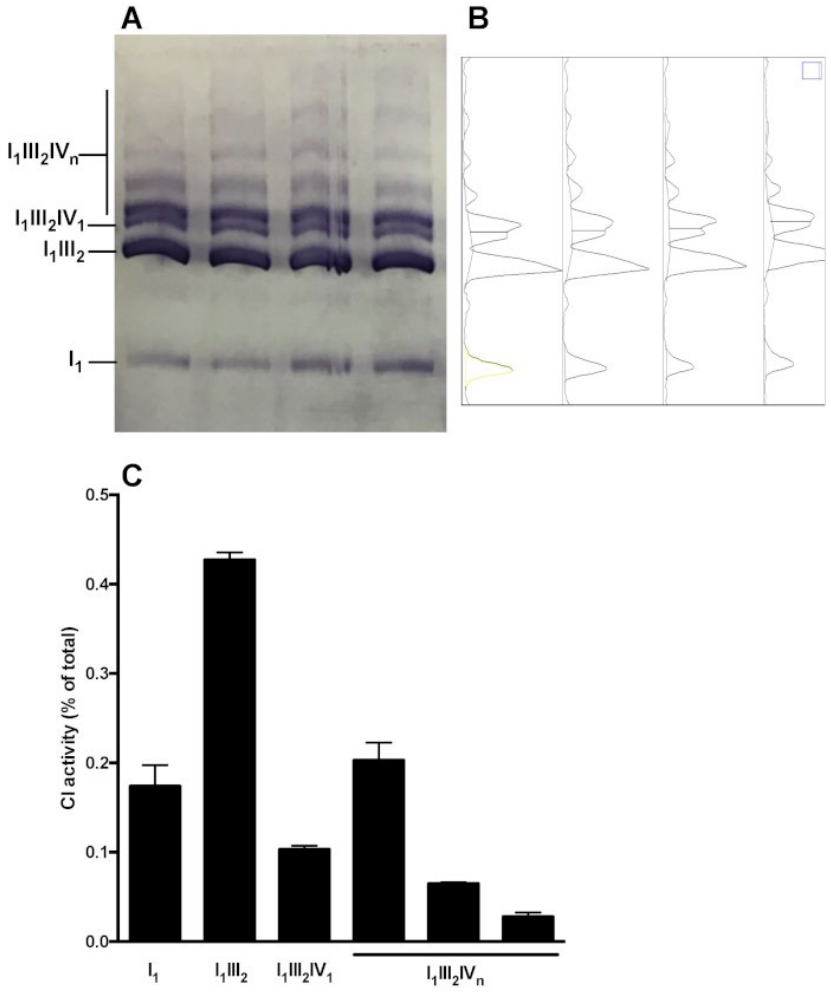

Quantification of CI distribution in monomeric and supramolecular assemblies. Panel A: CI in-gel activity determined following Hybrid CN/BN-PAGE of in liver mitochondria SC extracts obtained from 4 mice. Panel B: Densitograms obtained using ImageJ's Gel Analysis Tool showing distinct peaks corresponding to CI monomers (I1) and various CI-containing supramolecular complexes (I1III2, I1III2IV1, and I1III2IVn). Panel C: quantification of the relative distribution of C1 activity. The data represent mean and SEM of the 4 mice.

3.7 TABLE LEGENDS

Table 3.1: Volumes required to extract SCs from 5 mg of mitochondrial proteins using various digitonin/protein ratios.

Digitonin/protein ratio (g/ g)	**2 g/g**	**4 g/g**	**6 g/g**	**8 g/g**
Volume of extraction buffer (µL)	400	300	200	100
Volume of 10 % stock digitonin (µL)	100	200	300	400
Total extraction buffer volume (µL)	500	500	500	500

Table 3.2: SC extraction buffer (final concentrations). Keep at 4 °C for a maximum of 3 months.

Compound	**Final Concentration**
EDTA, pH 7. 5	1 mM
HEPES	30 mM
Potassium Acetate	150 mM
Glycerol	12%
6-aminocaproic Acid	2 mM

Table 3.3: Gel stock buffers.

Compound	Final Concentration
3X Gel Buffer: Aliquot and keep at -20 °C, pH 7. 5	
Imidazole/HCl pH-7. 0	75 mM
6-aminocaproic Acid	1.5 M
Acrylamide Buffer: Aliquot and keep at -20 °C	
Acrylamide	99. 5%
Bis-Acrylamide	3%

Table 3.4: 4%–12% gradient gel.

For 2 gels:	4% (60 mL)	12% (60 mL)	Stacking (4%) (25 mL)
3X Gel Buffer	19.8 mL	19.8 mL	8.25 mL
Acrylamide Buffer	4.8 mL	14.4 mL	2 mL
H_2O	35 mL	13.1 mL	14.6 mL
Glycerol	-	12 mL	-
APS 10%	360 µL	60 µL	150 µL
TEMED	24 µL	12 µL	10 µL

Table 3.5: Electrophoresis buffers.

Compound	**Final Concentration**
Anode Buffer: Keep at 4 °C, pH 7. 5	
Imidazole	25 mM
Cathode Buffer: Keep at 4 °C, pH 7. 5	
Tricine	50 mM
Imidazole	7.5 mM
With or without Coomassie Blue (G250)	0.022%

Table 3.6: In-gel activity assay buffers.

Compound	**Final Concentration**
Complex I activity Buffer: prepare fresh in 5 mM TRIS-HCl pH 7.4	
Nitrotetrazolium blue	3 mM
NADH	14 mM
Complex II activity Buffer: prepare fresh in 5 mM TRIS-HCl pH 7.4	
Succinate	20 mM
PMSF	0.2 mM
Nitrotetrazolium blue	3 mM
Complex IV activity Buffer: prepare fresh in 50 mM Na-Phosphate pH 7.2	
Cytochrome C	0.05 mM
Diaminobenzidine	2.3 mM
ATPsynthase activity Buffer: prepare fresh in water, adjust pH to 8 with KOH	
Glycine	50 mM
$MgCl_2$	5 mM
HEPES	50 mM
$CaCl_2$	30 mM
ATP	5 mM

Table 3.7: Immunoblotting buffers.

Compound	**Final Concentration**
Transfer Buffer	
Tris Base	25 mM
Glycine	192 mM
SDS	4%
Methanol	20%
TBST	
Tris Base	20 mM
NaCl	137 mM
Tween 20	0.1%

Table 3.8: Antibodies used for immunoblotting to detect respiratory chain SC. See Table of Materials for companies and lot numbers.

Complex	**Subunit**	**Clone**
I	NDUFA9	20C11B11B11
II	SDHA	2E3GC12FB2AE2
III	UQCRC2	13G12AF12BB11
IV	COX4	1D6E1A8
V	ATPB	3D5

3.8 DISCUSSION

Mitochondrial supercomplexes are being actively studied to elucidate their physiological role, and their importance in the pathogenesis of numerous human diseases, whether they are acquired or genetic mitochondrial diseases. [203-205, 349-351, 353] In order to obtain reliable results; several aspects need to be considered. This protocol has been tested with mouse liver mitochondria, mouse skeletal muscle mitochondria (results not shown), rat heart mitochondria, and human fibroblast mitochondria (results not shown), but could certainly be adapted to other sources of isolated mitochondria. The method optimally combines various aspects of BN and CN-PAGE protocols which allow to reduce exposure to detergents and anionic compounds to a minimum compared to published protocols. [358, 363, 364]

3.8.1 Sample preparation

Sample preparation represents a crucial step for successful separation of SCs. Buffer composition should be carefully selected in order to achieve proper solubilization of proteins and proteins assemblies, while preserving as much as possible their functional and structural integrity. Ionic strength and pH of the extraction buffer are two important factors to consider. Salt concentrations that are too low (< 50 mM K-Acetate or NaCl) will result in poor solubilization of proteins in presence of non-ionic detergents, while salt concentrations above 500 mM will promote protein stacking/aggregation, and precipitation of CB and proteins. [365] SCs should therefore be extracted using buffers at near physiological ionic strength. With regards to pH, the use of a near physiological pH is recommended.

Detergent type and detergent/protein ratio are also critical for optimal SC extraction. For maximal preservation of native SCs, digitonin should be preferred. [208] As shown in the present protocol and other published methods [199, 329, 360, 366], this mild detergent preserves the supramolecular composition of multiple SC assemblies, and the dimeric and oligomeric structure of ATPsynthase (Figure 3.3-3.4). Titration of the samples of interest with various amounts of digitonin is critical in order to identify the conditions that allow optimal solubilization, while preserving enzyme activity, and physiological protein interactions. Titration should be performed with ratios ranging between 2 and 8 g/g. [208] Optimal results for liver, skeletal muscle and cardiac mitochondria are respectively obtained with 4, 5 and 6 g digitonin/g protein. It should be noted that digitonin can be

replaced by Triton X-100, which under optimal conditions, results in similar migration and SC composition as those observed with digitonin. [200] However, this detergent should be used with caution since relatively small increase in the detergent/protein ratio (e.g. from 1 to 1.5 g/g) can result in a complete dissociation of SCs assemblies [200], which can result in experimental inconsistencies. After extraction, samples are traditionally supplemented with Coomassie Blue to give proteins a charge when applied to the gel, except for traditional CN-PAGE. [208, 358] In order to minimize protein exposure to Coomassie blue and potential dissociation of labile proteins, samples are not supplemented with Coomassie blue in this protocol.

3.8.2 Electrophoresis

Both CN-PAGE and BN-PAGE have been used to study mitochondrial OXPHOS complexes, each of them having distinct advantages and limitations. The milder conditions used under CN-PAGE (mainly the absence of CB which has a detergent-like effect), allows better preservation of ATP synthase in-gel activity, and limits the dissociation of labile proteins in high molecular weight SCs and ATP synthase assemblies. [208] However, the absence of the anionic dye CB in the protein extract, and electrophoresis buffers causes the proteins to migrate based on their intrinsic charge and isoelectric point, which reduces the electrophoretic mobility of proteins within the gel. [208] Moreover, in the absence of CB, proteins with insufficient negative charge tend to aggregate thus reducing the resolution of protein complexes in the gel. [208, 358] To circumvent these limitations, the so-called high-resolution CN-PAGE has been developed by Wittig and Schragger. [358] In this protocol, sodium deoxycholate (DOC) and various mild non-ionic detergents (DDM, Triton X100) are added to the cathode buffer to keep membrane proteins solubilized and impose a negative charge shift on proteins, which results in a considerable improvement of resolution. [358]

A distinctive feature of the present hybrid CN/BN protocol is that a comparable resolution can be reached without these detergents. Momentary addition of CB to the cathode buffer at the beginning of the electrophoresis is sufficient to limit protein aggregation and enhance mobility in the gel (Figure 3.3-3.4). As a result, this hybrid technique enables excellent resolution of distinct SC assemblies and very low or no exposure to detergents. The presence of low amounts of CB also allows better preservation of CV activity, improved preservation of dimeric and oligomeric CV assemblies (Figure 3.3 and [208]), and a reduction of the blue background noise that can hinder the quantification of in gel activities, particularly for CII and CIV (Figure 3.2). Moreover, the absence of CB in the protein extract limits the disruption of labile protein interactions within SCs. For

example, physical association of the ATP synthase with ANT to form the synthasome [367] or with Cyclophilin-D to regulate PTP opening [300] are better seen in absence of CB. Momentary exposure to CB during electrophoresis only may therefore be useful to reveal novel protein interactions within SCs. Overall, this hybrid CN/BN-PAGE protocol thus allows to combine precise and rapid in gel activity measurements with analytical techniques involving 2D electrophoresis, immuno-detection and/or proteomics for advanced analysis of SCs. It should be noted that with the growing interest for SCs, an increasing number of studies use small 10 x 10 cm gels for native PAGE. While this approach may be sufficient to identify gross changes in the abundance SC assemblies, the lower separation capacity of small gels is likely limited to resolve subtle rearrangements or to cut distinct bands for proteomic analysis. Moreover, several studies using smaller gels have reported that the respirasome migrates at the same size as the ATPsynthase dimer, making it difficult to dissociate them. [359] Therefore, the use of large gels should be favored.

3.9 ACKNOWLEDGMENTS

The authors would like to thank Jenna Rossi for technical assistance, and Dr. Mireille Khacho, Dr. David Patten and Dr. Ujval Anil Kumar for helpful discussion while developing this method. This work was funded by the Canadian Institutes of Health Research (CIHR) and the National Sciences and Engineering Council of Canada (NSERC). AC is a recipient of Doctoral Award - Frederick Banting and Charles Best Canada Graduate Scholarships (CIHR).

3.10 DISCLOSURES

None

Chapter 4

Adaptive Optimization of the OXPHOS Assembly Line Partially Compensates LRPPRC-Deficient Mitochondrial Translation Defect in Mice

Alexanne Cuillerier[1], Matthieu Ruiz[3,4], Caroline Daneault[3], Anik Forest[3], Jenna Rossi[1], Goutham Vasam[2], George Cairns[2], Virgilio Cadete[1,5], LSFC Consortium, Christine Des Rosiers[3,4], Yan Burelle[1,2]

[1]Department of Cellular and Molecular Medicine, Faculty of Medicine, University of Ottawa, Ottawa, ON, Canada

[2]Interdisciplinary School of Health Sciences, Faculty of Health Sciences, University of Ottawa, Ottawa, ON, Canada

[3]Research Center, Montreal Heart Institute, Montreal, Québec, Canada

[4] Department of Nutrition, Université de Montréal, Montréal, Québec, Canada

[5] Sinclair Centre for Regenerative Medicine, Ottawa Hospital Research Institute, Ottawa, ON, Canada

Communications Biology, 2021; PMID: 34413467; DOI: 10.1038/s42003-021-02492-5

4.1 ABSTRACT

Mouse models of genetic mitochondrial disorders are generally used to understand specific molecular defects and their biochemical consequences, but rarely to map compensatory changes allowing survival. Here we took advantage of the extraordinary mitochondrial resilience of hepatic *Lrpprc* knockout mice to explore this question using native proteomics profiling and lipidomics. In these mice, low levels of the mtRNA binding protein LRPPRC induce a global mitochondrial translation defect and a severe reduction (>80%) in the assembly and activity of the electron transport chain (ETC) complex IV (CIV). Yet, animals show no signs of overt liver failure and capacity of the ETC is preserved. Beyond stimulation of mitochondrial biogenesis, results show that the abundance of mitoribosomes per unit of mitochondria is increased and proteostatic mechanisms are induced in presence of low LRPPRC levels to preserve a balance in the availability of mitochondrial- vs nuclear-encoded ETC subunits. At the level of individual organelles, a stabilization of residual CIV in supercomplexes (SCs) is observed, pointing to a role of these supramolecular arrangements in preserving ETC function. While the SC assembly factor COX7A2L could not contribute to the stabilization of CIV, important changes in membrane glycerophospholipid (GPL), most notably an increase in SC-stabilizing cardiolipins species (CLs), were observed along with an increased abundance of other supramolecular assemblies known to be stabilized by, and/or participate in CL metabolism. Together these data reveal a complex in vivo network of molecular adjustments involved in preserving mitochondrial integrity in energy consuming organs facing OXPHOS defects, which could be therapeutically exploited.

4.2 SIGNIFICANCE STATEMENT

- Mouse models of genetic mitochondrial disorders are commonly used to understand specific molecular defects and their biochemical consequences, but rarely to map compensatory mechanisms allowing survival.
- We took advantage of the extraordinary mitochondrial resilience of hepatic *Lrpprc* knockout mice to explore this question.
- Our data reveal a complex network of molecular adjustments involved in preserving mitochondrial integrity in an energy consuming organ facing oxidative phosphorylation (OXPHOS) defects.
- These involve upregulation of mitochondrial content, maintenance of translation, and stabilization of residual electron transport chain complexes into bioenergetically more efficient supercomplexes (SCs), likely through upregulation of SC-stabilizing cardiolipins (CLs).
- Targeting these processes with compounds promoting mitochondrial biogenesis, and/or mitochondrial translation, and supplements for CL synthesis could therefore help compensate genetic mitochondrial defects in patients.

4.3 INTRODUCTION

Mitochondria are dynamic double membrane entities playing a central role in cellular homeostasis. In addition to their major contribution to cellular energy production through oxidative phosphorylation (OXPHOS) these organelles are functionally coupled to peroxisomes and the endoplasmic reticulum, and influence several facets of cellular biology such as lipid exchange, membrane dynamics and signaling. [368] Because of their bacterial origin, each organelle is endowed with multiple copies of circular DNA (mtDNA) comprising a total of 37 genes encoding for 13 core components of the OXPHOS machinery, and all RNA components required for their translation. Over the course of evolution, the remaining genes essential for the synthesis of the 1158 mitochondrial proteins have however been transferred to the nucleus. As a result, the biogenesis of these organelles has become one of the most complex biological processes requiring a fine intergenomic coordination, the import and assembly of protein subunits synthetized in distinct cellular compartments, and the incorporation of assembled multi-proteins complexes into specialized lipid bilayers.

Not surprisingly, mutations in mitochondrial genes encoded either in the mtDNA or nucleus underlie a broad spectrum of inherited disorders. [52, 72, 296] A large proportion of these mutations affect structural subunits of complex I, III, IV and V of the OXPHOS machinery, or factors involved in their translation or assembly. One such factor is Leucine Rich PentatricoPeptide Repeat Containing protein (LRPPRC; OMIM*607544), a protein predominantly localized to the mitochondria involved in the stabilization and translation of mtDNA-endoded mRNAs. Mutations in the *LRPPRC* gene have been identified as the root cause of a distinct monogenic form of Leigh Syndrome in the French-Canadian population of the northeastern region of Quebec (Leigh Syndrome French Canadian variant; LSFC; OMIM#220111) [84, 85], and recently in unrelated families in Europe and China. [87-89] Mutations in *LRPPRC* result in a severe loss of the protein in tissues, and consequently a drastic reduction in the steady-state levels of most mitochondrial mRNAs, resulting in a pronounced complex IV (CIV) deficiency in the liver and brain (20% of normal activity), a moderate CIV deficiency in fibroblasts and heart (50% of normal activity) and a combined CIV and complex I (CI) defect in the skeletal muscle (40% of normal activity). [85, 113, 122] LSFC patients also present high levels of circulating long-chain acyl-carnitines, which are proxies of mitochondrial fatty acid oxidation abnormalities, as well as a lipidomics signature of

perturbations in peroxisomal lipid metabolism characterized by lower levels of circulating ether lipids, which are precursors of plasmalogens, as well as conjugated bile acids. [90, 94]

Several features of the LSFC phenotype are also observed in mice harboring a liver-specific knockout of LRPPRC (H-*Lrpprc*$^{-/-}$), which includes a growth delay, a depletion of most mtDNA encoded transcripts, a severe disruption of CIV assembly and activity, and an impairment of mitochondrial long-chain fatty acid oxidation and peroxisomal function. [94, 360] However, mice behave normally and present a striking preservation of respiratory chain capacity. [360] Moreover, their ability to tolerate fasting through the energetically costly process of gluconeogenesis is preserved, and they show no evidence of overt liver failure [360], suggesting efficient adaptive changes are present to compensate for the translation defect resulting from LRPPRC deficiency. Better knowledge of those endogenous protective mechanisms has the potential to inform novel and unsuspected opportunities for therapeutic interventions, which are currently lacking for these patients.

In this study, native proteomics profiling and lipidomics in mitochondrial membranes were therefore used in our well-characterized mouse model of hepatic LRPPRC deficiency to explore and integrate various aspects that are critical for the maintenance of mitochondrial bioenergetics integrity. Our results point to several adaptive countermeasures which collectively allow for a relative preservation of mitochondrial and liver function despite the severity of the LRPPRC-dependent translation defect.

4.4 RESULTS

4.4.1 Hepatic Lrpprc deficiency triggers compensatory mitochondrial biogenesis and increased abundance of mitoribosome complexes.

Activation of mitochondrial biogenesis to compensate specific biochemical defects has been reported previously in patients with mitochondrial disorders caused by mtDNA mutations, particularly when the heteroplasmy threshold reaches 60-90%. [296, 369] To begin our investigation, we therefore examined whether this common adaptive mechanism was present in livers from H-*Lrpprc*$^{-/-}$ mice. As shown in Fig. 4.1A, copy number was more than doubled compared to WT controls, and mitochondria, although presenting clear ultrastructural abnormalities, were visibly larger and more numerous when visualized by electron microscopy (Fig. 4. 1B). Furthermore, protein expression levels for PGC1α, and the transcription factor TFAM were also upregulated, consistent with an increased drive for mitochondrial biogenesis in presence of low levels of LRPPRC (Fig. 4.1C).

In mitochondria, the main role of LRPPRC is to act as a global RNA chaperone which binds and stabilizes mt-DNA-encoded RNA structures to promote their translation. [122, 370] Therefore, we examined whether quantitative adjustments in the translational machinery were also present to compensate for the reduced levels of mitochondrial transcripts observed in absence of LRPPRC. To this end, proteomics profiling was performed on digitonin-extracted mitochondrial samples submitted to hybrid CN/BN-PAGE to resolve and quantify the abundance of mitochondrial ribosome complexes. A total of 24 Small and 39 Large Ribosomal Proteins (MRPS and MRPL) were consistently detected in all samples. In both genotypes, peak abundances for MRPS and MRPL proteins were observed in the 0.88-1.04, and 2.05-2.45 MDa regions respectively, which correspond to the migration pattern of the 28S and 39S mitoribosome complexes [371] (Fig. 4.1D-E). The global abundance of MRPS and MRPL proteins in both of these complexes was increased several folds in LRPPRC deficient mitochondria. Because equal amounts of mitochondrial protein extracts were loaded in the gels, these results suggest that the number of mitoribosomes per mitochondrial unit was substantially increased (Fig. 4.1D-E). Of note, LRPPRC was only detected in WT mitochondria and was mostly associated with the 28S mitoribosome complex together with prohibitins (PHB1, PHB2), and ATAD3, which are known mitoribosome-associated proteins (Fig. 4.1D). Altogether, these results indicate that in addition to a greater cellular mitochondrial content,

the density of ribosomes in each mitochondria is enhanced in H-*Lrpprc*$^{-/-}$ mice in order to compensate for the translation deficit.

Proteomic profiling also revealed that several proteins involved in the mitochondrial Unfolded Protein Response (mtUPR) were increased in response to the LRPPRC deficit, including mtHSP70/GRP75 (Hspa9), HSP60 (Hspa1), HSP10 (Hspe1), LONP1, AFG3L2, SPG7 and YME1L1 (Fig 4.1F). Several of these proteins were also found to be upregulated in confirmatory immunoblot experiments (Fig S4.1). Furthermore, transcript levels for the transcription factor CHOP, which mediates the mtUPR and more broadly the Integrated Stress Response 19, was increased 5-fold in H-*Lrpprc*$^{-/-}$ livers (Fig 4.1G), suggesting rewiring of cellular metabolism and maintenance of mito-nuclear balance likely involves these survival pathways.

Figure 4.1: Impact of LRPPRC Deficiency on Mitochondrial Biogenesis, Mitochondrial Ribosome Content and Proteostatic Systems

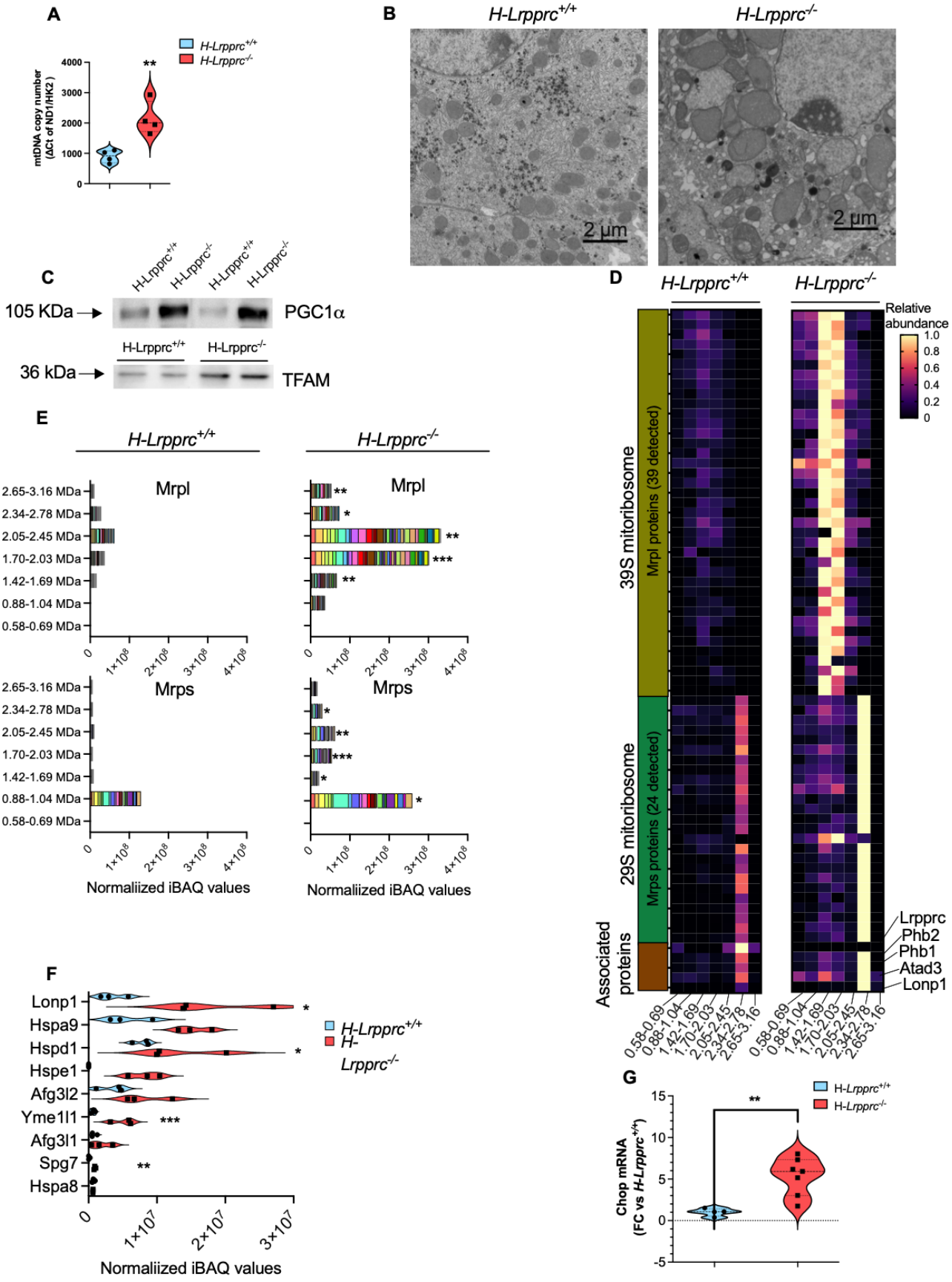

*Panel A: mitochondrial DNA copy numbers measured in whole liver homogenates from of H-Lrpprc$^{+/+}$ and H-Lrpprc$^{-/-}$ mice at 5 weeks of age. Values represent means ± sem of the ND1/HK2 ΔCt ratio (n=4). Student T test was used to assess significance (**: P<0.01). Panel B: Transmission Electron Micrographs of H-Lrpprc$^{+/+}$ and H-Lrpprc$^{-/-}$ livers at 5 weeks of age (magnification 1900x). Panel C: PGC1α and TFAM protein expression in whole liver homogenates from H-Lrpprc$^{+/+}$ and H-Lrpprc$^{-/-}$ mice. Panel D and E: Proteomic profiling of Large 39S and Small 29S mitochondrial ribosomal proteins (MRPL and MRPS proteins) in digitonin-solubilized mitochondria from H-Lrpprc$^{+/+}$ and H-Lrpprc$^{-/-}$ mice following separation by hybrid CN/BN-PAGE. The heatmap (Panel D) represents the average abundance (n=3 per group) of individual ribosomal protein in each of the gel bands analyzed relative to the maximal abundance observed for this protein in all samples analyzed. Each lane represents an individual subunit, and the range of molecular weight covered by each band is indicated at the bottom. To represent the abundance of mitoribosomes, iBAQ intensities for all of the large and small ribosomal subunits detected in each band were summed for each experimental replicate and the average values obtained for each genotype is presented in stacked histograms (Panel E). Panel F: Total abundance of selected mitochondrial proteases in digitonin-solubilized mitochondria from H-Lrpprc$^{+/+}$ and H-Lrpprc$^{-/-}$ mice. For a given protein, total abundance in a sample was calculated by summing the normalized iBAQ intensities observed in each band analyzed. Values presented represent the mean ± sem for n=3 in each group. Validation immunoblots for selected proteases are shown in Fig S1. One sample T tests corrected for multiple comparisons were performed to assess significance (***: Q < 0.01, **: Q < 0.01, *: Q < 0.05). Panel G: transcript level of Chop normalized to Tbp as housekeeping gene in whole liver homogenates from H-Lrpprc$^{+/+}$ (n=4) and H-Lrpprc$^{-/-}$(n=7).*

4.4.2 Hepatic Lrpprc deficiency triggers a remodelling of respiratory chain supercomplexes and stabilization of residual CIV into respirasomes

Studies on isolated mitochondria from H-*Lrpprc*$^{-/-}$ mice showed that maximal uncoupled flux through the electron transport chain (ETC) is completely preserved despite a drastic reduction (80-85%) in the amount of assembled CIV and in enzyme activity measured in solubilized extracts. [360] Even more striking is the fact that respiration in presence of the CIV substrate TMPD/ascorbate, which reflects CIV activity in its native membrane environment, is only reduced by 20-30%, as opposed to 80-85% following detergent extraction ([360] and Fig. S4.2). These results strongly suggest that beyond the above-mentioned increase in mitochondrial biogenesis and

mitoribosome density, additional mechanisms are in place to preserve residual CIV activity and maintain ETC function in presence of low LRPPRC levels.

We therefore tested whether the preservation of residual CIV was linked to remodeling of the ETC supercomplexes (SCs). Digitonin-solubilized mitochondria were subjected to hybrid CN/BN-PAGE, and the various supramolecular arrangements of ETC complexes were examined by immunoblot (Fig. 4.2A), in-gel activity (Fig. S4.3), and proteomics profiling (Fig. 4.2D). As expected, the total amount of assembled monomeric CIV was considerably reduced in LRPPRC deficient mitochondria compared to WT, with no apparent changes in the amount of CI monomers and CIII dimers (Fig. 4.2A). However, incorporation of CIV monomers into the S1 supercomplex composed of monomeric CI, dimeric CIII and monomeric CIV (I1-III2-IV1, termed respirasome) was relatively preserved (Fig. 4.2A). As a result, the proportion of CIV incorporated in the S1 respirasome relative to its monomeric form was increased (Fig. 4.2C, top and S4.3). Since only a few CIV monomers are available for assembly, higher molecular weight supercomplexes containing dimeric and multimetric CIV (e.g. S4.2-S4.4: I1-III2-IV2 and I1-III2-IVn) were nevertheless severely reduced in H-*Lrpprc*$^{-/-}$ mitochondria (Fig. 4.2A), albeit still detectable by proteomic analysis of the bands (Fig. 4.2D), and in gel activity measurement for a prolonged incubation period (Fig. S4.3). LRPPRC deficient mitochondria also presented a strong accumulation of CI and CIII in the region corresponding to the S4 supercomplex despite containing almost no CIV (Fig. 4.2A and 4.2D). This was accompanied by a reduction of CI and CIII in the region corresponding to S2 and S3 supercomplexes (Fig. 4.2A, 4.2D and S4.3) in H-*Lrpprc*$^{-/-}$ mitochondria, indicating a migration shift of CI-CIII containing arrangements toward a higher apparent molecular weight. Furthermore, S0 supercomplex composed of monomeric CI and dimeric CIII (I-III2) was slightly but significantly more abundant in H-*Lrpprc*$^{-/-}$ mitochondria (Fig 4.2D).

SCs were also extracted from LSFC patient fibroblasts and resolved under the same electrophoresis conditions. As shown in Fig. 4.2B and C (bottom), the abundance of CIV monomers was also severely reduced in LSFC patient mitochondria compared to control. However, the abundance of CIV present in S1-S2 SCs was relatively preserved, confirming the stabilization of residual CIV into supramolecular assemblies in these LSFC patient cells. Oligomeric forms of CIV found in control cells between the monomeric band and SCs assemblies, were however undetectable in patient samples. Stabilization of residual CIV in supercomplexes has also been reported in

fibroblasts from two patients harboring isolated CIV deficiencies linked to mutation of distinct nuclear encoded genes [203], suggesting this may be a common response to CIV deficiency.

Figure 4.2: Impact of LRPPRC Deficiency on Respiratory Chain Supercomplexes.

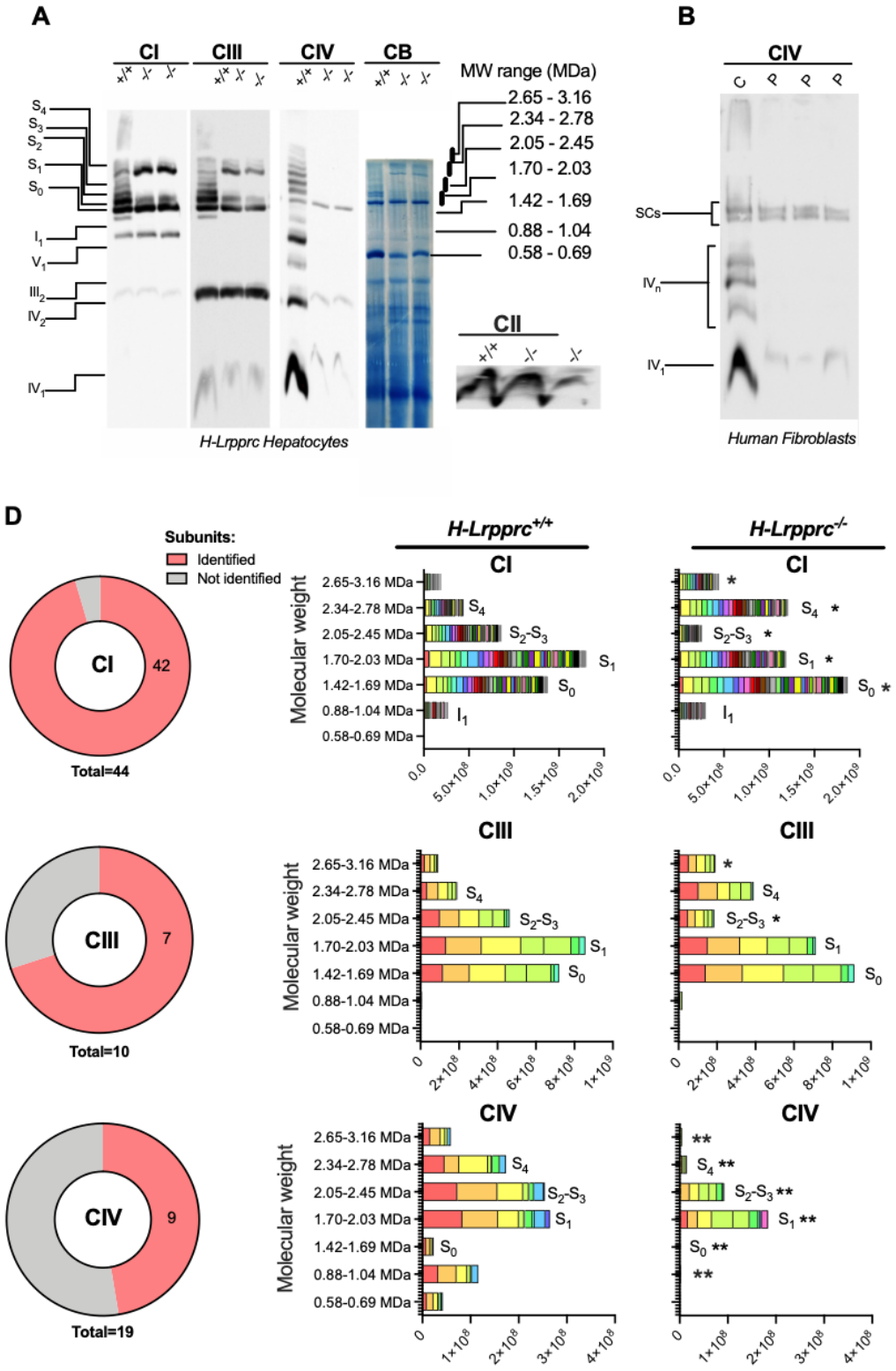

Panel A: Representative migration pattern of respiratory chain supercomplexes in digitonin-solubilized mitochondrial extracts from H-Lrpprc$^{+/+}$ and H-Lrpprc-/- mice resolved by hybrid CN/BN-PAGE. Replicates of the same 3 samples (1 H-Lrpprc$^{+/+}$ and 2 different H-Lrpprc$^{-/-}$) were loaded in multiple wells and migrated together. Following electrotransfer, replicate lanes were cut and probed with specific antibodies for CI, CII, CIII, and CIV. OXPHOS complexes and supramolecular assemblies are identified using the standard nomenclature, with numbers in indices indicating the molecular stoichiometry of each OXPHOS complex. Molecular weight ranges indicated on the right correspond to the size of the bands that were excised from a gel ran in parallel for proteomics profiling. Molecular weight calibration was performed using the migration pattern of CI, CII, CIV, and CV as assessed by in gel activity assays. Panel B: Representative migration pattern of CIV-containing supercomplexes in fibroblast mitochondria from controls and LSFC patients revealed by CIV immunostaining. Electrophoresis conditions were similar as in panel A. Panel C: Quantitative analysis of the proportion of CIV present in SCs relative to monomeric CIV in liver mitochondria and patient fibroblasts (n=3 per group). Panel D: Proteomics analysis of respiratory chain supercomplexes. For each complex, a pie chart illustrates the number of subunits reliably identified in the gel bands and the stacked histogram illustrates the mean (n=3 per group) abundance of complex subunits present in each band analyzed (see Fig. 1F legend for details).

4.4.3 Integration of residual CIV in respirasomes in LRPPRC deficient mitochondria is independent of COX7A2L

The molecular mechanisms regulating the formation of SCs are currently unclear and constitute a topic of debate[206]. Several proteins, including COX7A2L, RCF1/HIGD1A and RCF2/HIGD2A, have been identified using knockdown approaches in yeast and mammalian cells, and are suggested to affect SCs. However, controversy exists regarding their necessity, and whether they act directly in the formation/stability of SCs, or indirectly by promoting the assembly of individual ETC complexes.

As shown in Fig. 4.3A, LRPPRC deficiency caused a 2 fold increase in total COX7A2L protein abundance in whole mitochondrial lysates. When resolved under native conditions, COX7A2L was found mainly in CIII dimers and I1-III2 assemblies where its abundance was increased by ~1.5-2.0 fold in H-*Lrpprc*$^{-/-}$ samples (Fig 4.3B). However, COX7A2L was virtually absent from the respirasome and the larger molecular weight SCs (Fig 4. 3B), ruling out a potential contribution of

COX7A2L to the stabilization of CIV into SCs observed in *Lrpprc*-deficient mitochondria. This observation is consistent with the fact that mice were on a C57BL/6J background and thus expressed the short variant of COX7A2L which is able to interact with CIII assemblies, but lacks 2 critical residues found to mediate interactions with CIV. [143, 230, 231, 372] Of note, HIGD1A and HIGD2A (the mammalian orthologs of yeast's RCF1 and RCF2), which were recently suggested to promote SC assembly [223-225] could not be detected by proteomics profiling of the various SC bands (Supplemental table 1). Overall, our results suggested the possibility that factors other than assembly proteins could underlie the stabilization of CIV into SCs in *Lrpprc*-deficient mitochondria.

Figure 4.3: Impact of LRPPRC Deficiency on Supercomplexes Assembly Factor SCAF1.

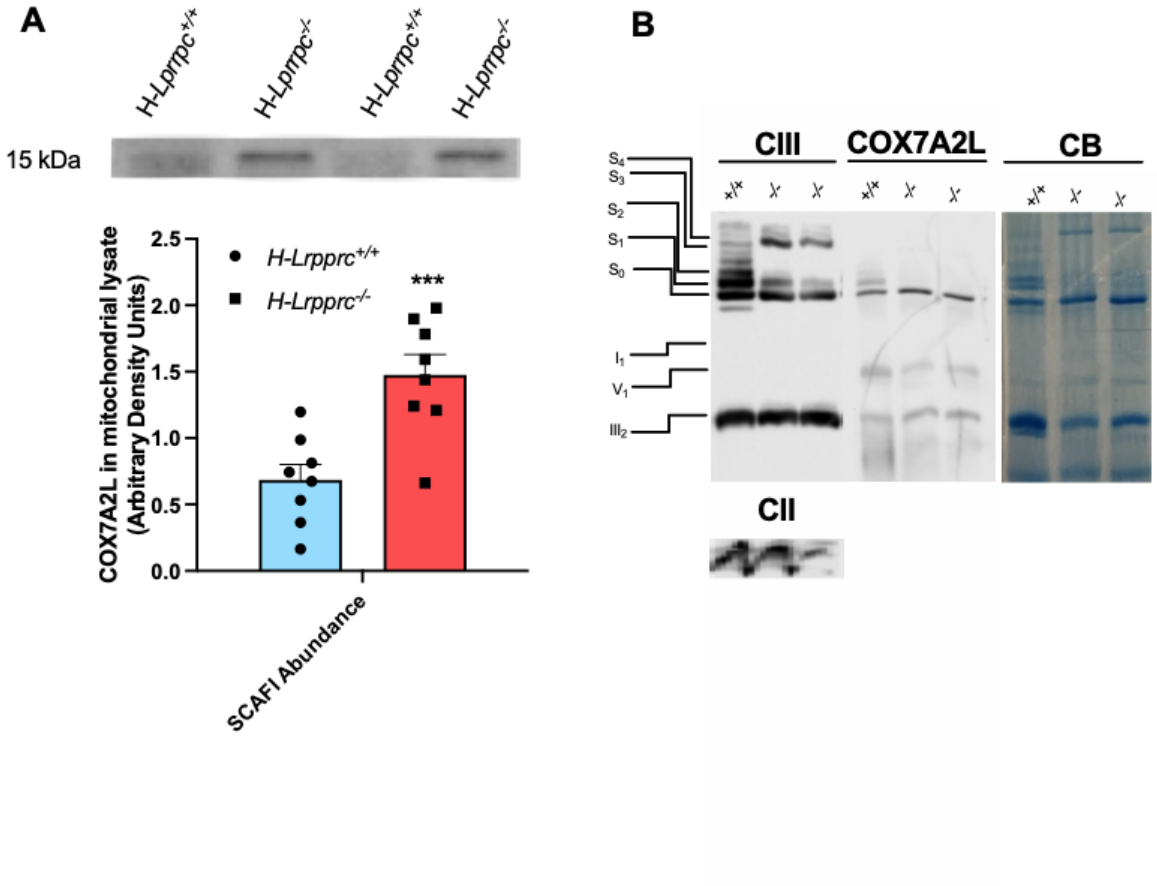

*Panel A: Western blot for quantification of SCAF1 abundance in liver mitochondria lysate (n= 8 per group) with representative image of the blot. (** = $p < 0.01$, Unpaired t test) Panel B: Representative migration pattern of CIV containing arrangements from digitonin solubilized extracts from H-Lrpprc$^{+/+}$ and H-Lrpprc$^{-/-}$ mice resolved by hybrid CN/BN-PAGE (n= 2 per group).*

After electrotransfer, one replicate was probed with antibody for CIII and CII, and the other replicate of the same gel with antibody for SCAF1 (COX7A2L).

4.4.4 Hepatic Lrpprc deficiency induces a remodeling of mitochondrial glycerophospholipids and increases multiple cardiolipin species.

Beyond assembly factors, increasing evidence indicates that membrane glycerophospholipid (GPL) composition exerts a strong influence on the assembly/stability of multi-protein complexes. [37, 233, 373] Thus, comprehensive untargeted lipidomics profiling, as previously described [94, 374], was performed in the digitonin-extracts used for hybrid CN/BN-PAGE in order to characterize potential changes in phospholipids that could promote SC stability in LRPPRC deficient mitochondria. Prior to performing these experiments, we validated the digitonin concentration used had a negligible impact on the GPL profile in the protein extract in order to exclude any biases related to small variations in the digitonin concentration across samples (Fig. S4.4). No significant changes in the proportion of the GPL (phosphatidylethanolamine and lysophosphatidylethanolamine (PE; LPE) shown as examples) and CL detected was noted between samples extracted with a digitonin ratio of 2 or 4 g/g of proteins.

In the digitonin-extracts, a total of 1176 mass spectrometry (MS) signals or features were reliably detected using high-resolution Liquid Chromatography quadrupole time-of-flight (LC-QTOF). These MS signals include, among other lipids, phosphatidylcholines (PCs), and the non-bilayer forming GPL phosphatidylethanolamines (PEs) as well as cardiolipin (CLs), which together make up ~90% of total mitochondrial GPL[37]. Volcano plot representation of the data highlighted the most significant changes, using a Q-value of <0.05 (corresponding to P<0.007) and a relative fold-change (FC) threshold of 1.5 and 0.75, in mitochondrial membrane lipids from H-*Lrpprc*$^{-/-}$ compared to H-*Lrpprc*$^{+/+}$ mice (Fig. 4A). MS/MS analysis of the most discriminant entities revealed changes in all the three major classes of mitochondrial GPL including PCs, PEs, and CLs (Fig. 4.4B). All of the differentially abundant PEs detected, except one (PE (20:0_20:4)), were increased in H-*Lrpprc*$^{-/-}$ mitochondria. For PCs, the proportion of increased and decreased species in H-*Lrpprc*$^{-/-}$ mice was more balanced; but interestingly those that were decreased were mostly enriched in DHA (22:6) in the sn-2 position (Fig. 4.4B). In addition to these changes, four sphingomyelins were also found to be significantly less abundant in LRPPRC deficient extracts (SM(d18:1/22:0):

FC 0.26, Q=0. 0217; SM(d18:1/20:4): FC 0.35, Q=0. 0358; SM(d18:2/18:1): FC 0.48, Q=0. 0047; SM(d40:2): FC 0.24, Q=0. 049) (Fig. 4A).

CLs being the mitochondrial GPL for which a role in SC assembly, stability, and function has been established [234-237], a targeted data mining approach was used to quantify all detectable CLs in the digitonin-extracts. Six species which collectively account for >90% of the total CL pool in the liver [375] were consistently identified in the digitonin extracts (Fig 4.4C). This included the symmetric CL species CL72:6, CL72:7, and CL72:8 which account for ~80% of the total CL pool [375], as well as less common asymmetric species (CL 70:7, CL 74:8 and CL 76:11: ~10% of total CL pool, [375]) in which one C18:2 acyl chain is substituted by either hexadecadienoic acid (C16:2), eicosadienoic acid (C20:2) or docosapentaenoic acid (C22:5) (Fig. 4.4C). Of those, only CL 74:8 was significantly more abundant H-*Lrpprc*$^{-/-}$ mitochondria (log2 FC: 0.9, Q 0.05) and MS/MS analysis confirmed the acyl chains composition (CL (18:2_18:2_18:2_20:2)). However, broader changes in the CL profile were observed in whole mitochondrial lysates, with four species being significantly more abundant in H-*Lrpprc*$^{-/-}$ mitochondria (Log2 FC 0.6-1. 2; $Q < 0.05$), namely CL 72:6, and CL 72:7 which account for ~30% of the total CL pool [375], as well as CL 74:8 and CL 74:9 (Fig. 4.4D). Collectively, these results indicate that LRPPRC deficiency leads to significant remodeling of the GPL landscape in mitochondria, including a relative increase in PE species compared to PC and an increase in the abundance of multiple CLs species, which may promote stabilization of residual CIV into SCs.

Figure 4.4: Impact of LRPPRC Deficiency on Mitochondrial Membrane Lipids.

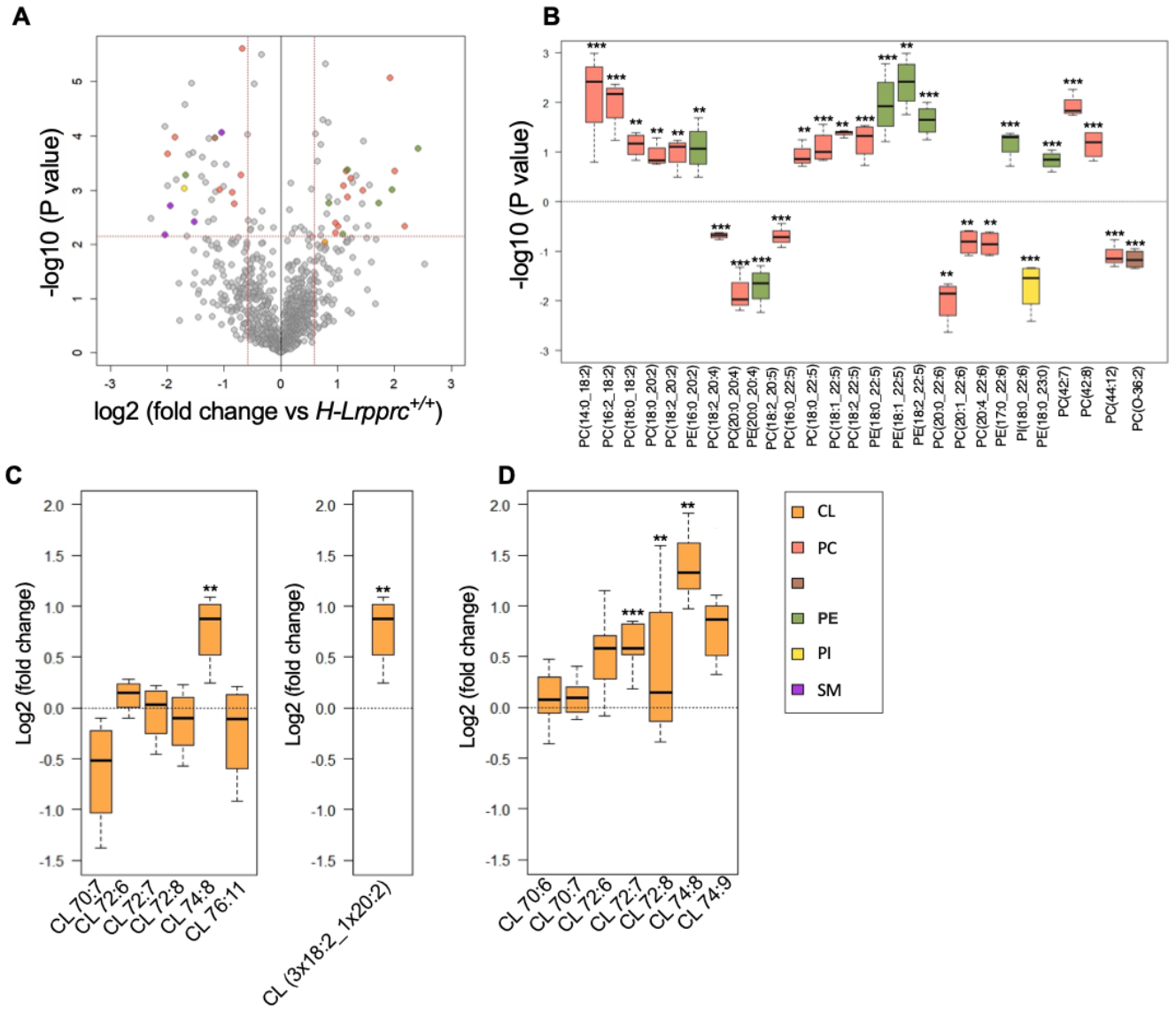

Comprehensive lipidomics of digitonin solubilized mitochondrial extracts (A-B) and targeted data mining of cardiolipin (CL) in digitonin-extracts (C) or isolated mitochondria (D). Panel A: Volcano plot from LC-QTOF-based untargeted lipidomics of digitonin solubilized mitochondria from H-Lrpprc$^{+/+}$ and H-Lrpprc$^{-/-}$ (n= 4 per group). The x axis represents fold changes (FCs) of MS signal intensity values for all these features in H-Lrpprc$^{-/-}$ vs H-Lrpprc$^{+/+}$ (log2) and the y axis represents p values (-log10). A corrected p value (Q-value) threshold of 0. 05 (corresponding to a P-value of 0. 007) and a relative FC of 1. 5 were used, leading to 69 significantly discriminant features among the 1176 MS features on which 31 were annotated. Panel B: Box plot of 27 selected lipids significantly discriminating H-Lrpprc$^{-/-}$ from H-Lrpprc$^{+/+}$, and annotated using MS/MS analysis. The midline represents the median fold change vs. H-Lrpprc$^{+/+}$, the box represents the interquartile range (IQR) between the first and third quartile, and whiskers represent the lowest or highest

*values. Panel C and D: Box plot of CL species annotated by MS/MS analysis in the digitonin-extracts (Panel C) and in isolated mitochondria (Panel D). Differences are shown according to a Q value of 0.056 (corresponding to a P-value of 0.009); (***: P < 0.01, **: P < 0.01).*

4.4.5 Hepatic Lrpprc-deficiency is associated with changes in protein complexes that are structurally and functionally linked to CL.

To further explore a potential role for increased CLs in promoting SC stability, native gel proteomics was used to probe selected supra-molecular complexes reported to be stabilized by CLs, or involved in the formation of CLs microdomains. To this end, we first determined whether the association of the ATP/ADP exchanger (ANT) with SCs was enhanced in H-*Lrpprc*$^{-/-}$ mitochondria, since the association of a minor fraction of ANT to SCs was previously shown to be strictly dependent on CLs. [233] As shown in Fig. 4.5A, ANT1 and ANT2 were both detected in high molecular weight bands corresponding to SCs, and their abundance was 2-3 folds greater in H-*Lrpprc*$^{-/-}$ mitochondria compared to WT, despite the fact that equal amounts of mitochondrial protein extracts were loaded in the gels. Similarly, CLs are involved in the oligomerization and stabilization of MICOS complexes in the inner mitochondrial membrane where they participate in the importation of precursors for CL synthesis and the formation of CL-rich microdomains. [35, 376] As shown in Fig 4.5B, MICOS subunits were found to migrate together in the 0. 58-0. 69 and 0.88-1.04 MDa regions, which corresponds to the known migration pattern of MICOS (0.5-1.1 MDa). In H-*Lrpprc*$^{-/-}$ mitochondria, the abundance of MICOS subunits, including the CL-binding subunits APOO and APOOL [377], was generally increased compared to WT.

Prohibitins were next examined as they are known to form large protein complexes that act as lipid scaffolds to regulate CL metabolism and other functions that are crucial for IMM homeostasis. [378, 379] As previously shown, the main prohibitin complex formed by PHB1 and PHB2 was detected in the 0.88-1.04 MDa region (Fig 4.5C) [39] together with the 29S mitoribosomes and other mitoribosome-associated proteins (see Fig. 4.2E). In H-*Lrpprc*$^{-/-}$ mitochondria, the abundance of this complex was increased by 2 folds (Fig. 4.5C). In addition, multiple other prohibitins-containing complexes running at 1.7 MDa and above were drastically increased in H-*Lrpprc*$^{-/-}$ mitochondria compared to WT (Fig. 4.5C). Several proteases, previously shown to associate with prohibitins to form proteolytic hubs (i.e. AFG3L2, SPG7, and YME1L1) were detected in these bands and they were generally more abundant in H-*Lrpprc*$^{-/-}$ livers (see confirmatory blots in Fig. S4.1). Notably,

prohibitins complexes above 2.0 MDa co-migrated with Stomatin-Like protein 2 (Stoml2), a member of the stomatin/prohibitin/flotillin/HflK/C (SPFH) family previously shown to interact with prohibitins [39, 379, 380], and to bind CLs to form CL-enriched microdomains for optimal assembly of the ETC complexes. [380] The abundance of Stoml2 in these putative prohibitin complexes was increased by 2.7, 3.5 and 3.7 folds respectively compared to WT.

Since contact sites between the Endoplasmic Reticulum (ER) and mitochondria play an important role in the transfer of lipid precursors required for mitochondrial CL synthesis [373] we finally looked for potential changes in proteins complexes involved in the maintenance of ER-mitochondria contact sites. In mammalian cells, maintenance of contacts sites is suggested to involve the Endoplasmic Reticulum Membrane Protein Complex (EMC), Mitofusin2 (MFN2) tethers, and Voltage Dependent Anion Channels (VDACs) - Glucose-Related Protein 75 (GRP75) complexes which are structurally linked to Inositol triphosphate Receptors (IP3R) at the ER surface. [381-383] Although EMC and MFN2 complexes were not captured in our proteomic profiling, VDAC1-3 and GRP75 were detected together in multiple bands, with a main peak in the 0.88-1.04 MDa region, suggesting these proteins migrated as part of a complex (Fig. 4.5D). In H-*Lrpprc*$^{-/-}$ mitochondria, the abundance of VDAC and GRP75 in the 0.88-1.04 MDa region was significantly increased compared to controls (VDACs: 2.7-3.6 fold; GRP75: 1.5 fold vs H-*Lrpprc*$^{+/+}$), as it was in mitochondrial lysates probed with anti-VDAC and GRP75 antibodies (Fig. S4.5). Furthermore, two additional VDAC-GRP75 containing complexes, which were absent in WT, were observed in the 0.58-0.69 MDa and 2.05-2.45 MDa regions, with a small amount of IP3R being present in the largest of these complexes. The increased abundance of VDAC-GRP75 complexes and their preserved association with IP3R in purified mitochondrial extracts suggest increased ER-mitochondria interactions in H-*Lrpprc*$^{-/-}$ mitochondria.

Figure 4.5: Impact of LRPPRC Deficiency on Protein Complexes Structurally and Functionally Linked to CL.

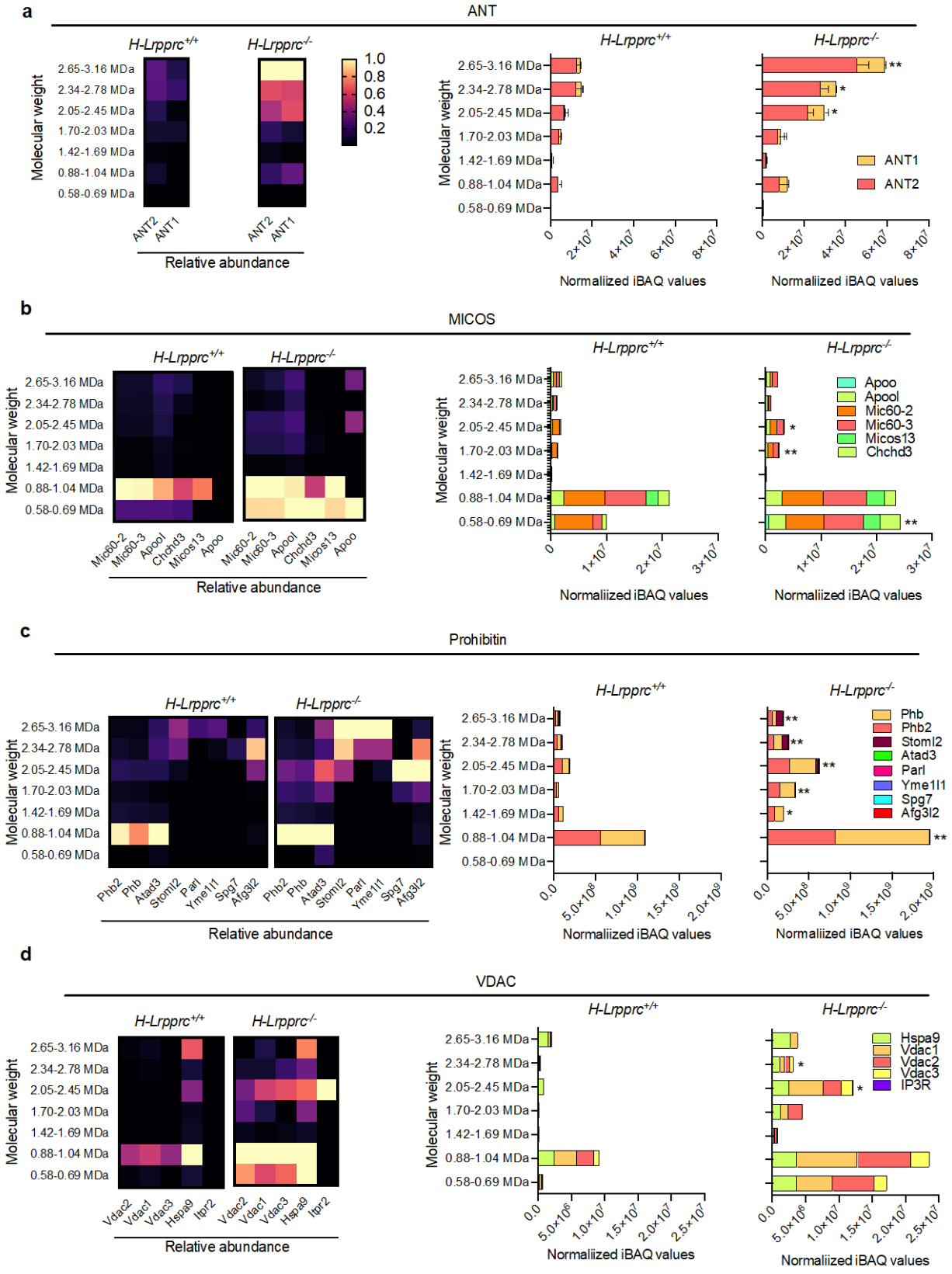

Proteomic profiling of ANT (panel A), MICOS (panel B), Prohibitin (panel C) and VDAC (panel D) complexes in digitonin-solubilized mitochondria from H-Lrpprc$^{+/+}$ and H-Lrpprc$^{-/-}$ mice

*following separation by hybrid CN/BN-PAGE. The heatmap represents the average abundance (n=3 per group) of individual protein within the complex in each of the gel bands analyzed relative to the maximal abundance observed for this protein in all samples analyzed. Each column represents an individual subunit, and the range of molecular weight covered by each band is indicated on the left side. To represent the abundance of ANT, MICOS, Prohibitin and VDAC, iBAQ intensities for all of the listed proteins forming each complex detected in each band were summed for each experimental replicate and the average values obtained for each genotype is presented in stacked histograms. Values represent the mean ± sem for n=3 in each group. One sample T tests corrected for multiple comparisons were performed to assess significance (***: Q < 0.01, **: Q < 0.01, *: Q < 0.05).*

4.5 Supplemental Material

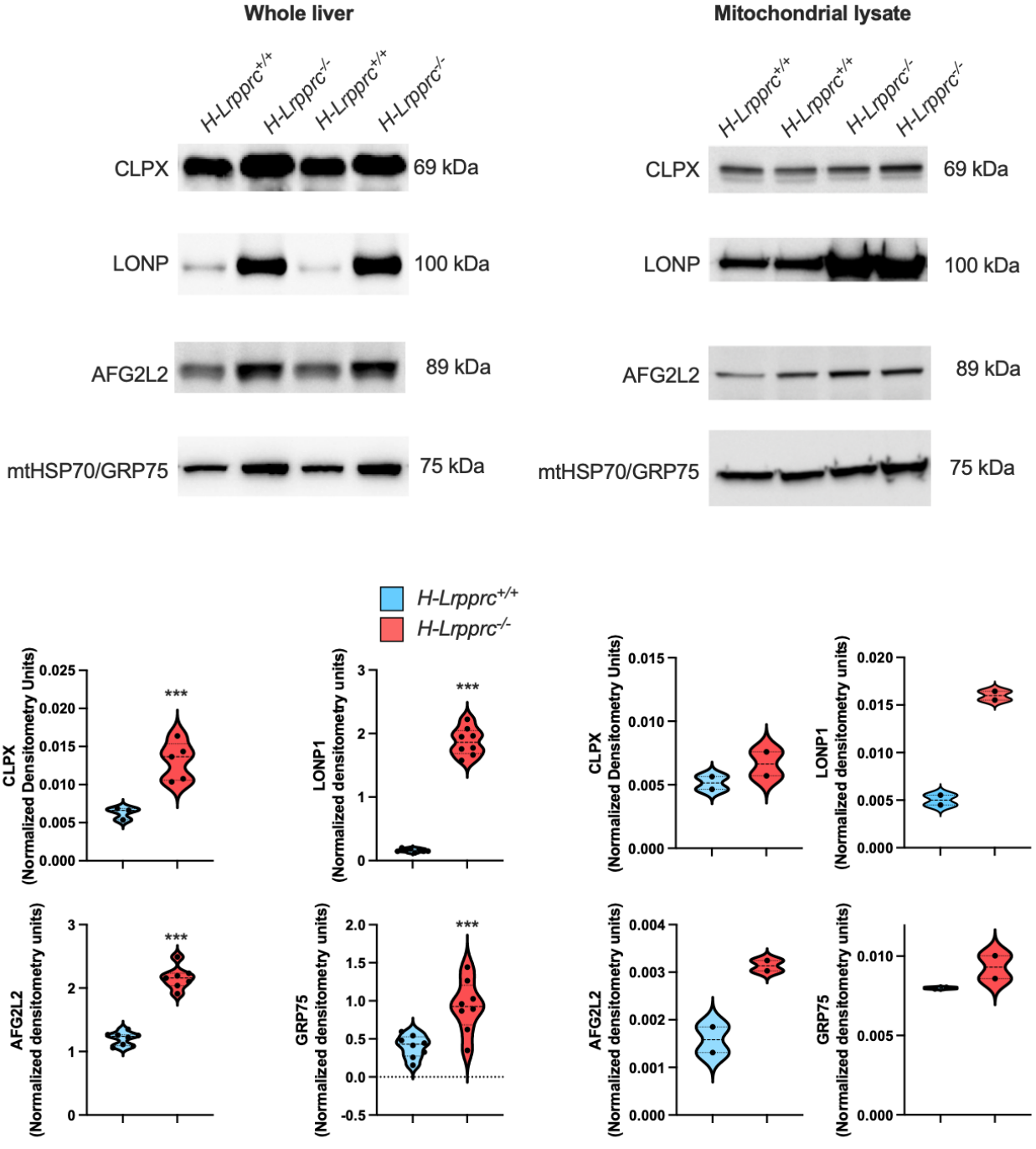

Fig S1: Impact of LRPPRC deficiency on protein abundance of selected proteases. Figure shows immunoblots performed following SDS-PAGE of liver lysates and mitochondrial lysates. Bar graphs represent mean ± sem of the quantitative analysis of protein expression performed on 5-8 animals per experimental groups. Densitometry values obtained for each protein was normalized against the Ponceau stain (provided in Fig S6). Unpaired two-sided T tests with Welsh's correction was used to assess significance (**: P<0.01).

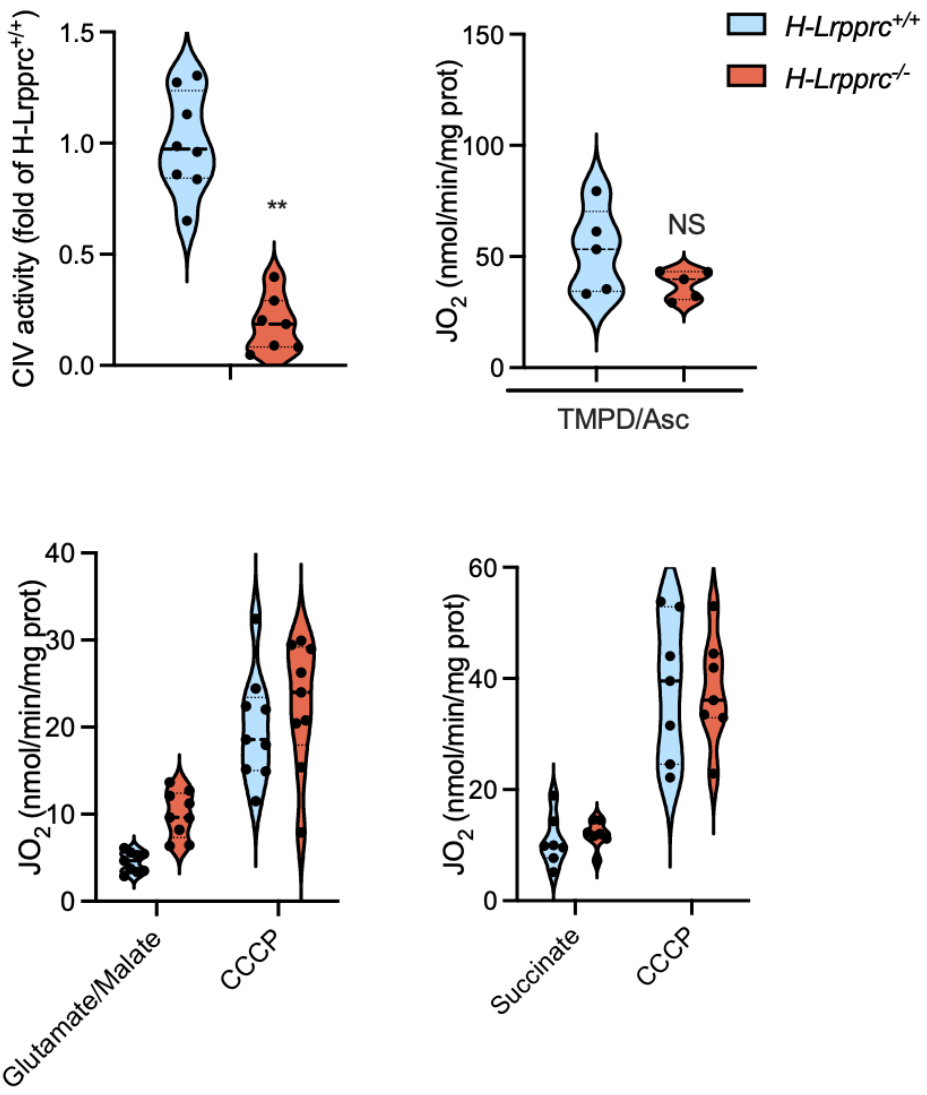

Fig S2: Impact of LRPPRC deficiency on CIV activity and respiratory capacity: Panel A: CIV activity measured spectrophotometrically in isolated liver mitochondria following detergent extraction. Panel B: Maximal state 3 respiration in isolated liver mitochondria energized with the CIV substrates TMPD and Ascorbate (9mM/0.9mM). Panel C-D: Baseline and maximal CCCP uncoupled respiration in mitochondria energized with CI (5 mM glutamate-0.5 mM malate) and CII (5 MM succinate) donors. Unpaired two-sided T tests with Welsh's correction was used to assess significance (**P<0.01).

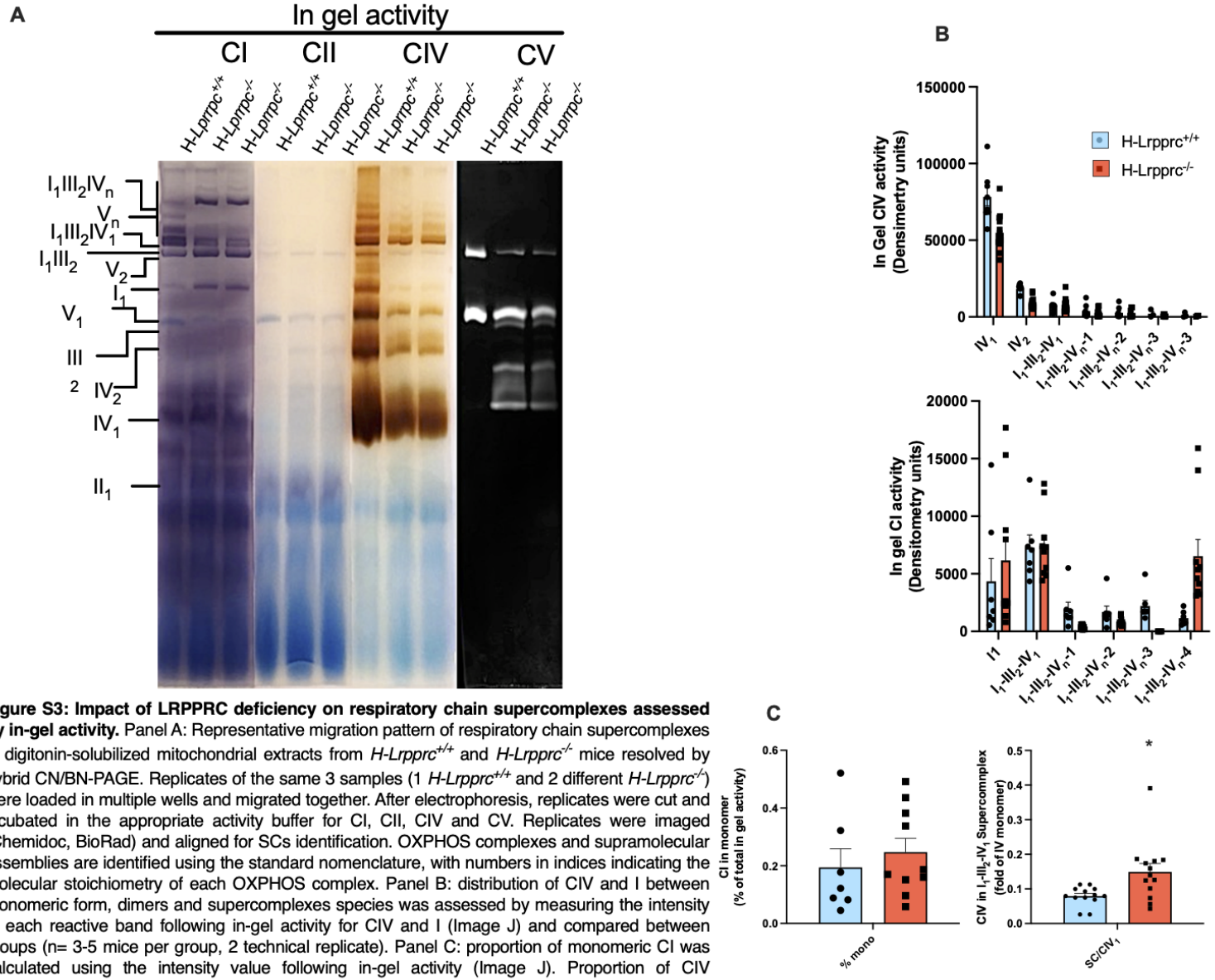

Figure S3: Impact of LRPPRC deficiency on respiratory chain supercomplexes assessed by in-gel activity. Panel A: Representative migration pattern of respiratory chain supercomplexes in digitonin-solubilized mitochondrial extracts from *H-Lrpprc*$^{+/+}$ and *H-Lrpprc*$^{-/-}$ mice resolved by hybrid CN/BN-PAGE. Replicates of the same 3 samples (1 *H-Lrpprc*$^{+/+}$ and 2 different *H-Lrpprc*$^{-/-}$) were loaded in multiple wells and migrated together. After electrophoresis, replicates were cut and incubated in the appropriate activity buffer for CI, CII, CIV and CV. Replicates were imaged (Chemidoc, BioRad) and aligned for SCs identification. OXPHOS complexes and supramolecular assemblies are identified using the standard nomenclature, with numbers in indices indicating the molecular stoichiometry of each OXPHOS complex. Panel B: distribution of CIV and I between monomeric form, dimers and supercomplexes species was assessed by measuring the intensity of each reactive band following in-gel activity for CIV and I (Image J) and compared between groups (n= 3-5 mice per group, 2 technical replicate). Panel C: proportion of monomeric CI was calculated using the intensity value following in-gel activity (Image J). Proportion of CIV incorporated in the respirasome was also calculated using the intensity value of the band following in-gel activity (Image J). Unpaired two-sided T tests with Welsh's correction was used to assess significance (*P<0.05).

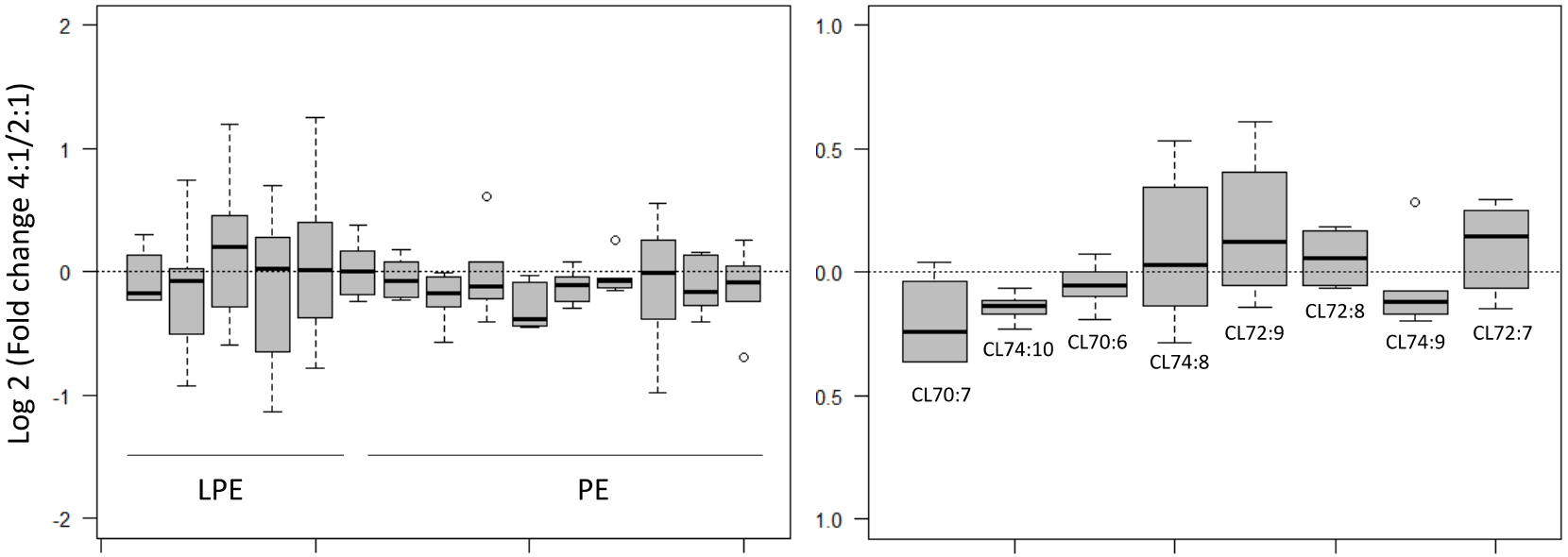

Figure S4: Impact of digitonin concentration on the glycerophospholipid (GPL) profile detected in supercomplex extracts. Figure shows box plots comparing the abundance of selected lysophosphatidyl ethanolamine (LPE), phosphatidylethanolamine (PE) and cardiolipin (CL) in supercomplexes extracted using a 4:1 or a 2:1 digitonin/protein ratio (n= 6-7 per condition). Data are presented as log2 ratio between abundancies measured at 4:1 vs 2:1. Absence of significant deviation from zero indicates that digitonin concentration has a negligible impact on the GPL profile in supercomplex extracts.

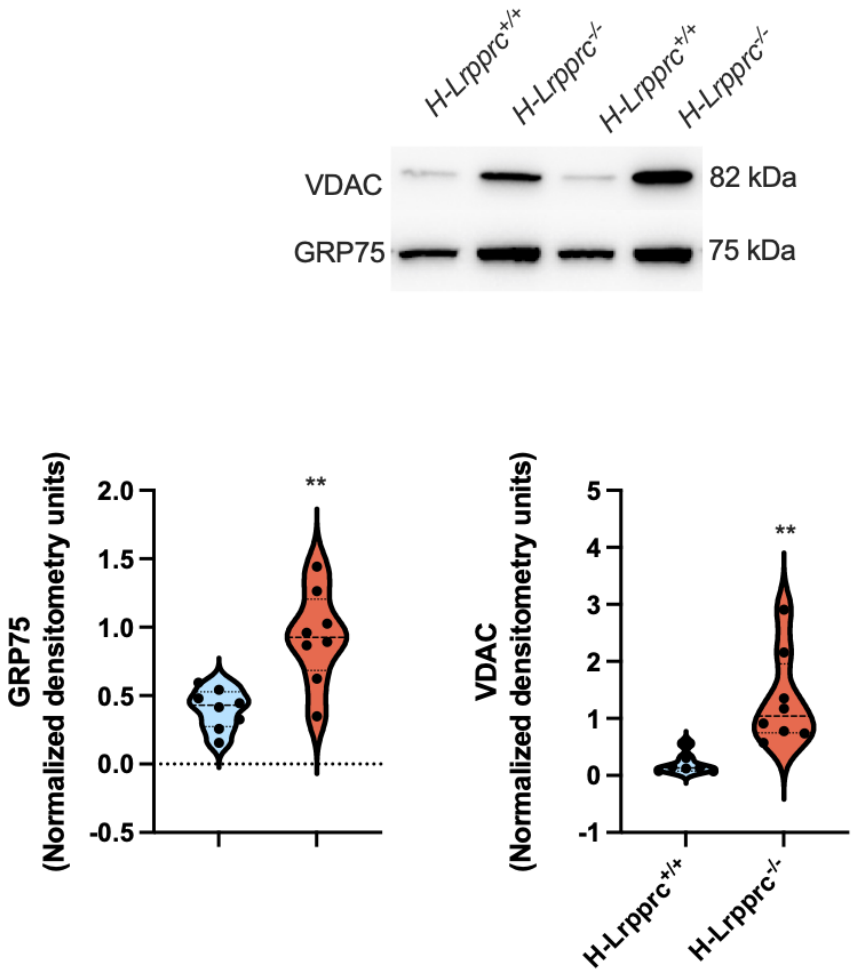

Fig S5: Impact of LRPPRC deficiency on the abundance of ER-mitochondria tethering proteins. Figure shows representative immunoblot performed following SDS-PAGE of whole liver lysates. Bar graphs represent mean ± sem of the quantitative analysis of protein expression performed on 7-8 animals per experimental groups. Densitometry values obtained for each protein was normalized against the Ponceau stain (provided in Fig S6). Unpaired two-sided T tests with Welsh's correction was used to assess significance (**: $P<0.01$).

Figure 1-C: PGC1-α

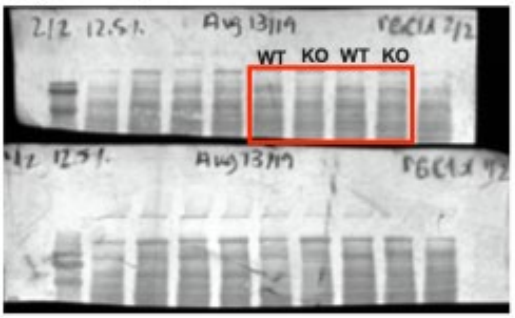

Figure 1-C: Tfam

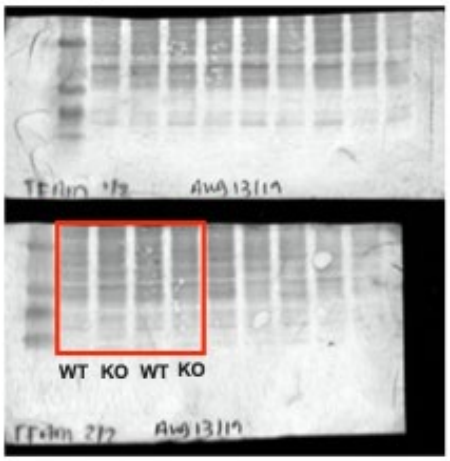

Figure 3-A: COX7A2L

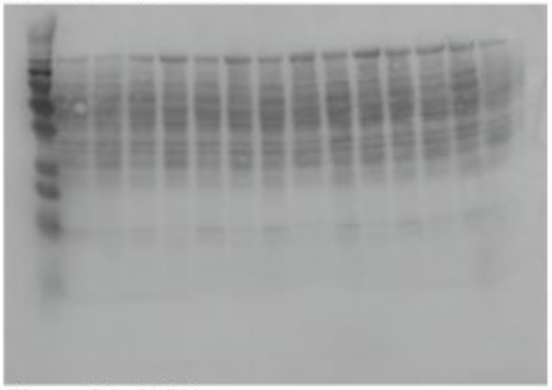

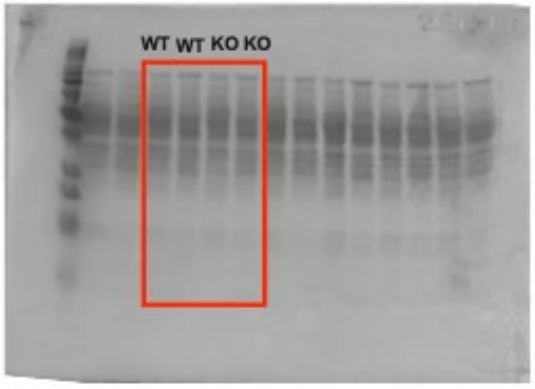

Figure S1: CLPX

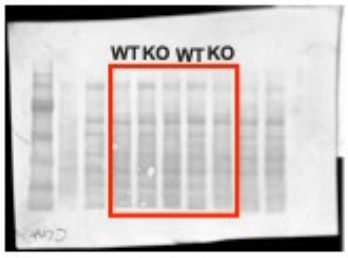

Figure S1: LONP

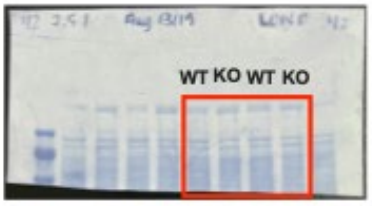

Figure S1: AFG3L2

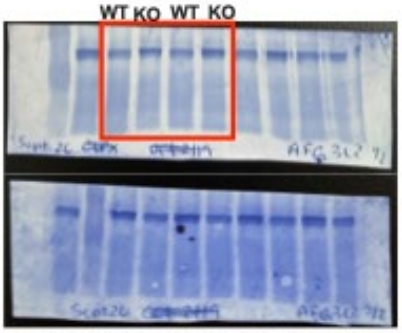

Figure S1: GRP75

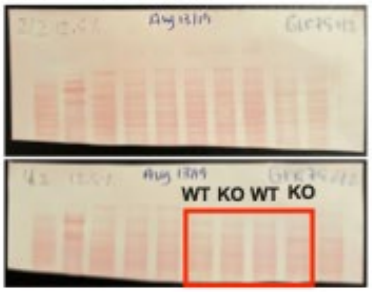

Figure S5: VDAC

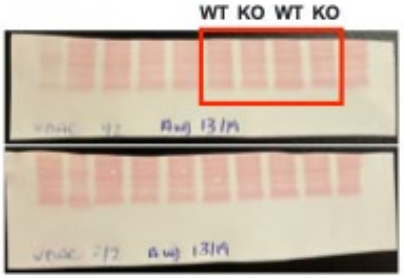

Fig S6: Coomassie blue and Ponceau straining of membranes used for immunoblot experiments reported in the indicated figures.

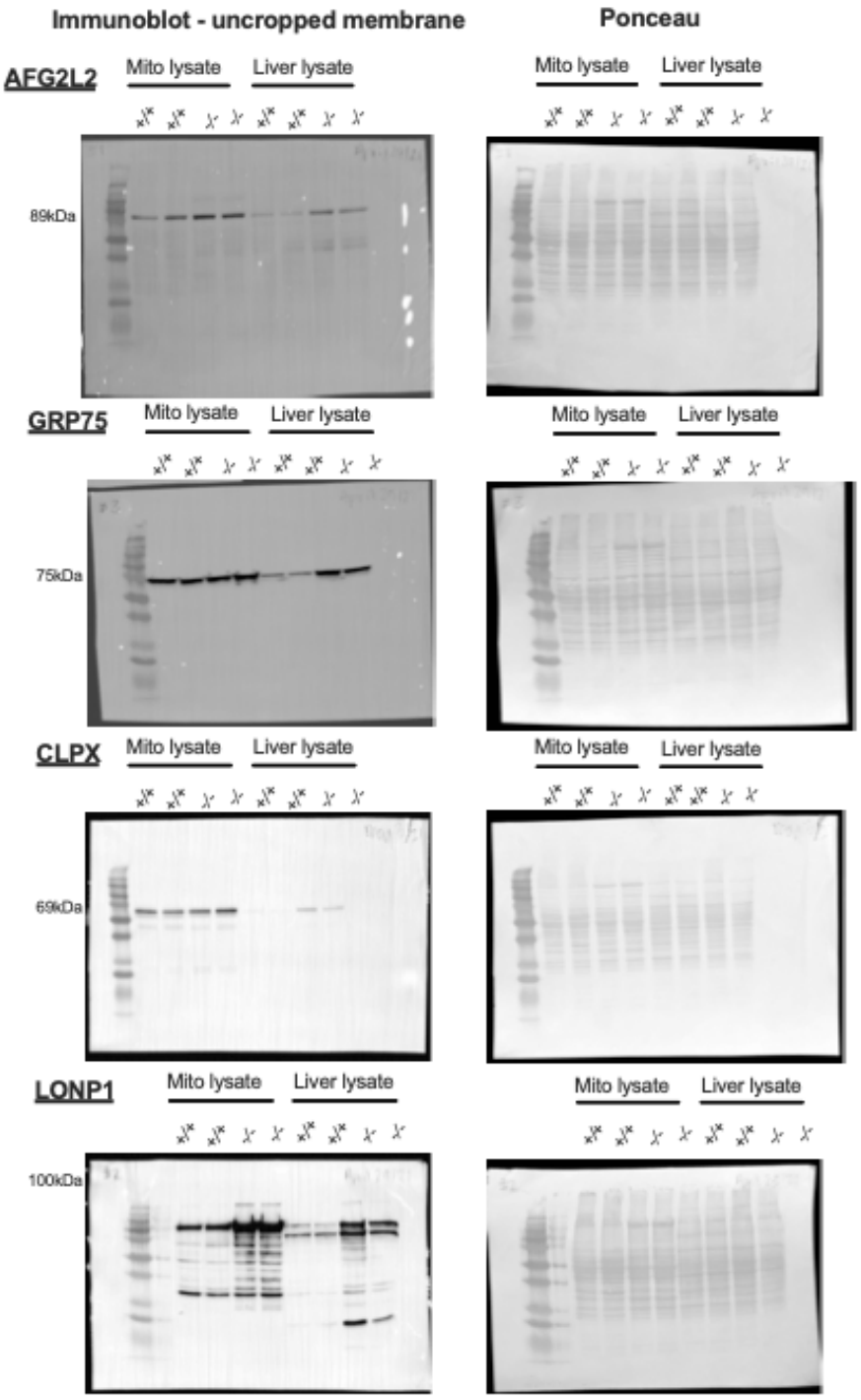

Fig S6B: Uncropped immunoblot membrane and Ponceau staining comparing mitochondrial proteases/ chaperones content in whole liver vs whole mitochondrial lysates.

Immunoblot - uncropped membrane

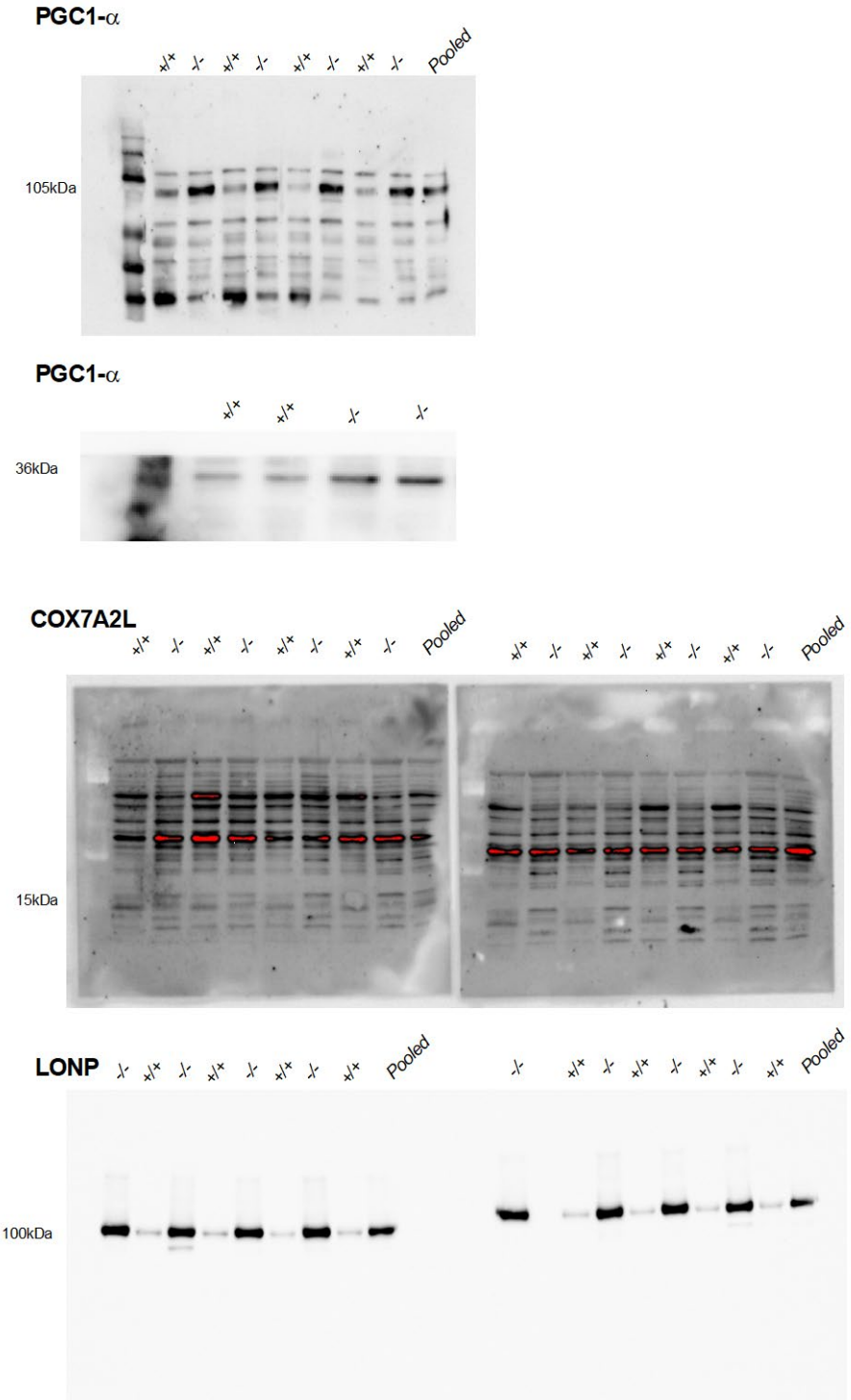

Fig S6C: Uncropped immunoblot membranes used for immunoblot experiments reported in the indicated figures.

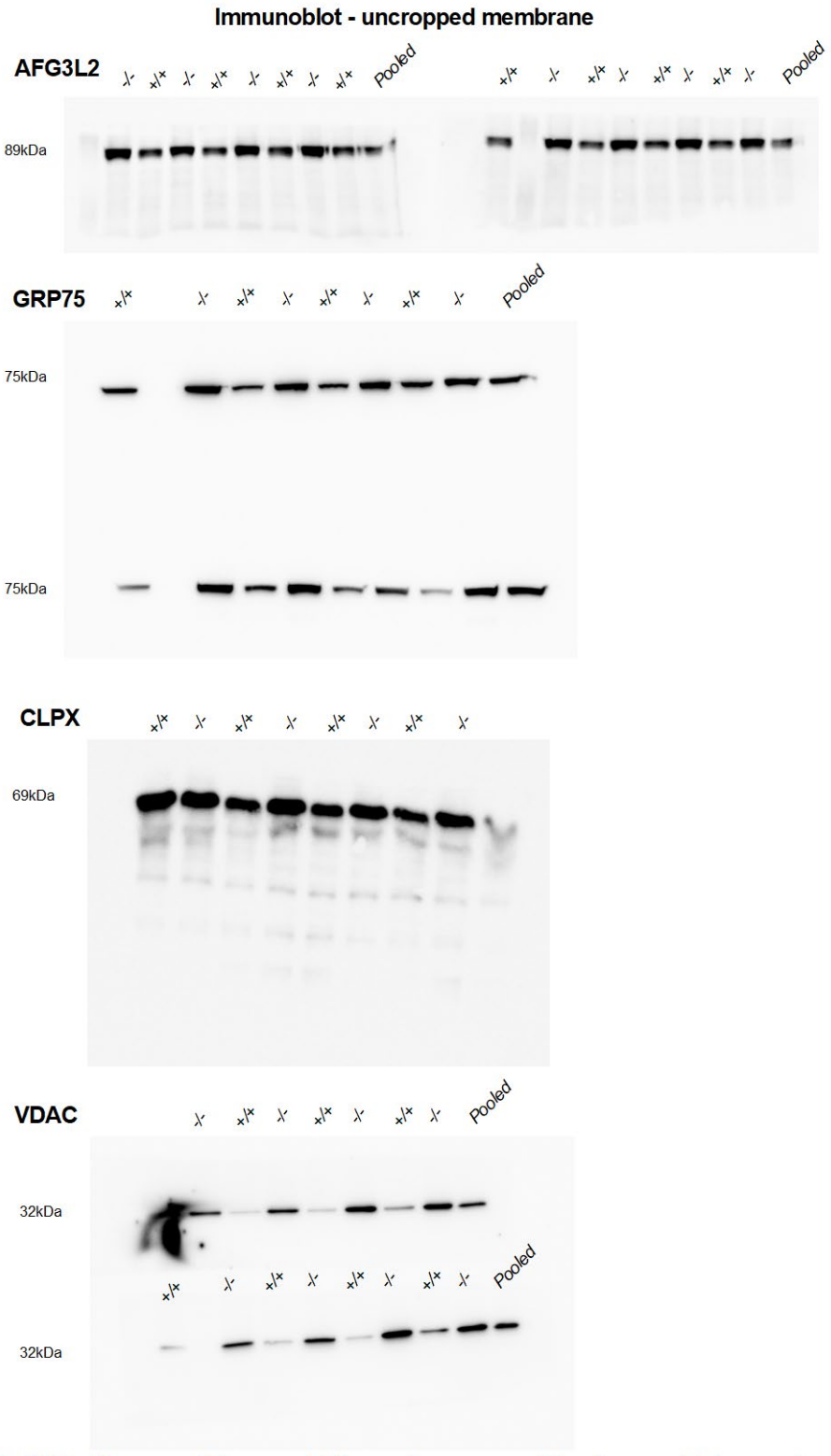

Fig S6C: Uncropped immunoblot membranes used for immunoblot experiments reported in the indicated figures.

4.6 DISCUSSION

Mouse models of genetic mitochondrial disorders are generally used to understand specific molecular defects and their biochemical consequences, but rarely to map in vivo compensatory mechanisms that allow maintenance of organ function and survival. Here we took advantage of the extraordinary mitochondrial resilience of hepatic *Lrpprc* knockout mice to explore this question using native proteomics and lipidomics. Our data reveals the presence of adaptive changes at multiple levels along the OXPHOS assembly line which likely allow to compensate the LRPPRC-dependent mitochondrial translation defect in the liver. We show that beyond stimulation of mitochondrial biogenesis, the abundance of mitoribosomes per unit of mitochondria is increased, and proteostatic mechanisms are stimulated. Furthermore, our results provide novel evidence for a stabilization of residual CIV in supercomplexes through a mechanism that may involve changes in the GPL composition of mitochondrial membranes, most notably CLs, which are reported to play a role in stabilizing protein-protein interactions in the inner membrane.

4.6.1 Balancing biogenesis, translation and proteostasis

Compensatory upregulation of mitochondrial content in response to LRPPRC deficiency is robust in the liver as shown by TEM imaging and several molecular markers of mitochondrial biogenesis. A similar response is also observed in the heart of cardiac-specific *Lrpprc* knockout mice. [85] Interestingly however, results from a recent study report a strikingly different phenotype following inactivation of *Lrpprc* in mouse brown adipose tissue (BAT), where lack of LRPPRC was associated with a downregulation of mitochondrial biogenesis signaling, a reduced expression of multiple nuclear-encoded oxidative and thermogenic genes, and an accumulation of intracellular triglycerides[384]. At least for mitochondrial biogenesis, there is thus a clear tissue-specificity in the response to the LRPPRC-dependent translation defect, which is likely attributable to differences in energy requirements across cell types and tissues. In BAT, metabolic reprogramming away from fuel oxidation and toward energy storage most likely represents the optimal compensatory response, while in energy demanding cells such as hepatocytes, which obligatorily rely of oxidative metabolism, upregulation of mitochondrial content to maintain oxidative capacity is probably crucial to support function and survival.

In this regard, is it interesting to note that in patients with mitochondrial diseases, massive mitochondrial proliferation is typically observed in muscle fibers [25, 369], which also supports the notion that compensatory mitochondrial biogenesis occurs preferentially in cells/tissues with high metabolic demands. Intriguingly, this mitochondrial proliferation phenotype is almost invariably observed in muscle fibers from patients harboring mtDNA mutations that affect global translation and result in multi-complex deficiencies, while it is always absent when mutations affect specific OXPHOS subunits. [25, 369] Based on the above mentioned dichotomic response of mitochondrial biogenesis to LRPPRC deficiency in liver and myocytes vs. BAT [384], the presence of compensatory mitochondrial biogenesis in patient muscle would therefore appear to be linked to the severity of the OXPHOS impairment as opposed to being specific to translation defects per se.

LRPPRC, in complex with its binding partner SLIRP, was recently shown to bind throughout the mitochondrial transcriptome (with a preference for mRNA) where it acts as a global RNA chaperone that stabilizes RNA structures, allowing exposure of the required sites for translation, stabilization, and polyadenylation of mitochondrial transcripts. [370] Therefore, although CIV is the main OXPHOS complex biochemically impaired in the liver [85, 113, 360], lack of LRPPRC clearly affects the secondary structure and stability of the entire mitochondrial transcriptome. [122, 360, 370] The present results provide evidence that in vivo this is compensated quantitatively by an increase in the number of mitoribosomes per mitochondrial unit, which was also reported in the cardiac-specific *Lrpprc* knockout mode. [369] This phenomenon is likely important for preserving a balance in the availability of mitochondrial- vs nuclear-encoded OXPHOS complex subunits in presence of a strong LRPPRC deficit, particularly in the face of a greater drive for mitochondrial biogenesis which increases the supply of nuclear-encoded polypeptides.

Over the last decade, studies have uncovered the mtUPR, a transcriptional program activated by mitochondrial proteotoxic stress, which aims to maintain proteostasis within the organelle. Studies in yeast and mammalian cell models have shown that this program triggers genetic activation of several mitochondrial chaperones and proteases. [162, 202, 385] The classic mtUPR also causes a reduction in the availability of mitochondrial transcripts, potentially through transcriptional repression at the level of the D-loop on mtDNA, and reduced expression of nuclear-encoded OXPHOS genes. [162] Furthermore, the mtUPR is reported to trigger broader changes such as the suppression of general translation and privileged translation of genes involved in cell survival, which in mammalian cells appears to be linked to the Integrated Stress Response pathway. [162]

However, limited data is available on the mtUPR response in the liver of in vivo models of genetic mitochondrial diseases. Our results show that LRPPRC deficiency in the liver potently induces the expression of CHOP, a key transcriptional activator of the mtUPR and ER stress responses and increases the steady state levels of several chaperones involved in mitochondrial proteostasis. However, this proteostatic response occurs without signs of reduced translation of nuclear and mitochondria-encoded mitochondrial genes, which are hallmarks of the classic mtUPR in yeast and mammalian cell models. [162, 385] Thus, in vivo, and in an energy demanding tissue such as the liver, the mtUPR differs from the classic response, which likely reflects the need to balance proteostasis while maintaining energy homeostasis. Therefore, our results suggest the mtUPR allows to achieve higher levels of chaperone and proteases required to support mitochondrial biogenesis in the context of a mitochondrial translation defect that inevitably perturbs the dynamic equilibrium between steady-state levels of mtDNA- and nuclear-encoded polypeptide.

4.6.2 Preserving residual CIV activity and OXPHOS function

Beyond quantitative adjustments in mitochondrial biomass and translation capacity, our study suggests that stabilization of CIV into SCs may optimize its residual activity. Stabilization of CIV was apparent both in liver mitochondria from LRPPRC-deficient mice and fibroblastic mitochondria from LSFC patients, where the proportion of CIV incorporated in the S1 respirasome relative to its monomeric form was increased. Although the high degree of conservation of SCs across species logically implies that they confer some functional advantages, the true physiological raison d'être of these supramolecular structures still remains unclear. [206] One possibility is that SCs formation increases ETC efficiency by facilitating electron flow between complexes through substrate channeling. [201, 202, 386, 387] This mechanism could explain why maximal uncoupled flux through the electron transport chain is completely preserved, and the respiratory rate in presence of CIV substrates (e.g. TMPD/Ascorbate) is only reduced by 20-30% in H-*Lrpprc*$^{-/-}$ mitochondria despite a drastic reduction (80-85%) in the amount of assembled CIV ([360, 388] and Fig. S2).

Formation of SCs is also suggested to reduce ROS production at the level of CI and/or CIII. [216, 389] Interestingly, our previous study showed that superoxide release by the ETC is increased in presence of low LRPPRC levels. [360] In this context, preferential integration of CIV in CI-CIII containing SCs could act as a compensatory mechanism to limit further oxidative damage to

mitochondria. Some studies [220, 390], but not all [388], have also suggested SCs could provide a scaffold for the completion of CI assembly and/or its stabilization. Accordingly, preferential integration of residual CIV in SCs could act to prevent CI abnormalities secondary to the CIV assembly defect. However, considering the severity of the CIV assembly deficit and the complete absence of CI defects observed in LRPPRC deficient mitochondria, this possibility seems unlikely.

Although the existence of SCs as physical entities is now well accepted, the molecular mechanisms regulating their formation remain poorly understood. [206] Previous studies have shown that the CIII-associated protein COX7A2L assists and/or stabilizes the interactions between CIII and CIV, and consequently the formation and/or stability of III2+IV1 and I/III2/IV supercomplexes. [143, 202, 229, 230] In the present study, we found that the expression of COX7A2L was increased in mitochondria from H-*Lrpprc*$^{-/-}$ mice and was stabilized in III2 and I1-III2 assemblies. As suggested recently, this could be part of a response to accelerate CIII-containing SCs assembly under stress conditions. [201] However, when the short variant of COX7A2L is expressed, as in our mouse model, this compensatory mechanism cannot successfully stabilize CIV since the 6 bp deletion prevents interactions with CIV [143, 206, 230], as shown by the near absence of COX7A2L in CIV-containing SCs both in WT and H-*Lrpprc* knockout mice. These results therefore provide clear evidence that the preferential integration of CIV is caused by other mechanisms.

Factors such as membrane GPL composition play a role in the assembly and maintenance of SCs. [37, 234, 373] Early studies in yeast have established an important contribution of CL in stabilizing respiratory chain SCs. [234, 237] Structural studies employing cryoelectron microscopy have estimated that 50 and 200 CL were present in yeast and bovine SCs respectively. [391, 392] Self-assembly molecular dynamics simulations performed in bovine heart complexes embedded in CL-containing bilayers, which aimed to mimic the crowdedness and complexity of mitochondrial membranes, have also revealed that CL enrichment at the SC interface precedes their assembly and act as a strong glue acting at specific sites on the surface of proteins. [235] Based on these studies, our results suggest that the upregulation of CLs may contribute to the stabilization of residual CIV in SCs. This stabilizing role of CLs is further suggested by our observation that in native gel studies, several protein complexes, known to require CLs for their assembly and/or stability are more abundant in H-*Lrpprc*$^{-/-}$ mitochondria. This includes a minor fraction of the mitochondrial ANT which is able to associate with SCs in a strict CL-dependent manner [233], as well as MICOS and Prohibitin/Stoml2 complexes which, apart from being stabilized by CLs, also play a role in CL

synthesis, and the formation of CL-rich microdomains in the inner mitochondrial membrane. [35, 376, 378, 379] Prohibitin/Stoml2 complexes in particular were suggested to form CL-enriched microdomains in which electron transport complexes are optimally assembled. [380]

Our native gel proteomics data also revealed that the abundance of GRP75-VDAC-IP3R complexes is increased in LRPPRC deficient mitochondria, which raises the intriguing possibility of an increased tethering between mitochondria and ER. [381, 382] By generating closely appositioned membranes, these tethers are increasingly viewed as being important for the movement of GPL across cellular compartments. [373] In yeast for instance, impairment of ER-mitochondria tethering was recently shown to decrease the transfer of PA from ER to mitochondria, resulting in a 40% reduction in CL levels. [393] Thus, increased tethering between mitochondria and ER could promote GPL trafficking between ER and mitochondria and at least partly account for the increased abundance of CLs. The fact that nearly all of the differentially abundant PEs detected in our lipidomics analysis were upregulated in LRPPRC-deficient mitochondria is also suggestive of altered phospholipid trafficking between ER and mitochondria, as the ER and ER-associated membranes (MAMs) play a key role in mitochondrial PE synthesis. [36]

Although indicative, these results only constitute indirect evidence. Further studies in which upregulation of CLs is prevented in liver specific *Lrpprc*-deficient mice will be required to confirm that changes in the lipid milieu underlies the stabilization of CIV. Interestingly, recent evidence indicates that greater mitochondrial PE could also potentiate respiratory enzymes activity. [394] Our lipidomic analysis pointing to a relative increase of PE species, compared to PC species, supports the notion that GPL remodeling may be a mechanism to preserve or potentiate the activity of the residual CIV in H-*Lrpprc*$^{-/-}$ mice.

4.7 METHODS

4.7.1 Animal care

All experiments on animals were approved by the University of Ottawa Institutional Animal Care Committee and conducted according to the directives of the Canadian Council on Animal Care. Mice were maintained in ventilated cage racks by groups of 5 mice. All mice of both sexes were kept on a regular 12–12h light-dark cycle, and had access to food and water ad libitum. Animals were used at 5 weeks of age for experiments and euthanized by cervical dislocation.

To disrupt LRPPRC expression in the liver, the *Lrpprc* knock-out mouse line *Lrpprc*$^{tm1a(KOMP)Wtsi}$ produced in C57BL/6N embryonic stem (ES) cells was acquired from the KOMP repository (University of California, California) as previously reported[360]. The mutated locus was transmitted through the germline to obtain heterozygous *Lrpprc*+/lox-neo animals. These animals were then bred with flp producing animal B6(C3)-Tg(Pgk1-FLPo)10Sykr/J (The Jackson Laboratory) in order to excise the neomycin resistance cassette, recreating a LRPPRC protein producing locus having lox sites in intron 3 and 5. The resulting *Lrpprc*$^{+/loxP}$ mice were then mated to get homozygous *Lrpprc*$^{loxP/loxP}$ mice and only animals that were exempt of the flp allele were kept. To achieve liver specific inactivation of *Lrpprc*, *Lrpprc*$^{loxP/loxP}$ mice were crossed with B6. Cg-Tg(Alb-cre)21Mgn/J (The Jackson Laboratory) mice producing the Cre recombinase under the control of the albumin promoter and bred to homozygous state, Hep-Cre$^{cre/cre}$. These mice were then bred with the *Lrpprc*$^{loxP/loxP}$ to generate double homozygous mice Hep-*Lrpprc*$^{loxP/loxP;cre/cre}$. However, in order to simultaneously generate homozygous knockout and wild type littermate controls, Hep-*Lrpprc* $^{loxP/loxP;cre/0}$ individuals were inter-crossed.

4.7.2 Transmission electron microscopy

Following anaesthesia (8% chloral hydrate; 600mg/kg), mice were perfused with 10ml PBS and 5ml 2,5% glutaraldehyde via the vena cava. Livers were excised, sliced and fixed overnight at 4 oC in 2,5% glutaraldehyde in phosphate buffer. After sample preparation, 90–100 nm thick sections were mounted onto a 200 mesh copper grid (Electron Microscopy Sciences) and imaged with a FEI Tecnai 12120kV transmission electron microscope equipped with an AMT XR80C 8 megapixel CCD camera as previously described. [341]

4.7.3 Mitochondria isolation

Hepatic mitochondria were isolated from 5 weeks old mice by differential centrifugation as described previously [360]. Isolated mitochondria were either kept on ice and immediately used to measure mitochondrial respiration or stored at -80°C until SCs sample preparation.

For fibroblasts mitochondria, confluent cells (total of 30-60 x 106 for one SCs extraction sample) were lifted using trypsin, washed with PBS and cell pellet was flash frozen and kept at -80°C. After thawing, cell pellet was resuspended in 500ul buffer A (220mM Mannitol, 20mM HEPES, 70mM Sucrose, 1mM EDTA, pH7,4, 1x protease inhibitor, 2mg/ml BSA), transferred to a glass-glass homogenizer and volume was completed to 5ml with buffer A. Cells were broken with 15 strokes with the loose pestle followed by 30 strokes with the tight pestle. Cell breakage was assessed using a light microscope. Homogenate was transferred to a Nalgene centrifuge tube, volume was completed to 30mL, and centrifuged at 700g for 5 minutes at 4°C. Supernatant was transferred in a new tube and centrifuged at 10,000g for 10 minutes at 4°C. Pellet was resuspended in 2mL buffer B (220mM Mannitol, 20mM HEPES, 70mM Sucrose, 1mM EDTA, pH7,4, 1x protease inhibitor), volume completed to 30mL, and centrifuged at 10,000g for 10 minutes at 4°C. Washing step was repeated a second time and final mitochondria pellet was resuspended in 1mL buffer B. From this point, fibroblasts mitochondria were treated like the liver mitochondria for SCs extraction, using a ratio of 5g digitonin/1g of mitochondria protein for the extraction.

4.7.4 mtDNA copy

mtDNA isolation and copy number analysis was performed as previously described [395]. Liver tissue (30mg) from 5 weeks old animals was digested in proteinase K (0.2mg/ml) for 3 hours at 55°C. Lysate was subjected to RNase A (100µg/ml) for 30 mins at 37°C. DNA was pelleted following the addition of ammonium acetate-isopropanol (7. 5M; 0.7 v/v) and centrifugation at 15,000g for 10 mins at 4°C. Pellet was washed with 70% ethanol and resuspended in TE buffer. DNA (20ng) was combined with SsoAdvanced Universal SYBR Green Supermix (Bio-Rad), with ND1(mtDNA) or HK2 (nuclear DNA) primer sets (ND1 FWD: 5'-CTAGCAGAAACAAACCGGGC-3'; REV: 5'-CCGGCTGCGTATTCTACGTT-3'; HK2: FWD: 5'-GCCAGCCTCTCCTGATTTTAGTGT-3'; REV: 5'-GGGAACACAAAAGACCTCTTCTGG-3'). Plate (96 well) was read using CFX Real-Time PCR (Bio-Rad; 95°C for 5 min, 45 cycles of

95°C for 10 s, 60°C for 10 s and 72°C for 20 s). The ΔCt of ND1/HK2 were used to calculate copy number using the equation 2ΔCt.

4.7.5 Electrophoresis

Western blotting: Whole livers were homogenized in RIPA buffer, centrifuged and supernatant was collected, proteins were quantified using Pierce BCA protein assay kit (Thermo Scientific). Extracts were mixed in a 1:1 ratio with laemlli buffer before being loaded on polyacrylamide gels (40 µg protein per well, 7. 5% to 15% gels depending on protein of interest). Gels were submitted to an 1h30 run at 150V, then retrieved and transferred to PVDF membranes at 110V for 1h at 4°C. Membranes were blocked in 5% milk in TBST and incubated in antibody solution (1:1000 dilution) O/N at 4°C. After incubation in secondary antibody solution for 1H, membranes were imaged with Chemidoc (Bio-Rad) using enhanced chemiluminescence (Amersham ECL prime detection reagent, GE). Protein abundance was normalized to Ponceau staining of membranes after antibody detection.

CN/BN-PAGE, 2D-SDS-PAGE, 2D-DDM-CN/BN-PAGE: Briefly, SCs were extracted from liver mitochondria using digitonin (4g digitonin/g of mitochondrial protein) solubilized in extraction buffer. SCs were resolved in large native gradient gels (4%-12%) with 175µg of proteins in each well as previously described[396]. For patient fibroblasts mitochondria, a digitonin ratio of 5g/1g was used, and 100µg of protein were loaded in each well of a 4%-12% gradient native gel. For hybrid CN/BN-PAGE, the first hour and a half of electrophoresis was performed in presence of 0.022% Coomasie Blue in cathode buffer, and the remaining without68. After an O/N electrophoresis at 4°C, gels were retrieved for either in-gel activity assays or transferred to PVDF membranes for antibody detection. Antibodies used at a 1:1000 dilution include: NDUFA9 (CI, Invitrogen, #459100); SDHA (CII, Abcam, #ab14715); UQCRC2 (CIII, Abcam, #ab14745); COX4 (CIV, Invitrogen, #459600), ATPB (CV, Abcam, #ab14730), and COX7A2L (Abcam #ab66107).

4.7.6 Proteomics profiling

For proteomics profiling, replicate samples from 6 mice (3 H-*Lrpprc*$^{-/-}$ and 3 H-*Lrpprc*$^{+/+}$) were resolved by Hybrid CN/BN PAGE. In gel activity assays for OXPHOS complexes were performed and the staining pattern obtained was aligned and used as guide to cut bands in the unstained

replicate that was migrated in parallel. For each sample, a total of seven bands of equal size (5 mm height) were cut covering the following molecular weight ranges (in MD): 2.9 ± 0.253, 2.6 ± 0.22, 2.25 ± 0.20, 1.85 ± 0.16, 1.55 ± 0.14, 1.0 ± 0.083 and 0.65 ± 0.05. Proteins were digested in gel using trypsin (Promega) according to the method of Shevchenko69. Peptide extracts were then concentrated by Vacufuge (Eppendorf), and diluted to 20 µl in 0. 1% formic acid/water.

5% of each digest was injected and analyzed by liquid chromatography tandem mass spectrometry (LC-MS/MS) in an Orbitrap Fusion Lumos Mass Spectrometry System (Thermo Scientific) with a Dionex Ultimate 3000 RSLC Nano High Performance Liquid Chromatrography system (Thermo Scientific) at the front end and the Xcalibur 4.0.27.10 sofware package. Peptides were separated on a C18 PepMap100 precolumn, and a C18 2µ, Acclaim PepMap RSLC column (Thermo Scientific) using a 15 min gradient of 5% to 36% acetonitrile with 0.1 % formic acid at a flow rate of 300 nL/min. Peptides were analyzed using Data Dependent Acquisition (DDA) mode. Full scan MS mode (400 to 1500 m/z) was operated at a resolution of 120 000 with an automatic gain control (AGC) target of 4 × 105 ions, and a maximum ion transfer of 35 ms. Selected ions for MS/MS were analyzed using the following parameters: resolution 120 000; AGC target of 4 × 105; maximum ion transfer of 35 ms; 1. 6 m/z isolation window; for CID a normalized collision energy 35% was used; and dynamic exclusion of 60.0 s. The Easy-IC was used for internal calibration.

4.7.7 Protein identification and data analysis

The analysis of the RAW files was performed using the MaxQuant software package (version 1.6.5.0). The extracted spectra were matched against the mouse sequences from SwissProt (version 2019-04). Sequences of known contaminants were added to this database, and the reverse decoy was strictly set to FDR of 0.01. Database searches were done with 20 ppm and 0.5 Da mass tolerances for precursor ions and fragmented ions respectively. Trypsin (two missed cleavages allowed) was selected as the protease. Dynamic modifications included N-terminal acetylation and oxidation of methionine, while Cystein carbamidomethylation was set as a fixed modification.

Protein abundances were determined by label-free quantitation using the composite iBAQ intensity values determined by MaxQuant and normalized within single or multiple migration profiles of individual proteins. Normalized protein quantification values were then imported in the Perseus 70 software platform for log transformation, data imputation, and statistical analysis. For proteins

missing values for 1 of the 3 experimental replicates in a particular band and genotype, the mean iBAQ value of the two other replicates was imputed. All proteins missing more than one value in a particular band and genotype were considered undetected. For each protein, gel migration profiles were created and normalized to the maximum abundance across all samples analyzed. The migration profile of proteins belonging to known multi-protein complexes were then manually extracted and heatmaps of relative abundance were generated using GraphPad Prism 8 software package (version 8.4.2) to visualize co-migration. The absolute abundance of selected protein complexes was also estimated by summing iBAQ values of all detected protein components co-migrating in the same band. For statistical analysis, one sample T tests comparing the two genotypes were performed for each band. A P value of less than 0.05 was set as the arbitray treshold for statistical significance. For each P value obtained, a corresponding False Discovery Rate (FDR) was calculated according to the Benjamini and Hochberg method and lists of significantly affected proteins were generated at FDR tresholds of <5, <10 and <15% FDR values. The mass spectrometry proteomics data have been deposited to the ProteomeXchange Consortium via the PRIDE 71 partner repository with the dataset identifier PXD021867.

4.7.8 Quantitative RT-PCR.

Chop transcript level from frozen liver tissue was assessed using an RNeasy kit (QIAGEN) for RNA extraction and reverse transcribed with the High-Capacity CDNA RT kit (Thermo Fisher Scientific) according to the manufacturer's recommendations. Quantification was allowed using the ΔΔCT method and the TATA Binding Protein gene expression was used as a housekeeping gene.

Primers used: Chop (NM_007837), sense 5'-TATCTCATCCCCAGGAAACG-3', anti-sense 5'-CAGGGTCAAGAGTAGTGAAGGTTT-3'; Tbp (NM_013684), sense 5'-GGCCTCTCAGAAGCATCACTA-3', anti-sense 5'-GCCAAGCCCTGAGCATAA-3'.

4.7.9 Lipidomics

Lipid extraction and data analysis were done as previously described [374] and adapted for isolated mitochondria [360]. In brief, lipids were extracted from isolated mitochondria or digitonin-extract and spiked with six internal standards: LPC 13:0, PC19:0/19:0, PC14:0/14:0, PS12:0/12:0, PG15:0/15:0 and PE17:0/17:0 (Avanti Polar Lipids Inc, Alabaster, USA). For both kinds of samples, protein concentration was determined using a colorimetric-based assay based on the Bradford dye-binding method to set the volume of injection. Samples were injected (isolated

mitochondria: from 1. 03 µl to 4 µl equivalent to 25µg of protein extract; digitonin-extract: from 0. 98 µl to 1. 20 µl equivalent to 1. 5 µg of protein extract) into a 1290 Infinity HPLC coupled with a 6530 Accurate Mass Q-TOF (Agilent Technologies Inc., Santa Clara, USA) via a dual electrospray ionization (ESI) source. Elution of lipids was assessed on a Zorbax Eclipse plus column (C18, 2.1 x 100 mm, 1.8 µm, Agilent Technologies Inc.) maintained at 40°C using a 83 minutes chromatographic gradient of solvent A (0.2% formic acid and 10 mM ammonium formate in water) and B (0.2% formic acid and 5 mM ammonium formate in methanol/acetonitrile/methyl tert-butyl ether [MTBE], 55:35:10 [v/v/v]). The analysis was performed in positive scan mode. MS data processing was achieved as previously describe31 using Mass Hunter B. 06.00 (Agilent Technologies Inc.) and a bioinformatics pipeline that we have developed to perform serveral steps including: (i) ensuring optimal MS alignment between chromatographic runs, (ii) filtering of adducts as well as subsequent data mining done using an in-house script that applies frequency filtering (80 % in one condition), (iii) signal intensity normalization using cyclic loess algorithm and (iv) imputation of missing values with k-nearest neighbor on scaled data. This yields a data set listing MS features characterized by mass, retention time and corrected signal intensity. Lipid annotation, including fatty acids side chains, was achieved by MS/MS on all discriminant MS features selected according to the following criteria of selection: Q-value < 0.05 (as an estimation of false discovery rate (FDR) < 5%) and a relative fold change (FC) of 1.5 or 0.75. Statistical analysis was performed on the data using an unpaired student's t-test with Storey correction for multiple testing using the Q-value package from Bioconductor. Data are depicted as volcano plots and box plots, where the midline represents the median fold change vs. controls, the box represents the interquartile range (IQR) between the first and third quartile, and whiskers represent the lowest or highest values.

4.8 STATISTICS AND REPRODUCIBILITY

For functional immunoblot and Q-PCR experiments, values are reported as mean ± sem for a minimum of 3 mice per experimental group and graphically represented as violin plots. Unpaired two-sided t tests with Welch's correction (GraphPad Prism 8.4.3) were used to determine statistical difference when two means were compared, with a significance threshold set at $p < 0.05$.

For lipidomics, data are depicted as volcano plots and box plots, where the midline represents the median fold change vs. controls, the box represents the interquartile range (IQR) between the first and third quartile, and whiskers represent the lowest or highest values (n=4 mice per group). All discriminant MS features were selected according to the following criteria of selection: Q-value < 0.05 (as an estimation of false discovery rate (FDR) < 5%) and a relative fold change (FC) of 1.5 or 0.75. Statistical analysis was performed on the data using an unpaired student's t-test with Storey correction for multiple testing using the Q-value package from Bioconductor.

For proteomics, replicate samples from 6 mice (3 H-*Lrpprc*$^{-/-}$ and 3 H-*Lrpprc*$^{+/+}$) were analyzed. Difference in the abundance of individual proteins between genotypes was determined in each band using unpaired two-tailed T tests. A p value of less than 0.05 was set as the arbitrary threshold for statistical significance. For each p value obtained, a corresponding FDR was calculated according to the Benjamini and Hochberg method, and lists of significantly affected proteins were generated at FDR thresholds of <5, <10 and <15% FDR values (Supplemental table 1). To test differences in the absolute abundance of selected multi-protein complexes across genotypes, unpaired two-sided t tests were performed. p values were corrected using the Benjamini & Hochberg method with a FDR cutoff of 5%. Corrected p values (Q)<0.05 were considered significant.

4.9 DATA AVAILABILITY STATEMENT

The mass spectrometry proteomics data have been deposited to the ProteomeXchange Consortium via the PRIDE 79 partner repository with the dataset identifier PXD021867. All other data are available from the corresponding authors upon reasonable request.

4.10 COMPETING INTERESTS

The authors declare no competing interests.

4.11 AUTHOR CONTRIBUTIONS

YB, AC, MR and CDR designed the study. YB and AC wrote the manuscript. MR, CDR reviewed and edited the manuscript. AC, MR, CD, AF, JR, GC and VC performed experiments. YB, AC, MR and GV analyzed data.

4.12 FUNDING

This work was funded by grants from the Natural Sciences and Engineering Council of Canada (RGPIN 2016-09932), The Canadian Institutes of Health Research (MOP 136999), the Fondation du Grand Défi Pierre Lavoie, and the Canadian Foundation for Innovation.

Chapter 5

Testing the potential of stem cell therapy for mitochondrial diseases using the French-Canadian variant of Leigh syndrome – a pilot study

Alexanne Cuillerier[1], Virgilio Cadete[4], Nicholas Cober[1,4], Conor O'Dwyer[5], Fengxia Xiao[1,2], George Cairns[3], Chantal Pileggi[5], Jenna Rossi[1], Mary-Ellen Harper[5], Morgan Fullerton[5], Dylan Burger[1,2], Duncan Stewart[1,4], Yan Burelle[1,3]

[1] Department of Cellular and Molecular Medicine, Faculty of Medicine, University of Ottawa, Ottawa, Canada

[2] Kidney Research Center, Ottawa Hospital Research Institute, Ottawa, Canada

[3] Interdisciplinary School of Health Sciences, Faculty of Health Sciences, University of Ottawa, Ottawa, Canada

[4] Sinclair Centre for Regenerative Medicine, Ottawa Hospital Research Institute, Ottawa, Canada

[5] Department of Biochemistry, Microbiology and Immunology, Faculty of Medicine, University of Ottawa, Ottawa, Canada

Unsubmitted Manuscript, 2021

5.1 Abstract

Genetic mitochondrial diseases affect 1 in 5000 and can present at any stage of life, usually following a nonlinear progression, with fatal outcome. Their clinical presentation and underlying biochemical defects are highly heterogeneous, making patient management and therapy development extremely challenging. Despite recent advances in molecular diagnosis and pathophysiology, mitochondrial diseases are still lacking effective and curative treatments. The recent emergence of mesenchymal stem cell (MSC) therapy, supported by pre-clinical and clinical data, has shown promises in the treatment of various human diseases. MSCs home to the effected tissue *in vivo*, modulate inflammation and promote repair through various mechanisms including the release of extracellular vesicles. Moreover, MSCs can transfer mitochondria directly to the target cell with impaired mitochondria, offering a possibility to replace mutant and dysfunctional organelles, which is relevant in the context of genetic mitochondrial diseases. In this pilot study, we decided to test the potential of MSC therapy, using the French-Canadian variant of Leigh Syndrome (LSFC) as a model. LSFC is a particularly severe form of Leigh Syndrome characterized by the onset of fatal lactic acidosis crises and a tissue involvement pattern affecting mainly the brain and liver. We treated our LSFC mouse model with murine bone marrow derived MSCs and established direct co-cultures systems *in vitro* using rodent and patient cells. We observed a non-significant trend towards improved mitochondrial respiration in both models, suggesting 24h might be too early to observe the full potential of MSC therapy. We also tested the contribution of the paracrine activity *in vitro* in patient fibroblasts and observed that extracellular vesicles alone were as efficient as MSCs, and after cell uptake they improve mitochondrial respiration after 24h. Altogether, the results of our pilot study suggest MSC therapy could be beneficial, but experiments need to be repeated at later time points to fully appreciate the effect. The extracellular vesicles show promise and further studies should investigate the underlying mechanism.

5.2 Introduction

Primary mitochondrial diseases form a group of genetic disorders characterized by dysfunctions of oxidative phosphorylation, mitochondrial function, and structure. They are among the most common groups of genetic disease and of inherited metabolic disorders. [2, 26, 397, 398] With an estimated prevalence of 1 in 5000 live births, mitochondrial diseases are highly heterogeneous on the clinical, genetic, and biochemical level, and can present at any age in any tissue. [4] To add to the complexity, these severe progressive disorders do not follow a linear evolution and often have a fatal outcome. [77] For a given syndrome, symptoms and organ involvement can drastically vary across variants, and even between patients harboring mutations of the same gene. [399] To date, nearly 600 mutations have been reported, and this number is expected to increase as molecular diagnostic methods are improving and becoming more available in the clinic. [13, 44, 47, 49] Despite remarkable progress in the knowledge on the molecular basis and the emergence of next generation sequencing, mitochondrial diseases are cruelly lacking therapies. Current options are limited and consist of vitamins, cofactors and dietary supplements, and their efficacy is controversial. [240, 400] Given the high heterogeneity of mitochondrial diseases, developing tailored treatments is not productive, and instead a promising therapy should be effective for most variants and target as many symptoms as possible.

Recently, extensive pre-clinical and clinical data supported the emergence and safety of mesenchymal stem cell (MSC) therapy in the treatment of various diseases. [253] MSCs can be isolated from various sources, including bone marrow, adipose tissue, placenta and umbilical cord/blood, and easily expand in cell culture. [258] These cells are immune evasive, can differentiate into multiple cell types and can act as cell modulators, making them interesting candidates as therapeutic agents. [259, 260] MSCs can reduce inflammation and promote tissue repair through their paracrine activity by secreting growth factors, cytokines, and hormones. [260] Interestingly, studies have shown the intercellular transfer of mitochondria between MSCs and target cells with mitochondrial dysfunctions through tunneling nanotubes (TNT). [272, 275, 401, 402] Following transfer, ATP levels and mitochondrial functions in the target cell are improved. [275, 283, 403] MSCs can transfer molecules to target cells via microvesicles and exosomes, which contain a cargo of lipids, proteins, and genetic material (mtDNA, mRNA and microRNA). [277, 280, 404] The therapeutic effect of these vesicles alone is comparable to MSCs, and can modulate

inflammation, decrease apoptosis and promote tissue repair. [276] Broadly, MSC therapy has a considerable impact on the target cells' mitochondria through various mechanisms.

The use of MSC therapy, including MSC-derived EVs, for mitochondrial diseases remains largely unexplored, except for one study. [405] Therefore, we decided to launch a pilot study to test the potential of stem cell therapy for mitochondrial diseases using the French-Canadian variant of Leigh Syndrome (LSFC) as a model. LSFC is a particularly severe form of Leigh Syndrome and has a high prevalence in the Saguenay-Lac-Saint-Jean region of Quebec in Canada. [85, 86, 92] It is caused by mutations in *LRPPRC*, encoding an mRNA binding protein of the same name which handles mitochondrial transcripts. [84, 91, 113] This results in a severe complex IV (cytochrome c oxidase) defect, mainly in the brain and liver, where the levels of LRPPRC are almost completely depleted. [113] The affected children undergo unpredicted acidotic crises, potentially triggered by metabolic stresses, that are fatal in 80% of them before the age of 3. [91] Studies performed on patient fibroblasts highlighted mitochondrial dysfunctions at baseline and an impaired capacity to respond to stress. [93] To gain better knowledge on the underlying mechanisms of LSFC, our research consortium has developed a mouse model of the disease, harboring a liver specific inactivation of *Lrpprc* (H-*Lrpprc* mouse). Our characterisation of this model has shown multiple mitochondrial dysfunctions in the liver, and also secondary cardiac involvement. [94, 360] We hypothesize that MSC therapy will alleviate the mitochondrial dysfunctions in the patient fibroblasts and in the H-*Lrpprc* mouse model.

5.3 Results

5.3.1 Impact of MSC Treatment on mitochondria in H-Lrpprc mouse liver

MSCs are being tested in an increasing number of disease models, including liver diseases. [267, 406] Following injection, MSCs home to the injured tissue and promote repair through various mechanisms. [407] We decided to begin our investigation by treating our H-*Lrpprc* mouse model, harboring a liver specific inactivation of *Lrpprc*, with bone marrow derived murine MSCs (M-MSCs). The cells were labelled with the membrane cross linker DiR and injected in the tail vein to favor distribution to the liver. At 6h and 24h post injection, animals were put in the IVIS scanner to confirm the M-MSCs homed to the liver (Figure 5.1A). As shown in figure 5.1A, DiR fluorescence at 24h was clearly visible in M-MCS injected mice and were concentrated in an anatomical location consistent with accumulation in the liver. We then measured mitochondrial respiration in isolated liver mitochondria 24h post-injection. As expected, ADP and CCCP stimulated respiration in presence of physiological substrates was decreased in H-*Lrpprc*$^{-/-}$ (Figure 5.1B,). No significant differences were observed between control and M-MSC treated animals due to a fairly large spread observed between experimental replicates. Inspection of results collected on each experimental day revealed variability between the different M-MSCs donors and in the response to the same donor between different hosts. In some experiments, treatment with M-MSCs increased ADP and CCCP respiration by up to 17.7%, while in others the stimulatory effect was marginal or absent. (Fig. Supp. 5.1)

Given the variability observed in the *in vivo* experiments, we decided to test the impact of M-MSCs treatment on our H-*Lrpprc* model *in vitro*. Therefore, we directly co-cultured M-MSCs and primary hepatocytes isolated from H-*Lrpprc* mice for 24h and measured mitochondrial respiration using Seahorse extracellular flux analysis. As shown in Figure 5.1C, mitochondrial respiration at baseline and after uncoupling with FCCP was not different between both groups after 24h. Variability across experimental replicates was fairly large, and statistical significance could not be reached. However, inspection of individual experimental days indicated a trend towards improved mitochondrial respiration when hepatocytes were co-cultured with MSCs of some donors. (Fig. Supp. 5.2) In these cases, the improvement in OCR was coming exclusively from the primary hepatocytes, since M-MSCs alone or M-MSCs treated with hepatocyte conditioned media had nearly absent OCR values. (Fig. Supp. 5.2) As for our *in vivo* experiments, we also observed variability in the response to M-

MSCs across M-MSC donors. (Fig. Supp. 5.2) The contribution of M-MSC treatment, corresponding to the difference between treated and untreated ORC values, was significantly greater in H-*Lrpprc*$^{+/+}$ after the addition of FCCP, and was not different between H-*Lrpprc*$^{+/+}$ and H-*Lrpprc*$^{-/-}$ in the other respiratory states measured (i.e. baseline, oligomycin, rotenone/antimycin A) (Figure 5.1D), indicating M-MSC treatment had a small and comparable effect in both groups under these conditions. In our experiments with the murine cells, we measured mitochondrial respiration of the M-MSCs alone and in presence of conditioned media to ensure the cells were not activated by factors secreted by the primary hepatocytes (Fig. supp. 5.2). In both conditions, M-MSC mitochondrial respiration was not different, and the values of the oxygen consumption rates were much smaller than the increase in mitochondrial respiration of the treated primary hepatocytes, suggesting that this respiration was by the hepatocytes.

Once MSCs are in contact with the affected tissue, they can fuse with the target cells and transfer their content or differentiate to replenish the tissue. [281] Studies have also shown MSCs can transfer mitochondria to target cells with mitochondrial dysfunctions. [270-272, 275, 281] To validate if this was occurring in our model, primary hepatocytes directly co-cultured with labelled M-MSCs (GFP mitochondria) were imaged by fluorescence microscopy 24h after treatment. Our observations suggest more M-MSCs remain in culture with the H-*Lrpprc*$^{-/-}$ primary hepatocytes as compared to H-*Lrpprc*$^{+/+}$ co-cultures, although this was not quantified (Figure 5.1E). Interestingly, we observed several physical contacts between M-MSCs and primary hepatocytes in the co-culture systems after 24h, but no evidence of mitochondrial transfer from M-MSCs to hepatocytes. We neither observed any evidence of cell fusion between M-MSCs and hepatocytes. It is probable that differentiation of M-MSCs does not occur at this early time point (24h), as we did not observe evidence of differentiation of M-MSCs into hepatocyte like cells either. Altogether, these results suggest there is M-MSCs donor variability and a potential positive impact of certain M-MSCs donors on murine liver mitochondria after 24h of treatment both *in vivo* and *in vitro*.

Figure 5.1: Impact of MSC Therapy on the H-Lrpprc Mouse Model, in vivo and in vitro.

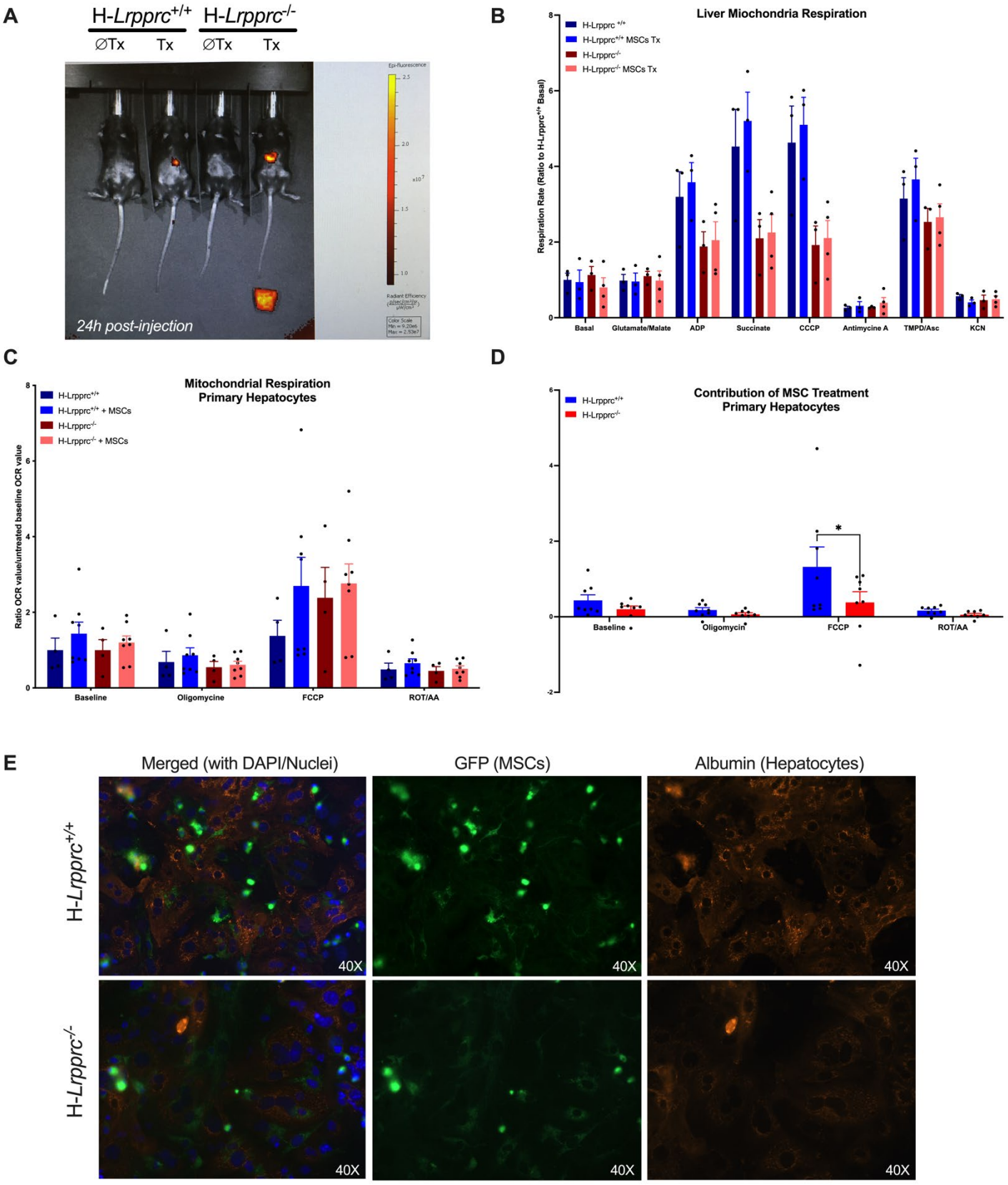

*A: Whole body scan of animals 24h post-injection of 500,000 M-MSCs (labelled with DiR) in 100uL PBS or 100uL PBS shows localization of M-MSCs in the liver. (n = 3 H-Lrpprc$^{+/+}$ and 4 H-Lrpprc$^{-/-}$) B: Liver mitochondria respiration tends to improve in both groups 24h post-injection with either M-MSCs. (n = 3 H-Lrpprc$^{+/+}$ and 4 H-Lrpprc$^{-/-}$; 2 technical replicates per animal) C: Oxygen consumption rate tends to increase in H-Lrpprc primary hepatocytes 24h after direct co-culture with M-MSCs (n = 4 animals per group, 1 pair per day of experiment and Seahorse run) and D: the contribution of M-MSC treatment is significantly greater in H-Lrpprc$^{+/+}$ after the addition of FCCP. E: Fluorescence microscopy showing the interaction of M-MSCs (GFP) with hepatocytes (Albumin). (n = 2 animals per groups, 2 technical replicates per animal) Differences were assessed by 2 way ANOVA, * corresponds to $p < 0.05$.*

Figure Supplemental 5.1: Impact of M-MSC Donor Variability on Liver Mitochondria Respiration After 24h Treatment.

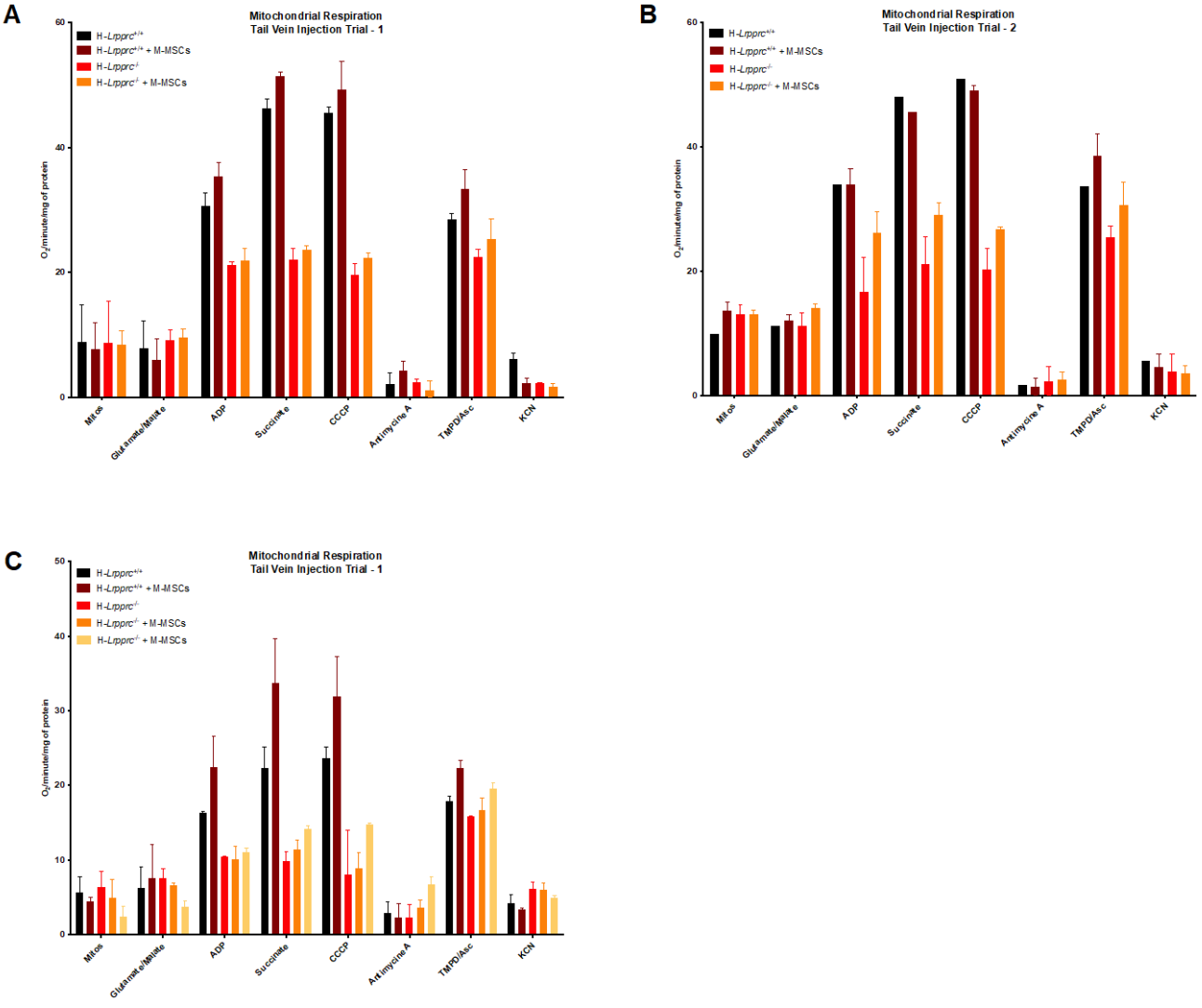

Figure Supplemental 5.2: Individual Seahorse Traces for Mitochondrial Respiration of H-Lrpprc Primary Hepatocytes 14h After Co-culture With M-MSCs.

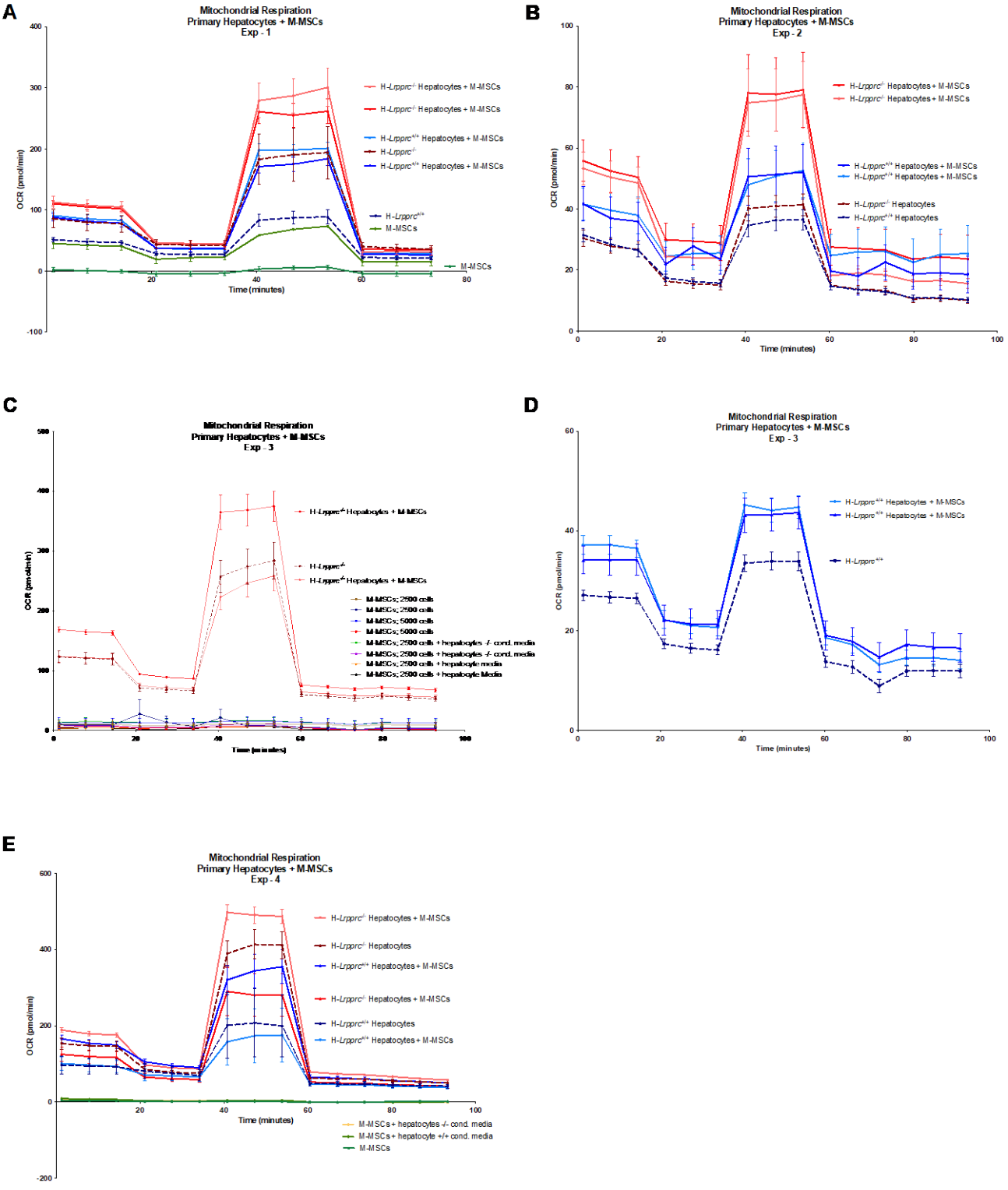

5.3.2 The effect of MSC treatment on Human cells is comparable to the H-Lrpprc mouse model

Several challenges are associated with MSC injection and cell therapy and can reduce the efficacy of the treatment. [265] Evidence suggest the paracrine activity of MSCs is as efficient as whole cell therapy, and the factors are easier to manage in the context of therapy development. [286-288] Therefore, we decided to investigate the contribution of MSCs paracrine activity on our disease model. For this part of our study, we took advantage of our access to healthy bone marrow derived Human MSCs (H-MSCs) and LSFC patient fibroblasts. We first reproduced the co-culture conditions established for the H-*Lrpprc* primary hepatocyte to validate if MSCs treatment had a similar effect in our Human *in vitro* model. As show in Figure 5.2A, after 24h of direct co-culture, mitochondrial respiration tends to improve in both groups, but not significantly. The contribution of treatment was not significantly different between control and patient (Figure 5.2B). These results suggest a similar functional impact of MSC treatment on our murine and Human models. We also performed fluorescence microscopy on our co-cultured Human cells to assess the fate of the H-MSCs and if there were any mitochondrial transfer. Fibroblasts were labelled with MitoTracker Red and exhibited a more fused mitochondrial network, whereas the H-MSCs were labelled with MitoTracker Green and exhibited a more fragmented mitochondrial network, facilitating cell identification. After 24h, some cells with the MSC morphology (fragmented mitochondrial network) were positive for both green and red fluorescence (yellow) in our two groups (Figure 5.2D), suggesting mitochondrial material transfer from the fibroblasts to the H-MSCs. Moreover, there were more yellow cells in direct contact with patient fibroblasts compared to control (Figure 5.2D).

To isolate the paracrine activity of H-MSCs, we established co-cultures using the Transwell system. Under those conditions, both cell types share the same culture media and communicate, but do not physically touch. Moreover, the pore size we chose for the inserts allows the passage of EVs. After 48h of co-culture, we measured mitochondrial respiration in the fibroblasts using Seahorse extracellular flux analysis. As shown in Figure 5.3A, there was no impact of H-MSCs treatment on mitochondrial respiration (noted “I” for culture with inserts), in both groups. Since 24h and 48h are early time points for therapy, we decided to remove the insert, on which the H-MSCs were plated, and culture the fibroblasts by themselves for seven additional days. Mitochondrial respiration in fibroblasts was measured after this culture period and seemed to improve in both patient and control (noted “w” for culture without inserts) (Figure 5.3A), although not significantly. Throughout our experiments, we used two different H-MSCs donors and we wanted to make sure their paracrine

effect on LSFC fibroblasts was comparable. As shown in figure 5.3B, both H-MSCs donors we had access to have a comparable impact on mitochondrial respiration under identical co-culture conditions in Transwell. (Figure 5.3B).

Figure 5.2: Impact of Direct Co-culture of LSFC Fibroblasts With H-MSCs.

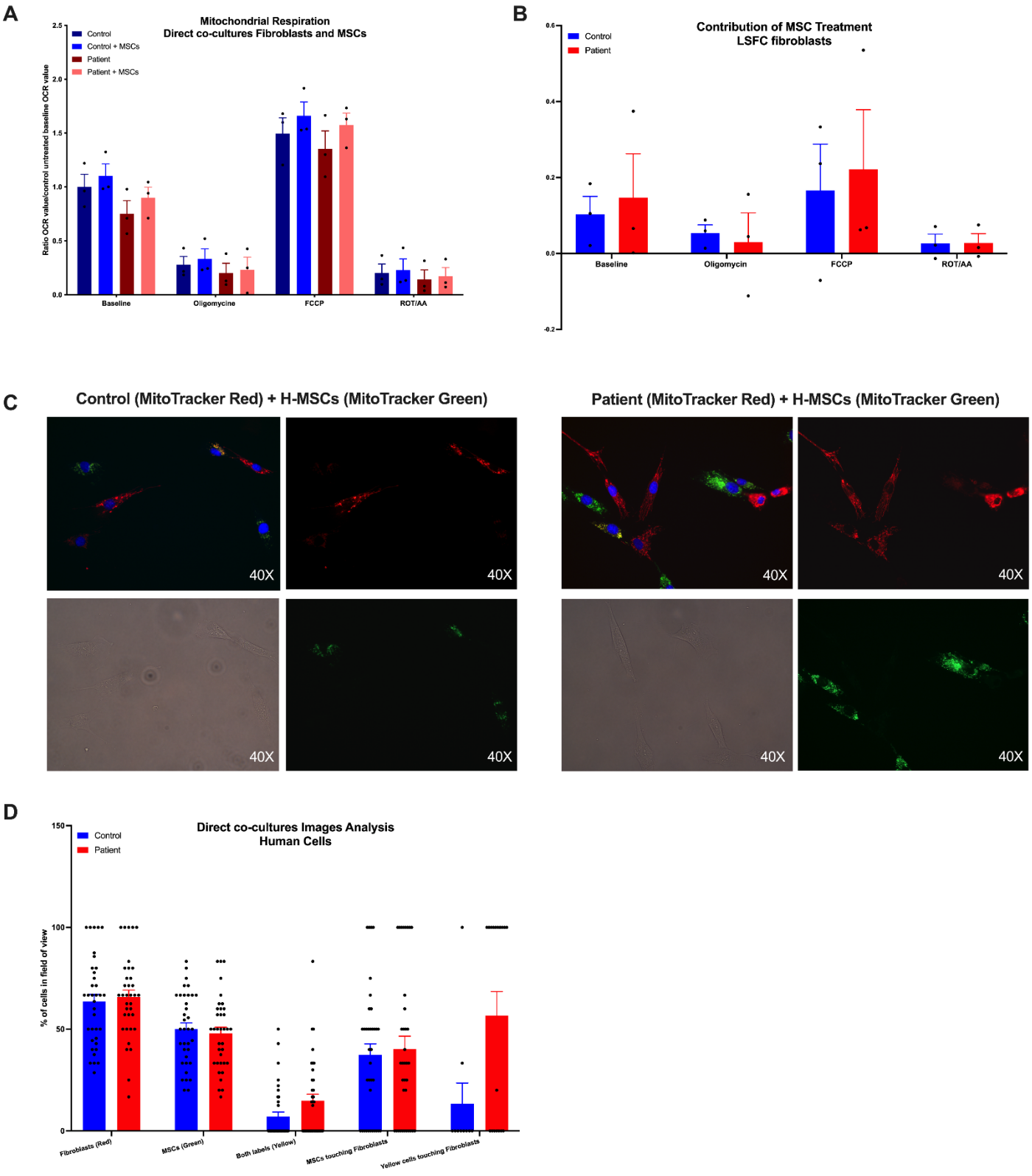

A: Oxygen consumption rate tends to increase in both groups 24h after co-culture with H-MSCs. (n = 3 Seahorse plates run on different days) B: Contribution of treatment (calculated as the

difference in OCR values between treated and non-treated) is similar between both groups. C: Fluorescence microscopy showing the preferential transfer of mitochondrial material from LSFC fibroblasts (red) to H-MSCs (green/yellow) 24h after co-culture (n = 3 technical replicates per group) and D: Image analysis, quantification of number of fibroblasts, H-MSCs, contacts between cell types and number of cells positive for both labels (yellow). Differences were assessed by 2 way ANOVA.

Figure Supplemental 5.3: Individual Seahorse Traces for Mitochondrial Respiration of LSFC Fibroblasts 24h After Direct Co-culture With H-MSCs.

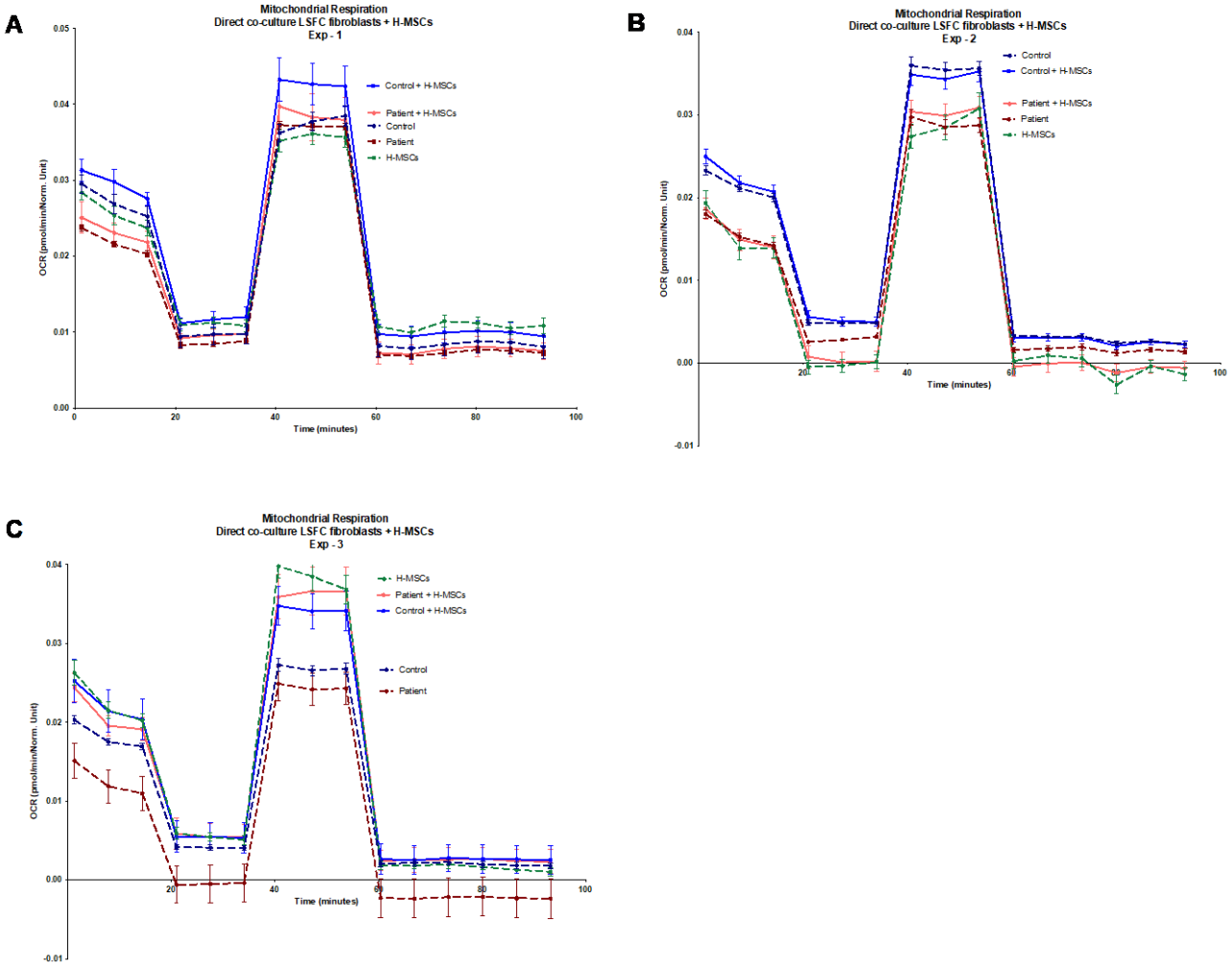

Figure 5.3: Impact of the Paracrine Activity of H-MSCs on LSFC Fibroblasts.

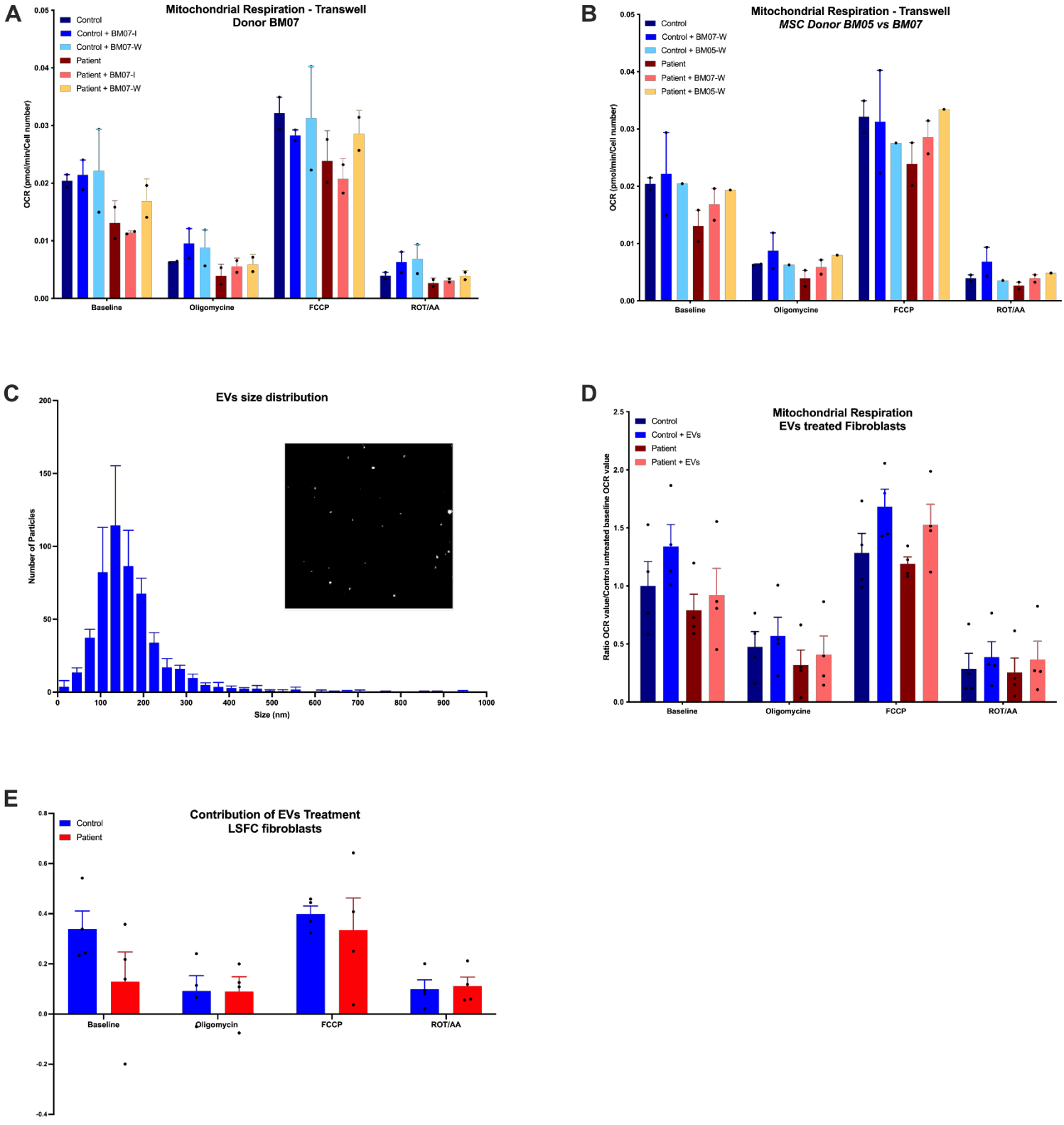

A: Oxygen consumption rates of LSFC fibroblasts tend to first decrease 48h after indirect co-culture with H-MSCs and improve 7 days after the interruption of indirect co-culture. (n = 2 Seahorse

plates run on different days) B: Both H-MSCs donors (BM05 and BM07) to which we had access have a comparable impact on oxygen consumption rates of LSFC fibroblasts. (n = 1 seahorse plate) C: H-MSCs derived EVs display normal size distribution and are positive for EV markers. D: Oxygen consumption rates tend to improve in LSFC fibroblasts 24h after treatment with EVs (n = 4 Seahorse plates run on different days) and E: contribution of treatment is comparable between the 2 groups. Differences were assessed by 2 way ANOVA.

5.3.3 Extracellular Vesicles improve mitochondrial respiration in LSFC fibroblasts

Recent studies compared the therapeutic effect between MSC treatment and their conditioned media. [286] The effect on target cells is similar, and the further isolation of EVs from this conditioned media is as efficient. [286-288] Given the advantages of EV based therapies and the trends we observed using MSCs, we decided to investigate the potential of EVs on mitochondrial respiration in LSFC fibroblasts. EVs were isolated by ultracentrifugation and the isolated fraction displayed the specific size distribution with a peak around 120nm (Figure 5.3C). We treated fibroblasts with an average dose of 30µg of EVs (corresponding to a volume of 10µL) for 24h before measuring mitochondrial respiration. After treatment, mitochondrial respiration was not significantly different. (Fig. 5.3D) However, when examining the results from each individual experimental day, EVs increased maximal respiration (FCCP) in 87. 5% of cases. (Fig. Supp. 5.5) The contribution of EV treatment to fibroblasts respiration is comparable between our two groups, suggesting a similar impact of EVs on both control and LSFC cells. (Fig 5.3E) We then performed fluorescence microscopy to see if the EVs were internalized by the LSFC fibroblasts. Using confocal microscopy and z stacks, we observed the EVs are internalized in fibroblasts of both groups (Figure 5.4A). The vesicles seemed intact and distributed uniformly within the cells and about 20% of EV colocalized with the mitochondrial network in both control and patient fibroblasts at 24h and 48h. We attempted to investigate the humoral effect of M-MSCs *in vitro* on our primary hepatocytes. We treated H-*Lrpprc* primary hepatocytes with M-MSCs, conditioned media and EVs isolated from the same M-MSCs donor for 24h before measuring mitochondrial respiration. Unfortunately, due to technical difficulties we performed this experiment once and only have the values for the H-*Lrpprc*$^{-/-}$ cells. Both treatments increase oxygen consumption rates in a comparable manner, except upon uncoupling where M-MSCs have a significantly greater impact than EVs. (Fig Supp. 5.4) Altogether, these observations suggest that after a 24h treatment period, EVs have a positive impact on mitochondrial respiration *in vitro* ion our LSFC model.

Figure 5.4: EVs are Uptaken by LSFC Fibroblasts Within 24h and Remain Intact.

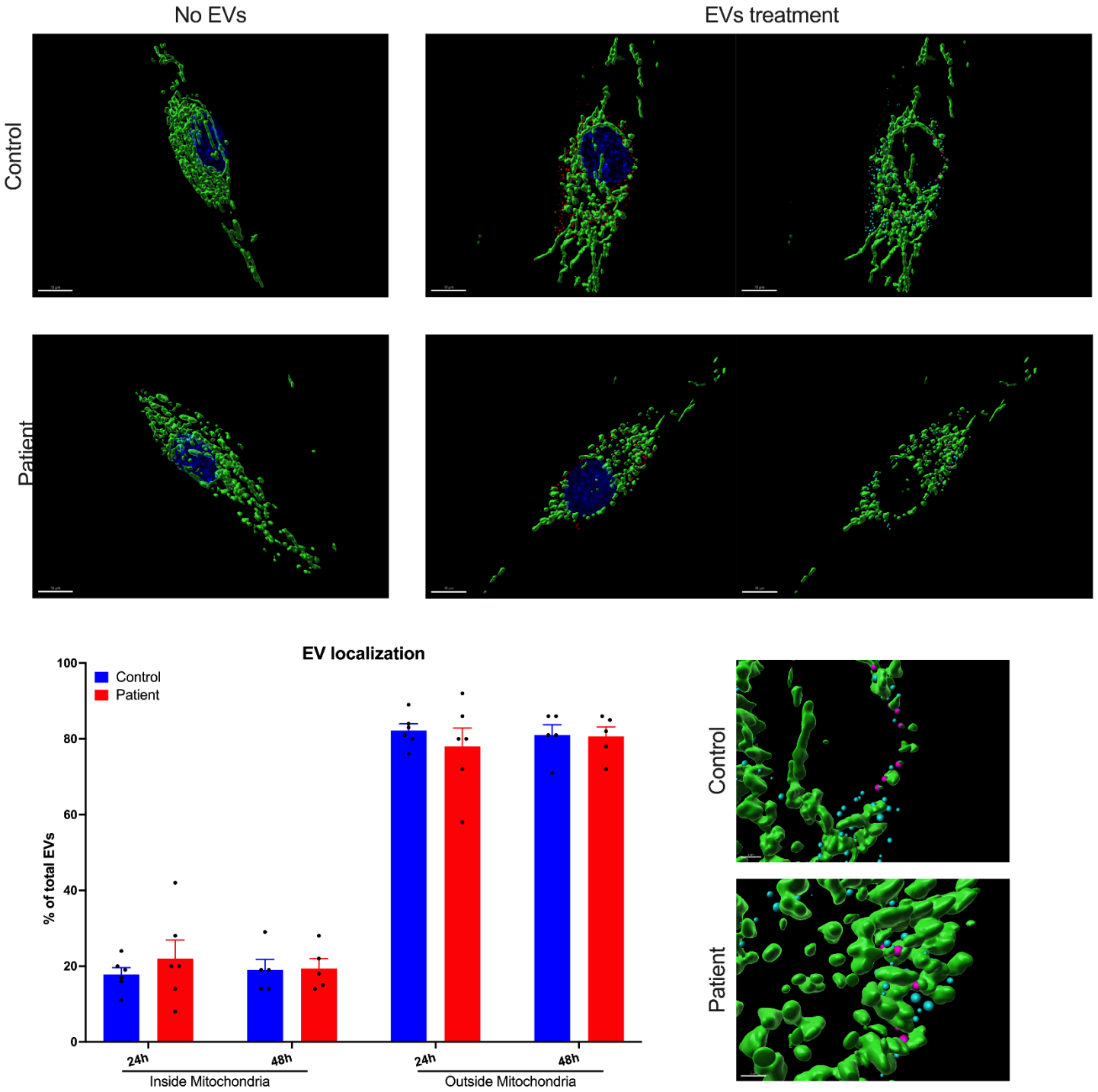

LSFC fibroblasts treated with EVs for 24h and imaged on a confocal microscope (Zeiss). Stacks were grouped and images deconvolved. EVs (PKH26, red) are evenly distributed within LSFC fibroblasts. EV population outside of the mitochondrial network (MitoTracker Green) is

represented in blue, and EV population co-localized with the mitochondrial network is represented in pink.

Figure Supplemental 5.4: Comparison of the Impact of MSCs and EVs on Mitochondrial Respiration in H-Lrpprc$^{-/-}$ Primary Hepatocytes.

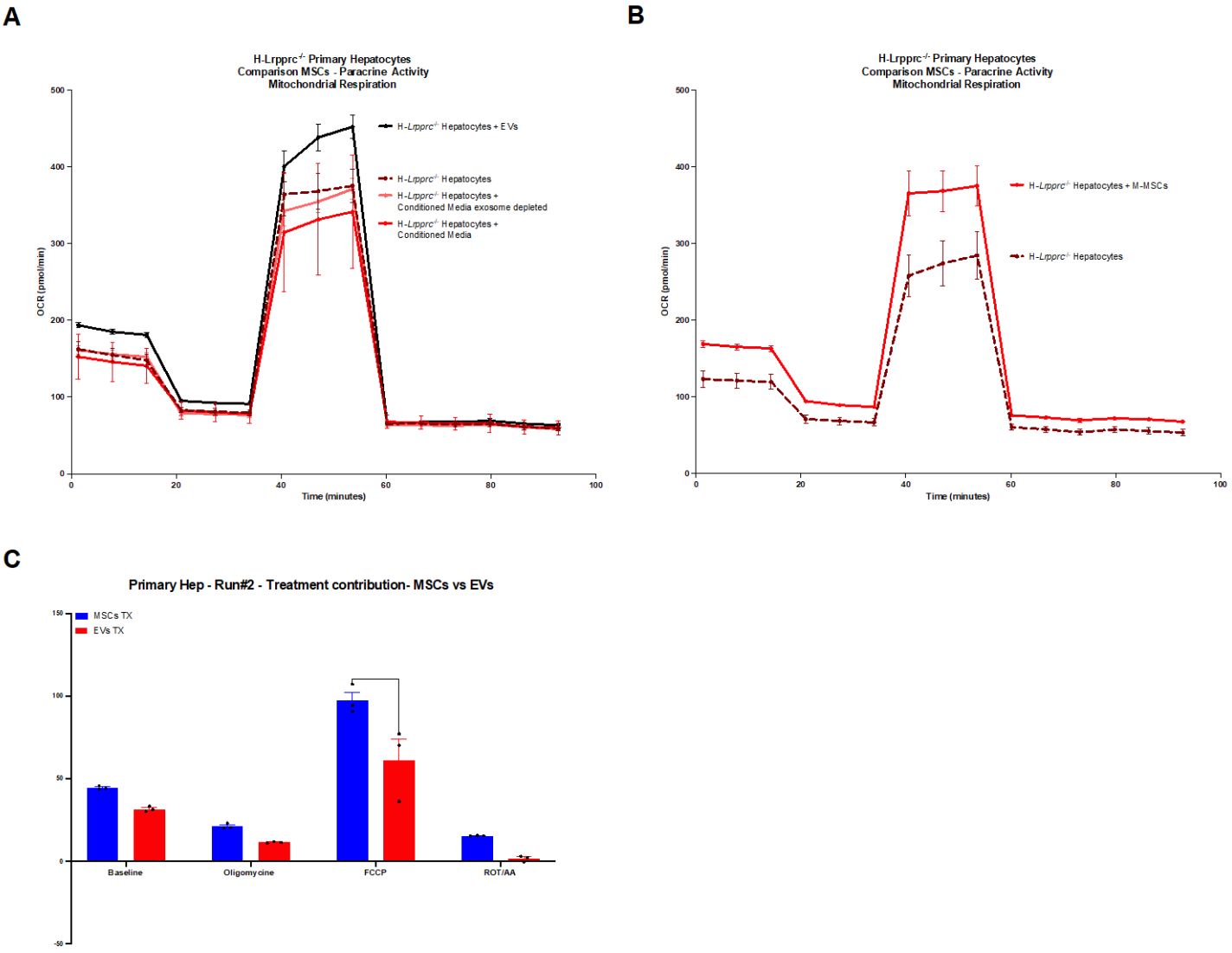

Figure Supplemental 5.5: Individual Seahorse Traces for Mitochondrial Respiration of LSFC Fibroblasts 24h after EV Treatment.

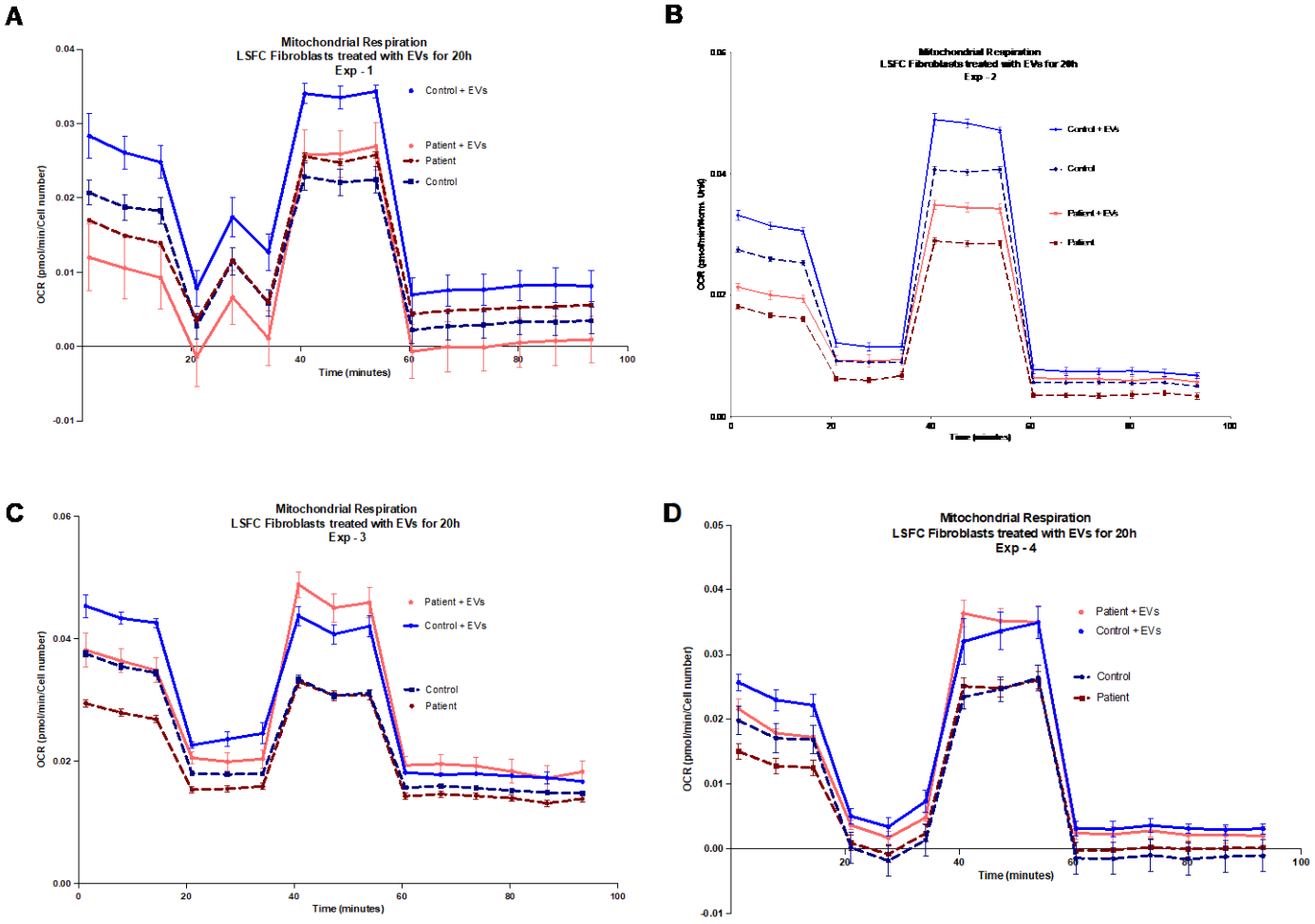

5.4 Discussion

In this pilot study, we tested the potential of MSC therapy for mitochondrial diseases using LSFC as a model and taking advantage of our access to the H-*Lrpprc* mouse model, healthy Human MSCs and LSFC patient fibroblasts. We investigated the contribution MSCs and MSC-derived humoral factors using a combination of *in vitro* and *in vivo* approaches. Our pilot study using various experimental approaches and various MSC donors revealed large variability in the individual responses, across MSC donors and from one recipient to the other, and between experimental days. Consequently, this makes it challenging to observe statistically significant results with restricted sample sizes. Nevertheless, our preliminary data suggest the impact of MSC therapy on mitochondrial function tends to be positive in our various models, and with an increased sample number, some of the results will likely reach significance.

5.4.1 In vivo effects of MSCs on liver mitochondrial function

Mesenchymal stem cells can be isolated from various tissues, are easy to culture and purify, and retain their multipotent properties despite multiple passaging in culture. [258] Their therapeutic potential has been explored in various Human diseases, which are currently under clinical trial, including central nervous system and liver diseases. [256] In the context of liver diseases, MSCs have been shown to contribute to the production of new hepatocytes, to promote tissue repair, modulate inflammation and prevent the activation of hepatic stellate cells, and therefore fibrosis. [267, 408, 409] Liver is mainly affected in LSFC, and we have previously shown microsteatosis and multiple mitochondrial dysfunctions in our mouse model harboring a liver specific inactivation of *Lrpprc* (H-*Lrpprc* mouse). [86, 360] A number of studies have looked at the outcome of MSC therapy after several days and weeks of treatment, while others investigated the acute effect of MSC treatment. In MSC therapy studies in rodent models of liver fibrosis and fatty liver, labelled MSCs were injected in the tail vein and detected at a peak signal in the liver at 24h post-injection [289, 405], which decreased afterwards. [410] Over that period of time, MSCs reduced fibrosis [289] and improved mitochondrial respiration and functions [405] after homing to the liver. Based on these findings, we decided to treat our H-*Lrpprc* mice for 24h before measuring liver mitochondria respiration as an outcome of mitochondrial function. At 24h, we do see a stimulatory effect on respiration, although it is inconsistent and seems dependent on donor source and donor-host specific response. We did try to limit variability using various strategies and control conditions. We used

murine bone marrow derived MSCs to treat our H-*Lrpprc* mice, and one donor could only yield enough M-MSCs to treat two to three animals. Consequently, each animal pair was treated with a different M-MSC donor. We isolated M-MSCs from animals of the same age (6 weeks), cultured them for one passage and subsequently stored the cells in liquid nitrogen until use to ensure consistency. We observed M-MSCs donor variability between our respirometry experiments (Supp. Fig. 5.1), with some donors having an effect only in one of the two groups (Supp. Fig. 5.1-A, B) and one donor having a different effect in two animals of the same group (Supp. Fig. 5.1C). Studies measuring the outcome of MSC therapy at 24h saw similar results which were more consistent, perhaps because they used a single commercial source of human MSCs for all their experiments or expanded their murine MSCs in culture, allowing the use of one donor for all the experiments and reducing variability. [289, 405] Although not mentioned, these studies potentially tested different donors before selecting the most potent one. Donor variability is reported in the literature and the main contributing factors are the age of the donor and the handling of the cells prior to treatment. [411] Another factor that might have contributed to the lower efficiency of our treatment is the use of frozen cells. The thawing step is a stress and not all cells survive. It is likely that the surviving stressed M-MSCs were not be as potent as their fresh equivalent. Supporting this possibility, studies have shown only healthy MSCs are able to transfer material to target cells and tissue, and the stressed ones do not. [282, 412] If these experiments were to be repeated, it would be worth keeping the M-MSCs in culture for a few days to allow them to recover from the thawing before injecting them. Together, these results suggest that at least acutely, MSCs may be able to increase respiration of liver mitochondria, but this effect is likely variable. Longer time course would be required to see whether this translates into benefits on liver microvesicular steatosis.

5.4.2 In vitro effects of MSCs in co-culture systems

Benefits from direct co-culture of MSCs and recipient cells at 24h have been shown in various studies. Improvement in mitochondrial morphology occurs within 8h of co-culture in human fibroblasts [405], and improves mitochondrial respiration within 48h of co-culture [281]. As opposed to these findings, in neither of our co-culture models (murine and human) we observed a significant improvement of mitochondrial function. As for our *in vivo* experiments, mitochondrial respiration *in vitro* tends to improve in both groups after treatment, but not significantly (Fig. 5.2). It is difficult to assess the functional impact of MSC in target cells when they are directly co-cultured *in vitro* since the two cell types cannot be separated before measurement. Most studies separate their cell populations by flow cytometry before measurements. [256] Instead, and to avoid

the stress of cell sorting, we decided to include multiple control conditions in an attempt to separate the contribution of MSC respiration from the mitochondrial respiration of our target cells. The M-MSC minimally responded to any of the substrates and inhibitors used in the Seahorse experiment, displaying a more quiescent profile consistent with stemness. (Supp. Fig. 5.3) In contrast, Human bone marrow derived MSCs are naturally more activated and their respiration profile is similar to Human fibroblasts [413], making it more challenging to separate them. We plated H-MSCs and LSFC fibroblasts in a 1:1 ratio for a total of 15,000 cells per Seahorse well, and our control condition was 15,000 fibroblasts since the metabolic profile depends on cell density and cell contact. [414] Further work is required to optimize a way to separate the cell populations with minimal stress to better assess the functional impact *in vitro* of MSC therapy on mitochondria.

Among the mechanisms by which MSCs can promote repair of the target tissue, the transfer of intact mitochondria is the most relevant in the context of therapy development for mitochondrial diseases. Intercellular mitochondria transfer has been shown in various conditions, both non-pathological and pathological, in primary cells, cell lines and *in vivo*. [281, 285, 415] The donor cells transfer their mitochondria through the formation of TNT, by direct contact and GAP junctions or through microvesicles. In some studies, mitochondrial transfer between MSCs and recipient cells occurs as early as 2h after co-cultures, reaching a transfer peak at 24h. [281] The ability of MSCs from various sources to transfer mitochondria is linked with the health of their mitochondria, and among stem cells, bone marrow derived MSCs have the greatest mitochondrial transfer potential. [416] Mitochondria transfer is associated with increased respiration and restoration of mitochondrial function in the target cells. [272, 274, 282] Our H-MSCs are bone marrow derived and have respiration rates comparable to what is found in the literature [413] (Fig. Supp. 5.3), gathering the perfect conditions for mitochondrial transfer to the recipient cells. Thus, we were surprised by the absence of mitochondrial transfer from our H-MSCs to LSFC fibroblasts *in vitro*. (Fig. 5.2) In the case of our murine *in vitro* experiments, we did not find any evidence of mitochondrial transfer from M-MSCs to primary hepatocytes at 24h. In contrast, our microscopy data suggest fibroblasts from both groups transfer mitochondria to H-MSCs. Previous reports have observed mitochondrial transfer in one direction, from MSCs to stressed recipient cells, and failed to observe transfer in the opposite direction. [282, 401] However, bi-directional mitochondrial transfer, with a predominant transfer to MSCs, is observed under non-pathological conditions in renal tubular cells and vascular smooth muscle cells. [285] These findings suggest the direction of mitochondria transfer depends on the health of the target cells. The major difference between these

experiments and ours is the level of stress of the recipient cells. In most studies, the recipient cells are under severe mitochondrial stress conditions induced by poisons of the respiratory chain such as rotenone, complete depletion of mitochondrial DNA, or under chronic inflammation stress. [272, 274, 282] However, we did not observed mitochondrial transfer in our primary hepatocytes co-cultures either, although they present a more severe phenotype, and this in spite of numerous cell-to-cell contacts between M-MSCs and H-*Lrpprc* hepatocytes. (Fig. 5.1) Unfortunately, because primary hepatocytes de-differentiate rapidly in culture, we could not investigate if mitochondrial transfer occurred at a further time point. For our experiments with the human cells, we used LSFC fibroblasts under basal conditions without any additional stress. Although we have previously reported several dysfunctions in these cells, the damage remains mild, as for most fibroblasts sampled from patients suffering of a mitochondrial disease. [93] Based on our observations, it could be possible that H-MSCs trigger quality control mechanisms in our fibroblasts at baseline and stimulate the elimination of less efficient mitochondria followed by an enhanced biogenesis in the fibroblasts. The H-MSCs, in this case, would act as scavengers and accept the dysfunctional organelles. Additional experiments could confirm this possibility, by measuring the levels of quality control (PINK1/Parkin) and biogenesis (PCG1-α, TFAM) markers in fibroblasts by western blots after co-culture with H-MSCs. Our microscopy experiments should also be repeated, at further time points (36h, 72h), to validate if the transfer eventually becomes bi-directional or if it remains strictly from the fibroblasts to the H-MSCs under basal condition. It is likely that the number of H-MSCs positive for both MitoTracker green (MSCs mitochondria marker) and MitoTracker red (fibroblasts mitochondria marker) will increase over time, since there were several H-MSCs touching fibroblasts in both groups, but no evidence of mitochondrial transfer yet at 24h. (Fig. 5.2) We could also stimulate intercellular mitochondrial transfer from H-MSCs to recipient cells by stressing our fibroblasts, and image the cells at various time points (24h, 36h, 72h), to maximise our chances of witnessing these events. The use of KCN in this condition would be interesting given the complex IV deficiency in LSFC and the greater susceptibility of LSFC fibroblasts to stress. [93] These additional experiments would highlight how H-MSCs favor different repair mechanisms depending on the level of damage to the mitochondria in the same cell type. Another difference between our study and previous reports is the recipient cell type. Intercellular mitochondrial transfer has been reported in cardiomyocytes, renal cells, and neurons; all very metabolically active cell types that highly rely on healthy mitochondria to function. We took advantage of our access to LSFC patient cells for our experiments, but fibroblasts do not display a high energetic profile, and this could have blunted our results.

We based our pilot study on findings of improved mitochondrial function within 24h, both *in vivo* and *in vitro* in models of mitochondrial disease. [405] Moreover, we wanted to perform our experiments in our different models at the same time point to allow comparison. Primary hepatocytes quickly lose their phenotype when they are cultured in 2D. [417] We tried to measure mitochondrial respiration at 48h of co-culture with M-MSCs to obtain additional time points, but the results were not conclusive because the hepatocytes were not responding anymore and there was a lot of cell death in the culture plate (data not shown). Overall, 24h might be too early to observe major changes. In support of this, the original papers reporting intercellular mitochondrial transfer [272, 274] co-cultured their recipient cells with MSCs for at least four days prior to imaging and measuring the functional impact. It would definitely be relevant to repeat our experiments, especially microscopy, at further time points to validate if the effect of MSC therapy occurs later than 24h.

5.4.3 In vitro effects of the humoral contribution, particularly EVs, of MSCs

An increasing number of studies are highlighting how the paracrine activity of MSCs is as potent as MSC therapy. [286] Among the factors and material secreted by MSCs, EVs have been shown to be responsible for the beneficial effects observed upon treatment. [286, 294] The difficulty in reproducing therapeutic effects of cell-based therapy can be attributed to cell preservation, donor-to-donor variability, cell storage issues, handling and culture variations. Given these, EVs represent an interesting alternative to cell-based therapy since they exhibit similar trophic and immunomodulatory functions. [286-288] Studies comparing the effect of MSC therapy and MSC-derived EVs in models of cutaneous wound, acute kidney injury and multiple sclerosis have shown both options had similar effect. [418-420] The potential of EV therapy has been explored in rodent models of liver disease, and treatments alleviated inflammation, liver fibrosis, apoptosis, and oxidative stress. [421-423] In other models with mitochondrial dysfunctions, exosomes increased mitochondrial respiration in a dose dependent manner. [294] Our results show EVs have an effect on mitochondrial respiration in H-*Lrpprc*$^{-/-}$ primary hepatocytes and LSFC fibroblasts. Conditioned media and exosome depleted media seem to have a lesser effect than EVs purified from the same conditioned media on H-*Lrpprc*$^{-/-}$ primary hepatocytes at 24h, which supports the notion that EVs may constitute the mechanism underlying the paracrine effect of MSCs on mitochondrial respiration of host cells. In our Human LSFC fibroblasts, H-MSCs derived EVs had a positive, but not significant, impact on mitochondrial respiration in both groups. (Figure 5.3-D) Our low sample

number (4) likely contributes to the non-significance of our results since looking at our four different Seahorse experiments individually, EVs increased oxygen consumption rates of all our samples except once for our patient cells. (Supp. Fig. 5.5) Our results seem in line with a beneficial effect of H-MSCs residing in the paracrine activity of MSCs, more precisely in the EVs. Approximately 20% of EVs internalized by fibroblasts co-localized with the mitochondrial network in both groups at 24h and remained at 48h. This suggests the content of EVs could modulate mitochondrial function directly. We did not investigate the content of our EVs, but we can suspect the presence of molecules able to stimulate mitochondria and more broadly metabolism. The EV cargo is large and depends on the cell culture conditions and the source of MSCs. [280] A study reported the presence of five enzymes involved in ATP synthesis through glycolysis in their EVs, including glyceraldehyde 3-phosphate dehydrogenase, phosphoglycerate kinase, phosphoglucomutase, enolase and pyruvate kinase m2 isoform. In this study, EVs restored ATP production and reduced oxidative stress in a rodent model of ischemia/reperfusion. [424] In a model of pulmonary hypertension with mitochondrial dysfunctions, EVs impact the pyruvate and glutamine pathways, and increase the flux to the TCA cycle. Additional studies using proteomics and RNA sequencing identified several mitochondrial proteins and metabolic genes in the EV cargo. [277, 294, 425, 426] Other reports mention the presence of complete mitochondrial DNA in exosomes derived from stem like cancer cells, capable of restoring metabolic activity of recipient cells. [293] Moreover, an increasing number of studies are focusing on identifying microRNAs in EVs and their impact on recipient cells. These single strand non-coding RNA molecules are involved in post-translational modifications, and a few microRNAs have been shown to target mitochondria. [256, 277] We cannot exclude the possibility our EVs contain microRNAs, potentially contributing to improved mitochondrial function.

Despite tremendous advances, the precise nature of the content of EVs remains elusive. At baseline, MSCs and other cell types secrete EVs containing mitochondrial proteins, likely as an internal quality control mechanism. Therefore, it is difficult to conclude if the released mitochondrial cargo is healthy and if MSCs are secreting mitochondrial proteins specifically to repair dysfunctional organelles in the recipient cells. It is possible the secreted mitochondrial cargo is not defective, but simply less efficient compared with the rest, and eliminated. These undamaged proteins could still have a beneficial impact on the target cells' mitochondria, especially if they harbor dysfunctions. Usually, when MSC conditioned media is collected prior to EV isolation, the MSCs were not in co-culture with the target cells, preventing communication between cell types and a tailored secretion.

Nonetheless, the EV cargo has a positive impact on mitochondria in various models, including ours. It would be interesting to pre-treat the MSCs with conditioned media collected from the target cells prior to EV isolation. This would allow the comparison with the EV cargo at baseline and investigate if the effect on the target cells is greater after this pre-treatment.

Overall, EVs seem to be the mechanism by which MSC therapy is most potent in our LSFC models and the next step following this exploratory study should focus on EV therapy and include an *in vivo* component.

5.5 Perspectives and Conclusion

MSC therapy remains challenging despite incredible progress and promising pre-clinical and clinical results, mainly because the therapeutic mechanisms are still poorly understood and of inconsistencies between studies. Donor variability and cell handling prior to treatment greatly affects the efficiency of therapy and is highly variable between studies. Standardized parameters are required to ensure better reproducibility, and include, but are not limited to, the choice of culture media, donor selection, sample handling, freezing protocols, storage conditions. Novel techniques involving 3D culture methods and hypoxic environments are slowly being favored as they best reproduce the natural environment of the stem cells niche and ensure the maintenance of quiescence and stemness. Circumventing these drawbacks, EVs are a promising option and present several advantages over cell-based therapy. Their surface markers make them more likely to avoid immune rejection compared to MSCs, and their small size allows them to be transported through the pulmonary circulation and the blood-brain barrier, where MSCs usually accumulate due to their size. [291, 292, 427] Increasing evidence suggests the possibility to pre-treat MSCs to obtain a specific cargo in the EVs, and more tailored therapeutic options. The surface of EVs can even be modified to favor an increased uptake in the liver [428], making customized EVs an interesting option in the treatment of LSFC. More broadly, mitochondrial diseases are highly heterogeneous from the genetic, molecular and clinical point of view and would benefit from a therapy targeting several cellular defects, alleviating as many symptoms as possible. This pilot study suggests MSC therapy could be beneficial for LSFC and mitochondrial diseases. Additional experiments are required to draw a conclusion, but EVs seem to be the most efficient mechanism and the easiest to handle in therapy.

5.6 Methods

5.6.1 Cell Culture

All cells were cultured at 37°C and 5% CO_2 in Nunc tissue culture treated flasks (ThermoFisher). LSFC fibroblasts we obtained after written informed consent from skin biopsies of patients (A354V mutation in *LRPPRC*) and healthy controls aged between 8 and 39 years (LSFC Consortium Biobank, Chicoutimi, Quebec, Canada). LSFC fibroblasts were grown in high glucose (4.5g/L) DMEM (Wisent) supplemented with serum (fetal bovine serum, 10%; Wisent) and antibiotics (1% penicillin/streptomycin; Wisent). Experiments were performed at passages between 5 and 15.

Healthy Human MSCs (H-MSCs) were obtained from bone marrow of three different donors (BM05, BM07 and BM08) as described previously. [429] H-MSCs were processed and cultured in accordance with all requirements in the Ottawa Hospital Research Institute's Cell Manufacturing Facility. H-MSCs were maintained in culture in fibronectin (5μg/cm^2, Roche) coated flasks in NutriStem XF media with supplement mix (Sartorius), and were kept in culture for a maximum of 4 passages. Trypl-E (Thermofisher) was used to lift H-MSCs instead of trypsin.

5.6.2 Primary Hepatocyte Isolation

Primary hepatocytes were isolated from 5 weeks old H-*Lrpprc*$^{-/-}$ mice and wild-type littermate controls H-*Lrpprc*$^{+/+}$ as previously described [430] with slight modifications. Animals were anesthetized with ketamine/xylazine (150/10 mg/kg) and livers perfused using a syringe pump at a rate of 7 mL/min with 25 mL of an EGTA solution (140 mM NaCl, 6.7 mM KCl, 10 mM HEPES, and 50 μM EGTA, pH 7. 4) followed by a collagenase solution (67 mM NaCl, 6.7 mM KCl, 5 mM $CaCl_2{\cdot}2H_2O$, and 100 mM HEPES, pH 7.6) through the inferior veina cava after cutting the portal vein and clamping the superior veina cava. Livers were removed, cells dissociated manually in 10 mL of William's medium E (Gibco) and suspension passed through a 100μm cell strainer. Cells were washed in complete Wiliam's medium E (supplemented with 10% fetal bovine serum (Wisent), 1% penicillin/streptomycin (Wisent), 1% Glutamax (Gibco)), counted using trypan blue and the automated cell counter Countess II (Thermofisher), and plated on collagen (Fisher) coated plates at: 20,000 cells per well in a 96-well Seahorse plate; 250,000 cells per well on glass coverslip in 24-well plates; 1,000,000 cells per well in glass bottom black edges 6-well plates. Cells were washed with PBS 4h after plating, media replenished and left overnight before experiments.

5.6.3 Murine MSC Isolation

Bone marrow derived MSCs (M-MSCs) were isolated from 6 weeks old wild-type MitoQC mice, harboring dual GFP and mCherry mitochondria label. [431] Isolation was adapted from previous protocol optimized for rats. Briefly, both femurs and tibias were removed, transferred in cold sterile PBS (Wisent) and cleaned with scalpel blade in a sterile fume hood. Bones were flushed with 3 mL of cold complete (10% fetal bovine serum, 1% penicillin/streptomycin; Wisent) DMEM (Wisent) using a syringe with 26G needle. Bone marrow was broken down and homogenized in complete DMEM using a 1mL pipet. Suspension was transferred to a 50 mL tube and cells were pelleted at 300g for 5 minutes. Cell pellet was resuspended in 20 mL pre-warmed complete DMEM and transferred to a T75 Nunc culture flask (Thermofisher). Media was refreshed 24h later and cells maintained in culture for 1 passage before use or freezing.

5.6.4 Extracellular Vesicles Isolation

Conditioned media (Nutristem) was collected from H-MSCs donor BM07, aliquoted in 250mL bottles and stored at -80°C until processing. Conditioned media was thawed and transferred to sterile centrifuge tubes (Nalgene). Apoptotic bodies and cellular fragments were pelleted at 20,000g for 20 minutes at 4°C. Supernatant was transferred to ultracentrifuge tubes and extracellular vesicles were pelleted at 100,000g for 90 minutes at 4°C. All but ~1mL of the supernatant was discarded and the remaining 1 mL was used to resuspended pellet. When needed, EVs were labelled at this step with PKH26 (Sigma) following manufacturer's instructions. Suspension was transferred to 1,5 mL tubes (Eppendorf) and centrifuged at 100,000g for 90 minutes at 4°C. Final pellet was resuspended in sterile PBS (Wisent) and stored at -80°C. Extracellular vesicles were quantified for proteins (BCA, Pierce, Thermofisher) and analyzed using the Zeta view for size distribution before use.

5.6.5 MSC Therapy in vivo

MitoQc murine MSCs (M-MSCs) we used for MSC therapy *in vivo* of 5 weeks old H-*Lrpprc* mice. Each pair of animals (ie each day of therapy) received cells isolated from the same murine donor. Cells stored in liquid nitrogen were thawed and labelled with DiR (Thermofisher) according to manufacturer's instructions. After washing excess probe, M-MSCs were resuspended in sterile PBS

at 500,000 cells per 100 µL. Each animal was injected with 100 µL of M-MSCs (treated) or PBS (control) in the tail vein using insulin syringes with 29G needles. Each day of experiment, a minimum of 4 animals were injected (2 treated, 2 controls) and more animals received treatment if M-MSCs cell number was sufficient. Animals were imaged at 6h and 24h post-injection using the IVIS Spectrum optical imager to confirm labelled M-MSCs homed to the liver. Animals were sacrificed 24h post-injection.

5.6.6 MSC Therapy in vitro

LSFC fibroblasts were directly co-cultured with H-MSCs in a 1:1 ratio in complete DMEM for mitochondrial respiration and microscopy. LSFC fibroblasts were indirectly co-cultured with H-MSCs in 6 well plates with Transwell inserts (Corning) where fibroblasts were plated at 50,000 cells per well, 9,600 H-MSCs were plated on each insert and both cell types shared the same culture media (complete DMEM).

H-*Lrpprc* primary hepatocytes were directly co-cultured with M-MSCs in a 1:8 ratio (M-MSCs:primary hepatocytes) for the Seahorse experiments; in a 1:4 ratio on the glass coverslips for microscopy to maximize cell-to-cell contacts and chances of witnessing mitochondrial transfer events; and in a 1:10 ratio on the glass bottom 6-well plate based on MSCs availability.

LSFC fibroblasts plated in either Seahorse plates or in 8-well Ibidi slides (Ibidi) were treated for 24h with 30µg of EVs.

5.6.7 Liver mitochondria isolation

Liver mitochondria were isolated from 5 weeks old H-*Lrpprc* mice by differential centrifugation 24h after MSC therapy, as described previously. [360]

5.6.8 Mitochondrial Respiration

Mitochondrial respiration was measured on isolated liver mitochondria using Clark-type electrodes at 23°C under continuous stirring as previously described. [360] Mitochondria (0.5 mg/mL) were suspended in MiR05 buffer (in mM: 0.5 EGTA, 3 $MgCl_2$, 60 lactobionic acid, 20 taurine, 10 KH_2PO_4, 20 HEPES, 110 D-sucrose, and 1g/L BSA). Following baseline recording, oxygen consumption was measured following sequential additions: i) glutamate malate (5:2.5 mM) for

Complex-I (CI), ii) ADP (1 mM), succinate (5 mM) for complex-II (CII), and iii) and carbonyl cyanide m-chlorophenylhydrazone (CCCP: 0.03 mM), antimycin A (8μM), TMPD/Ascorbate (5/0. 3mM) for complex IV (CIV), and potassium cyanide (0. 6 mM).

Mitochondrial respiration (oxygen consumption rate) in intact cells was measured using extra cellular flux analysis (Seahorse) in 96 well plates. Measurements were performed after subsequent additions of Oligomycin (1μg/mL), FCCP (1μM), and Antimycin A (1μM) plus Rotenone (1μM) in HCO3-free DMEM supplemented with L-Glutamine (4mM), Na-Pyruvate (1mM) and D-Glucose (5mM), at pH 7.4. Cell count was assessed after OCR measurements by microscopy (Evos, Thermo Fisher) after incubating cells with DAPI.

5.6.9 Fluorescence Microscopy

Primary hepatocytes and M-MSCs plated on glass coverslips were fixed with 4% PFA and permeabilized with 1% Triton prior to immunolabelling with mouse anti-Albumin (Novus). Coverslips were mounted using Prolong Gold with DAPI (Thermofisher) and imaged with a 40X objective (Zeiss) at the EVOS (Thermofisher).

Prior to microscopy, mitochondrial network of LSFC fibroblasts was labelled with MitoTracker RED (Thermofisher) and H-MSCs with MitoTracker GREEN (Thermofisher), following manufacturer's instructions. Cells were plated in a 1:1 ratio for a total of 5,000 cells per well in 8-well Ibidi slides (Ibidi) and imaged using the EVOS microscope (Thermofisher) with the 40X objective (Zeiss). To visualize EV uptake by fibroblasts, MitoTracker RED labelled cells were plated at 5,000 cells per well in 8-well Ibidi slides (Ibidi) and labelled (PKH26) EVs were added to well 24h before imaging at the confocal (Zeiss AxioObserver).

5.7 Acknowledgements

The authors would like to thank Dr. Ozge Kizilay Mancini and Dr. David Patten for insights on stem cells and useful discussions regarding the interpretation of results.

Chapter 6: Discussion and Conclusion

The work of this thesis brought light on the pathophysiology of LSFC in a novel mouse model of the disease, investigated the underlying compensatory mechanisms that grant a remarkable resilience to this model, and finally explored the therapeutic potential of stem cell therapy for mitochondrial diseases.

The H-*Lrpprc* mouse model, harboring a liver specific inactivation of *Lrpprc*, reproduces some of the hallmarks of hepatic mitochondrial diseases, including generalized growth delay and microvesicular steatosis of the liver. [432] At the molecular level, LRPPRC deficiency results in the depletion of most mtDNA encoded transcripts, a severe CIV and ATPsynthase assembly defect and reduced enzymatic activity. The impact is not limited to OXPHOS, and includes alteration of fatty acid oxidation, PTP dysregulation, caused by the ATPsynthase assembly defect, and altered transmembrane diffusion of ROS, linked to mitochondrial membrane lipid remodeling.

Despite these severe perturbations, H-*Lrpprc*$^{-/-}$ mice present a remarkable preservation of respiratory chain capacity. Mitochondria integrity is preserved through a complex network of molecular adjustments, which appear to include the upregulation of mitochondrial mass through mitochondrial biogenesis, enhanced translation capacity through increased number of mitoribosomes, and activation of elements of the mtUPR and the integrated stress response. Our data also indicate that stabilization of OXPHOS complexes into bioenergetically more efficient SCs is favored in *Lrpprc* deficient mitochondria, likely supported by the upregulation of cardiolipins.

Although significant progress is being made on the molecular/biochemical causes and pathophysiology of mitochondrial diseases, these disorders cruelly lack effective and curative treatments. Stem cell therapy has shown great promises in various human diseases and its therapeutic potential for mitochondrial diseases was explored using our LSFC models. Our data shows that MSCs and MSC-derived humoral factors display donor and recipient variability but have shown benefits in some experiments. EVs demonstrated an efficiency that is comparable to cell therapy and offer several technical advantages. The positive effect of EVs on our LSFC models and the underlying mechanisms deserve to be further investigated.

6.1 Impact of LRPPRC deficiency on liver, a clinically relevant organ in LSFC

Results from the characterization of the H-*Lrpprc* mouse model demonstrate the impact of LRPPRC ablation goes beyond OXPHOS and affects other facets of mitochondrial biology, including alteration of PTP regulation and transmembrane ROS diffusion. These dysfunctions likely have a clinical impact and could hardly be predicted based on the knowledge of the genetic defect. Most mitochondrial disease reports mainly focus on the impact of the OXHPOS defect on mitochondrial respiration, especially with the recent advancement of techniques such as extracellular flux analysis (e.g. Seahorse) which facilitates measurement of respiration, is high throughput and becomes useful when sample size is limited. In light of our findings and given the numerous roles of the mitochondria within the cell, other aspect of mitochondria functions should also be described when characterizing mitochondrial diseases.

6.1.1 Bioenergetics

Similar to what is reported in LSFC patients, hepatic LRPRPC depletion causes a severe CIV deficiency in the H-*Lrpprc* mouse, where enzyme activity is reduced by 80% after detergent extraction. [113, 121] However, functionally CIV is only reduced by 30% in H-*Lrpprc*$^{-/-}$ mitochondria when the complex is embedded in its native lipid environment. This suggests the detergents used in enzyme assay protocols exacerbate the defect, and CIV activity in its native state is not as severely affected (Chapter 2 and 4). [310] This is an important factor to consider since OXPHOS enzyme assays usually consist in the first line of investigation when characterizing mitochondrial diseases. Therefore, the reported defects are likely exaggerated and do not take into account the contribution of the surroundings of complexes. Membrane lipids are crucial for the proper assembly and function of individual OXPHOS complexes and their supra-arrangements [35, 37, 239], and among them cardiolipins, PC, PE, PG and TG are known to specifically support CIV. [235, 433] Our lipidomics analysis of mitochondrial membrane fragments containing SCs and OXPHOS complexes revealed a broad remodeling of membrane lipids, including various species belonging to classes of lipids indispensable for CIV. We observed an increase in the total amount of cardiolipins, in addition to individual variations in the six species of cardiolipin we identified. We also noted differences among the lipids within PC and PE classes. supporting their role in maintaining the activity of residual CIV in absence of LRPPRC (Chapter 4).

As found in LSFC patients, the CIV defect in H-*Lrpprc*$^{-/-}$ can be tracked down to the reduced levels of mitochondrially encoded transcripts COX-I, COX-II and COX-III, encoding the catalytic core of the complex, resulting in a decreased in fully assembled CIV. [113, 122, 125] To our surprise, we incidentally found the impact of reduced LRPPRC on mitochondrial transcripts also severely affects ATPsynthase in H-*Lrpprc*$^{-/-}$ mice, causing an assembly defect specific to murine model. The secondary impact on ATPsynthase, and its assembly defect, is also reported in a mouse model with conditional inactivation of cardiac *Lrpprc* [126], but the underlying mechanisms have not been investigated. The difference found between human and mouse could be explained by species specificity in mitochondrial transcripts handling by LRPPRC. [370] The complex formed by LRPPRC and its partner SLIRP, globally binds throughout the mitochondrial DNA, preferentially interacting with single-stranded mRNAs and rRNAs, and disruption of the complex results in generalized transcript impairment. [370] Investigations of RNA-protein interaction revealed differences in the favored binding sites between human and rodents LRPPRC. [370] Although the binding sites are generally conserved across species, there are slight differences in the surroundings of *ATP6/8* between humans and rodents, with a moderate increase of binding by LRPPRC in rodents for this region. [370] Other factors are involved in the transcription of the mitochondrial genome, some still elusive, and could be regulated differently in human and mouse. This could also be the case for the other PPR proteins. While the seven members of this protein family are highly conserved [106, 109], their regulation could also differ between human and mouse, and some species could potentially compensate, to some extent, for the LRPPRC deficiency preferentially in one species.

6.1.2 PTP dysregulation

The ATPsynthase assembly defect triggered by LRPPRC deficiency resulted in a dramatic PTP dysregulation in the H-*Lrpprc* mouse. The PTP plays important physiological roles in the cell. [299] Notably, prolonged PTP opening is associated with membrane permeabilization, impaired respiratory chain function, and release of cytochrome c leading to apoptosis. [434] Acute opening and flickering of the pore are involved in Ca^{2+} handling in various cell types and cell differentiation in the cardiac tissue. [315] Previous work from our research consortium on LSFC fibroblasts showed an increased sensitivity to PTP opening in patient cells. In contrast, and to our surprise at first, PTP opening is drastically delayed in H-*Lrpprc*$^{-/-}$ mitochondria despite an increased amount of pore sensitizer cyclophilin D. The nature of the molecular components of the PTP has been a

subject of debate, but extensive recent work has convincingly demonstrated ATPsynthase dimers structurally rearrange to form the pore. [319, 322] While the PTP dysregulation seems specific to the H-*Lrpprc* mouse, our results strongly support this hypothesis of a PTP formed by ATPsynthase. Although the ATPsynthase defect caused by depleted LRPPRC is absent in LSFC patients, our results could be transposed to other mitochondrial diseases caused by primary defects of ATPsynthase where decreased sensitivity to pore opening could contribute to pathogenesis. [435] However, it is impossible to predict if the primary ATPsynthase defect will result in a premature or delayed PTP opening. Otherwise, in most mitochondrial diseases without a primary involvement of ATPsynthase, increased sensitivity to PTP opening is likely to be more common, as these disorders are often associated with increased ROS release, and impaired capacity to maintain membrane potential and changes in other factors that may promote pore opening. [435] This is consistent with the fact that in LSFC fibroblasts, in which the ATPsynthase assembly defect is absent, PTP opening occurs prematurely as previously reported. [93]

Clinically, the impact of PTP dysregulation in mitochondrial diseases may be greater than suspected. PTP dysregulation can have a severe impact in tissues, especially in the nervous system where a tight regulation of the pore is required for proper neuronal function. [436] A prolonged opening of the pore or interruption of PTP flickering can lead to premature cell death and impaired synaptic transmission caused by altered Ca^{2+} buffering in axon terminals, respectively. [437] Dysregulation of the PTP and altered Ca^{2+} handling have been reported in various neurodegenerative disorders, including Charcot-Marie-Tooth, Alzheimer's disease, Parkinson's disease and forms of ataxia. [437] In an amyotrophic lateral sclerosis (ALS) mouse model, the use of cyclosporin A, a pharmacologic agent able to bind the PTP sensitizer cyclophilin D and delay pore opening, has been shown to be neuroprotective and increase lifespan of animals. [436] These findings highlighted both the implication of mitochondria in the pathogenesis of ALS and the consequences of hypersensitivity of the PTP. On the other hand, in rodent and Human models of hereditary spastic paraplegia caused by mutations in the mitochondrial protein SPG7, the use of benzodiazepine Bz-423 triggered pore opening and restored neuronal function. [437] Given the importance of PTP function in the nervous system and the neurodegenerative component of LSFC, it is plausible that dysregulation of the PTP contributes to the pathophysiology of the brain. Based on our findings, the type of PTP dysregulation will depend in part on the assembly of ATPsynthase in neurons. In patient fibroblasts, showing no ATPsynthase dysfunction, PTP sensitivity is enhanced whereas PTP opening is delayed in H-*Lrpprc*$^{-/-}$ mice with an ATPsyntahse assembly

defect. These contrasting results makes it difficult to predict which alteration prevails in LSFC neurons, but investigating the status of the ATPsynthase could provide an indication. To this end, LSFC fibroblasts could be transdifferentiated into neurons and ATPsynthase assembly be assessed by large gel electrophoresis. It would also be relevant to test the effect of either pore sensitizer Bz-423 or pore inhibitor cyclosporin A, previously reported to have a beneficial effect on the nervous system, on our models' phenotypes.

6.1.3 Changes in mitochondrial ROS transmembrane diffusion

Another unexpected and surprising phenotypic trait of H-*Lrpprc*$^{-/-}$ mice unraveled through our characterization, is the alteration of normal transmembrane ROS diffusion. Our data shows that both ROS emission and scavenging rates are almost null in H-*Lrpprc*$^{-/-}$ mitochondria, and that this is independent of antioxidant systems and mitochondrial membrane potential. Increased H_2O_2 release is only observed when measured in inside-out sub-mitochondrial particles, which allows the bypass of the normal diffusion step across the inner mitochondrial membrane. In this situation, the respiratory chain produces more ROS in absence of hepatic LRPPRC. These results, and the release of H_2O_2 following progressive permeabilization of liver mitochondria support the hypothesis of altered transmembrane diffusion. We did not investigate the underlying mechanisms, but evidence in the literature suggest that modulation of membrane permeability to ROS is an adaptive mechanism in yeast. Throughout its different stages of life, yeast will become more or less permeable by modulating the levels of membrane ergosterol (i.e. cholesterol in eucaryotic cells). Increased H_2O_2 diffusion is associated to increased ergosterol content whereas reduced H_2O_2 diffusion is associated with reduced ergosterol content. [336, 337] The structure of cholesterol and its embedding in lipid bilayers creates voids, which facilitate the transmembrane diffusion of gases, peroxide and quinone. [338, 438] Mitochondrial membranes are naturally poor in cholesterol, and our lipidomics analysis revealed lower levels of cholesterol and cholesterol esters in absence of LRPPRC. We cannot conclude that the transmembrane diffusion alteration we observed is caused by the lowered levels of cholesterol. Additional experiments to test this hypothesis could include modulation of membrane cholesterol using conjugated BSA-cholesterol for enrichment and MBCD for depletion of liver mitochondria [439, 440], followed by H_2O_2 release measurement. This would allow to measure the impact of increased and lowered membrane cholesterol content on ROS transmembrane diffusion. Otherwise, the specific involvement of this lipid could be targeted by further knocking down mitochondrial cholesterol transporter START domain protein family members or HMG-CoA synthase/reductase involved in cholesterol synthesis. [441] Beyond

cholesterol, alterations of other mitochondrial membrane phospholipids could play a role, possibly through altering membrane fluidity, which could also interfere with normal diffusion. We did not perform lipidomics screens in LSFC fibroblasts and we do not know if transmembrane diffusion is altered in their mitochondria. Given the lipid perturbations reported in patient plasma and in the H-*Lrpprc* mouse, we could suspect mitochondrial membrane lipids alterations are also present in fibroblasts. but further experiments are required to investigate this possibility.

6.1.4 Metabolism alteration beyond OXPHOS in absence of LRPPRC

As a consequence of mutations of LRPPRC, LSFC patients present high circulating levels of long-chain acylcarnitines, which are known proxies of beta-oxidation alteration. [90] Moreover, both LSFC patients and H-*Lrpprc*$^{-/-}$ mice display hepatic microvesicular steatosis which is another clear indicator of abnormal lipid metabolism. [94] This phenotypic trait is alleviated in mice by the overexpression of LRPPRC, confirming the involvement of the protein. [108, 118] The lipid handling defect is not limited to the mitochondria, and also impacts the peroxisomes as indicated by decreased levels of plasmalogens in LSFC patient plasma and H-*Lrpprc* mice plasma and liver. [94] Perturbations in peroxisomal lipid metabolism can have a significant negative impact on the brain, and could contribute to LSFC pathogenesis, since plasmalogens account for approximately 20% of the brain's phospholipids. [442] Overall, LRPPRC probably exerts broad effects on lipid metabolism which potentially contribute to the pathogenesis of LSFC beyond OXPHOS. Lipid dyshomeostasis could be more common than expected, given the neurodegenerative nature of Leigh syndrome, and of most mitochondrial diseases, and would be worth investigating more often in the clinic. Moreover, work from our research consortium revealed a lipidomics signature in LSFC patient plasma, which could be used for screening patients and follow disease progression, facilitating disease management. [90]

6.2 Compensatory mechanisms in place to compensate and palliate primary defects caused by LRPPRC deficiency

Despite a severe OXPHOS primary defect, LSFC fibroblasts and H-*Lrpprc* mice maintain normal levels of energy, suggesting compensatory responses are in place to help palliate the defects. The compensatory mechanisms we have reported in the H-*Lrpprc* livers (Chapter 4), which include increased mitochondrial biogenesis and mass, and favored incorporation of residual CIV into SCs, likely contribute to the resilience of this model. This is shown by the ability of LRPPRC knockout liver mitochondria to maintain near normal respiration rates under uncoupled state and in presence of the artificial electron donor TMPD feeding electrons directly to CIV (Chapter 2).

6.2.1 Stress responses

Mouse models of genetic mitochondrial diseases are mainly used to gain better knowledge on the molecular defects and their biochemical consequences, and rarely to identify compensatory mechanisms allowing survival *in vivo.* The onset of compensatory mechanisms has been shown to be responsible for the spontaneous recovery of patients suffering of a muscle myopathy named reversible infantile respiratory chain deficiency caused by dual mutations in the nuclear and mitochondrial DNA. [66, 134] This evidence in humans highlights the strength of endogenous compensatory mechanisms triggered by primary mitochondrial defects. In the case of mouse models of Leigh syndrome with *Surf1* deficiency, the phenotype is surprisingly mild despite a profound CIV defect. [443] *Surf1*$^{-/-}$ mice have higher blood lactate levels and significantly reduced CIV activity in the highly energetic tissues heart and muscle, but mitochondrial respiration and ATP levels are unaltered, and their median lifespan is increased. [444] Further studies aiming to elucidate the mechanisms associated with this resilience showed an activation of the mtUPR and increased mitochondrial biogenesis. [444] In a similar manner, mitochondrial biogenesis and mitochondrial mass are increased in absence of hepatic LRPRPC, and this is accompanied by increased transcript levels for master regulators of mitochondrial biogenesis PGC1a and TFAM. In the H-*Lrpprc* liver, both small and large mitochondria ribosomes are increased as a compensatory mechanism part of the mtUPR. This upregulation of mitochondrial ribosomes is likely to compensate for the reduced mitochondrial transcript levels in absence of LRPPRC. Moreover, several chaperones and proteases, which play a key role in the mtUPR, are also increased in H-*Lrpprc*$^{-/-}$ mitochondria. [173] The mtUPR has not been much studied in the liver and in *in vivo* models of mitochondrial diseases.

In absence of hepatic LRPPRC, we observed an increase of mtUPR markers accompanied by an increased mitochondrial transcription, which is the opposite to the classic mtUPR, which is accompanied by transcriptional suppression. [173, 445] This suggests the mtUPR we observed in the liver differs from the classic response and allows the increase of chaperones and proteases to support mitochondrial biogenesis and energy demand. This potentially occurs in other highly energetic tissue and should be further investigated in *in vivo* models. Although compensatory mechanisms seem beneficial for the survival of some mouse models of mitochondrial diseases, evidence suggest they can also contribute to the pathogenesis of others. [166] For instance, in a mouse model of mitochondrial myopathy (Deletor mouse), chronic activation of the mtUPR and the integrated mitochondrial stress response is detrimental and their inhibition by rapamycin reverses the progression of the disease. [166] This evidence suggest that chronic activation of these mechanisms could be harmful and a balance in these stress responses is necessary for them to be effective.

6.2.2 SCs rearrangements stabilize CIV in absence of LRPPRC

In our first study, the striking difference in CIV activity after detergent extraction versus when the complex is found in its native environment in absence of LRPPRC cannot be solely explained by the above-mentioned compensatory mechanisms. This suggests additional responses are in place to preserve residual CIV activity and function. A compensatory stabilization of CIV by SCs has been reported in patient with CIV deficiency caused by an unidentified gene mutation. [203] This has also been reported in Surf1 patients' fibroblasts, where CIV is mainly found assembled in I-III_2-IV_n SC. [203, 443] Our studies have shown a preferential incorporation of remaining CIV into SCs arrangements, more specifically in the respirasome, at the expense of the monomeric form in both LSFC fibroblasts and H-*Lrpprc*$^{-/-}$ mitochondria. This likely contributes to explain how the activity of CIV extracted from this protective environment by detergents exaggerates the defect in absence of LRPPRC.

SCAF1 is involved in the formation of III_2-IV SCs, and its role in the formation of respirasome is debated. Studies have shown mice with the C57BL/6 background harbor a mutation in the gene encoding for SCAF1, resulting in the production of a shorter dysfunctional protein. As a result, mouse models generated on this background are unable to form III_2-IV SCs. [202] The functional impact on mitochondrial function has not been investigated much, but a recent report demonstrated

no impact of the short form of SCAF1 on bioenergetics. [372] Our H-*Lrpprc* model is bred on the C57BL/6 background, and therefore cannot form the III_2-IV SCs, but is still able to form the SC respirasome. Based on these evidence, we can clearly rule out any contribution of SCAF1 in the preferential incorporation of residual CIV into respirasome observed in absence of LRPPRC. Our data thus suggest that other factors probably played a role, particularly mitochondrial membrane lipids.

6.2.3 Broad lipid remodeling in absence of LRPPRC

The broad lipid remodeling occurring in absence of LRPPRC is linked with several aspects of the phenotype observed in LSFC. Evidence suggesting the lipid remodeling potentially participate in compensatory response in our model is through the mitochondria specific anionic lipid cardiolipin. Cardiolipin is involved in CIV, and SCs, assembly and stabilization. [40] We observed an increase in four species of cardiolipin, and also an increase in protein complexes linked to cardiolipin. These include the MICOS and prohibitins complexes involved in the regulation of cardiolipin metabolism and the formation of cardiolipin enriched microdomains. We also observed an increase in proteins forming contact sites between the endoplasmic reticulum and mitochondria, favoring the transport of cardiolipin precursors. Although not confirmatory, our observations suggest a possible role for cardiolipin in the SCs remodeling occurring in H-*Lrpprc* mitochondria. Interestingly, cardiolipin's stabilizing role is not limited to CIV and also includes ATPsynthase. [446] Cardiolipin transiently interacts with the c-ring of ATPsynthase, participating in the viscosity and sealing of the membrane surrounding this complex, enabling rotation of the c-ring and preventing proton leak. [446] Studies have also reported a correlation between levels and alterations of cardiolipin and ATP levels, more specifically a decrease in ATP production in the presence of peroxidated cardiolipins in rat liver mitochondria. [447] This suggests the stabilization of ATPsynthase by cardiolipin contributes to the maintenance of ATP production, and this could be promoted in the absence of hepatic LRPPRC. The contribution of cardiolipin to the resilience of H-*Lrpprc* mice could be further studied by preventing the upregulation of cardiolipin. This would reveal if SCs can still form in the absence of LRPPRC and reduced levels of cardiolipin, and by this the extent of the impact of SCs in cell survival. Conversely, we could look into strategies that could promote cardiolipins and assess if it further stabilizes CIV in the absence of LRPPRC.

6.3 Potential of stem cell therapy for mitochondrial diseases using LSFC as a model

Because of the high heterogeneity in the clinical presentation and in the genetic causes of mitochondrial diseases, a successful treatment needs to act broadly in the cell and across tissues in the body. Based on our MSC therapy pilot study and on evidence in the literature, an effective therapy for mitochondrial diseases will likely have an indirect effect on the OXPHOS complex or the mitochondria.

MSC therapy for mitochondrial disease is understudied and prompted us to test its potential in LSFC. [405] After characterizing the H-*Lrpprc* mouse and investigating the mechanisms responsible for its resilience, exploring therapeutic avenues was the logic following step. We took advantage of our access to LSFC patient fibroblasts, healthy human MSCs and our hepatic LRPPRC knockout mouse. Our pilot study indicates MSC therapy has variable biological effects in our LSFC models, with no obvious evidence of mitochondrial transfer from MSCs to LSFC cells despite cell-to-cell contacts. Nevertheless, some of our MSC donors had a beneficial impact on mitochondrial respiration within 24h in both *in vitro* and *in vivo* experiments and with both rodent and human samples. This suggests an acute effect of stem cells on mitochondria function cannot be attributable to direct transfer of mitochondria. Because of technical challenges and variations in protocols and responses across studies, the field of regenerative medicine is moving towards to use of extracellular vesicles, which represent a safer and easier product to handle. [276] The benefits, although variable, of cell therapy we initially observed are found using exosomes in our LSFC models. This suggests EVs could be an interesting therapy for mitochondrial diseases. Although the precise content of EVs is not fully elucidated, studies have reported mitochondrial material, microRNA targeting the mitochondria, and various lipids, depending on the secreting cell type[294, 404], which could prove relevant in the context of mitigating mitochondrial dysfunction in patient cells. Moreover, an increasing number of studies are exploring the possibility to engineer exosomes and to customize the cargo, enabling their use for personalized medicine. [448] A lot of work in the field of regenerative medicine is still required, especially to better understand the mechanisms through which EVs are beneficial.

Unfortunately, our pilot study does not allow us to validate if the multiple dysfunctions and molecular defects we previously reported are fully alleviated by stem cell therapy. Especially, after

24h of treatment it is impossible to say if the treatment activated cellular repair mechanisms, as these likely need more time. To complete our pilot study, additional experiments are indispensable. We need to increase our sample number for the measurement of mitochondrial respiration using the Seahorse after exosome treatment and indirect co-cultures of H-MSCs and LSFC fibroblasts in Transwell. We also need to investigate by which mechanism MSCs and exosomes are having a beneficial impact on mitochondrial function by repeating our indirect co-culture experiments with the Transwell and exosome treatment and collecting the cells for western blot analysis. We will probe for markers of mitochondria biogenesis to validate if the increased respiration rates are caused by increased mitochondrial mass.

6.3.1 LSFC and LRPPRC study models

The impact of LRPPRC on cellular biology has been investigated in LSFC patient samples and fibroblasts harboring the A354V mutation, in cell models with depleted or upregulated LRPPRC, and in tissue specific knockout of LRPPRC mouse models. Responses to reduced or increased levels of LRPPRC yield similar and different results in the various models and are summarized in Table 3. Despite their differences, all the listed models greatly contributed to the improvement of our knowledge on the biology of LRPPRC.

Several elements likely contribute to the variation of the impact of mutated or reduced levels of LRPPRC on metabolism. Among them, the lower energetic demand of fibroblasts compared to hepatocytes could explain the milder phenotype observed in LSFC fibroblasts as opposed the H-*Lrpprc* mouse. Mitochondrial disease patient fibroblasts are useful since they harbor the specific causative mutation(s), but their phenotype is often masked and will manifests under stressed conditions [449], making it more challenging to appreciate the full range of defects. On the other hand, LSFC fibroblasts are easily obtained from patients through minimally invasive biopsies and are useful tools for therapy testing and compound screening. ([93], Chapter 5)

Another important factor to consider is the variation in the compensation to LRPPRC depletion across tissues in LSFC patients. Brain and liver are severely affected whereas heart and muscle are spared, suggesting different compensatory stress responses are triggered across these tissues. [113, 121] A better understanding of these differential mechanisms would be useful and could help identifying therapeutic targets. This difference in compensatory responses is also present across the

various models of LRPPRC deficiency reported in the literature. These models and their corresponding phenotype are listed in Table 3. When comparing the impact of the levels of LRPPRC on the various sample types listed in Table 3, the combined CIV and ATPsynthase defect seems restricted to mouse model or mouse cells lines and is associated with very low amounts of LRPPRC (below 10%). [112, 126] This additional ATPsynthase deficiency in rodents could be explained by differences in mtRNA handling and binding by LRPPRC specific to species, as discussed previously. [370] In the case of human cells, as the LRPPRC levels are depleted due either to the natural degradation of mutated LRPPRC or the experimental knock-down of the wildtype protein, the impact on OXPHOS becomes generalized. [107, 111, 113, 121, 122] In LSFC patient liver and heart samples where levels of mutated LRPPRC are lower than 10%, ATPsynthase is unaffected and the abundance of assembled CI and CIII is increased, likely as a compensation to the CIV defect. [113, 121] This compensatory increase of CI, CII and CIII is only observed later in life in the H-*Lrpprc* mouse model at 10 weeks, indicating this compensatory increase is delayed in the mouse model. [450] These differences among the different models do not diminish their usefulness but should be kept in mind when interpreting data.

Table 6.1: Comparison of LRPPRC Models.

Paper	**Sample**	**Levels of LRPPRC**	**Increased transcripts**	**Decreased transcripts**	**Assembled mtRibosomes**	**OXPHOS assembly defect**	**OXPHOS enzyme activity**	**Respiration**
Sondheimer, 2010 [107]	HeLa cells	35%		ND1, ND6, COX I, mTmP, CIDEA				↓ basal and maximal (uncoupled)
Xu, 2004 [121]	LSFC patient liver and fibroblasts	< 25%		COX I, COX III, ND1				
	LSFC patient tissues	skeletal muscle > heart > placenta > kidney > liver > lung = brain		COX I-II-III: heart > liver > skeletal muscle > kidney > brain = placenta > lung			CIV: ↓ activity inversely proportional to levels of LRPPRC	
Xu, 2012 [125]	Whole mouse embryo	0%					↓ CIV	
	Murin embryonic fibroblasts (MEFs)		CYTB; PGC1a (by WB)	COX I, COX III, ATP6, PTCD2 and MRSP27 (by WB)			↓ CIV > 60% ↓ CI+CIII	
Sasarman, 2010 [122]	LSFC patient cell lines (fibroblasts)	< 30%		All OXPHOS except ND3 and ND6	rRNAs transcripts unchanged	CIV	↓ by 64%	
		< 30%		All OXPHOS except ND3 and ND6		CIV		

		< 10%		Generalized		Generalized		
Sasarman, 2015 [113]	LSFC patient muscle sample	20-30%	12S rRNA	Generalized		CI and CIV		
	LSFC patient muscle sample	< 10%				Generalized		
	LSFC patient heart sample		12S and 16S rRNA			CIV ↓ by 50%; ↑ CI and CIII		
	LSFC patient liver sample				↓ small ribosome	undetectable CIV; ↑ CI and CIII		
Ruzzenente, 2012 [112]	Mouse	0%	12S, 16S, 28S and 39S rRNA	COX I, COX II, COX III, ND1, ND5 **ATP6/8 not measured*	↑ 55S	CIV; CV later in life	↓ CIV; ↓ CII later in life	
Mourier, 2014 [126]	Mouse	0%				CIV and CV	↓ CIV; CV less sensitive to oligomycin	↓ ADP stimulated, Uncoupled unchanged, ↓ state 3 later in life
Gohil, 2010 [111]	Human fibroblasts	Various knock-down		extend of transcript affected correlates with decrease in LRPPRC levels				↓ OCR ↑ ECAR

Cooper, 2006 [108]	H2. 35 hepatoma murine cells	↓		PGC1a, PRPCK, G6P				
		↑						
	Murine primary hepatocytes	< 15%		COX I, COX II, COX III (other transcripts not shown)				
Liu, 2011 and 2014 [118, 119]	Murine primary hepatocytes							
	H2. 35 hepatoma murine cells	< 15%						impaired b-oxidation, ↓ maximal respiration
	LRP130 mice	↓		ND1, ND4, COX I, COX II, COX III, ATP6, ATP8				
		↑						↑ + ↑ fatty acid oxidation
Akie, 2015 [120]	Mouse - diet induced obisity	↑					↑ CI, III, IV and V	no change in state 2 and 4; ↑ in ADP stimulated

Cuillerier, 2016 and 2021 *(in press)* [360]	Mouse liver	< 10%	PGC1a and TFAM (by WB)	COX I, COX II, COX III, ATP6	↑ small and large	CIV and CV	↓ CIV and CV; CV less sensitive to oligomycin	impaired b-oxidation, unchanged maximal and TMPD/ASC, ↓ ADP stimulated

Increased/decreased transcripts are mtDNA encoded and exclude tRNA and rRNA, unless otherwise specified. Levels are unchanged or uninvestigated if nothing is mentioned.

6.4 Conclusion

In conclusion, the work from this thesis used the available LSFC models to their full potential. We have characterized the H-*Lrpprc* mouse model and used it to test the potential of therapies, increasing our knowledge on the role of LRPPRC in the process. Unfortunately, although this model was extremely useful, it is imperfect and has reached its limit for the study of LSFC. This mouse model harbors a liver specific inactivation of LRPPRC and limits the study of other tissues. Moreover, gene inactivation in the liver can be diluted over time with the regeneration of non-genetically modified hepatocytes. [298] Although the levels of LRPPRC are drastically reduced in the liver of patients with the A354V mutation, the protein is still present, and studies have shown mutated LRPPRC is still functional. [113] Consequently, a complete depletion of LRPPRC is not representative of what is observed in patients.

Our research consortium has worked on the development of multiple mouse models of LSFC. One model consisted of a ubiquitous knock-in of the A354V mutation in *LRPPRC*, but unfortunately this was lethal at embryonic day 8. [450] We and others [112] have also tried to generate a ubiquitous knockout of LRPPRC and as this was unsuccessful, it showed LRPPRC is essential for embryonic development in mice. Given the impact of LSFC in liver and brain, our group decided to develop tissue specific inactivation of LRPPRC in these organs using the CRE-LOX system. For the neuronal model, synapsin driven CRE caused death at 14 days of age, and we could not use this model. At the beginning of the work of this thesis, the hepatic model using albumin-CRE successfully generated a viable model for the study of the pathogenesis of LSFC in the liver. Our consortium is still working on the development of more relevant mouse models.

To this end, we recently developed a mouse model in which one of the wild type allele has been replaced by the A354V mutant, and the other by a floxed *Lrpprc* allele that can be deleted using a tamoxifen inducible cre-recombinase under the control of the endogenous mouse promoter Gt(ROSA)26Sor. After treatment with tamoxifen, the normal floxed allele is inactivated, and only the mutated form of *Lrpprc* is expressed throughout the body, thereby reproducing the molecular defect observed in patients. This model will need to be characterized in future studies.

Another option will be to use the LSFC fibroblasts and trans-differentiate them into hepatocytes or neuronal cells. However, the multistep process required for trans-differentiation is challenging, requires expertise, is expensive and yields a few cells, limiting the number of experiments we can perform.

References

1. Wallace, D.C., *Mitochondrial Diseases in Man and Mouse.* Science, 1999. **283**(5407): p. 1482-1488.
2. Nunnari, J. and A. Suomalainen, *Mitochondria: in sickness and in health.* Cell, 2012. **148**(6): p. 1145-59.
3. Rahman, J. and S. Rahman, *Mitochondrial medicine in the omics era.* The Lancet, 2018. **391**(10139): p. 2560-2574.
4. Rahman, S., *Mitochondrial disease in children.* J Intern Med, 2020. **287**(6): p. 609-633.
5. Taanman, J.-W., *The mitochondrial genome: structure, transcription, translation and replication.* Biochimica et Biophysica Acta (BBA) - Bioenergetics, 1999. **1410**(2): p. 103-123.
6. Taarnman, J.-W., *The mitochondrial genome: structure, transcription, translation and replication.* Biochumuca et Biophysica Acta, 1998. **1410**(2): p. 103-123.
7. Robin, E.D. and R. Wong, *Mitochondrial DNA molecules and virtual number of mitochondria per cell in mammalian cells.* J Cell Physiol, 1988. **136**(3): p. 507-13.
8. Anderson, S., et al., *Sequence and organization of the human mitochondrial genome.* Nature, 1981. **290**(5806): p. 457-65.
9. Lopez, M.F., et al., *High-throughput profiling of the mitochondrial proteome using affinity fractionation and automation.* Electrophoresis, 2000. **21**(16): p. 3427-3440.
10. Calvo, S.E., K.R. Clauser, and V.K. Mootha, *MitoCarta2.0: an updated inventory of mammalian mitochondrial proteins.* Nucleic Acids Res, 2016. **44**(D1): p. D1251-7.
11. Pagliarini, D.J., et al., *A mitochondrial protein compendium elucidates complex I disease biology.* Cell, 2008. **134**(1): p. 112-23.
12. PF., C., *Mitochondrial Disorders Overview.* . Adam MP, Ardinger HH, Pagon RA, et al., editors. ed. GeneReviews® [Internet]. 2000.
13. Schon, K.R., et al., *Mitochondrial Diseases: A Diagnostic Revolution.* Trends Genet, 2020. **36**(9): p. 702-717.
14. Schon, E.A., S. DiMauro, and M. Hirano, *Human mitochondrial DNA: roles of inherited and somatic mutations.* Nat Rev Genet, 2012. **13**(12): p. 878-90.
15. Gorman, G.S., et al., *Mitochondrial diseases.* Nat Rev Dis Primers, 2016. **2**: p. 16080.
16. Wallace, D.C., *Diseases of the mitochondrial DNA.* Annual Review of Biochemistry, 1992. **61**: p. 1175-1212.
17. Sunnucks, P., et al., *Integrative Approaches for Studying Mitochondrial and Nuclear Genome Co-evolution in Oxidative Phosphorylation.* Front Genet, 2017. **8**: p. 25.
18. Grady, J.P., et al., *mtDNA heteroplasmy level and copy number indicate disease burden in m.3243A>G mitochondrial disease.* EMBO Mol Med, 2018. **10**(6).
19. Picard, M., et al., *Progressive increase in mtDNA 3243A>G heteroplasmy causes abrupt transcriptional reprogramming.* Proc Natl Acad Sci U S A, 2014. **111**(38): p. E4033-42.
20. Korzeniewski, B., et al., *Effect of 'binary mitochondrial heteroplasmy' on respiration and ATP synthesis: implications for mitochondrial diseases.* Biochem J, 2001. **357**(Pt 3): p. 835-42.
21. Stewart, J.B. and P.F. Chinnery, *The dynamics of mitochondrial DNA heteroplasmy: implications for human health and disease.* Nat Rev Genet, 2015. **16**(9): p. 530-42.
22. de Laat, P., et al., *Intra-patient variability of heteroplasmy levels in urinary epithelial cells in carriers of the m.3243A>G mutation.* Mol Genet Genomic Med, 2019. **7**(2): p. e00523.
23. van den Ameele, J., et al., *Mitochondrial heteroplasmy beyond the oocyte bottleneck.* Semin Cell Dev Biol, 2020. **97**: p. 156-166.
24. Calvo, S.E. and V.K. Mootha, *The mitochondrial proteome and human disease.* Annu Rev Genomics Hum Genet, 2010. **11**: p. 25-44.
25. DiMauro, S., *Mitochondrial diseases.* Biochim Biophys Acta, 2004. **1658**(1-2): p. 80-8.
26. Chinnery, P.F., *Mitochondrial Disorders Overview*, in *GeneReviews® [Internet]*. 2000.
27. Civiletto, G., et al., *Opa1 overexpression ameliorates the phenotype of two mitochondrial disease mouse models.* Cell Metab, 2015. **21**(6): p. 845-54.

28. Viscomi, C. and M. Zeviani, *MtDNA-maintenance defects: syndromes and genes.* J Inherit Metab Dis, 2017. **40**(4): p. 587-599.
29. Marusich, M.F.R., Brian H.; Taanman, Jan-Willem.; Jin Kim, Soo.; and R.S. Schillace, Jordan L.; Capaldi, Roderick A. , *Expression of mtDNA and nDNA encoded respiratory chain proteins in chemically and genetically-derived Rho0 human fibroblasts: a comparison of subunit proteins in normal fibroblasts treated with ethidium bromide and fibroblasts from a patient with mtDNA depletion syndrome.* Biochimica et Biophysica Acta, 1997. **1362**(2-3): p. 145-159.
30. Wiedemann, N. and N. Pfanner, *Mitochondrial Machineries for Protein Import and Assembly.* Annu Rev Biochem, 2017. **86**: p. 685-714.
31. Palmer, C.S., A.J. Anderson, and D. Stojanovski, *Mitochondrial protein import dysfunction: mitochondrial disease, neurodegenerative disease and cancer.* FEBS Lett, 2021. **595**(8): p. 1107-1131.
32. Franco-Iborra, S., et al., *Defective mitochondrial protein import contributes to complex I-induced mitochondrial dysfunction and neurodegeneration in Parkinson's disease.* Cell Death Dis, 2018. **9**(11): p. 1122.
33. Holthuis, J.C. and A.K. Menon, *Lipid landscapes and pipelines in membrane homeostasis.* Nature, 2014. **510**(7503): p. 48-57.
34. Horvath, S.E. and G. Daum, *Lipids of mitochondria.* Prog Lipid Res, 2013. **52**(4): p. 590-614.
35. Colina-Tenorio, L., et al., *Shaping the mitochondrial inner membrane in health and disease.* J Intern Med, 2020.
36. Basu Ball, W., et al., *Ethanolamine ameliorates mitochondrial dysfunction in cardiolipin-deficient yeast cells.* J Biol Chem, 2018. **293**(28): p. 10870-10883.
37. Basu Ball, W., J.K. Neff, and V.M. Gohil, *The role of nonbilayer phospholipids in mitochondrial structure and function.* FEBS Lett, 2018. **592**(8): p. 1273-1290.
38. Tatsuta, T., M. Scharwey, and T. Langer, *Mitochondrial lipid trafficking.* Trends Cell Biol, 2014. **24**(1): p. 44-52.
39. Chatzispyrou, I.A., et al., *Barth syndrome cells display widespread remodeling of mitochondrial complexes without affecting metabolic flux distribution.* Biochim Biophys Acta Mol Basis Dis, 2018. **1864**(11): p. 3650-3658.
40. McKenzie, M., et al., *Mitochondrial Respiratory Chain Supercomplexes Are Destabilized in Barth Syndrome Patients.* Journal of Molecular Biology, 2006. **361**(3): p. 462-469.
41. Rahman, S. and W.C. Copeland, *POLG-related disorders and their neurological manifestations.* Nat Rev Neurol, 2019. **15**(1): p. 40-52.
42. Grier, J., et al., *Diagnostic odyssey of patients with mitochondrial disease: Results of a survey.* Neurol Genet, 2018. **4**(2): p. e230.
43. McFarland, R., R.W. Taylor, and D.M. Turnbull, *A neurological perspective on mitochondrial disease.* The Lancet Neurology, 2010. **9**(8): p. 829-840.
44. Witters, P., et al., *Revisiting mitochondrial diagnostic criteria in the new era of genomics.* Genet Med, 2018. **20**(4): p. 444-451.
45. Rodenburg, R.J., et al., *A multi-center comparison of diagnostic methods for the biochemical evaluation of suspected mitochondrial disorders.* Mitochondrion, 2013. **13**(1): p. 36-43.
46. Taylor, R.W., et al., *The diagnosis of mitochondrial muscle disease.* Neuromuscul Disord, 2004. **14**(4): p. 237-45.
47. Frazier, A.E., D.R. Thorburn, and A.G. Compton, *Mitochondrial energy generation disorders: genes, mechanisms and clues to pathology.* J Biol Chem, 2017.
48. Calvo, S.E., et al., *Molecular diagnosis of infantile mitochondrial disease with targeted next-generation sequencing.* Sci Transl Med, 2012. **4**(118): p. 118ra10.
49. Carroll, C.J., V. Brilhante, and A. Suomalainen, *Next-generation sequencing for mitochondrial disorders.* Br J Pharmacol, 2014. **171**(8): p. 1837-53.
50. Duan, M., et al., *Evaluating heteroplasmic variations of the mitochondrial genome from whole genome sequencing data.* Gene, 2019. **699**: p. 145-154.
51. Guo, Y., et al., *MitoSeek: extracting mitochondria information and performing high-throughput mitochondria sequencing analysis.* Bioinformatics, 2013. **29**(9): p. 1210-1.
52. Dimauro, S., *A history of mitochondrial diseases.* J Inherit Metab Dis, 2011. **34**(2): p. 261-76.

53. DiMauro, S. and C. Garone, *Historical perspective on mitochondrial medicine.* Dev Disabil Res Rev, 2010. **16**(2): p. 106-13.
54. Andreu, A.L. and S. DiMauro, *Current classification of mitochondrial disorders.* J Neurol, 2003. **250**(12): p. 1403-6.
55. Chinnery, P.F., *Mitochondrial Disorders Overview*, in *GeneReviews*, E.-i.-c. Roberta A Pagon, Margaret P Adam, Holly H Ardinger, Stephanie E Wallace, Anne Amemiya, Lora JH Bean, Thomas D Bird, Chin-To Fong, Heather C Mefford, Richard JH Smith, and Karen Stephens, Editor. 2000: Seattle (WA); University or Washington, Seattle.
56. Suomalainen, A. and B.J. Battersby, *Mitochondrial diseases: the contribution of organelle stress responses to pathology.* Nat Rev Mol Cell Biol, 2018. **19**(2): p. 77-92.
57. Palmieri, F., P. Scarcia, and M. Monne, *Diseases Caused by Mutations in Mitochondrial Carrier Genes SLC25: A Review.* Biomolecules, 2020. **10**(4).
58. Lake, N.J., et al., *Leigh syndrome: One disorder, more than 75 monogenic causes.* Ann Neurol, 2016. **79**(2): p. 190-203.
59. Chinnery, P.F., *Mitochondrial Disorders Overview.* 2000.
60. Moraes, C.T., et al., *Mitochondrial DNA deletions in progressive external ophthalmoplegia and Kearns-Sayre syndrome.* N Engl J Med, 1989. **320**(20): p. 1293-9.
61. Hirano, M., et al., *MELAS: An original case and clinical criteria for diagnosis.* Neuromuscular Disorders, 1992. **2**(2): p. 125-135.
62. Hammans, S.R., et al., *The mitochondrial DNA transfer RNA(Lys)A-->G(8344) mutation and the syndrome of myoclonic epilepsy with ragged red fibres (MERRF). Relationship of clinical phenotype to proportion of mutant mitochondrial DNA.* Brain, 1993. **116 (Pt 3)**: p. 617-32.
63. Holt IJ, H.A., Petty RK, Morgan-Hughes JA. , *A new mitochondrial disease associated with mitochondrial DNA heteroplasmy.* Am J Hum Genet. , 1990. **46**(3): p. 428-433.
64. Ciafaloni, E., et al., *Maternally inherited Leigh syndrome.* The Journal of Pediatrics, 1993. **122**(3): p. 419-422.
65. Brito, S., et al., *Long-term survival in a child with severe encephalopathy, multiple respiratory chain deficiency and GFM1 mutations.* Front Genet, 2015. **6**: p. 102.
66. Horvath, R., et al., *Molecular basis of infantile reversible cytochrome c oxidase deficiency myopathy.* Brain, 2009. **132**(Pt 11): p. 3165-74.
67. Scaglia, F., et al., *Clinical spectrum, morbidity, and mortality in 113 pediatric patients with mitochondrial disease.* Pediatrics, 2004. **114**(4): p. 925-31.
68. van den Ouweland, J.M., et al., *Mutation in mitochondrial tRNA(Leu)(UUR) gene in a large pedigree with maternally transmitted type II diabetes mellitus and deafness.* Nat Genet, 1992. **1**(5): p. 368-71.
69. DiMauro, S.H., Michio.; NAini, Ali B.; Tanji, Kurenai.; Schon, Eric A.; Nagy, Peter L., *The Diagnosis of Mitochondrial Diseases*, C.U.M. Center, Editor.
70. Munnich, A., et al., *Clinical presentation of mitochondrial disorders in childhood.* J Inherit Metab Dis, 1996. **19**(4): p. 521-7.
71. Boenzi, S. and D. Diodato, *Biomarkers for mitochondrial energy metabolism diseases.* Essays Biochem, 2018. **62**(3): p. 443-454.
72. Rahman, S., et al., *Leigh Syndrome: Clinical Features and Biochemical and DNA Abnormalities.* Annals of Neurology, 1996. **39**(3): p. 343-351.
73. Leigh, D., *Subacute necrotizing encephalomyelopathy in an infant.* Journal of Neurology, Neurosurgery & Psychiatry, 1951. **3**(14): p. 216-221.
74. Baertling, F., et al., *A guide to diagnosis and treatment of Leigh syndrome.* J Neurol Neurosurg Psychiatry, 2014. **85**(3): p. 257-65.
75. Chen, L., et al., *Management of Leigh syndrome: Current status and new insights.* Clin Genet, 2017.
76. Lake, N.J.B., M. J.; Isohanni, P.; Paetau, A., *Leigh Syndrome: Neuropathology and Pathogenesis.* Journal of Neuropathology & Experimental Neurology, 2015. **6**(74): p. 482-492.
77. Steele, H.E., et al., *Monitoring clinical progression with mitochondrial disease biomarkers.* Brain, 2017. **140**(10): p. 2530-2540.
78. Hommes, F.A.P., H. A.; Reerink, J. D., *Leigh's Encephalomyelopathy: an Inborn Error of Gluconeogenesis.* Archives of Disease in Childhood, 1968(230): p. 423-426.

79. Rahman, S., *Gastrointestinal and hepatic manifestations of mitochondrial disorders.* J Inherit Metab Dis, 2013. **36**(4): p. 659-73.
80. Debray, F.G., et al., *Long-term outcome and clinical spectrum of 73 pediatric patients with mitochondrial diseases.* Pediatrics, 2007. **119**(4): p. 722-33.
81. Crave, L.A., C. L.; Taylor, R. W.; Turnbull, D. M., *Recent Advances in Mitochondrial Diseases.* Annual Review of Genomics and Human Genetics, 2017. **18**: p. 257-275.
82. Finsterer, J., *Leigh and Leigh-like syndrome in children and adults.* Pediatr Neurol, 2008. **39**(4): p. 223-35.
83. Lee, N., et al., *A genomewide linkage-disequilibrium scan localizes the Saguenay-Lac-Saint-Jean cytochrome oxidase deficiency to 2p16.* Am J Hum Genet, 2001. **68**(2): p. 397-409.
84. Mootha, V.K., et al., *Identification of a gene causing human cytochrome c oxidase deficiency by integrative genomics.* Proc Natl Acad Sci U S A, 2003. **100**(2): p. 605-10.
85. Merante, F.P.-B., R.; MacKay, N.; Mitchell, G.; Lambert, M.; Morin, C.; De Braekeleer, M.; Laframboise, R.; Gagné, R.; Robinson, B. H., *A Biochemically Distinct Form of Cytochrome Oxidase (COX) Deficiency in the Saguenay-Lac-Saint-Jean Region of Quebec.* Am J Hum Genet, 1993. **2**(53): p. 481-487.
86. Morin, C.M., G.; Larochelle, J.; Lambert, M.; Ogier, H.; Robinson, B. H.; De Braekeleer, M., *Clinical, Metabolic, and Genetic Aspects of Cytochrome C Oxidase Deficiency in Saguenay-Lac-Saint-Jean.* Am J Hum Genet, 1993. **2**(53): p. 488-496.
87. Olahova, M., et al., *LRPPRC mutations cause early-onset multisystem mitochondrial disease outside of the French-Canadian population.* Brain, 2015. **138**(Pt 12): p. 3503-19.
88. Piro, E., et al., *Novel LRPPRC compound heterozygous mutation in a child with early-onset Leigh syndrome French-Canadian type: case report of an Italian patient.* Ital J Pediatr, 2020. **46**(1): p. 140.
89. Han, V.X., et al., *Novel LRPPRC Mutation in a Boy With Mild Leigh Syndrome, French-Canadian Type Outside of Quebec.* Child Neurol Open, 2017. **4**: p. 2329048X17737638.
90. Thompson Legault, J., et al., *A Metabolic Signature of Mitochondrial Dysfunction Revealed through a Monogenic Form of Leigh Syndrome.* Cell Rep, 2015. **13**(5): p. 981-9.
91. Debray, F.G., et al., *LRPPRC mutations cause a phenotypically distinct form of Leigh syndrome with cytochrome c oxidase deficiency.* J Med Genet, 2011. **48**(3): p. 183-9.
92. Morin, C.D., J.; Robinson, B. H.; Lacroix, J.; Michaud, J.; De Braekeleer, M.; Geoffroy, G.; Lortie, A.; Blanchette, C.; Lambert, M. A.; Mitchell, G. A., *Stroke-Like Episodes in Autosomal Recessive Cytochrome Oxidase Deficiency.* Annals of Neurology, 1999. **3**(45): p. 389-392.
93. Burelle, Y., et al., *Mitochondrial vulnerability and increased susceptibility to nutrient-induced cytotoxicity in fibroblasts from leigh syndrome French canadian patients.* PLoS One, 2015. **10**(3): p. e0120767.
94. Ruiz, M., et al., *Lipidomics unveils lipid dyshomeostasis and low circulating plasmalogens as biomarkers in a monogenic mitochondrial disorder.* JCI Insight, 2019. **4**(14).
95. Lee, N.D., M. J.; Delmonte, T.; Lander, E. S.; Xu, F.; Hudson, T. J.; Mitchell, G. A.; Morin, C. C.; Robinson, B. H., *A Genomewide Linkage-Disequilibrium Scan Localizes the Saguenay– Lac-Saint-Jean Cytochrome Oxidase Deficiency to 2p16.* Am J Hum Genet, 2001. **68**(2): p. 397-409.
96. Small, I.D., O. Rackham, and A. Filipovska, *Organelle transcriptomes: products of a deconstructed genome.* Curr Opin Microbiol, 2013. **16**(5): p. 652-8.
97. Schmitz-Linneweber, C. and I. Small, *Pentatricopeptide repeat proteins: a socket set for organelle gene expression.* Trends Plant Sci, 2008. **13**(12): p. 663-70.
98. Delannoy, E., et al., *Pentatricopeptide repeat (PPR) proteins as sequence-specificity factors in post-transcriptional processes in organelles.* Biochem Soc Trans, 2007. **35**(Pt 6): p. 1643-7.
99. Aubourg, S., et al., *In Arabidopsis thaliana, 1% of the genome codes for a novel protein family unique to plants.* Plant Mol Biol, 2000. **42**(4): p. 603-13.
100. Small, I.D. and N. Peeters, *The PPR motif – a TPR-related motif prevalent in plant organellar proteins.* Trends in Biochemical Sciences, 2000. **25**(2): p. 45-47.
101. Ke, J., et al., *Structural basis for RNA recognition by a dimeric PPR-protein complex.* Nat Struct Mol Biol, 2013. **20**(12): p. 1377-82.
102. Yin, P., et al., *Structural basis for the modular recognition of single-stranded RNA by PPR proteins.* Nature, 2013. **504**(7478): p. 168-71.

103. Barkan, A., et al., *A combinatorial amino acid code for RNA recognition by pentatricopeptide repeat proteins.* PLoS Genet, 2012. **8**(8): p. e1002910.
104. Small, I. and H. Puchta, *Emerging tools for synthetic biology in plants.* Plant J, 2014. **78**(5): p. 725-6.
105. Yagi, Y., T. Nakamura, and I. Small, *The potential for manipulating RNA with pentatricopeptide repeat proteins.* Plant J, 2014. **78**(5): p. 772-82.
106. Manna, S., *An overview of pentatricopeptide repeat proteins and their applications.* Biochimie, 2015. **113**: p. 93-9.
107. Sondheimer, N., et al., *Leucine-rich pentatricopeptide-repeat containing protein regulates mitochondrial transcription.* Biochemistry, 2010. **49**(35): p. 7467-73.
108. Cooper, M.P., et al., *Defects in energy homeostasis in Leigh syndrome French Canadian variant through PGC-1alpha/LRP130 complex.* Genes Dev, 2006. **20**(21): p. 2996-3009.
109. Lightowlers, R.N. and Z.M. Chrzanowska-Lightowlers, *Human pentatricopeptide proteins: only a few and what do they do?* RNA Biol, 2013. **10**(9): p. 1433-8.
110. Chujo, T., et al., *LRPPRC/SLIRP suppresses PNPase-mediated mRNA decay and promotes polyadenylation in human mitochondria.* Nucleic Acids Res, 2012. **40**(16): p. 8033-47.
111. Gohil, V.M., et al., *Mitochondrial and nuclear genomic responses to loss of LRPPRC expression.* J Biol Chem, 2010. **285**(18): p. 13742-7.
112. Ruzzenente, B., et al., *LRPPRC is necessary for polyadenylation and coordination of translation of mitochondrial mRNAs.* EMBO J, 2012. **31**(2): p. 443-56.
113. Sasarman, F., et al., *Tissue-specific responses to the LRPPRC founder mutation in French Canadian Leigh Syndrome.* Hum Mol Genet, 2015. **24**(2): p. 480-91.
114. Lagouge, M., et al., *SLIRP Regulates the Rate of Mitochondrial Protein Synthesis and Protects LRPPRC from Degradation.* PLoS Genet, 2015. **11**(8): p. e1005423.
115. Wu, Z., et al., *Mechanisms Controlling Mitochondrial Biogenesis and Respiration through the Thermogenic Coactivator PGC-1.* Cell, 1999. **98**(1): p. 115-124.
116. St-Pierre, J., et al., *Bioenergetic analysis of peroxisome proliferator-activated receptor gamma coactivators 1alpha and 1beta (PGC-1alpha and PGC-1beta) in muscle cells.* J Biol Chem, 2003. **278**(29): p. 26597-603.
117. Scarpulla, R.C., *Transcriptional activators and coactivators in the nuclear control of mitochondrial function in mammalian cells.* Gene, 2002. **286**(1): p. 81-89.
118. Liu, L., et al., *LRP130 protein remodels mitochondria and stimulates fatty acid oxidation.* J Biol Chem, 2011. **286**(48): p. 41253-64.
119. Liu, L., et al., *Nutrient sensing by the mitochondrial transcription machinery dictates oxidative phosphorylation.* J Clin Invest, 2014. **124**(2): p. 768-84.
120. Akie, T.E., et al., *OXPHOS-Mediated Induction of NAD+ Promotes Complete Oxidation of Fatty Acids and Interdicts Non-Alcoholic Fatty Liver Disease.* PLoS One, 2015. **10**(5): p. e0125617.
121. Xu, F.M., C.; Mitchel, G.; Ackerley, C.; Robinson, B. H., *The role of the LRPPRC (leucine-rich pentatricopeptide repeat cassette) gene in cytochrome oxidase assembly: mutation causes lowered levels of COX (cytochrome c oxidase) I and COX III mRNA.* Biochem J, 2004(382): p. 331-336.
122. Sasarman, F.B.-G., C.; Antonicka, H.; Wai, T.; Shoubridge, E. A.; LSFC Consortium., *LRPPRC and SLIRP Interact in a Ribonucleoprotein Complex That Regulates Posttranscriptional Gene Expression in Mitochondria.* Molecular Biology of the Cell, 2010. **21**(8): p. 1315-1323.
123. Sinkler, C.A., et al., *Tissue- and Condition-Specific Isoforms of Mammalian Cytochrome c Oxidase Subunits: From Function to Human Disease.* Oxid Med Cell Longev, 2017. **2017**: p. 1534056.
124. Vijayasarathy, C., et al., *Variations in the subunit content and catalytic activity of the cytochrome c oxidase complex from different tissues and different cardiac compartments.* Biochimica et Biophysica Acta (BBA) - Biomembranes, 1998. **1371**(1): p. 71-82.
125. Xu, F., et al., *LRPPRC mutation suppresses cytochrome oxidase activity by altering mitochondrial RNA transcript stability in a mouse model.* Biochem J, 2012. **441**(1): p. 275-83.
126. Mourier, A., et al., *Loss of LRPPRC causes ATP synthase deficiency.* Hum Mol Genet, 2014. **23**(10): p. 2580-92.

127. Mukaneza, Y., et al., *mTORC1 is required for expression of LRPPRC and cytochrome-c oxidase but not HIF-1alpha in Leigh syndrome French Canadian type patient fibroblasts.* Am J Physiol Cell Physiol, 2019. **317**(1): p. C58-C67.
128. Elstner, M. and D.M. Turnbull, *Transcriptome analysis in mitochondrial disorders.* Brain Res Bull, 2012. **88**(4): p. 285-93.
129. Zhang, Z., et al., *Primary respiratory chain disease causes tissue-specific dysregulation of the global transcriptome and nutrient-sensing signaling network.* PLoS One, 2013. **8**(7): p. e69282.
130. Latorre-Pellicer, A., et al., *Mitochondrial and nuclear DNA matching shapes metabolism and healthy ageing.* Nature, 2016. **535**(7613): p. 561-5.
131. Picard, M., D.C. Wallace, and Y. Burelle, *The rise of mitochondria in medicine.* Mitochondrion, 2016. **30**: p. 105-16.
132. Shadel, G.S. and T.L. Horvath, *Mitochondrial ROS signaling in organismal homeostasis.* Cell, 2015. **163**(3): p. 560-9.
133. Salo, M.K., et al., *Reversible mitochondrial myopathy with cytochrome c oxidase deficiency.* Arch Dis Child, 1992. **67**(8): p. 1033-5.
134. Hathazi, D., et al., *Metabolic shift underlies recovery in reversible infantile respiratory chain deficiency.* EMBO J, 2020. **39**(23): p. e105364.
135. Costa-Mattioli, M. and P. Walter, *The integrated stress response: From mechanism to disease.* Science, 2020. **368**(6489).
136. Mick, E., et al., *Distinct mitochondrial defects trigger the integrated stress response depending on the metabolic state of the cell.* Elife, 2020. **9**.
137. Ignatenko, O., et al., *Mitochondrial spongiotic brain disease: astrocytic stress and harmful rapamycin and ketosis effect.* Life Sci Alliance, 2020. **3**(9).
138. Pakos-Zebrucka, K., et al., *The integrated stress response.* EMBO Rep, 2016. **17**(10): p. 1374-1395.
139. Harding, H.P., Y. Zhang, and D. Ron, *Protein translation and folding are coupled by an endoplasmic-reticulum-resident kinase.* Nature, 1999. **397**(6716): p. 271-4.
140. Marciniak, S.J., et al., *Activation-dependent substrate recruitment by the eukaryotic translation initiation factor 2 kinase PERK.* J Cell Biol, 2006. **172**(2): p. 201-9.
141. Samluk, L., et al., *Cytosolic translational responses differ under conditions of severe short-term and long-term mitochondrial stress.* Mol Biol Cell, 2019. **30**(15): p. 1864-1877.
142. Balsa, E., et al., *ER and Nutrient Stress Promote Assembly of Respiratory Chain Supercomplexes through the PERK-eIF2alpha Axis.* Mol Cell, 2019. **74**(5): p. 877-890 e6.
143. Perez-Perez, R., et al., *COX7A2L Is a Mitochondrial Complex III Binding Protein that Stabilizes the III2+IV Supercomplex without Affecting Respirasome Formation.* Cell Rep, 2016. **16**(9): p. 2387-98.
144. Bota, D.A. and K.J. Davies, *Mitochondrial Lon protease in human disease and aging: Including an etiologic classification of Lon-related diseases and disorders.* Free Radic Biol Med, 2016. **100**: p. 188-198.
145. Vazquez de Aldana, C.R., et al., *Multicopy tRNA genes functionally suppress mutations in yeast eIF-2 alpha kinase GCN2: evidence for separate pathways coupling GCN4 expression to unchanged tRNA.* Mol Cell Biol, 1994. **14**(12): p. 7920-32.
146. Ishimura, R., et al., *Activation of GCN2 kinase by ribosome stalling links translation elongation with translation initiation.* Elife, 2016. **5**.
147. Inglis, A.J., et al., *Activation of GCN2 by the ribosomal P-stalk.* Proc Natl Acad Sci U S A, 2019. **116**(11): p. 4946-4954.
148. Guo, F. and D.R. Cavener, *The GCN2 eIF2alpha kinase regulates fatty-acid homeostasis in the liver during deprivation of an essential amino acid.* Cell Metab, 2007. **5**(2): p. 103-14.
149. Dey, M., et al., *Mechanistic link between PKR dimerization, autophosphorylation, and eIF2alpha substrate recognition.* Cell, 2005. **122**(6): p. 901-13.
150. Gal-Ben-Ari, S., et al., *PKR: A Kinase to Remember.* Front Mol Neurosci, 2018. **11**: p. 480.
151. Patel, C.V., et al., *PACT, a stress-modulated cellular activator of interferon-induced double-stranded RNA-activated protein kinase, PKR.* J Biol Chem, 2000. **275**(48): p. 37993-8.
152. Nakamura, T., et al., *Double-stranded RNA-dependent protein kinase links pathogen sensing with stress and metabolic homeostasis.* Cell, 2010. **140**(3): p. 338-48.

153. Kim, Y., et al., *PKR is activated by cellular dsRNAs during mitosis and acts as a mitotic regulator.* Genes Dev, 2014. **28**(12): p. 1310-22.
154. Rath, E., et al., *Induction of dsRNA-activated protein kinase links mitochondrial unfolded protein response to the pathogenesis of intestinal inflammation.* Gut, 2012. **61**(9): p. 1269-1278.
155. Abdel-Nour, M., et al., *The heme-regulated inhibitor is a cytosolic sensor of protein misfolding that controls innate immune signaling.* Science, 2019. **365**(6448).
156. Zhang, S., et al., *HRI coordinates translation necessary for protein homeostasis and mitochondrial function in erythropoiesis.* Elife, 2019. **8**.
157. Guo, X., et al., *Mitochondrial stress is relayed to the cytosol by an OMA1-DELE1-HRI pathway.* Nature, 2020. **579**(7799): p. 427-432.
158. Vattem, K.M. and R.C. Wek, *Reinitiation involving upstream ORFs regulates ATF4 mRNA translation in mammalian cells.* Proc Natl Acad Sci U S A, 2004. **101**(31): p. 11269-74.
159. Palam, L.R., T.D. Baird, and R.C. Wek, *Phosphorylation of eIF2 facilitates ribosomal bypass of an inhibitory upstream ORF to enhance CHOP translation.* J Biol Chem, 2011. **286**(13): p. 10939-49.
160. Jousse, C., et al., *Inhibition of CHOP translation by a peptide encoded by an open reading frame localized in the chop 5'UTR.* Nucleic Acids Res, 2001. **29**(21): p. 4341-51.
161. Watatani, Y., et al., *Stress-induced translation of ATF5 mRNA is regulated by the 5'-untranslated region.* J Biol Chem, 2008. **283**(5): p. 2543-53.
162. Anderson, N.S. and C.M. Haynes, *Folding the Mitochondrial UPR into the Integrated Stress Response.* Trends Cell Biol, 2020. **30**(6): p. 428-439.
163. Zhao, Q., et al., *A mitochondrial specific stress response in mammalian cells.* EMBO J, 2002. **21**(17): p. 4411-9.
164. Aldridge, J.E., T. Horibe, and N.J. Hoogenraad, *Discovery of genes activated by the mitochondrial unfolded protein response (mtUPR) and cognate promoter elements.* PLoS One, 2007. **2**(9): p. e874.
165. Zurita Rendon, O. and E.A. Shoubridge, *LONP1 Is Required for Maturation of a Subset of Mitochondrial Proteins, and Its Loss Elicits an Integrated Stress Response.* Mol Cell Biol, 2018. **38**(20).
166. Khan, N.A., et al., *mTORC1 Regulates Mitochondrial Integrated Stress Response and Mitochondrial Myopathy Progression.* Cell Metab, 2017. **26**(2): p. 419-428 e5.
167. Durieux, J., S. Wolff, and A. Dillin, *The cell-non-autonomous nature of electron transport chain-mediated longevity.* Cell, 2011. **144**(1): p. 79-91.
168. Haynes, C.M., et al., *The matrix peptide exporter HAF-1 signals a mitochondrial UPR by activating the transcription factor ZC376.7 in C. elegans.* Mol Cell, 2010. **37**(4): p. 529-40.
169. Houtkooper, R.H., et al., *Mitonuclear protein imbalance as a conserved longevity mechanism.* Nature, 2013. **497**(7450): p. 451-7.
170. Nargund, A.M., et al., *Mitochondrial import efficiency of ATFS-1 regulates mitochondrial UPR activation.* Science, 2012. **337**(6094): p. 587-90.
171. Sorrentino, V., et al., *Enhancing mitochondrial proteostasis reduces amyloid-beta proteotoxicity.* Nature, 2017. **552**(7684): p. 187-193.
172. Nargund, A.M., et al., *Mitochondrial and nuclear accumulation of the transcription factor ATFS-1 promotes OXPHOS recovery during the UPR(mt).* Mol Cell, 2015. **58**(1): p. 123-33.
173. Shpilka, T. and C.M. Haynes, *The mitochondrial UPR: mechanisms, physiological functions and implications in ageing.* Nat Rev Mol Cell Biol, 2018. **19**(2): p. 109-120.
174. Harding, H.P., et al., *An Integrated Stress Response Regulates Amino Acid Metabolism and Resistance to Oxidative Stress.* Molecular Cell, 2003. **11**(3): p. 619-633.
175. Teske, B.F., et al., *CHOP induces activating transcription factor 5 (ATF5) to trigger apoptosis in response to perturbations in protein homeostasis.* Mol Biol Cell, 2013. **24**(15): p. 2477-90.
176. Dey, S., et al., *Both transcriptional regulation and translational control of ATF4 are central to the integrated stress response.* J Biol Chem, 2010. **285**(43): p. 33165-33174.
177. Quiros, P.M., et al., *Multi-omics analysis identifies ATF4 as a key regulator of the mitochondrial stress response in mammals.* J Cell Biol, 2017. **216**(7): p. 2027-2045.
178. Bao, X.R., et al., *Mitochondrial dysfunction remodels one-carbon metabolism in human cells.* Elife, 2016. **5**.

179. Celardo, I., et al., *dATF4 regulation of mitochondrial folate-mediated one-carbon metabolism is neuroprotective.* Cell Death Differ, 2017. **24**(4): p. 638-648.
180. Fiorese, C.J. and C.M. Haynes, *Integrating the UPR(mt) into the mitochondrial maintenance network.* Crit Rev Biochem Mol Biol, 2017. **52**(3): p. 304-313.
181. Suomalainen, A., et al., *FGF-21 as a biomarker for muscle-manifesting mitochondrial respiratory chain deficiencies: a diagnostic study.* The Lancet Neurology, 2011. **10**(9): p. 806-818.
182. Dogan, S.A., et al., *Tissue-specific loss of DARS2 activates stress responses independently of respiratory chain deficiency in the heart.* Cell Metab, 2014. **19**(3): p. 458-69.
183. Straub, I.R., W. Weraarpachai, and E.A. Shoubridge, *Multi-OMICS study of a CHCHD10 variant causing ALS demonstrates metabolic rewiring and activation of endoplasmic reticulum and mitochondrial unfolded protein responses.* Hum Mol Genet, 2021. **30**(8): p. 687-705.
184. Jornayvaz, F.R. and G.I. Shulman, *Regulation of mitochondrial biogenesis.* Essays Biochem, 2010. **47**: p. 69-84.
185. Puigserver, P., et al., *A Cold-Inducible Coactivator of Nuclear Receptors Linked to Adaptive Thermogenesis.* Cell, 1998. **92**(6): p. 829-839.
186. Virbasius, J.V. and R.C. Scarpulla, *Activation of the human mitochondrial transcription factor A gene by nuclear respiratory factors: a potential regulatory link between nuclear and mitochondrial gene expression in organelle biogenesis.* Proc Natl Acad Sci U S A, 1994. **91**(4): p. 1309-13.
187. Meirhaeghe, A., et al., *Characterization of the human, mouse and rat PGC1 beta (peroxisome-proliferator-activated receptor-gamma co-activator 1 beta) gene in vitro and in vivo.* Biochem J, 2003. **373**(Pt 1): p. 155-65.
188. Morrow, R.M., et al., *Mitochondrial energy deficiency leads to hyperproliferation of skeletal muscle mitochondria and enhanced insulin sensitivity.* Proc Natl Acad Sci U S A, 2017. **114**(10): p. 2705-2710.
189. Heddi, A., et al., *Coordinate induction of energy gene expression in tissues of mitochondrial disease patients.* J Biol Chem, 1999. **274**(33): p. 22968-76.
190. Chabi, B., et al., *How is mitochondrial biogenesis affected in mitochondrial disease?* Med Sci Sports Exerc, 2005. **37**(12): p. 2102-10.
191. Einer, C., et al., *A High-Calorie Diet Aggravates Mitochondrial Dysfunction and Triggers Severe Liver Damage in Wilson Disease Rats.* Cell Mol Gastroenterol Hepatol, 2019. **7**(3): p. 571-596.
192. Reginald H. Garret, C.M.G., *Biochemistry*. 4 ed. 2010: Mary Finch.
193. Warburg, O., *On the origin of cancer cells.* Science, 1956. **123**(3191): p. 309-14.
194. Gillies, R.J., I. Robey, and R.A. Gatenby, *Causes and consequences of increased glucose metabolism of cancers.* J Nucl Med, 2008. **49 Suppl 2**: p. 24S-42S.
195. Saxton, R.A. and D.M. Sabatini, *mTOR Signaling in Growth, Metabolism, and Disease.* Cell, 2017. **168**(6): p. 960-976.
196. Duvel, K., et al., *Activation of a metabolic gene regulatory network downstream of mTOR complex 1.* Mol Cell, 2010. **39**(2): p. 171-83.
197. Altomare, D.A. and A.R. Khaled, *Homeostasis and the importance for a balance between AKT/mTOR activity and intracellular signaling.* Curr Med Chem, 2012. **19**(22): p. 3748-62.
198. Sage-Schwaede, A., et al., *Exploring mTOR inhibition as treatment for mitochondrial disease.* Ann Clin Transl Neurol, 2019. **6**(9): p. 1877-1881.
199. Schägger, H. and K. Pfeiffer, *Supercomplexes in the respiratory chains of yeast and mammalian mitochondria.* The EMBO journal, 2000. **19**(8): p. 1777-1783.
200. Acin-Perez, R., et al., *Respiratory active mitochondrial supercomplexes.* Mol Cell, 2008. **32**(4): p. 529-39.
201. Acin-Perez, R. and J.A. Enriquez, *The function of the respiratory supercomplexes: the plasticity model.* Biochim Biophys Acta, 2014. **1837**(4): p. 444-50.
202. Lapuente-Brun, E., et al., *Supercomplex Assembly Determines Electron Flux in the Mitochondrial Electron Transport Chain.* Science, 2013. **340**(6140): p. 1567-1570.
203. Lazarou, M., et al., *Assembly of nuclear DNA-encoded subunits into mitochondrial complex IV, and their preferential integration into supercomplex forms in patient mitochondria.* FEBS J, 2009. **276**(22): p. 6701-13.

204. Greggio, C., et al., *Enhanced Respiratory Chain Supercomplex Formation in Response to Exercise in Human Skeletal Muscle.* Cell Metab, 2017. **25**(2): p. 301-311.
205. D'Aurelio, M., et al., *Respiratory chain supercomplexes set the threshold for respiration defects in human mtDNA mutant cybrids.* Hum Mol Genet, 2006. **15**(13): p. 2157-69.
206. Milenkovic, D., et al., *The Enigma of the Respiratory Chain Supercomplex.* Cell Metab, 2017. **25**(4): p. 765-776.
207. Salway, J.G., *Metabolism at a Glance*. 2004: Balckwell Publishing.
208. Wittig, I. and H. Schägger, *Advantages and limitations of clear-native PAGE.* PROTEOMICS, 2005. **5**(17): p. 4338-4346.
209. Wittig, I., H.P. Braun, and H. Schagger, *Blue native PAGE.* Nat Protoc, 2006. **1**(1): p. 418-28.
210. Schagger, H. and K. Pfeiffer, *The ratio of oxidative phosphorylation complexes I-V in bovine heart mitochondria and the composition of respiratory chain supercomplexes.* J Biol Chem, 2001. **276**(41): p. 37861-7.
211. Stroud, D.A., et al., *Accessory subunits are integral for assembly and function of human mitochondrial complex I.* Nature, 2016. **538**(7623): p. 123-126.
212. Letts, J.A., K. Fiedorczuk, and L.A. Sazanov, *The architecture of respiratory supercomplexes.* Nature, 2016. **537**(7622): p. 644-648.
213. Wu, M., et al., *Structure of Mammalian Respiratory Supercomplex I1III2IV1.* Cell, 2016. **167**(6): p. 1598-1609 e10.
214. Blaza, J.N., et al., *Kinetic evidence against partitioning of the ubiquinone pool and the catalytic relevance of respiratory-chain supercomplexes.* Proc Natl Acad Sci U S A, 2014. **111**(44): p. 15735-40.
215. Maranzana, E., et al., *Mitochondrial respiratory supercomplex association limits production of reactive oxygen species from complex I.* Antioxid Redox Signal, 2013. **19**(13): p. 1469-80.
216. Lopez-Fabuel, I., et al., *Complex I assembly into supercomplexes determines differential mitochondrial ROS production in neurons and astrocytes.* Proc Natl Acad Sci U S A, 2016. **113**(46): p. 13063-13068.
217. Acín-Pérez, R., et al., *Respiratory Complex III Is Required to Maintain Complex I in Mammalian Mitochondria.* Molecular Cell, 2004. **13**(6): p. 805-815.
218. Diaz, F., et al., *Cytochrome c oxidase is required for the assembly/stability of respiratory complex I in mouse fibroblasts.* Mol Cell Biol, 2006. **26**(13): p. 4872-81.
219. Schagger, H., et al., *Significance of respirasomes for the assembly/stability of human respiratory chain complex I.* J Biol Chem, 2004. **279**(35): p. 36349-53.
220. Calvaruso, M.A., et al., *Mitochondrial complex III stabilizes complex I in the absence of NDUFS4 to provide partial activity.* Hum Mol Genet, 2012. **21**(1): p. 115-20.
221. Chatfield, K.C., et al., *Elamipretide Improves Mitochondrial Function in the Failing Human Heart.* JACC Basic Transl Sci, 2019. **4**(2): p. 147-157.
222. Khacho, M., et al., *Acidosis overrides oxygen deprivation to maintain mitochondrial function and cell survival.* Nat Commun, 2014. **5**: p. 3550.
223. Chen, Y.C., et al., *Identification of a protein mediating respiratory supercomplex stability.* Cell Metab, 2012. **15**(3): p. 348-60.
224. Strogolova, V., et al., *Rcf1 and Rcf2, members of the hypoxia-induced gene 1 protein family, are critical components of the mitochondrial cytochrome bc1-cytochrome c oxidase supercomplex.* Mol Cell Biol, 2012. **32**(8): p. 1363-73.
225. Vukotic, M., et al., *Rcf1 mediates cytochrome oxidase assembly and respirasome formation, revealing heterogeneity of the enzyme complex.* Cell Metab, 2012. **15**(3): p. 336-47.
226. Rydstrom Lundin, C., et al., *Regulatory role of the respiratory supercomplex factors in Saccharomyces cerevisiae.* Proc Natl Acad Sci U S A, 2016. **113**(31): p. E4476-85.
227. Timon-Gomez, A., et al., *Distinct Roles of Mitochondrial HIGD1A and HIGD2A in Respiratory Complex and Supercomplex Biogenesis.* Cell Rep, 2020. **31**(5): p. 107607.
228. Hock, D.H., et al., *HIGD2A is Required for Assembly of the COX3 Module of Human Mitochondrial Complex IV.* Mol Cell Proteomics, 2020. **19**(7): p. 1145-1160.
229. Ikeda, K., et al., *A stabilizing factor for mitochondrial respiratory supercomplex assembly regulates energy metabolism in muscle.* Nat Commun, 2013. **4**: p. 2147.

230. Mourier, A., et al., *The respiratory chain supercomplex organization is independent of COX7a2l isoforms.* Cell Metab, 2014. **20**(6): p. 1069-75.
231. Cogliati, S., et al., *Mechanism of super-assembly of respiratory complexes III and IV.* Nature, 2016. **539**(7630): p. 579-582.
232. Calvo, E., et al., *Functional role of respiratory supercomplexes in mice: SCAF1 relevance and segmentation of the Qpool.* Sci Adv, 2020. **6**(26): p. eaba7509.
233. Claypool, S.M., et al., *Cardiolipin defines the interactome of the major ADP/ATP carrier protein of the mitochondrial inner membrane.* J Cell Biol, 2008. **182**(5): p. 937-50.
234. Pfeiffer, K., et al., *Cardiolipin stabilizes respiratory chain supercomplexes.* J Biol Chem, 2003. **278**(52): p. 52873-80.
235. Arnarez, C., S.J. Marrink, and X. Periole, *Molecular mechanism of cardiolipin-mediated assembly of respiratory chain supercomplexes.* Chem Sci, 2016. **7**(7): p. 4435-4443.
236. Bazan, S., et al., *Cardiolipin-dependent reconstitution of respiratory supercomplexes from purified Saccharomyces cerevisiae complexes III and IV.* J Biol Chem, 2013. **288**(1): p. 401-11.
237. Zhang, M., E. Mileykovskaya, and W. Dowhan, *Gluing the respiratory chain together. Cardiolipin is required for supercomplex formation in the inner mitochondrial membrane.* J Biol Chem, 2002. **277**(46): p. 43553-6.
238. Bottinger, L., et al., *Phosphatidylethanolamine and cardiolipin differentially affect the stability of mitochondrial respiratory chain supercomplexes.* J Mol Biol, 2012. **423**(5): p. 677-86.
239. Baker, C.D., et al., *Specific requirements of nonbilayer phospholipids in mitochondrial respiratory chain function and formation.* Mol Biol Cell, 2016. **27**(14): p. 2161-71.
240. Hirano, M., V. Emmanuele, and C.M. Quinzii, *Emerging therapies for mitochondrial diseases.* Essays Biochem, 2018. **62**(3): p. 467-481.
241. Pfeffer, G., et al., *Treatment for mitochondrial disorders.* Cochrane Database Syst Rev, 2012(4): p. CD004426.
242. Karaa, A., et al., *Mitochondrial disease patients' perception of dietary supplements' use.* Mol Genet Metab, 2016. **119**(1-2): p. 100-8.
243. Blanchet, L., et al., *Quantifying small molecule phenotypic effects using mitochondrial morpho-functional fingerprinting and machine learning.* Sci Rep, 2015. **5**: p. 8035.
244. Blankenberg, F.G., et al., *Brain uptake of Tc99m-HMPAO correlates with clinical response to the novel redox modulating agent EPI-743 in patients with mitochondrial disease.* Mol Genet Metab, 2012. **107**(4): p. 690-9.
245. Martinelli, D., et al., *EPI-743 reverses the progression of the pediatric mitochondrial disease--genetically defined Leigh Syndrome.* Mol Genet Metab, 2012. **107**(3): p. 383-8.
246. Johnson, S.C., et al., *mTOR inhibition alleviates mitochondrial disease in a mouse model of Leigh syndrome.* Science, 2013. **342**(6165): p. 1524-8.
247. Siegmund, S.E., et al., *Low-dose rapamycin extends lifespan in a mouse model of mtDNA depletion syndrome.* Hum Mol Genet, 2017. **26**(23): p. 4588-4605.
248. Huang, Q., et al., *Delivering genes across the blood-brain barrier: LY6A, a novel cellular receptor for AAV-PHP.B capsids.* PLoS One, 2019. **14**(11): p. e0225206.
249. Reynaud-Dulaurier, R., et al., *Gene replacement therapy provides benefit in an adult mouse model of Leigh syndrome.* Brain, 2020. **143**(6): p. 1686-1696.
250. Jain, I.H.Z., L.; Goli, R.; Alexa, K.; Schatzman-Bone, S.; Dhillon, H.; Goldberger, O.; Peng, J.; Shalem, O.; Sanjana, N. E.; Zhang, F.; Goessling, W.; Zapol, W. M.; Mootha, V. K., *Hypoxia as a therapy for mitochondrial disease.* Science, 2016. **352**(6281): p. 54-61.
251. Ferrari, M., et al., *Hypoxia treatment reverses neurodegenerative disease in a mouse model of Leigh syndrome.* Proc Natl Acad Sci U S A, 2017. **114**(21): p. E4241-E4250.
252. Jain, I.H., et al., *Leigh Syndrome Mouse Model Can Be Rescued by Interventions that Normalize Brain Hyperoxia, but Not HIF Activation.* Cell Metab, 2019. **30**(4): p. 824-832 e3.
253. Watanabe, Y., A. Tsuchiya, and S. Terai, *The development of mesenchymal stem cell therapy in the present, and the perspective of cell-free therapy in the future.* Clin Mol Hepatol, 2021. **27**(1): p. 70-80.
254. Du, W.J., et al., *Heterogeneity of proangiogenic features in mesenchymal stem cells derived from bone marrow, adipose tissue, umbilical cord, and placenta.* Stem Cell Res Ther, 2016. **7**(1): p. 163.

255. Pittenger, M.F., et al., *Mesenchymal stem cell perspective: cell biology to clinical progress.* NPJ Regen Med, 2019. **4**: p. 22.
256. Zhuang, W.Z., et al., *Mesenchymal stem/stromal cell-based therapy: mechanism, systemic safety and biodistribution for precision clinical applications.* J Biomed Sci, 2021. **28**(1): p. 28.
257. Lou, S., et al., *Mesenchymal stem cells: Biological characteristics and application in disease therapy.* Biochimie, 2021. **185**: p. 9-21.
258. Dominici, M., et al., *Minimal criteria for defining multipotent mesenchymal stromal cells. The International Society for Cellular Therapy position statement.* Cytotherapy, 2006. **8**(4): p. 315-7.
259. Caplan, A.I. and D. Correa, *The MSC: an injury drugstore.* Cell Stem Cell, 2011. **9**(1): p. 11-5.
260. Spees, J.L., R.H. Lee, and C.A. Gregory, *Mechanisms of mesenchymal stem/stromal cell function.* Stem Cell Res Ther, 2016. **7**(1): p. 125.
261. Iso, Y., et al., *Multipotent human stromal cells improve cardiac function after myocardial infarction in mice without long-term engraftment.* Biochem Biophys Res Commun, 2007. **354**(3): p. 700-6.
262. Hofstetter, C.P., et al., *Marrow stromal cells form guiding strands in the injured spinal cord and promote recovery.* Proc Natl Acad Sci U S A, 2002. **99**(4): p. 2199-204.
263. Lee, R.H., et al., *The CD34-like protein PODXL and alpha6-integrin (CD49f) identify early progenitor MSCs with increased clonogenicity and migration to infarcted heart in mice.* Blood, 2009. **113**(4): p. 816-26.
264. Lee, R.H., et al., *Intravenous hMSCs improve myocardial infarction in mice because cells embolized in lung are activated to secrete the anti-inflammatory protein TSG-6.* Cell Stem Cell, 2009. **5**(1): p. 54-63.
265. Garcia-Bernal, D., et al., *The Current Status of Mesenchymal Stromal Cells: Controversies, Unresolved Issues and Some Promising Solutions to Improve Their Therapeutic Efficacy.* Front Cell Dev Biol, 2021. **9**: p. 650664.
266. Xu, X., et al., *Effects of mesenchymal stem cell transplantation on extracellular matrix after myocardial infarction in rats.* Coron Artery Dis, 2005. **16**(4): p. 245-55.
267. Tanimoto, H., et al., *Improvement of liver fibrosis by infusion of cultured cells derived from human bone marrow.* Cell Tissue Res, 2013. **354**(3): p. 717-28.
268. Lee, M.J., et al., *Anti-fibrotic effect of chorionic plate-derived mesenchymal stem cells isolated from human placenta in a rat model of CCl(4)-injured liver: potential application to the treatment of hepatic diseases.* J Cell Biochem, 2010. **111**(6): p. 1453-63.
269. Melcher, M., et al., *Modulation of oxidative phosphorylation and redox homeostasis in mitochondrial NDUFS4 deficiency via mesenchymal stem cells.* Stem Cell Res Ther, 2017. **8**(1): p. 150.
270. Figeac, F., Lesault, P. F., Le Coz, O., Damy, T., Souktani, R., Trébeau, C., Schmitt, A., Ribot, J., Mounier, R., Guguin, A., Manier, C., Surenaud, M., Hittinger, L., Dubois-Randé, J. L., & Rodriguez, A. M., *Nanotubular crosstalk with distressed cardiomyocytes stimulates the paracrine repair function of mesenchymal stem cells.* Stem Cells, 2014. **32**(1): p. 216-230.
271. Plotnikov, E.Y., et al., *Cell-to-cell cross-talk between mesenchymal stem cells and cardiomyocytes in co-culture.* J Cell Mol Med, 2008. **12**(5A): p. 1622-31.
272. Islam, M.N., et al., *Mitochondrial transfer from bone-marrow-derived stromal cells to pulmonary alveoli protects against acute lung injury.* Nat Med, 2012. **18**(5): p. 759-65.
273. Sanchez, V., Villalba, N., Fiore, L., Luzzani, C., Miriuka, S., Boveris, A., Gelpi, R. J., Brusco, A., & Poderoso, J. J. , *Characterization of Tunneling Nanotubes in Wharton's jelly Mesenchymal Stem Cells. An Intercellular Exchange of Components between Neighboring Cells.* Stem Cell reviews and reports, 2017. **13**(4): p. 491-498.
274. Jeffrey L. Spees, S.D.O., Mandolin J. Whitney, Darwin J. Prockop, *Mitochondrial transfer between cells can rescue aerobic respiration.* Proceedings of the National Academy of Sciences, 2006. **103**(5): p. 1283-1288.
275. Cho, Y.M., et al., *Mesenchymal stem cells transfer mitochondria to the cells with virtually no mitochondrial function but not with pathogenic mtDNA mutations.* PLoS One, 2012. **7**(3): p. e32778.
276. Keshtkar, S., N. Azarpira, and M.H. Ghahremani, *Mesenchymal stem cell-derived extracellular vesicles: novel frontiers in regenerative medicine.* Stem Cell Research & Therapy, 2018. **9**(1).

277. Phinney, D.G., et al., *Mesenchymal stem cells use extracellular vesicles to outsource mitophagy and shuttle microRNAs.* Nat Commun, 2015. **6**: p. 8472.
278. Tieu, A., et al., *An Analysis of Mesenchymal Stem Cell-Derived Extracellular Vesicles for Preclinical Use.* ACS Nano, 2020. **14**(8): p. 9728-9743.
279. Mulcahy, L.A., R.C. Pink, and D.R. Carter, *Routes and mechanisms of extracellular vesicle uptake.* J Extracell Vesicles, 2014. **3**.
280. Haraszti, R.A., et al., *High-resolution proteomic and lipidomic analysis of exosomes and microvesicles from different cell sources.* J Extracell Vesicles, 2016. **5**: p. 32570.
281. Jiang, D., et al., *Mitochondrial transfer of mesenchymal stem cells effectively protects corneal epithelial cells from mitochondrial damage.* Cell Death Dis, 2016. **7**(11): p. e2467.
282. Ahmad, T., et al., *Miro1 regulates intercellular mitochondrial transport & enhances mesenchymal stem cell rescue efficacy.* EMBO J, 2014. **33**(9): p. 994-1010.
283. Babenko, V.A., et al., *Miro1 Enhances Mitochondria Transfer from Multipotent Mesenchymal Stem Cells (MMSC) to Neural Cells and Improves the Efficacy of Cell Recovery.* Molecules, 2018. **23**(3).
284. Li, C.J., et al., *Enhancement of Mitochondrial Transfer by Antioxidants in Human Mesenchymal Stem Cells.* Oxid Med Cell Longev, 2017. **2017**: p. 8510805.
285. Liu, D., et al., *Intercellular mitochondrial transfer as a means of tissue revitalization.* Signal Transduct Target Ther, 2021. **6**(1): p. 65.
286. Timmers, L., et al., *Reduction of myocardial infarct size by human mesenchymal stem cell conditioned medium.* Stem Cell Res, 2007. **1**(2): p. 129-37.
287. Ghittoni, R., et al., *Simvastatin inhibits T-cell activation by selectively impairing the function of Ras superfamily GTPases.* FASEB J, 2005. **19**(6): p. 605-7.
288. Aslam, M., et al., *Bone marrow stromal cells attenuate lung injury in a murine model of neonatal chronic lung disease.* Am J Respir Crit Care Med, 2009. **180**(11): p. 1122-30.
289. Li, Q., et al., *In vivo tracking and comparison of the therapeutic effects of MSCs and HSCs for liver injury.* PLoS One, 2013. **8**(4): p. e62363.
290. Liang, X., et al., *Paracrine mechanisms of mesenchymal stem cell-based therapy: current status and perspectives.* Cell Transplant, 2014. **23**(9): p. 1045-59.
291. Batsali, A.K., et al., *The Role of Bone Marrow Mesenchymal Stem Cell Derived Extracellular Vesicles (MSC-EVs) in Normal and Abnormal Hematopoiesis and Their Therapeutic Potential.* J Clin Med, 2020. **9**(3).
292. Bang, O.Y. and E.H. Kim, *Mesenchymal Stem Cell-Derived Extracellular Vesicle Therapy for Stroke: Challenges and Progress.* Front Neurol, 2019. **10**: p. 211.
293. Pasquale Sansone, C.S., Ivana Kurelac, Qing Chang, Laura Benedetta Amato, Antonio Strillacci, Anna Stepanova, Luisa Iommarini, Chiara Mastroleo, Laura Daly, Alexander Galkin, Basant Kumar Thakur, Nadine Soplop, Kunihiro Uryu, Ayuko Hoshino, Larry Norton, Massimiliano Bonafé, Monica Cricca, Giuseppe Gasparre, David Lyden, Jacqueline Bromberg, *Packaging and transfer of mitochondrial DNA via exosomes regulate escape from dormancy in hormonal therapy-resistant breast cancer.* Proc Natl Acad Sci U S A, 2017. **114**(47): p. E10255.
294. Hogan, S.E., et al., *Mesenchymal stromal cell-derived exosomes improve mitochondrial health in pulmonary arterial hypertension.* Am J Physiol Lung Cell Mol Physiol, 2019. **316**(5): p. L723-L737.
295. Debray, F.G.L., M.; Mitchell, G. A., *Disorders of mitochondrial function.* current opinion in pediatry, 2008. **4**(20): p. 471-482.
296. DiMauro, S. and E.A. Schon, *Mitochondrial disorders in the nervous system.* Annu Rev Neurosci, 2008. **31**: p. 91-123.
297. Zhiqing Zhu, J.Y., Timothy Johns, Katherine Fu, Isabelle De Bie, Carol Macmillan, Andrew P. Cuthbert, Robert F. Newbold, Jia-chi Wang, Mario Chevrette, Garry K. Brown, Ruth M. Brown & Eric A. Shoubridge, *SURF1, encoding a factor involved in the biogenesis of cytochrome c oxidase, is mutated in Leigh syndrome.* Nature Genetics, 1998. **20**(337-343).
298. Diaz, F., et al., *Pathophysiology and fate of hepatocytes in a mouse model of mitochondrial hepatopathies.* Gut, 2008. **57**(2): p. 232-42.

299. Bernardi, P., et al., *From ATP to PTP and Back: A Dual Function for the Mitochondrial ATP Synthase.* Circ Res, 2015. **116**(11): p. 1850-62.
300. Giorgio, V., et al., *Dimers of mitochondrial ATP synthase form the permeability transition pore.* Proceedings of the National Academy of Sciences, 2013. **110**(15): p. 5887.
301. Eliseev, R.A., et al., *Role of cyclophilin D in the resistance of brain mitochondria to the permeability transition.* Neurobiol Aging, 2007. **28**(10): p. 1532-42.
302. Li, B., et al., *Inhibition of complex I regulates the mitochondrial permeability transition through a phosphate-sensitive inhibitory site masked by cyclophilin D.* Biochim Biophys Acta, 2012. **1817**(9): p. 1628-34.
303. Daussin, F.N., et al., *Cyclophilin-D is dispensable for atrophy and mitochondrial apoptotic signalling in denervated muscle.* J Physiol, 2011. **589**(Pt 4): p. 855-61.
304. Distelmaier, F., et al., *The antioxidant Trolox restores mitochondrial membrane potential and Ca2+ -stimulated ATP production in human complex I deficiency.* J Mol Med (Berl), 2009. **87**(5): p. 515-22.
305. Verkaart, S., et al., *Superoxide production is inversely related to complex I activity in inherited complex I deficiency.* Biochim Biophys Acta, 2007. **1772**(3): p. 373-81.
306. Starkov, A.A. and G. Fiskum, *Regulation of brain mitochondrial H2O2 production by membrane potential and NAD(P)H redox state.* J Neurochem, 2003. **86**(5): p. 1101-7.
307. Sergey S. Korshunov, V.P.S., Anatoly A. Starkov, *High protonic potential actuates a mechanism of production of reactive oxygen species in mitochondria.* FEBS Letters, 1997. **416**: p. 15-18.
308. Ikaga, R., et al., *Knockdown of aquaporin-8 induces mitochondrial dysfunction in 3T3-L1 cells.* Biochem Biophys Rep, 2015. **4**: p. 187-195.
309. Marchissio, M.J., et al., *Mitochondrial aquaporin-8 knockdown in human hepatoma HepG2 cells causes ROS-induced mitochondrial depolarization and loss of viability.* Toxicol Appl Pharmacol, 2012. **264**(2): p. 246-54.
310. Pecina, P., et al., *Functional alteration of cytochrome c oxidase by SURF1 mutations in Leigh syndrome.* Biochimica et Biophysica Acta (BBA) - Molecular Basis of Disease, 2003. **1639**(1): p. 53-63.
311. Shinzawa-Itoh, K., et al., *Structures and physiological roles of 13 integral lipids of bovine heart cytochrome c oxidase.* EMBO J, 2007. **26**(6): p. 1713-25.
312. Tracey D. SPURWAY, H.S.A.S., Christopher I. POGSON and Loranne AGIUS, *The flux control coefficient of carnitine palmitoyltransferase I on palmitate β-oxidation in rat hepatocyte cultures.* Biochem J, 1997. **323**: p. 119-122.
313. Fritzen, A.J., N. Grunnet, and B. Quistorff, *Flux control analysis of mitochondrial oxidative phosphorylation in rat skeletal muscle: pyruvate and palmitoyl-carnitine as substrates give different control patterns.* Eur J Appl Physiol, 2007. **101**(6): p. 679-89.
314. Lei, S., et al., *Increased Hepatic Fatty Acids Uptake and Oxidation by LRPPRC-Driven Oxidative Phosphorylation Reduces Blood Lipid Levels.* Front Physiol, 2016. **7**: p. 270.
315. Kwong, J.Q. and J.D. Molkentin, *Physiological and pathological roles of the mitochondrial permeability transition pore in the heart.* Cell Metab, 2015. **21**(2): p. 206-214.
316. Kuei WOODFIELD, A.R., Dieter BRDICZKA and Andrew P. HALESTRAP, *Direct demonstration of a specific interaction between cyclophilin-D and the adenine nucleotide translocase confirms their role in the mitochondrial permeability transition.* Biochem J, 1998. **336**: p. 287-290.
317. Ildiko Szabo, M.Z., *The mitochondrial permeability transition pore may comprise VDAC molecules.* FEBS J, 1993. **330**(2): p. 201-205.
318. Leung, A.W., P. Varanyuwatana, and A.P. Halestrap, *The mitochondrial phosphate carrier interacts with cyclophilin D and may play a key role in the permeability transition.* J Biol Chem, 2008. **283**(39): p. 26312-23.
319. Carraro, M., et al., *Channel formation by yeast F-ATP synthase and the role of dimerization in the mitochondrial permeability transition.* J Biol Chem, 2014. **289**(23): p. 15980-5.
320. Alavian, K.N., et al., *An uncoupling channel within the c-subunit ring of the F1FO ATP synthase is the mitochondrial permeability transition pore.* Proc Natl Acad Sci U S A, 2014. **111**(29): p. 10580-5.

321. Solesio, M.E., et al., *Inorganic polyphosphate (polyP) as an activator and structural component of the mitochondrial permeability transition pore.* Biochem Soc Trans, 2016. **44**(1): p. 7-12.
322. Bernardi, P., *The mitochondrial permeability transition pore: a mystery solved?* Front Physiol, 2013. **4**: p. 95.
323. Christelle Spannagel, J.V., Genevi+ve Arselin, Pierre-Vincent Graves, Xavier Grandier-Vazeille, Jean Velours, *Evidence of a subunit 4 (subunit b) dimer in favor of the proximity of ATP synthase complexes in yeast inner mitochondrial membrane.* biochimica et Biophysica Acta (BBA), 1998. **1414**: p. 260-264.
324. Everard-Gigot, V., et al., *Functional analysis of subunit e of the F1Fo-ATP synthase of the yeast Saccharomyces cerevisiae: importance of the N-terminal membrane anchor region.* Eukaryot Cell, 2005. **4**(2): p. 346-55.
325. Bisetto, E., et al., *Functional and stoichiometric analysis of subunit e in bovine heart mitochondrial F(0)F(1)ATP synthase.* J Bioenerg Biomembr, 2008. **40**(4): p. 257-67.
326. Bustos, D.M. and J. Velours, *The modification of the conserved GXXXG motif of the membrane-spanning segment of subunit g destabilizes the supramolecular species of yeast ATP synthase.* J Biol Chem, 2005. **280**(32): p. 29004-10.
327. Davies, K.M., et al., *Structure of the yeast F1Fo-ATP synthase dimer and its role in shaping the mitochondrial cristae.* Proc Natl Acad Sci U S A, 2012. **109**(34): p. 13602-7.
328. Davies, K.M., et al., *Macromolecular organization of ATP synthase and complex I in whole mitochondria.* Proc Natl Acad Sci U S A, 2011. **108**(34): p. 14121-6.
329. Strauss, M., et al., *Dimer ribbons of ATP synthase shape the inner mitochondrial membrane.* The EMBO journal, 2008. **27**(7): p. 1154-1160.
330. He, J., et al., *Persistence of the mitochondrial permeability transition in the absence of subunit c of human ATP synthase.* Proc Natl Acad Sci U S A, 2017. **114**(13): p. 3409-3414.
331. Wittig, I., et al., *Assembly and oligomerization of human ATP synthase lacking mitochondrial subunits a and A6L.* Biochim Biophys Acta, 2010. **1797**(6-7): p. 1004-11.
332. Giorgio, V., et al., *Cyclophilin D modulates mitochondrial F0F1-ATP synthase by interacting with the lateral stalk of the complex.* J Biol Chem, 2009. **284**(49): p. 33982-8.
333. Lee, C.F., et al., *Normalization of NAD+ Redox Balance as a Therapy for Heart Failure.* Circulation, 2016. **134**(12): p. 883-94.
334. Bigay, J. and B. Antonny, *Curvature, lipid packing, and electrostatics of membrane organelles: defining cellular territories in determining specificity.* Dev Cell, 2012. **23**(5): p. 886-95.
335. Sousa-Lopes, A., et al., *Decreased cellular permeability to H2O2 protects Saccharomyces cerevisiae cells in stationary phase against oxidative stress.* FEBS Lett, 2004. **578**(1-2): p. 152-6.
336. Folmer, V., et al., *H2O2 induces rapid biophysical and permeability changes in the plasma membrane of Saccharomyces cerevisiae.* Biochim Biophys Acta, 2008. **1778**(4): p. 1141-7.
337. Branco, M.R., et al., *Decrease of H2O2 plasma membrane permeability during adaptation to H2O2 in Saccharomyces cerevisiae.* J Biol Chem, 2004. **279**(8): p. 6501-6.
338. Dominique Dumas, S.M., Frederique Gouin, Francis Baros, Marie-Laure Viriot, and Jean-Francois Stoltz, *Membrane Fluidity and Oxygen Diffusion in Cholesterol- Enriched Erythrocyte Membrane.* Archives of Biochemistry and Biophysics, 1997. **341**(1): p. 34-39.
339. Strott, C.A. and Y. Higashi, *Cholesterol sulfate in human physiology: what's it all about?* J Lipid Res, 2003. **44**(7): p. 1268-78.
340. Picard, M., et al., *Mechanical ventilation triggers abnormal mitochondrial dynamics and morphology in the diaphragm.* J Appl Physiol (1985), 2015. **118**(9): p. 1161-71.
341. Cadete, V.J., et al., *Formation of mitochondrial-derived vesicles is an active and physiologically relevant mitochondrial quality control process in the cardiac system.* J Physiol, 2016. **594**(18): p. 5343-62.
342. Marcil, M., et al., *Compensated volume overload increases the vulnerability of heart mitochondria without affecting their functions in the absence of stress.* J Mol Cell Cardiol, 2006. **41**(6): p. 998-1009.
343. Matas, J., et al., *Increased expression and intramitochondrial translocation of cyclophilin-D associates with increased vulnerability of the permeability transition pore to stress-induced opening during compensated ventricular hypertrophy.* J Mol Cell Cardiol, 2009. **46**(3): p. 420-30.

344. Ronald K. Emaus, R.G.a.J.J.L., *Biochimica et Biophysica Acta 850 (1986)436-448 Elsevier. Rhodamine 123 as a probe of transmembrane potential in isolated rat-liver mitochondria: spectral and metabolic properties.* biochimica et Biophysica Acta (BBA), 1986. **850**: p. 436-448.

345. Godin, R., et al., *Peroxisome proliferator-activated receptor gamma coactivator1- gene alpha transfer restores mitochondrial biomass and improves mitochondrial calcium handling in post-necrotic mdx mouse skeletal muscle.* J Physiol, 2012. **590**(21): p. 5487-502.
346. Liza A. Pom, E.A.S., *Mitochondria*. Methods in Cell Biology. Vol. 80.
347. Temperley, R.J., et al., *Investigation of a pathogenic mtDNA microdeletion reveals a translation-dependent deadenylation decay pathway in human mitochondria.* Hum Mol Genet, 2003. **12**(18): p. 2341-8.
348. Shagger, H., *Respiratory Chain Supercomplexes.* IUBMB Life, 2001. **52**(3-5): p. 119-128.
349. Vartak, R., C.A. Porras, and Y. Bai, *Respiratory supercomplexes: structure, function and assembly.* Protein Cell, 2013. **4**(8): p. 582-90.
350. Sun, D., et al., *Cell Type-Specific Modulation of Respiratory Chain Supercomplex Organization.* Int J Mol Sci, 2016. **17**(6).
351. Antoun, G., et al., *Impaired mitochondrial oxidative phosphorylation and supercomplex assembly in rectus abdominis muscle of diabetic obese individuals.* Diabetologia, 2015. **58**(12): p. 2861-2866.
352. Kanaan, G.N., et al., *Atrial Fibrillation Is Associated With Impaired Atrial Mitochondrial Energetics and Supercomplex Formation in Adults With Type 2 Diabetes.* Canadian Journal of Diabetes, 2018.
353. Kuter, K., et al., *Adaptation within mitochondrial oxidative phosphorylation supercomplexes and membrane viscosity during degeneration of dopaminergic neurons in an animal model of early Parkinson's disease.* Biochim Biophys Acta, 2016. **1862**(4): p. 741-53.
354. Rosca, M.G., et al., *Cardiac mitochondria in heart failure: decrease in respirasomes and oxidative phosphorylation.* Cardiovascular Research, 2008. **80**(1): p. 30-39.
355. Jang, S., et al., *Elucidating Mitochondrial Electron Transport Chain Supercomplexes in the Heart During Ischemia-Reperfusion.* Antioxidants & redox signaling, 2017. **27**(1): p. 57-69.
356. Frenzel, M., et al., *Ageing alters the supramolecular architecture of OxPhos complexes in rat brain cortex.* Experimental Gerontology, 2010. **45**(7): p. 563-572.
357. Krause, F., *Detection and analysis of protein-protein interactions in organellar and prokaryotic proteomes by native gel electrophoresis: (Membrane) protein complexes and supercomplexes.* Electrophoresis, 2006. **27**(13): p. 2759-81.
358. Wittig, I., M. Karas, and H. Schagger, *High Resolution Clear Native Electrophoresis for In-gel Functional Assays and Fluorescence Studies of Membrane Protein Complexes.* Mol Cell Proteoics, 2007. **6**: p. 1215-1225.
359. Jang, S. and S. Javadov, *Current Challenges in Elucidating Respiratory Supercomplexes in Mitochondria: Methodological Obstacles.* Frontiers in physiology, 2018. **9**: p. 238-238.
360. Cuillerier, A., et al., *Loss of hepatic LRPPRC alters mitochondrial bioenergetics, regulation of permeability transition and trans-membrane ROS diffusion.* Hum Mol Genet, 2017. **26**(16): p. 3186-3201.
361. Pallotti, F. and G. Lenaz, *Isolation and Subfractionation of Mitochondria from Animal Cells and Tissue Culture Lines*, in *Methods in Cell Biology*. 2007, Academic Press. p. 3-44.
362. Wieckowski, M.R., et al., *Isolation of mitochondria-associated membranes and mitochondria from animal tissues and cells.* Nature Protocols, 2009. **4**: p. 1582.
363. Jha, P., X. Wang, and J. Auwerx, *Analysis of Mitochondrial Respiratory Chain Supercomplexes Using Blue Native Polyacrylamide Gel Electrophoresis (BN-PAGE).* Current protocols in mouse biology, 2016. **6**(1): p. 1-14.
364. Au - Beutner, G. and G.A. Au - Porter Jr, *Analyzing Supercomplexes of the Mitochondrial Electron Transport Chain with Native Electrophoresis, In-gel Assays, and Electroelution.* JoVE, 2017(124): p. e55738.
365. Von Hagen, J., *Proteomics Sample Preperation*. 2008: Wiley InterScience.
366. Couoh-Cardel, S.J., et al., *Structure of dimeric F1F0-ATP synthase.* The Journal of biological chemistry, 2010. **285**(47): p. 36447-36455.

367. Wittig, I. and H. Schägger, *Structural organization of mitochondrial ATP synthase.* Biochimica et Biophysica Acta (BBA) - Bioenergetics, 2008. **1777**(7): p. 592-598.
368. Murley, A. and J. Nunnari, *The Emerging Network of Mitochondria-Organelle Contacts.* Mol Cell, 2016. **61**(5): p. 648-653.
369. Leonard, J.V. and A.H.V. Schapira, *Mitochondrial respiratory chain disorders I: mitochondrial DNA defects.* The Lancet, 2000. **355**(9200): p. 299-304.
370. Siira, S.J., et al., *LRPPRC-mediated folding of the mitochondrial transcriptome.* Nat Commun, 2017. **8**(1): p. 1532.
371. Wessels, H.J., et al., *Analysis of 953 human proteins from a mitochondrial HEK293 fraction by complexome profiling.* PLoS One, 2013. **8**(7): p. e68340.
372. Lobo-Jarne, T., et al., *Human COX7A2L Regulates Complex III Biogenesis and Promotes Supercomplex Organization Remodeling without Affecting Mitochondrial Bioenergetics.* Cell Rep, 2018. **25**(7): p. 1786-1799 e4.
373. Lu, Y.W. and S.M. Claypool, *Disorders of phospholipid metabolism: an emerging class of mitochondrial disease due to defects in nuclear genes.* Front Genet, 2015. **6**: p. 3.
374. Forest, A., et al., *Comprehensive and Reproducible Untargeted Lipidomic Workflow Using LC-QTOF Validated for Human Plasma Analysis.* J Proteome Res, 2018. **17**(11): p. 3657-3670.
375. Oemer, G., et al., *Phospholipid Acyl Chain Diversity Controls the Tissue-Specific Assembly of Mitochondrial Cardiolipins.* Cell Rep, 2020. **30**(12): p. 4281-4291 e4.
376. Rampelt, H., et al., *Role of the mitochondrial contact site and cristae organizing system in membrane architecture and dynamics.* Biochim Biophys Acta Mol Cell Res, 2017. **1864**(4): p. 737-746.
377. Weber, T.A., et al., *APOOL is a cardiolipin-binding constituent of the Mitofilin/MINOS protein complex determining cristae morphology in mammalian mitochondria.* PLoS One, 2013. **8**(5): p. e63683.
378. Osman, C., et al., *The genetic interactome of prohibitins: coordinated control of cardiolipin and phosphatidylethanolamine by conserved regulators in mitochondria.* J Cell Biol, 2009. **184**(4): p. 583-96.
379. Richter-Dennerlein, R., et al., *DNAJC19, a mitochondrial cochaperone associated with cardiomyopathy, forms a complex with prohibitins to regulate cardiolipin remodeling.* Cell Metab, 2014. **20**(1): p. 158-71.
380. Christie, D.A., et al., *Stomatin-like protein 2 binds cardiolipin and regulates mitochondrial biogenesis and function.* Mol Cell Biol, 2011. **31**(18): p. 3845-56.
381. Matsuzaki, H., et al., *Tespa1 is a novel component of mitochondria-associated endoplasmic reticulum membranes and affects mitochondrial calcium flux.* Biochem Biophys Res Commun, 2013. **433**(3): p. 322-6.
382. Szabadkai, G., et al., *Chaperone-mediated coupling of endoplasmic reticulum and mitochondrial Ca2+ channels.* J Cell Biol, 2006. **175**(6): p. 901-11.
383. de Brito, O.M. and L. Scorrano, *Mitofusin 2 tethers endoplasmic reticulum to mitochondria.* Nature, 2008. **456**(7222): p. 605-10.
384. Nam, M., et al., *Mitochondrial retrograde signaling connects respiratory capacity to thermogenic gene expression.* Sci Rep, 2017. **7**(1): p. 2013.
385. Qureshi, M.A., C.M. Haynes, and M.W. Pellegrino, *The mitochondrial unfolded protein response: Signaling from the powerhouse.* J Biol Chem, 2017. **292**(33): p. 13500-13506.
386. Lenaz, G., et al., *Complex I function in mitochondrial supercomplexes.* Biochim Biophys Acta, 2016. **1857**(7): p. 991-1000.
387. Enriquez, J.A., *Supramolecular Organization of Respiratory Complexes.* Annu Rev Physiol, 2016. **78**: p. 533-61.
388. Guerrero-Castillo, S., et al., *The Assembly Pathway of Mitochondrial Respiratory Chain Complex I.* Cell Metab, 2017. **25**(1): p. 128-139.
389. Sarewicz, M. and A. Osyczka, *Electronic connection between the quinone and cytochrome C redox pools and its role in regulation of mitochondrial electron transport and redox signaling.* Physiol Rev, 2015. **95**(1): p. 219-43.
390. Moreno-Lastres, D., et al., *Mitochondrial complex I plays an essential role in human respirasome assembly.* Cell Metab, 2012. **15**(3): p. 324-35.

391. Althoff, T., et al., *Arrangement of electron transport chain components in bovine mitochondrial supercomplex I1III2IV1.* EMBO J, 2011. **30**(22): p. 4652-64.
392. Mileykovskaya, E., et al., *Arrangement of the respiratory chain complexes in Saccharomyces cerevisiae supercomplex III2IV2 revealed by single particle cryo-electron microscopy.* J Biol Chem, 2012. **287**(27): p. 23095-103.
393. Elbaz-Alon, Y., et al., *A dynamic interface between vacuoles and mitochondria in yeast.* Dev Cell, 2014. **30**(1): p. 95-102.
394. Timothy D. Heden, J.M.J., Patrick J. Ferrara, Hiroaki Eshima, Anthony R. P. Verkerke, Edward J. Wentzler, Piyarat Siripoksup, Tara M. Narowski, *Mitochondrial PE potentiates respiratory enzymes to amplify skeletal muscle aerobic capacity.* Science Advances, 2019. **5**.
395. Quiros, P.M., et al., *Analysis of mtDNA/nDNA Ratio in Mice.* Curr Protoc Mouse Biol, 2017. **7**(1): p. 47-54.
396. Cuillerier, A. and Y. Burelle, *Hybrid Clear/Blue Native Electrophoresis for the Separation and Analysis of Mitochondrial Respiratory Chain Supercomplexes.* J Vis Exp, 2019(147).
397. Vafai, S.B. and V.K. Mootha, *Mitochondrial disorders as windows into an ancient organelle.* Nature, 2012. **491**(7424): p. 374-83.
398. Ng, Y.S. and D.M. Turnbull, *Mitochondrial disease: genetics and management.* J Neurol, 2016. **263**(1): p. 179-91.
399. Wallace, D.C., *Mitochondrial genetic medicine.* Nat Genet, 2018. **50**(12): p. 1642-1649.
400. Khayat, D., T.L. Kurtz, and P.W. Stacpoole, *The changing landscape of clinical trials for mitochondrial diseases: 2011 to present.* Mitochondrion, 2020. **50**: p. 51-57.
401. Li, X., et al., *Mitochondrial transfer of induced pluripotent stem cell-derived mesenchymal stem cells to airway epithelial cells attenuates cigarette smoke-induced damage.* Am J Respir Cell Mol Biol, 2014. **51**(3): p. 455-65.
402. Jackson, M.V., et al., *Mitochondrial Transfer via Tunneling Nanotubes is an Important Mechanism by Which Mesenchymal Stem Cells Enhance Macrophage Phagocytosis in the In Vitro and In Vivo Models of ARDS.* Stem Cells, 2016. **34**(8): p. 2210-23.
403. Boukelmoune, N., et al., *Mitochondrial transfer from mesenchymal stem cells to neural stem cells protects against the neurotoxic effects of cisplatin.* Acta Neuropathol Commun, 2018. **6**(1): p. 139.
404. Colombo, M., G. Raposo, and C. Thery, *Biogenesis, secretion, and intercellular interactions of exosomes and other extracellular vesicles.* Annu Rev Cell Dev Biol, 2014. **30**: p. 255-89.
405. Newell, C., et al., *Mesenchymal Stem Cells Shift Mitochondrial Dynamics and Enhance Oxidative Phosphorylation in Recipient Cells.* Front Physiol, 2018. **9**: p. 1572.
406. Zhao, W., et al., *Intravenous injection of mesenchymal stem cells is effective in treating liver fibrosis.* World J Gastroenterol, 2012. **18**(10): p. 1048-58.
407. Li, Z.H., X.; Mao, J.; Liu, X.; Zhang, L.; Liu, J.; Li, D.; Shan, H., *Optimization of Mesenchymal Stem Cells (MSCs) Delivery Dose and Route in Mice with Acute Liver Injury by Bioluminescence Imaging.* Molecular Imaging and Biology, 2015. **17**: p. 185-194.
408. Volarevic, V., et al., *Concise review: Therapeutic potential of mesenchymal stem cells for the treatment of acute liver failure and cirrhosis.* Stem Cells, 2014. **32**(11): p. 2818-23.
409. Nasir, G.A.M., S.; Khan, M.; Shams, S.; Alo, G.; Khan, S. N.; Riazuddin, S., *Mesenchymal stem cells and Interleukin-6 attenuate liver fibrosis in mice.* Journal of Translational Medicine, 2013. **11**(78).
410. Kanazawa, H., et al., *Bone marrow-derived mesenchymal stem cells ameliorate hepatic ischemia reperfusion injury in a rat model.* PLoS One, 2011. **6**(4): p. e19195.
411. Lavrentieva, A., A. Hoffmann, and C. Lee-Thedieck, *Limited Potential or Unfavorable Manipulations? Strategies Toward Efficient Mesenchymal Stem/Stromal Cell Applications.* Front Cell Dev Biol, 2020. **8**: p. 316.
412. Amin Rustom, R.S., Ivanka Markovic, and H.-H.G. Paul Walther, *Nanotubular Highways for Intercellular Organelle Transport.* Science, 2004. **303**: p. 1007-1010.
413. Patten, D.A., et al., *Mitochondrial adaptation in human mesenchymal stem cells following ionizing radiation.* FASEB J, 2019. **33**(8): p. 9263-9278.
414. Bereiter-Hahn, J., A. Munnich, and P. Woiteneck, *Dependence of energy metabolism on the density of cells in culture.* Cell Struct Funct, 1998. **23**(2): p. 85-93.

415. Berridge, M.V., et al., *Horizontal transfer of mitochondria between mammalian cells: beyond co-culture approaches.* Curr Opin Genet Dev, 2016. **38**: p. 75-82.
416. Paliwal, S., et al., *Human tissue-specific MSCs demonstrate differential mitochondria transfer abilities that may determine their regenerative abilities.* Stem Cell Res Ther, 2018. **9**(1): p. 298.
417. Kiamehr, M., et al., *Dedifferentiation of Primary Hepatocytes is Accompanied with Reorganization of Lipid Metabolism Indicated by Altered Molecular Lipid and miRNA Profiles.* Int J Mol Sci, 2019. **20**(12).
418. Pelizzo, G., et al., *Extracellular vesicles derived from mesenchymal cells: perspective treatment for cutaneous wound healing in pediatrics.* Regen Med, 2018. **13**(4): p. 385-394.
419. Gatti, S., et al., *Microvesicles derived from human adult mesenchymal stem cells protect against ischaemia-reperfusion-induced acute and chronic kidney injury.* Nephrol Dial Transplant, 2011. **26**(5): p. 1474-83.
420. Clark, K., et al., *Placental Mesenchymal Stem Cell-Derived Extracellular Vesicles Promote Myelin Regeneration in an Animal Model of Multiple Sclerosis.* Cells, 2019. **8**(12).
421. Li, T., et al., *Exosomes derived from human umbilical cord mesenchymal stem cells alleviate liver fibrosis.* Stem Cells Dev, 2013. **22**(6): p. 845-54.
422. Rong, X., et al., *Human bone marrow mesenchymal stem cells-derived exosomes alleviate liver fibrosis through the Wnt/beta-catenin pathway.* Stem Cell Res Ther, 2019. **10**(1): p. 98.
423. Damania, A., et al., *Mesenchymal stromal cell-derived exosome-rich fractionated secretome confers a hepatoprotective effect in liver injury.* Stem Cell Res Ther, 2018. **9**(1): p. 31.
424. Arslan, F., et al., *Mesenchymal stem cell-derived exosomes increase ATP levels, decrease oxidative stress and activate PI3K/Akt pathway to enhance myocardial viability and prevent adverse remodeling after myocardial ischemia/reperfusion injury.* Stem Cell Res, 2013. **10**(3): p. 301-12.
425. Kowal, J., et al., *Proteomic comparison defines novel markers to characterize heterogeneous populations of extracellular vesicle subtypes.* Proc Natl Acad Sci U S A, 2016. **113**(8): p. E968-77.
426. van Balkom, B.W., et al., *Quantitative and qualitative analysis of small RNAs in human endothelial cells and exosomes provides insights into localized RNA processing, degradation and sorting.* J Extracell Vesicles, 2015. **4**: p. 26760.
427. Lai, R.C., et al., *Exosome secreted by MSC reduces myocardial ischemia/reperfusion injury.* Stem Cell Res, 2010. **4**(3): p. 214-22.
428. Tamura, R., S. Uemoto, and Y. Tabata, *Immunosuppressive effect of mesenchymal stem cell-derived exosomes on a concanavalin A-induced liver injury model.* Inflamm Regen, 2016. **36**: p. 26.
429. McIntyre, L.A., et al., *Cellular Immunotherapy for Septic Shock. A Phase I Clinical Trial.* Am J Respir Crit Care Med, 2018. **197**(3): p. 337-347.
430. Fullerton, M.D., et al., *The development of a metabolic disease phenotype in CTP:phosphoethanolamine cytidylyltransferase-deficient mice.* J Biol Chem, 2009. **284**(38): p. 25704-13.
431. McWilliams, T.G., et al., *mito-QC illuminates mitophagy and mitochondrial architecture in vivo.* J Cell Biol, 2016. **214**(3): p. 333-45.
432. Chinnery, P.F. and S. DiMauro, *Mitochondrial hepatopathies.* J Hepatol, 2005. **43**(2): p. 207-9.
433. Signes, A. and E. Fernandez-Vizarra, *Assembly of mammalian oxidative phosphorylation complexes I-V and supercomplexes.* Essays Biochem, 2018. **62**(3): p. 255-270.
434. Rasola, A. and P. Bernardi, *The mitochondrial permeability transition pore and its involvement in cell death and in disease pathogenesis.* Apoptosis, 2007. **12**(5): p. 815-33.
435. Sileikyte, J. and M. Forte, *The Mitochondrial Permeability Transition in Mitochondrial Disorders.* Oxid Med Cell Longev, 2019. **2019**: p. 3403075.
436. Keep, M., et al., *Intrathecal cyclosporin prolongs survival of late-stage ALS mice.* Brain Research, 2001. **894**(2): p. 327-331.
437. Sambri, I., et al., *Impaired flickering of the permeability transition pore causes SPG7 spastic paraplegia.* EBioMedicine, 2020. **61**: p. 103050.
438. Mathai, J.C. and V. Sitaramam, *Stretch sensitivity of transmembrane mobility of hydrogen peroxide through voids in the bilayer. Role of cardiolipin.* Journal of Biological Chemistry, 1994. **269**(27): p. 17784-17793.

439. Mahammad, S. and I. Parmryd, *Cholesterol depletion using methyl-beta-cyclodextrin.* Methods Mol Biol, 2015. **1232**: p. 91-102.
440. Solsona-Vilarrasa, E., et al., *Cholesterol enrichment in liver mitochondria impairs oxidative phosphorylation and disrupts the assembly of respiratory supercomplexes.* Redox Biol, 2019. **24**: p. 101214.
441. Martin, L.A., B.E. Kennedy, and B. Karten, *Mitochondrial cholesterol: mechanisms of import and effects on mitochondrial function.* J Bioenerg Biomembr, 2016. **48**(2): p. 137-51.
442. Berger, J., et al., *Peroxisomes in brain development and function.* Biochim Biophys Acta, 2016. **1863**(5): p. 934-55.
443. Kovarova, N., et al., *Tissue- and species-specific differences in cytochrome c oxidase assembly induced by SURF1 defects.* Biochim Biophys Acta, 2016. **1862**(4): p. 705-715.
444. Pulliam, D.A., et al., *Complex IV-deficient Surf1(-/-) mice initiate mitochondrial stress responses.* Biochem J, 2014. **462**(2): p. 359-71.
445. Walter, P. and D. Ron, *The unfolded protein response: from stress pathway to homeostatic regulation.* Science, 2011. **334**(6059): p. 1081-6.
446. Mehdipour, A.R. and G. Hummer, *Cardiolipin puts the seal on ATP synthase.* Proc Natl Acad Sci U S A, 2016. **113**(31): p. 8568-70.
447. Santiago, E., N. López-Moratalla, and J.L. Segovia, *Correlation between losses of mitochondrial ATPase activity and cardiolipin degradation.* Biochemical and Biophysical Research Communications, 1973. **53**(2): p. 439-445.
448. Murphy, D.E., et al., *Extracellular vesicle-based therapeutics: natural versus engineered targeting and trafficking.* Exp Mol Med, 2019. **51**(3): p. 1-12.
449. Soiferman, D.a.S., A. , *The Use of Fibroblasts from Patients with Inherited Mitochondrial Disorders for Pathomechanistic Studies and Evaluation of Therapies.* 2015.
450. Honarmand, S., *Molecular Mechanisms Underlying the Pathogenesis of Leigh Syndrome French Canadian*, in *Human Genetics*. 2018, Faculty of Medicine: Montreal, Quebec, Canada.